

Lecture Note

Exotic Superconductivity

Department of Physics, University of Illinois at Urbana-Champaign

Anthony J. Leggett



These are the lecture notes for a series of lectures “Exotic Superconductivity” done at the Graduate School of Science of The University of Tokyo, Japan, in May-June, 2011. These lectures are an introduction to those superconductors, all discovered since the 1970s, which do not appear to be well described by the traditional BCS theory. While the main emphasis will be on the most spectacular member of this class, the cuprates, I shall also discuss briefly the heavy fermion, organic, ruthenate and ferropnictide superconductors as well as superfluid ^3He for reference. I shall try to provide a general framework for the analysis of all-electronic superconductivity (i.e. that in which the Cooper pairing is induced wholly or mainly by the repulsive Coulomb interaction).

These lecture notes were written by the following graduate students at The University of Tokyo: Haruki Watanabe (UC Berkeley from Aug. 2011, Lec. 4, 7, 8), Hakuto Suzuki (Lec. 5, 6), Yuya Tanizaki (Lec. 1, 4, 6), Masaru Hongo (Lec. 2, 3), Kota Masuda (Lec. 1, 2, 3), and Shimpei Endo (Lec. 1, 5, 7, 8). We would like to thank Profs. Hiroshi Fukuyama and Masahito Ueda for the organization of the lecture series as well for the critical reading of these notes. We also thank Office of Communication and Office of Internationalization Planning at the Graduate School of Science, and Office of Student Affairs at Physics Department of The University of Tokyo for their supports. The lectures were hosted as the Sir Anthony James Leggett Visit Program 2011-2013, financially supported by the JSPS Award for Eminent Scientists (FY2011-2013).

Slides and videos of the lectures are available at UT OpenCourseWare:
http://ocw.u-tokyo.ac.jp/eng_courselist/828.html

Contents

Lec. 1 Reminders of the BCS theory	10
1.1 Basic model	10
1.2 BCS theory at $T = 0$	11
1.2.1 BCS wave function	11
1.2.2 Alternative form of the BCS wave function	12
1.2.3 Pair wave function	13
1.2.4 Quantitative development of the BCS theory	15
1.3 BCS theory at finite temperature	18
1.3.1 Derivation of the gap equation	18
1.3.2 $F_{\mathbf{k}}$ at finite temperature	20
1.3.3 $\langle n_{\mathbf{k}} \rangle$ at finite temperature	20
1.3.4 Properties of the BCS gap equation	20
1.3.5 Properties of the Fock term	23
1.3.6 Pair wave function	23
1.4 Generalization of the BCS theory	25
Lec. 2 Superfluid ^3He: basic description	28
2.1 Introduction	28
2.2 Landau Fermi liquid theory	29
2.3 Effects of (spin) molecular field in ^3He	31
2.3.1 Enhanced low-energy spin fluctuations	31
2.3.2 Coupling of atomic spins through the exchange of virtual paramagnons	32
2.3.3 Pairing interaction in liquid ^3He	32
2.4 Anisotropic spin-singlet pairing (for orientation only)	33
2.5 Digression: macroscopic angular momentum problem	34
2.6 Spin-triplet pairing	35
2.6.1 Equal spin pairing (ESP) state	36
2.6.2 General case	36
2.6.3 \mathbf{d} -vector (unitary states)	37
2.7 Ginzburg–Landau theory	38
2.7.1 Spin-singlet case	38
2.7.2 Spin-triplet case	39

A. J. Leggett

Lec. 3 Superfluid ^3He (continued)	42
3.1 Experimental phases of liquid ^3He	42
3.2 Nature of the order parameter of different phases	43
3.2.1 A phase	43
3.2.2 A1 phase	44
3.2.3 B phase: naive identification	45
3.3 Why A phase?	45
3.3.1 Generalized Ginzburg–Landau approach	46
3.3.2 Spin fluctuation feedback	48
3.4 NMR in the new phase	49
3.5 What can be inferred from the sum rules?	50
3.6 Spontaneously broken spin-orbit symmetry	51
3.7 Microscopic spin dynamics (schematic)	54
3.8 Illustration of NMR behavior: A phase longitudinal resonance	55
3.9 Digression: possibility of the “fragmented” state	55
3.10 Superfluid ^3He : supercurrents, textures, and defects	57
3.10.1 Supercurrents	57
3.10.2 Mermin–Ho vortex and topological singularities	58
Lec. 4 Definition and diagnostics of “exotic” superconductivity	61
4.1 Diagnostics of the non-phonon mechanism	62
4.1.1 Absence of isotope effect	62
4.1.2 Absence of phonon structure in tunneling I-V characteristics	64
4.2 General properties of the order parameter	65
4.2.1 Definition of the order parameter	65
4.2.2 Order parameter in a crystal	67
4.3 Diagnostics of the symmetry of the order parameter	69
4.3.1 Diagnostics of the spin state	69
4.3.2 Diagnostics of the orbital state	71
4.3.3 Effect of impurities	73
4.4 Addendum: the effect of spin-orbit coupling	74
Lec. 5 Non-cuprate exotic superconductivity	77
5.1 Alkali fullerides	77
5.1.1 Structure	77
5.1.2 Fullerene crystals	77
5.1.3 Alkali fullerides	78
5.1.4 Superconducting state	79
5.2 Organics	80
5.2.1 Normal state	80
5.2.2 Superconducting state	81

A. J. Leggett

5.3	Heavy fermions	82
5.3.1	Normal-state behavior	82
5.3.2	Superconducting phase	84
5.4	Strontium ruthenate: Sr_2RuO_4	86
5.4.1	History	86
5.4.2	Experimental properties of Sr_2RuO_4	87
5.5	Ferropnictides	91
5.5.1	Composition	91
5.5.2	Structure (1111 compounds)	91
5.5.3	Phase diagram	92
5.5.4	Experimental properties (normal state)	92
5.5.5	Band structure	93
5.5.6	Superconductivity	94
5.5.7	Experimental properties (superconducting state)	94
5.5.8	Pairing state	95
Lec. 6	Cuprates: generalities, and normal state properties	98
6.1	Basic chemical properties	98
6.1.1	Composition	98
6.1.2	Structure	98
6.2	Doping	99
6.3	Construction of phase diagram	101
6.4	Determinants of T_c	103
6.5	Other remarks: carrier density and list of cuprate superconductors	104
6.6	Experimental properties of the normal state: general discussion	105
6.7	Experimental properties at the optimal doping	106
6.7.1	Electronic specific heat	106
6.7.2	Magnetic properties	106
6.7.3	Transport	106
6.7.4	Spectroscopic probes: Fermi surface	108
6.7.5	Results of ARPES experiments at the optimal doping	109
6.7.6	Neutron scattering	110
6.7.7	Optics (ab -plane)	110
6.8	Experimental properties at the underdoped regime	111
6.8.1	Pseudogap	111
6.8.2	ARPES in the pseudogap regime: the puzzle of the Fermi surface	113
Lec. 7	Cuprates: superconducting state properties	117
7.1	Experimental properties	117
7.1.1	Structural and elastic properties and electron density distribution	117
7.1.2	Macroscopic electromagnetic properties	117

A. J. Leggett

7.1.3	Specific heat and condensation energy	118
7.1.4	NMR	118
7.1.5	Penetration depth	118
7.1.6	AC conductivity	120
7.1.7	Thermal conductivity	121
7.1.8	Tunneling	121
7.1.9	ARPES	122
7.1.10	Neutron scattering (YBCO, LSCO, and Bi-2212)	123
7.1.11	Optics	123
7.1.12	Electron energy loss spectroscopy (EELS)	125
7.2	What do we know for sure about superconductivity in the cuprates?	125
7.3	Symmetry of the order parameter (gap)	128
7.4	Josephson experiment in cuprate (and other exotic) superconductors	131
7.5	What is a “satisfactory” theory of the high- T_c superconductivity in the cuprates?	133
Lec. 8	Exotic superconductivity: discussion	136
8.1	Common properties of all exotic superconductors	136
8.2	Phenomenology of superconductivity	137
8.2.1	Meissner effect	138
8.2.2	Persistent current	138
8.2.3	Summary	138
8.3	What else do exotic superconductors have in common?	140
8.4	Theoretical approaches (mostly for the cuprates)	140
8.5	Which energy is saved in the superconducting phase transition?	143
8.5.1	Virial theorem	144
8.5.2	Energy consideration in “all-electronic” superconductors	147
8.5.3	Eliashberg vs. Overscreening	148
8.5.4	Role of two-dimensionality	149
8.5.5	Constraints on the Coulomb saved at small q	150
8.5.6	Mid-infrared optical and EELS spectra of the cuprates	152
8.6	How can we realize room temperature superconductors?	154

A. J. Leggett

List of Symbols

Symbol	Meaning	Page where defined /introduced
$ \uparrow\rangle$	spin up state	11
$ \downarrow\rangle$	spin down state	11
$ 00\rangle$	state with $(\mathbf{k} \uparrow, -\mathbf{k} \downarrow)$ states unoccupied	12
$ 11\rangle$	state with $(\mathbf{k} \uparrow, -\mathbf{k} \downarrow)$ states occupied	12
a, a^\dagger	creation/annihilation operators	10
$\alpha_{\mathbf{k}\sigma}, \alpha_{\mathbf{k}\sigma}^\dagger$	creation/annihilation operators for quasi-particles (not for bare particles)	33
$A(\mathbf{k}, \varepsilon)$	spectral function	108
$c_{\mathbf{k}}$	coefficient of the pair wave function	36
C_V	specific heat	28
\mathbf{d}	\mathbf{d} -vector	38
$dn/d\varepsilon$	density of states of both spins at the Fermi surface	21
$d_{x^2-y^2}$	most popular symmetry of cuprate order parameter	130
D_s	spin diffusion constant	28
e	electron charge	26
E_0	ground state energy of the interacting system	29
$E_{\mathbf{k}}$	BCS excitation energy	16
E_{BP}	energy of the broken-pair state	18
E_{EP}	energy of the excited-pair state	18
E_{GP}	energy of the ground-pair state	18
E_J	Josephson coupling energy	131
F	free energy	39
$F(\mathbf{k})$	relative wave function of the Cooper pair	23
$f(\mathbf{p}\mathbf{p}'\sigma\sigma')$	Landau interaction function	29
$F(\omega)$	phonon density of states	63
F_ℓ^s, F_ℓ^a	Landau parameters	30
g_D	nuclear dipole coupling constant	52
H_{c1}	lower critical field	81
H_{c2}	upper critical field	81
\hat{H}_D	nuclear dipole energy	51
H_{ext}	external magnetic field	50
\mathbf{k}	wave vector	10
k_B	Boltzmann's constant	21

A. J. Leggett

Symbol	Meaning	Page where defined /introduced
k_F	Fermi wave number	10
K_s	Knight shift	73
$\hat{\ell}$	direction of relative orbital angular momentum of pairs in the A phase	43
ℓ_{el}	mean free paths of electrons	121
ℓ_{ph}	mean free paths of phonons	121
\mathbf{L}	orbital angular momentum	45
$L(\omega)$	loss function	110
m	mass of atoms/electrons	10
m^*	effective mass of atoms/electrons	30
n	particle density	13
$N(0)$	density of states of one spin at the Fermi surface ($\equiv 1/2(dn/d\varepsilon)$)	21
N_{Cooper}	number of the Cooper pairs	24
N_s	density of states	72
p	doping (of cuprates)	101
p_F	Fermi momentum	29
q_{TF}	Thomas-Fermi wave number	26
\mathbf{Q}	pseudo-Bragg vector	142
\mathbf{R}	center-of-mass coordinate	72
$R(\omega)$	optical reflectivity	110
\mathbf{S}	total spin	31
T^*	crossover line (in the phase diagram of cuprates)	102
T_1	nuclear spin relaxation time	73
T_c	critical temperature	20
T_{Curie}	Curie temperature	85
T_N	Nèel temperature	85
$u_{\mathbf{k}}$	coefficient in the BCS wave function	12
v_F	Fermi velocity	25
$v_{\mathbf{k}}$	coefficient in the BCS wave function	12
v_s	superfluid velocity	57
α_I	isotope exponent	63
$\alpha(\omega)$	phonon coupling function	63
β	$1/k_B T$	19
γ	coefficient of the linear term in the specific heat	87
Γ_1	relaxation rate of ℓ -symmetry distortion	74

A. J. Leggett

Symbol	Meaning	Page where defined /introduced
Γ_U	relaxation rate of the T -reversal operator	74
δn	deviation of (quasi)particle occupation number from the normal-state value	29
$\Delta_{\mathbf{k}}$	BCS gap parameter	16
ε_c	cutoff energy in the BCS model	21
ε_F	Fermi energy	10
$\varepsilon_{\mathbf{k}}$	kinetic energy relative to the Fermi energy	10
η	viscosity	28
Θ_D	Debye temperature	63
κ	thermal conductivity	28
κ_0	static bulk modulus of the non-interacting Fermi gas	26
λ	London penetration depth	79
μ	chemical potential	10
μ^*	Coulomb pseudopotential	63
μ_B	Bohr magneton	52
μ_n	nuclear magnetic moment	50
ξ	healing length	24
ξ_{PR}	pair radius	14
ξ_{ab}	in-plane Ginzburg-Landau healing length	117
$\xi_{\mathbf{k}}$	kinetic energy	10
ξ_c	c -axis Ginzburg-Landau healing length	117
$\rho(T)$	resistivity	80
ρ_1, ρ_2	single-particle/two-particle density matrices	65
$\rho_{\mathbf{k}}$	single-particle density	18
ρ_s	superfluid density	57
$\sigma(\omega)$	AC conductivity	107
τ	relaxation time	107
$\phi(\mathbf{k})$	phase of the condensate wave function	13
$\phi(\mathbf{r}_1\sigma_1; \mathbf{r}_2\sigma_2)$	pseudo-molecular wave function in the BCS problem	11
Φ_0	(superconducting) flux quantum ($\equiv h/2e$)	131
χ	Pauli spin susceptibility	28
χ^{sp}	spin response	31
$\Psi(\hat{\mathbf{n}})$	Ginzburg-Landau order parameter	38
$\Psi(\mathbf{r}_1\sigma_1, \mathbf{r}_2\sigma_2 \cdots \mathbf{r}_N\sigma_N)$	many-body wave function	11
ω_D	Debye frequency	21

A. J. Leggett

Symbol	Meaning	Page where defined /introduced
$\bar{\omega}_e$	some characteristic frequency of the order of the plasma frequency	153
ω_p	plasma frequency	153
ω_{ph}	frequency of the longitudinal sound waves (phonons)	64
ω_{res}	response frequency	50
ω_{SF}	AF fluctuation frequency	142

Lec. 1 Reminders of the BCS theory

First we give a brief review of the theory of conventional superconductors, namely the BCS theory. In this section, we start with the singlet pairing case to describe the basic physics of the superconductivity.

1.1 Basic model

Just as in the original BCS theory, we consider here the Sommerfeld model for simplicity: we consider N spin-1/2 fermions in a free space. We assume N to be sufficiently large and even. For such a system, the kinetic energy for a free particle is

$$\varepsilon_{\mathbf{k}} \equiv \xi_{\mathbf{k}} - \mu(T), \quad (1.1)$$

where $\xi_{\mathbf{k}} = \frac{\mathbf{k}^2}{2m}$, and $\mu(T)$ is the chemical potential of the system. We note here that $\mu(T)$ can be regarded as a constant¹, and it is equal to the Fermi energy

$$\mu(T) = \varepsilon_F = \frac{k_F^2}{2m}. \quad (1.2)$$

We assume that the fermions are interacting via an attractive potential, so that the interaction part can be represented as

$$\hat{V} = \frac{1}{2} \sum_{\substack{\mathbf{p}, \mathbf{p}', \mathbf{q} \\ \sigma, \sigma'}} V_{\mathbf{p}, \mathbf{p}', \mathbf{q}} a_{\mathbf{p}+\frac{\mathbf{q}}{2}, \sigma}^\dagger a_{\mathbf{p}'-\frac{\mathbf{q}}{2}, \sigma'}^\dagger a_{\mathbf{p}'+\frac{\mathbf{q}}{2}, \sigma'} a_{\mathbf{p}-\frac{\mathbf{q}}{2}, \sigma}. \quad (1.3)$$

We do not discuss here the origin of this interaction (we will present the discussion in Sec. 1.3.4), but rather try to see how the system behaves under such an attractive interaction.

¹In fact, the temperature in question is very small in discussing the BCS theory, and thus the temperature dependence of the chemical potential due to the Fermi statistics is negligible. In addition, the effect of the superconducting phase transition to the chemical potential is very small in the BCS theory. Therefore, we can regard $\mu(T)$ as a constant.

1.2 BCS theory at $T = 0$

1.2.1 BCS wave function

Under an attractive interaction, the Fermi system forms Cooper pairs and they undergo Bose-Einstein condensation. When the Bose-Einstein condensation occurs, a macroscopic number of bosons occupy the same state. Therefore, as a fundamental assumption, we think that all the pairs of fermions occupy the same pair wave function ϕ :

$$\Psi_N = \Psi(\mathbf{r}_1\sigma_1, \mathbf{r}_2\sigma_2 \dots \mathbf{r}_N\sigma_N) = \mathcal{A}[\phi(\mathbf{r}_1\sigma_1; \mathbf{r}_2\sigma_2)\phi(\mathbf{r}_3\sigma_3; \mathbf{r}_4\sigma_4) \cdots \phi(\mathbf{r}_{N-1}\sigma_{N-1}; \mathbf{r}_N\sigma_N)], \quad (1.4)$$

where \mathcal{A} is the antisymmetrizer. For now, we restrict our attention to the case where pairs are formed in the spin-singlet, s -wave orbital angular momentum state, and the center of mass of the pairs is at rest. Then the pair wave function ϕ becomes

$$\phi(\mathbf{r}_1\sigma_1; \mathbf{r}_2\sigma_2) = \frac{1}{\sqrt{2}} \left[|\uparrow\rangle_1 |\downarrow\rangle_2 - |\downarrow\rangle_1 |\uparrow\rangle_2 \right] \phi(\mathbf{r}_1 - \mathbf{r}_2), \quad (1.5)$$

where $\phi(\mathbf{r}) = \phi(-\mathbf{r})$. If we define the Fourier transform $\chi(\mathbf{k})$ by

$$\phi(\mathbf{r}) = \sum_{\mathbf{k}} \chi(\mathbf{k}) e^{i\mathbf{k}\mathbf{r}}, \quad (1.6)$$

then we find

$$\begin{aligned} \phi(\mathbf{r}_1\sigma_1; \mathbf{r}_2\sigma_2) &= \frac{1}{\sqrt{2}} \left[|\uparrow\rangle_1 |\downarrow\rangle_2 - |\downarrow\rangle_1 |\uparrow\rangle_2 \right] \sum_{\mathbf{k}} \chi(\mathbf{k}) e^{i\mathbf{k}(\mathbf{r}_1 - \mathbf{r}_2)} \\ &= \sum_{\mathbf{k}} \frac{\chi(\mathbf{k})}{\sqrt{2}} \left[|\mathbf{k}\uparrow\rangle_1 |-\mathbf{k}\downarrow\rangle_2 - |\mathbf{k}\downarrow\rangle_1 |-\mathbf{k}\uparrow\rangle_2 \right] \\ &= \sum_{\mathbf{k}} \frac{\chi(\mathbf{k})}{\sqrt{2}} \left[|\mathbf{k}\uparrow\rangle_1 |-\mathbf{k}\downarrow\rangle_2 - |-\mathbf{k}\downarrow\rangle_1 |\mathbf{k}\uparrow\rangle_2 \right] \\ &= \sum_{\mathbf{k}} \chi(\mathbf{k}) a_{\mathbf{k}\uparrow}^\dagger a_{-\mathbf{k}\downarrow}^\dagger |\text{vac}\rangle, \end{aligned} \quad (1.7)$$

where we have used $\chi(\mathbf{k}) = \chi(-\mathbf{k})$ in the second last line. Therefore, if we define

$$\Omega^\dagger \equiv \sum_{\mathbf{k}} \chi(\mathbf{k}) a_{\mathbf{k}\uparrow}^\dagger a_{-\mathbf{k}\downarrow}^\dagger, \quad (1.8)$$

the N -body wave function defined in Eq. (1.4) is rewritten as

$$\Psi_N = (\Omega^\dagger)^{N/2} |\text{vac}\rangle = \left[\sum_{\mathbf{k}} \chi(\mathbf{k}) a_{\mathbf{k}\uparrow}^\dagger a_{-\mathbf{k}\downarrow}^\dagger \right]^{N/2} |\text{vac}\rangle. \quad (1.9)$$

Note that this is automatically an eigenstate of \hat{N} . We also note that the normal ground state is a special case of this form of the wave function, since we can see

$$\Psi_N^{\text{norm}} = \prod_{k < k_F} a_{\mathbf{k}\uparrow}^\dagger a_{-\mathbf{k}\downarrow}^\dagger |\text{vac}\rangle = \left(\sum_{k < k_F} a_{\mathbf{k}\uparrow}^\dagger a_{-\mathbf{k}\downarrow}^\dagger \right)^{N/2} |\text{vac}\rangle \quad (1.10)$$

from the Fermi statistics, and the final expression corresponds to the BCS wave function with $\chi(\mathbf{k}) = \theta(k_F - |\mathbf{k}|)$.

1.2.2 Alternative form of the BCS wave function

In the previous subsection, we have obtained the many-body wave function which automatically conserves the number of particles N . In principle, we can minimize the free energy with this class of wave functions and study the thermodynamic properties of the system, but it is a tough work. Therefore, we replace the wave function in the following way:

$$(\Omega^\dagger)^{N/2} \rightarrow \exp \Omega^\dagger \equiv \sum_{N/2=0}^{\infty} \frac{1}{(N/2)!} (\Omega^\dagger)^{N/2}, \quad (1.11)$$

and we try to minimize $\hat{H} - \mu \hat{N}$ instead of \hat{H} . Hence, up to the normalization, the wave function becomes

$$\Psi \propto \exp \left(\sum_{\mathbf{k}} \chi(\mathbf{k}) a_{\mathbf{k},\uparrow}^\dagger a_{-\mathbf{k},\downarrow}^\dagger \right) |\text{vac}\rangle = \prod_{\mathbf{k}} \exp \left(\chi(\mathbf{k}) a_{\mathbf{k},\uparrow}^\dagger a_{-\mathbf{k},\downarrow}^\dagger \right) |\text{vac}\rangle. \quad (1.12)$$

Since $(a_{\mathbf{k},\uparrow}^\dagger a_{-\mathbf{k},\downarrow}^\dagger)^2 = 0$ due to the Fermi statistics, it reads

$$\Psi \propto \prod_{\mathbf{k}} (1 + \chi(\mathbf{k}) a_{\mathbf{k},\uparrow}^\dagger a_{-\mathbf{k},\downarrow}^\dagger) |\text{vac}\rangle. \quad (1.13)$$

To make clear the physical meanings of the following calculations, we go over to the representation in terms of occupation spaces of $\mathbf{k} \uparrow, -\mathbf{k} \downarrow$; let $|00\rangle_{\mathbf{k}}$ be the corresponding vacuum, and define

$$|10\rangle_{\mathbf{k}} = a_{\mathbf{k},\uparrow}^\dagger |00\rangle_{\mathbf{k}}, \quad |01\rangle_{\mathbf{k}} = a_{-\mathbf{k},\downarrow}^\dagger |00\rangle_{\mathbf{k}}, \quad \text{and} \quad |11\rangle_{\mathbf{k}} = a_{\mathbf{k},\uparrow}^\dagger a_{-\mathbf{k},\downarrow}^\dagger |00\rangle_{\mathbf{k}}. \quad (1.14)$$

Then the wave function Ψ can be represented as

$$\Psi = \prod_{\mathbf{k}} \Phi_{\mathbf{k}}, \quad (1.15)$$

where

$$\Phi_{\mathbf{k}} \propto |00\rangle_{\mathbf{k}} + \chi_{\mathbf{k}} |11\rangle_{\mathbf{k}}. \quad (1.16)$$

To satisfy the normalization condition, multiply by the factor $1/\sqrt{1 + |\chi_{\mathbf{k}}|^2}$, and then we obtain

$$\Phi_{\mathbf{k}} = u_{\mathbf{k}} |00\rangle_{\mathbf{k}} + v_{\mathbf{k}} |11\rangle_{\mathbf{k}}, \quad (1.17)$$

with $u_{\mathbf{k}} = \frac{1}{\sqrt{1 + |\chi_{\mathbf{k}}|^2}}$ and $v_{\mathbf{k}} = \frac{\chi_{\mathbf{k}}}{\sqrt{1 + |\chi_{\mathbf{k}}|^2}}$. Thus, we have obtained the general form of the BCS wave function as

$$\Psi_{\text{BCS}} = \prod_{\mathbf{k}} (u_{\mathbf{k}} |00\rangle_{\mathbf{k}} + v_{\mathbf{k}} |11\rangle_{\mathbf{k}}) = \prod_{\mathbf{k}} \left(u_{\mathbf{k}} + v_{\mathbf{k}} a_{\mathbf{k},\uparrow}^\dagger a_{-\mathbf{k},\downarrow}^\dagger \right) |\text{vac}\rangle, \quad (1.18)$$

which does not conserve the number of particles. The normal ground state corresponds to a special case of this wave function, which can be obtained by setting $u_{\mathbf{k}} = 0, v_{\mathbf{k}} = 1$ for $k < k_F$ and $u_{\mathbf{k}} = 1, v_{\mathbf{k}} = 0$ for $k > k_F$.

We should make some remarks on the BCS wave function and the above derivation. At first we should notice that this is the very general result for the spin-singlet pairing systems in the sense that the coefficients $u_{\mathbf{k}}$ and $v_{\mathbf{k}}$ can depend on the direction of the momentum \mathbf{k} . Since the phase transformation $(u_{\mathbf{k}}, v_{\mathbf{k}}) \rightarrow e^{i\phi_{\mathbf{k}}}(u_{\mathbf{k}}, v_{\mathbf{k}})$ has no physical effect, we can choose all $u_{\mathbf{k}}$ to be real.

As a consequence of the number conservation, we can find that the transformation $v_{\mathbf{k}} \rightarrow e^{i\phi}v_{\mathbf{k}}$, where ϕ is independent of \mathbf{k} , has no physical effects either. To see this, let us define

$$\Psi_{\text{BCS}}(\phi) = \prod_{\mathbf{k}} \left(u_{\mathbf{k}} + e^{i\phi} v_{\mathbf{k}} a_{\mathbf{k},\uparrow}^{\dagger} a_{-\mathbf{k},\downarrow}^{\dagger} \right) |\text{vac}\rangle. \quad (1.19)$$

From this, we can easily check that $\frac{\partial}{\partial\phi}\Psi_{\text{BCS}}(\phi) = i\hat{N}\Psi_{\text{BCS}}(\phi)$. When we define

$$\langle \hat{A} \rangle_{\phi} = \Psi_{\text{BCS}}^{\dagger}(\phi) \hat{A} \Psi_{\text{BCS}}(\phi), \quad (1.20)$$

where \hat{A} is a physical (hence number-conserving) operator, we can see that this expectation value does not depend on the phase ϕ :

$$\frac{d}{d\phi} \langle \hat{A} \rangle_{\phi} = i \Psi_{\text{BCS}}^{\dagger}(\phi) [\hat{A}, \hat{N}] \Psi_{\text{BCS}}(\phi) = 0. \quad (1.21)$$

We can, therefore, construct the number-conserving many body wave function:

$$\Psi_N = \frac{1}{2\pi} \int_0^{2\pi} d\phi \Psi_{\text{BCS}}(\phi) e^{-i\phi \frac{N}{2}}. \quad (1.22)$$

1.2.3 Pair wave function

Let us discuss the relative wave function of a Cooper pair. In the BCS theory, the pair wave function at $T = 0$ is expressed as

$$F_{\mathbf{k}} = u_{\mathbf{k}} v_{\mathbf{k}}, \quad (1.23)$$

or as its Fourier transformation $F(\mathbf{r}) = \sum_{\mathbf{k}} F_{\mathbf{k}} e^{i\mathbf{k}\mathbf{r}}$.

The physical meaning of the pair wave function becomes clearer if we evaluate the expectation value of the potential energy $\langle \hat{V} \rangle$:

$$\langle \hat{V} \rangle = \frac{1}{2} \sum_{\substack{\mathbf{p}\mathbf{p}'\mathbf{q} \\ \sigma\sigma'}} V_{\mathbf{p}\mathbf{p}'\mathbf{q}} \langle a_{\mathbf{p}+\mathbf{q}/2,\sigma}^{\dagger} a_{\mathbf{p}'-\mathbf{q}/2,\sigma'}^{\dagger} a_{\mathbf{p}'+\mathbf{q}/2,\sigma'} a_{\mathbf{p}-\mathbf{q}/2,\sigma} \rangle. \quad (1.24)$$

For the BCS wave function, only three types of terms contribute to the expectation value: the Hartree term ($\mathbf{q} = 0$), the Fock term ($\sigma = \sigma', \mathbf{p} = \mathbf{p}'$), and the pairing term ($\mathbf{p} + \frac{\mathbf{q}}{2} = -(\mathbf{p}' - \frac{\mathbf{q}}{2}), \sigma = -\sigma'$). The Hartree term can be evaluated as

$$\langle \hat{V} \rangle_{\text{Hartree}} = \frac{1}{2} \sum_{\substack{\mathbf{p}\mathbf{p}' \\ \sigma\sigma'}} V_{\mathbf{p}\mathbf{p}'\mathbf{0}} \langle n_{\mathbf{p}\sigma} n_{\mathbf{p}'\sigma'} \rangle. \quad (1.25)$$

Especially, for the case of the local potential $V = V(\mathbf{r})$, the Hartree term $\langle \hat{V} \rangle_{\text{Hartree}}$ becomes a constant $\frac{1}{2}V(\mathbf{q} = 0)\langle \hat{N}^2 \rangle$.

The Fock term, corresponding to $\sigma = \sigma', \mathbf{p} = \mathbf{p}'$, is given by

$$\langle \hat{V} \rangle_{\text{Fock}} = -\frac{1}{2} \sum_{\mathbf{p}\mathbf{q}\sigma} V_{\mathbf{p}\mathbf{p}\mathbf{q}} \langle n_{\mathbf{p}+\mathbf{q}/2, \sigma} n_{\mathbf{p}-\mathbf{q}/2, \sigma} \rangle = -\frac{1}{2} \sum_{\mathbf{p}\mathbf{q}} |v_{\mathbf{p}+\mathbf{q}/2}|^2 |v_{\mathbf{p}-\mathbf{q}/2}|^2. \quad (1.26)$$

The last equality is a consequence of the uncorrelated nature of the BCS wave function, and it can be easily checked by a direct calculation.

Finally we evaluate the pairing term. For convenience, we introduce the following variables: $\mathbf{k} = \mathbf{p} + \mathbf{q}/2$ and $\mathbf{k}' = \mathbf{p} - \mathbf{q}/2$. Then, we have

$$\langle \hat{V} \rangle_{\text{pair}} = \frac{1}{2} \sum_{\mathbf{k}, \mathbf{k}'} V_{\mathbf{k}\mathbf{k}'} \langle a_{\mathbf{k}', \sigma}^\dagger a_{-\mathbf{k}', -\sigma'}^\dagger a_{-\mathbf{k}, -\sigma} a_{\mathbf{k}, \sigma} \rangle, \quad (1.27)$$

where $V_{\mathbf{k}\mathbf{k}'} = V_{\mathbf{k}+\mathbf{q}/2, \mathbf{k}'-\mathbf{q}/2, \mathbf{k}-\mathbf{k}'}$, which is $V(\mathbf{k} - \mathbf{k}')$ for a local potential $V(\mathbf{r})$. Again using the factorizable nature of the BCS wave function except for the $\mathcal{O}(1/N)$ contributions, this reduces to

$$\begin{aligned} \langle \hat{V} \rangle_{\text{pair}} &= \frac{1}{2} \sum_{\mathbf{k}\mathbf{k}'\sigma} V_{\mathbf{k}\mathbf{k}'} \langle a_{\mathbf{k}', \sigma}^\dagger a_{-\mathbf{k}', -\sigma'}^\dagger \rangle \langle a_{-\mathbf{k}, -\sigma} a_{\mathbf{k}, \sigma} \rangle \\ &= \frac{1}{2} \sum_{\mathbf{k}\mathbf{k}'\sigma} V_{\mathbf{k}\mathbf{k}'} \langle a_{\mathbf{k}'\uparrow}^\dagger a_{-\mathbf{k}'\downarrow}^\dagger \rangle \langle a_{-\mathbf{k}\downarrow} a_{\mathbf{k}\uparrow} \rangle. \end{aligned} \quad (1.28)$$

At last, we have used the spin-singlet nature of the BCS wave function. We can find by an explicit calculation that

$$\langle a_{-\mathbf{k}\downarrow} a_{\mathbf{k}\uparrow} \rangle = u_{\mathbf{k}}^* v_{\mathbf{k}} \langle 00 | a_{-\mathbf{k}\downarrow} a_{\mathbf{k}\uparrow} | 11 \rangle = u_{\mathbf{k}} v_{\mathbf{k}} = F_{\mathbf{k}}. \quad (1.29)$$

Similarly, we can obtain that $\langle a_{\mathbf{k}\uparrow}^\dagger a_{-\mathbf{k}\downarrow}^\dagger \rangle = u_{\mathbf{k}} v_{\mathbf{k}}^* = F_{\mathbf{k}}^*$. Hence, the pairing interaction is

$$\langle \hat{V} \rangle_{\text{pair}} = \sum_{\mathbf{k}\mathbf{k}'} V_{\mathbf{k}\mathbf{k}'} F_{\mathbf{k}} F_{\mathbf{k}'}^*. \quad (1.30)$$

In the case of a local potential $V(\mathbf{r})$, we can rewrite this in terms of the Fourier component of $F(\mathbf{r})$:

$$\langle \hat{V} \rangle_{\text{pair}} = \int d^3\mathbf{r} V(\mathbf{r}) |F(\mathbf{r})|^2. \quad (1.31)$$

The comparison of this result with the interaction between two particles in free space $\langle \hat{V} \rangle = \int d^3\mathbf{r} V(\mathbf{r}) |\Psi(\mathbf{r})|^2$ tells us that $F(\mathbf{r})$ essentially works as the relative wave function $\Psi(\mathbf{r})$ of the pair in the superfluid Fermi system. It is a much simpler quantity to deal with than the quantity $\phi(\mathbf{r})$, which appears in the N -conserving formalism.

We do not yet know the specific form of u 's and v 's in the ground state, and we cannot calculate the form of $F(\mathbf{r})$ now. We, however, anticipate that it will be bound in relative space and that we will be able to define a ‘‘pair radius’’ by the quantity

$$\xi_{\text{PR}}^2 = \frac{\int d^3\mathbf{r} |F(\mathbf{r})|^2 |\mathbf{r}|^2}{\int d^3\mathbf{r} |F(\mathbf{r})|^2}. \quad (1.32)$$

It cannot be too strongly emphasized that everything above is very general and true whether or not the state we are considering is actually the ground state.

1.2.4 Quantitative development of the BCS theory

We consider a fully condensed BCS state described by the N -nonconserving wave function:

$$\Psi = \prod_{\mathbf{k}} \Phi_{\mathbf{k}}, \quad \Phi_{\mathbf{k}} \equiv u_{\mathbf{k}} |00\rangle_{\mathbf{k}} + v_{\mathbf{k}} |11\rangle_{\mathbf{k}}. \quad (1.33)$$

From the normalization condition, $u_{\mathbf{k}}$ and $v_{\mathbf{k}}$ should satisfy the following relation:

$$|u_{\mathbf{k}}|^2 + |v_{\mathbf{k}}|^2 = 1. \quad (1.34)$$

The values of $u_{\mathbf{k}}, v_{\mathbf{k}}$ are determined by minimizing the free energy:

$$\langle \hat{H} \rangle = \langle \hat{T} - \mu \hat{N} + \hat{V} \rangle. \quad (1.35)$$

Let us neglect² the Fock term in $\langle \hat{V} \rangle$ unless mentioned otherwise (we have already seen below Eq. (1.25) that the Hartree term contributes only a constant for the local potential case). Then, the contribution of $\langle \hat{V} \rangle$ comes only from the pairing terms

$$\langle \hat{V} \rangle = \sum_{\mathbf{k}, \mathbf{k}'} V_{\mathbf{k}\mathbf{k}'} F_{\mathbf{k}} F_{\mathbf{k}'}^*, \quad F_{\mathbf{k}} \equiv u_{\mathbf{k}} v_{\mathbf{k}}. \quad (1.36)$$

Here, $V_{\mathbf{k}\mathbf{k}'}$ is a matrix element for the process where fermions change the state from $(\mathbf{k} \downarrow, -\mathbf{k} \uparrow)$ to $(\mathbf{k}' \uparrow, \mathbf{k}' \downarrow)$. Let us consider the term

$$\hat{T} - \mu \hat{N} = \sum_{\mathbf{k}, \sigma} \hat{n}_{\mathbf{k}\sigma} (\xi_{\mathbf{k}} - \mu) \equiv \sum_{\mathbf{k}, \sigma} \hat{n}_{\mathbf{k}\sigma} \varepsilon_{\mathbf{k}}. \quad (1.37)$$

It is clear that $|00\rangle_{\mathbf{k}}$ and $|11\rangle_{\mathbf{k}}$ are eigenstates of $\hat{n}_{\mathbf{k}\sigma}$ with their eigenvalues 0 and 2, respectively. Taking the sum of the spins, we find

$$\langle \hat{T} - \mu \hat{N} \rangle = 2 \sum_{\mathbf{k}} \varepsilon_{\mathbf{k}} |v_{\mathbf{k}}|^2, \quad (1.38)$$

and therefore we obtain

$$\langle \hat{H} \rangle = 2 \sum_{\mathbf{k}} \varepsilon_{\mathbf{k}} |v_{\mathbf{k}}|^2 + \sum_{\mathbf{k}, \mathbf{k}'} V_{\mathbf{k}\mathbf{k}'} (u_{\mathbf{k}} v_{\mathbf{k}}) (u_{\mathbf{k}'} v_{\mathbf{k}'}^*). \quad (1.39)$$

This $\langle \hat{H} \rangle$ must be minimized under the constraint $|u_{\mathbf{k}}|^2 + |v_{\mathbf{k}}|^2 = 1$.

We introduce a pretty way of visualizing the problem. Let us put

$$u_{\mathbf{k}} (= \text{real}) = \cos \frac{\theta_{\mathbf{k}}}{2}, \quad v_{\mathbf{k}} = \sin \frac{\theta_{\mathbf{k}}}{2} \exp i \phi_{\mathbf{k}}, \quad (1.40)$$

and rewrite the Hamiltonian as

$$\langle \hat{H} \rangle = \sum_{\mathbf{k}} (-\varepsilon_{\mathbf{k}} \cos \theta_{\mathbf{k}}) + \frac{1}{4} \sum_{\mathbf{k}, \mathbf{k}'} V_{\mathbf{k}\mathbf{k}'} \sin \theta_{\mathbf{k}} \sin \theta_{\mathbf{k}'} \cos(\phi_{\mathbf{k}} - \phi_{\mathbf{k}'}) + \sum_{\mathbf{k}} \varepsilon_{\mathbf{k}}. \quad (1.41)$$

²In fact, we can show that the Fock term has little effects. We will consider this effect later.

The last term is a mere constant, so that we can neglect it. Next, we introduce the Anderson pseudospin representation of the BCS Hamiltonian. We introduce a unit vector $\sigma_{\mathbf{k}}$ with its polar angle given by $(\theta_{\mathbf{k}}, \phi_{\mathbf{k}})$:

$$\begin{aligned}\sin\theta_{\mathbf{k}}\cos\phi_{\mathbf{k}} &= \sigma_{x\mathbf{k}}, \\ \sin\theta_{\mathbf{k}}\sin\phi_{\mathbf{k}} &= \sigma_{y\mathbf{k}}, \\ \cos\theta_{\mathbf{k}} &= \sigma_{z\mathbf{k}}.\end{aligned}\tag{1.42}$$

With this representation, the expectation value is rewritten as

$$\langle \hat{H} \rangle = - \sum_{\mathbf{k}} \varepsilon_{\mathbf{k}} \sigma_{z\mathbf{k}} + \frac{1}{4} \sum_{\mathbf{k}, \mathbf{k}'} V_{\mathbf{k}\mathbf{k}'} \sigma_{\mathbf{k}\perp} \cdot \sigma_{\mathbf{k}'\perp} = - \sum_{\mathbf{k}} \sigma_{\mathbf{k}} \cdot \mathcal{H}_{\mathbf{k}},\tag{1.43}$$

where $\sigma_{\mathbf{k}\perp}$ is the xy -component of $\sigma_{\mathbf{k}}$, and the pseudo-magnetic field $\mathcal{H}_{\mathbf{k}}$ is defined as

$$\mathcal{H}_{\mathbf{k}} \equiv -\varepsilon_{\mathbf{k}} \hat{z} - \Delta_{\mathbf{k}},\tag{1.44}$$

$$\Delta_{\mathbf{k}} \equiv -\frac{1}{2} \sum_{\mathbf{k}'} V_{\mathbf{k}\mathbf{k}'} \sigma_{\mathbf{k}'\perp}.\tag{1.45}$$

Thus, the z -component of $\mathcal{H}_{\mathbf{k}}$ gives the kinetic energy, while the xy -component is the potential energy (see Fig. 1.1).

It is actually very convenient to represent $\Delta_{\mathbf{k}}$ and $\sigma_{\mathbf{k}\perp}$ as complex numbers $\Delta_{\mathbf{k}} \equiv \Delta_{kx} + i\Delta_{ky}$, $\sigma_{\mathbf{k}\perp} \equiv \sigma_{kx} + i\sigma_{ky}$ rather than representing them as vectors. Evidently, the magnitude of the field $\mathcal{H}_{\mathbf{k}}$ is

$$|\mathcal{H}_{\mathbf{k}}| = (\varepsilon_{\mathbf{k}}^2 + |\Delta_{\mathbf{k}}|^2)^{1/2} \equiv E_{\mathbf{k}},\tag{1.46}$$

In the ground state the spin $\sigma_{\mathbf{k}}$ lies along the field $\mathcal{H}_{\mathbf{k}}$, giving an energy $-E_{\mathbf{k}}$. If the spin is reversed, this costs $2E_{\mathbf{k}}$ (not $E_{\mathbf{k}}!$). This reversal corresponds to

$$\theta_{\mathbf{k}} \rightarrow \pi - \theta_{\mathbf{k}}, \quad \phi_{\mathbf{k}} \rightarrow \phi_{\mathbf{k}} + \pi,\tag{1.47}$$

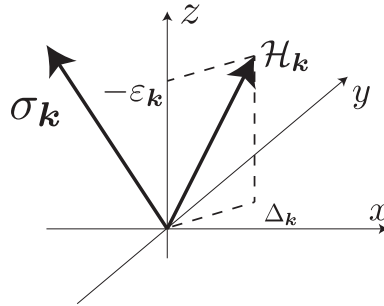


Fig. 1.1. Schematic illustration of the vectors $\mathcal{H}_{\mathbf{k}}$ and $\sigma_{\mathbf{k}}$. At equilibrium, $\mathcal{H}_{\mathbf{k}}$ and $\sigma_{\mathbf{k}}$ should point the same direction.

and

$$\begin{aligned} u_{\mathbf{k}} &\rightarrow \sin \frac{\theta_{\mathbf{k}}}{2} \exp(-i\phi_{\mathbf{k}}) = v_{\mathbf{k}}^*, \\ v_{\mathbf{k}} &\rightarrow -\cos \frac{\theta_{\mathbf{k}}}{2} = -u_{\mathbf{k}}. \end{aligned} \quad (1.48)$$

Therefore, the wave function of the excited state generated in this way is

$$\Psi_{\mathbf{k}}^{\text{EP}} = v_{\mathbf{k}}^* |00\rangle - u_{\mathbf{k}} |11\rangle, \quad (1.49)$$

We can easily verify that this excited state is orthogonal to the ground state $\Phi_{\mathbf{k}} \equiv u_{\mathbf{k}} |00\rangle + v_{\mathbf{k}} |11\rangle$ (remember we take $u_{\mathbf{k}}$ to be real).

Let us derive the BCS gap equation. Since the vector $\sigma_{\mathbf{k}}$ must point along the field $\mathcal{H}_{\mathbf{k}}$ in the ground state, this gives a set of self-consistent conditions for $\Delta_{\mathbf{k}}$; since $\sigma_{\mathbf{k}'\perp} = -\Delta_{\mathbf{k}'}/E_{\mathbf{k}'}$, we have

$$\Delta_{\mathbf{k}} = - \sum_{\mathbf{k}'} V_{\mathbf{k}\mathbf{k}'} \frac{\Delta_{\mathbf{k}'}}{2E_{\mathbf{k}'}}. \quad (1.50)$$

This is the BCS gap equation. Note that the above derivation is quite general. In particular, we have never assumed the s -wave state (though we did assume the spin-singlet pairing).

Let us also introduce an alternative derivation of the BCS gap equation. We simply parametrize $u_{\mathbf{k}}$ and $v_{\mathbf{k}}$ by $\Delta_{\mathbf{k}}$ and $E_{\mathbf{k}}$ as

$$u_{\mathbf{k}} \equiv \frac{E_{\mathbf{k}} + \varepsilon_{\mathbf{k}}}{\sqrt{|\Delta_{\mathbf{k}}|^2 + (E_{\mathbf{k}} + \varepsilon_{\mathbf{k}})^2}}, \quad (1.51)$$

$$v_{\mathbf{k}} \equiv \frac{\Delta_{\mathbf{k}}}{\sqrt{|\Delta_{\mathbf{k}}|^2 + (E_{\mathbf{k}} + \varepsilon_{\mathbf{k}})^2}}. \quad (1.52)$$

This clearly satisfies the normalization condition $|u_{\mathbf{k}}|^2 + |v_{\mathbf{k}}|^2 = 1$, and gives

$$|u_{\mathbf{k}}|^2 = \frac{1}{2} \left[1 + \frac{\varepsilon_{\mathbf{k}}}{E_{\mathbf{k}}} \right], \quad |v_{\mathbf{k}}|^2 = \frac{1}{2} \left[1 - \frac{\varepsilon_{\mathbf{k}}}{E_{\mathbf{k}}} \right], \quad u_{\mathbf{k}} v_{\mathbf{k}} = \frac{\Delta_{\mathbf{k}}}{2E_{\mathbf{k}}}. \quad (1.53)$$

The BCS ground state energy can therefore be written in the form

$$\langle \hat{H} \rangle = \sum_{\mathbf{k}} \varepsilon_{\mathbf{k}} \left(1 - \frac{\varepsilon_{\mathbf{k}}}{E_{\mathbf{k}}} \right) + \sum_{\mathbf{k}\mathbf{k}'} V_{\mathbf{k}\mathbf{k}'} \frac{\Delta_{\mathbf{k}}}{2E_{\mathbf{k}}} \frac{\Delta_{\mathbf{k}'}}{2E_{\mathbf{k}'}}. \quad (1.54)$$

Here, $\Delta_{\mathbf{k}}$ for each \mathbf{k} are independent variational parameters. By using $\partial E_{\mathbf{k}}/\partial \Delta_{\mathbf{k}} = \Delta_{\mathbf{k}}^*/E_{\mathbf{k}}$, we find

$$\frac{\varepsilon_{\mathbf{k}}^2}{E_{\mathbf{k}}^3} \left[\Delta_{\mathbf{k}}^* - \sum_{\mathbf{k}'} V_{\mathbf{k}\mathbf{k}'} \frac{\Delta_{\mathbf{k}'}}{2E_{\mathbf{k}'}} \right] = 0, \quad (1.55)$$

so that we again obtain the standard gap equation.

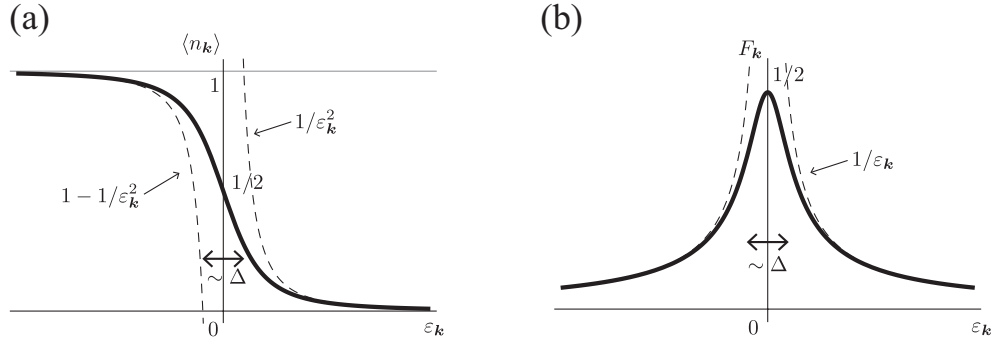


Fig. 1.2. (a) The number distribution and (b) the pair wave function for the BCS ground state.

For the s -wave state, $\Delta_{\mathbf{k}}$ is independent of the direction of \mathbf{k} and depends only on its magnitude $|\mathbf{k}|$. Let us expect that, as in most cases of interests, $\Delta_{\mathbf{k}}$ is approximately a constant Δ over a wide range of energy $\varepsilon \gg \Delta$. Then, we obtain

$$\langle n_{\mathbf{k}} \rangle = |v_{\mathbf{k}}|^2 = \frac{1}{2} \left(1 - \frac{\varepsilon_{\mathbf{k}}}{\sqrt{\varepsilon_{\mathbf{k}}^2 + |\Delta|^2}} \right), \quad (1.56)$$

and

$$F_{\mathbf{k}} = u_{\mathbf{k}}v_{\mathbf{k}} = \frac{\Delta}{2E_{\mathbf{k}}}. \quad (1.57)$$

The behavior of $\langle n_{\mathbf{k}} \rangle$ and $F_{\mathbf{k}}$ are illustrated in Fig. 1.2: $\langle n_{\mathbf{k}} \rangle$ behaves qualitatively similarly to the normal-state at $T = T_c$, but falls off very slowly $\approx \varepsilon^{-2}$, rather than exponentially. On the other hand, $F_{\mathbf{k}}$ falls off as $|\varepsilon|^{-1}$ for large ε .

1.3 BCS theory at finite temperature

1.3.1 Derivation of the gap equation

To generalize the BCS theory to a finite temperature, we have to use the density matrix formalism. An obvious way is to assume that the many-body density matrix can be written in a product form just like the ground state wave function:

$$\hat{\rho} = \prod_{\mathbf{k}} \rho_{\mathbf{k}}. \quad (1.58)$$

Here, each Hilbert space labeled by \mathbf{k} is spanned by the following four states:

$$\Psi_{\text{GP}} = u_{\mathbf{k}} |00\rangle + v_{\mathbf{k}} |11\rangle : \text{“Ground pair states”} ; \quad (1.59)$$

$$\Psi_{\text{EP}} = v_{\mathbf{k}}^* |00\rangle - u_{\mathbf{k}} |11\rangle : \text{“Excited pair states”} ; \quad (1.60)$$

$$\Psi_{\text{BP}}^{(1)} = |10\rangle \quad \Psi_{\text{BP}}^{(2)} = |01\rangle : \text{“Broken pair states”} . \quad (1.61)$$

As regards the first two states, they can be parametrized by the Anderson variables $\theta_{\mathbf{k}}$ and $\phi_{\mathbf{k}}$. The difference from $T = 0$ is that there is a finite probability $P_{\text{EP}}^{(\mathbf{k})}$ for a given “spin” $\sigma_{\mathbf{k}}$ to be reversed, i.e., the pair is in the Ψ_{EP} state rather than the Ψ_{GP} state. There is also finite probability, $P_{\text{BP}}^{(\mathbf{k},1)}$ and $P_{\text{BP}}^{(\mathbf{k},2)}$, that the pair is a broken-pair state. As to the broken-pair states, they clearly do not contribute to $\langle \hat{V} \rangle$ and thus do not to the effective field. Thus, we can go through the argument as above and obtain the result

$$\Delta_{\mathbf{k}} = -\frac{1}{2} \sum_{\mathbf{k}'} V_{\mathbf{k},\mathbf{k}'} \langle \sigma_{\perp \mathbf{k}'} \rangle, \quad (1.62)$$

where $\langle \sigma_{\perp \mathbf{k}'} \rangle$ is now given as

$$\langle \sigma_{\perp \mathbf{k}'} \rangle = \left(P_{\text{GP}}^{(\mathbf{k}')} - P_{\text{EP}}^{(\mathbf{k}')} \right) \frac{\Delta_{\mathbf{k}'}}{E_{\mathbf{k}'}}. \quad (1.63)$$

Therefore, the gap equation becomes

$$\Delta_{\mathbf{k}} = - \sum_{\mathbf{k}'} V_{\mathbf{k},\mathbf{k}'} \left(P_{\text{GP}}^{(\mathbf{k}')} - P_{\text{EP}}^{(\mathbf{k}')} \right) \frac{\Delta_{\mathbf{k}'}}{2E_{\mathbf{k}'}}. \quad (1.64)$$

We therefore need to calculate the quantities $P_{\text{GP}}^{(\mathbf{k})}$ and $P_{\text{EP}}^{(\mathbf{k})}$ ³. This is simply given by the canonical distribution⁴

$$P_{\text{GP}}^{(\mathbf{k})} : P_{\text{BP}}^{(\mathbf{k})} : P_{\text{EP}}^{(\mathbf{k})} = \exp(-\beta E_{\text{GP}}) : \exp(-\beta E_{\text{BP}}) : \exp(-\beta E_{\text{EP}}). \quad (1.65)$$

As we already noted in the discussion below Eq. (1.46), the energy difference between the ground pair and excited pair states is $E_{\text{EP}} - E_{\text{GP}} = 2E_{\mathbf{k}}$ ⁵. What is $E_{\text{BP}} - E_{\text{GP}}$? Here, a special care should be paid. If all energies are taken relative to the normal-state Fermi sea, then evidently the energy of the “broken pair” states $|01\rangle$ and $|10\rangle$ is $\varepsilon_{\mathbf{k}}$ (which can be negative!). In writing down the Anderson pseudospin Hamiltonian, we omitted the constant term $\sum_{\mathbf{k}} \varepsilon_{\mathbf{k}}$. Hence, the energy of the GP state relative to the normal Fermi sea is not $-E_{\mathbf{k}}$, but $\varepsilon_{\mathbf{k}} - E_{\mathbf{k}}$. Thus, we have

$$E_{\text{BP}} - E_{\text{GP}} = E_{\mathbf{k}}, \quad (1.66)$$

$$E_{\text{EP}} - E_{\text{GP}} = 2E_{\mathbf{k}}. \quad (1.67)$$

The broken-pair states can be regarded as states with one quasi-particle, the excited pair state as one with two quasi-particles.

From Eqs. (1.66) and (1.67), we obtain

$$P_{\text{EP}}^{(\mathbf{k})} - P_{\text{GP}}^{(\mathbf{k})} = \frac{1 + \exp(-\beta E_{\mathbf{k}})}{1 + 2 \exp(-\beta E_{\mathbf{k}}) + \exp(-2\beta E_{\mathbf{k}})} = \tanh\left(\frac{\beta E_{\mathbf{k}}}{2}\right), \quad (1.68)$$

³Since the states $|10\rangle$ and $|01\rangle$ are degenerate, we can calculate $P_{\text{BP}}^{(\mathbf{k})}$ immediately from these quantities and from $P_{\text{GP}}^{(\mathbf{k})} + P_{\text{EP}}^{(\mathbf{k})} + 2P_{\text{BP}}^{(\mathbf{k})} = 1$.

⁴Since we are talking about different occupation states, Fermi/Bose statistics are irrelevant, and the probability of a given state with its energy E is simply proportional to $\exp(-\beta E)$.

⁵Note that $E_{\mathbf{k}}$ here is temperature dependent!

and can derive the gap equation:

$$\Delta_{\mathbf{k}} = - \sum_{\mathbf{k}'} V_{\mathbf{k},\mathbf{k}'} \frac{\Delta_{\mathbf{k}'}}{2E_{\mathbf{k}'}} \tanh\left(\frac{\beta E_{\mathbf{k}'}}{2}\right). \quad (1.69)$$

Note that this gap equation can also be derived in a brute force manner: by minimizing the the free energy $F(\Delta_{\mathbf{k}})$ with respect to $\Delta_{\mathbf{k}}$ (see appendix 5D of Ref. [1]).

1.3.2 $F_{\mathbf{k}}$ at finite temperature

As for $\langle \sigma_{\perp \mathbf{k}} \rangle$, if we recall the definition $\langle \sigma_{\perp \mathbf{k}} \rangle \equiv \langle a_{-\mathbf{k}\downarrow} a_{\mathbf{k}\uparrow} \rangle$, we can easily see that the broken pair states do not contribute to this quantity. Recalling that the EP and GP states have the opposite direction in the Anderson pseudospin representation, and that the magnitude of its xy -component is $\Delta_{\mathbf{k}}/2E_{\mathbf{k}}$, we obtain

$$\langle \sigma_{\perp \mathbf{k}} \rangle = F_{\mathbf{k}} = \left(P_{\text{GP}}^{(\mathbf{k})} - P_{\text{EP}}^{(\mathbf{k})} \right) \frac{\Delta_{\mathbf{k}}}{2E_{\mathbf{k}}} = \frac{\Delta_{\mathbf{k}}}{2E_{\mathbf{k}}} \tanh\left(\frac{\beta E_{\mathbf{k}}}{2}\right). \quad (1.70)$$

Thus, the pair wave function is also reduced by a factor of $\tanh\left(\frac{\beta E_{\mathbf{k}}}{2}\right)$ from the ground state⁶.

1.3.3 $\langle n_{\mathbf{k}} \rangle$ at finite temperature

By using Eqs. (1.59) to (1.61) and recalling that $n_{\mathbf{k}} - \frac{1}{2}$ is zero for the BP states, we obtain

$$\langle n_{\mathbf{k}} \rangle - \frac{1}{2} = (|v_{\mathbf{k}}|^2 - |u_{\mathbf{k}}|^2) P_{\text{GP}}^{(\mathbf{k})} + (|u_{\mathbf{k}}|^2 - |v_{\mathbf{k}}|^2) P_{\text{EP}}^{(\mathbf{k})} = -\frac{\varepsilon_{\mathbf{k}}}{E_{\mathbf{k}}} \tanh\left(\frac{\beta E_{\mathbf{k}}}{2}\right). \quad (1.71)$$

By introducing the occupation number of the ideal Fermi gas $\langle n_{\mathbf{k}} \rangle_0 = \theta(k_F - |\mathbf{k}|)$, we find

$$\langle n_{\mathbf{k}} \rangle - \langle n_{\mathbf{k}} \rangle_0 = \left[\frac{1}{2} - \frac{|\varepsilon_{\mathbf{k}}|}{E_{\mathbf{k}}} \tanh\left(\frac{\beta E_{\mathbf{k}}}{2}\right) \right] \text{sgn}(\varepsilon_{\mathbf{k}}). \quad (1.72)$$

From this, we can see that the occupation number will reduce to that for the normal Fermi gas as $T \rightarrow T_c$ and $\Delta \rightarrow 0$.

1.3.4 Properties of the BCS gap equation

We can immediately see that the BCS gap equation always has a trivial solution $\Delta_{\mathbf{k}} = 0$ regardless of the form of the potential $V_{\mathbf{k}\mathbf{k}'}$, which corresponds to the normal state. Thus, we concentrate only on nontrivial solutions, which, as we shall see soon, depend significantly on the form of the potential $V_{\mathbf{k}\mathbf{k}'}$ and the temperature T .

⁶Note that the value itself is far more reduced than this factor, since the value of gap $\Delta_{\mathbf{k}}$ decreases from its ground state value as the temperature is raised.

We can find two rather simple cases where no nontrivial solution exists. One is when all Legendre components V_ℓ of $V_{\mathbf{k}\mathbf{k}'}$ are non-negative; see Sec. 2.4. The other case is the high temperature limit $T \rightarrow \infty$. In this limit, the right-hand side of the BCS gap equation (1.50) reduces to

$$\sum_{\mathbf{k}'} V_{\mathbf{k}\mathbf{k}'} \frac{\Delta_{\mathbf{k}'}}{2E_{\mathbf{k}'}} \frac{\beta E_{\mathbf{k}'}}{2} = \frac{1}{4k_B T} \sum_{\mathbf{k}'} V_{\mathbf{k}\mathbf{k}'} \Delta_{\mathbf{k}'}. \quad (1.73)$$

For the existence of the nontrivial solution, the potential $-V_{\mathbf{k}\mathbf{k}'}$ should have the eigenvalue $4k_B T$, which is impossible in the high-temperature limit. Thus, there is no nontrivial solution in the limit $T \rightarrow \infty$. We can also conclude that if there is a nontrivial solution at $T = 0$, there must exist a critical temperature T_c at which this solution vanishes.

So far, we have considered the general features of the BCS theory, but in order to obtain further insights, we confine ourselves to the case of the original BCS form, where we approximate the potential as $V_{\mathbf{k}\mathbf{k}'} \simeq V_o$ with an energy cutoff ε_c around the Fermi surface. Let us introduce the density of states at the Fermi surface by $N(0) = \frac{1}{2} \left. \frac{dn}{d\varepsilon} \right|_{\varepsilon=\varepsilon_F}$.

With the replacement $\sum_{\mathbf{k}} \rightarrow N(0) \int d\varepsilon$, we have

$$\lambda^{-1} = \int_{-\varepsilon_c}^{\varepsilon_c} \frac{\tanh \beta E/2}{2E} d\varepsilon = \int_0^{\varepsilon_c} \frac{\tanh \beta E/2}{E} d\varepsilon \quad (1.74)$$

with $\lambda = -N(0)V_o$. It is obvious that nontrivial solutions do not exist for $V_o > 0$, as already remarked. We therefore consider the case $V_o < 0$ below.

At first, we calculate the critical temperature T_c . Put $\beta = \beta_c$, then Δ goes to zero and $E \rightarrow |\varepsilon|$:

$$\lambda^{-1} = \int_0^{\varepsilon_c} d\varepsilon \frac{\tanh(\beta_c \varepsilon/2)}{\varepsilon} = \ln(1.14\beta_c \varepsilon). \quad (1.75)$$

Thus the critical temperature T_c is given by

$$k_B T_c = 1.14\varepsilon_c \exp(-\lambda^{-1}) = 1.14\varepsilon_c \exp\left(-\frac{1}{N(0)|V_o|}\right). \quad (1.76)$$

This expression does not depend on the choice of the cutoff ε_c because the renormalized potential $|V_o| \sim \text{const.} + \ln \varepsilon_c$ ⁷ cancels its dependence. Therefore, it is plausible to set the value of the energy cutoff to be $\varepsilon_c \sim \omega_D$ as in the original BCS paper. By recalling that the Debye frequency depends on the mass of the ions M as $\omega_D \sim M^{-1/2}$, this predicts $T_c \sim M^{-1/2}$, which explains the isotope effect. It also ensures the self-consistency of the above calculations: we focus on the energy region close to the Fermi surface, which can be seen to be true since it is known experimentally that the transition temperature scales as $T_c \ll \omega_c$.

⁷In the renormalization group analysis, the four-Fermi coupling turns out to obey the flow $V(\varepsilon) = \frac{V}{1+N(0)V \ln(\varepsilon_c/\varepsilon)}$, where ε is the characteristic energy scale of the system, and V is the bare coupling constant.

At zero temperature, the gap equation reads

$$\lambda^{-1} = \int_0^{\varepsilon_c} \frac{d\varepsilon}{\sqrt{\varepsilon^2 + |\Delta(0)|^2}} \simeq \ln \frac{2\varepsilon_c}{\Delta(0)}. \quad (1.77)$$

Then, we can find the ratio between the energy gap and the transition temperature as follows

$$\frac{\Delta(0)}{T_c} = 1.76. \quad (1.78)$$

Note that this ratio is a universal constant independent of the detail of the materials. Since $\Delta(0)$ can be measured by tunneling experiments, we can confirm this relation experimentally. This relation usually works quite well for weak coupling superconductors, while the ratio becomes usually somewhat larger than 1.76 for “strong-coupling” superconductors, where T_c/ω_c is not very small.

At finite temperature $T < T_c$, the gap equation can be written as

$$\int_0^{\infty} d\varepsilon \left[\frac{\tanh(\beta E(T))}{E(T)} - \frac{\tanh(\beta_c \varepsilon)}{\varepsilon} \right] = 0. \quad (1.79)$$

Since this integral converges, we can extend ε_c to $\varepsilon_c \rightarrow \infty$. Then, we can easily see that the energy gap should be written as

$$\Delta(T) = T_c f(T/T_c), \quad (1.80)$$

or equivalently,

$$\frac{\Delta(T)}{\Delta(0)} = \tilde{f}(T/T_c). \quad (1.81)$$

The temperature dependence of the energy gap is pretty close to the following form⁸

$$\frac{\Delta(T)}{\Delta(0)} = \left[1 - \left(\frac{T}{T_c} \right)^4 \right]^{1/2}. \quad (1.82)$$

On the other hand, near T_c , we can obtain the following result from the gap equation

$$\frac{\Delta(T)}{\Delta(0)} \sim 1.74 \left(1 - \frac{T}{T_c} \right)^{1/2}, \quad (1.83)$$

or equivalently,

$$\frac{\Delta(T)}{T_c} \sim 3.06 \left(1 - \frac{T}{T_c} \right)^{1/2}. \quad (1.84)$$

⁸Before the BCS theory, this temperature dependence of the energy gap was presented theoretically by Casimir and Gorter with a phenomenological two-fluid model, which agrees well with experiments.

1.3.5 Properties of the Fock term

In the calculation above, we have neglected the Fock term

$$\langle H - \mu N \rangle_{\text{Fock}} = -\frac{1}{2} \sum_{\mathbf{k}, \mathbf{k}' \sigma} V_{\mathbf{k}, \mathbf{k}'} \langle n_{\mathbf{k}\sigma} \rangle \langle n_{\mathbf{k}'\sigma} \rangle. \quad (1.85)$$

For a weak coupling *s*-wave superconductor, this is indeed a valid approximation. In fact, if we look at the Fock term we can regard

$$-\sum_{\mathbf{k}'} V_{\mathbf{k}, \mathbf{k}'} \langle n_{\mathbf{k}'\sigma} \rangle \quad (1.86)$$

as a molecular field acting on $n_{\mathbf{k}}$, changing the single particle energy as

$$\varepsilon_{\mathbf{k}} \rightarrow \tilde{\varepsilon}_{\mathbf{k}, \sigma} \equiv \varepsilon_{\mathbf{k}} - \sum_{\mathbf{k}'} V_{\mathbf{k}, \mathbf{k}'} \langle n_{\mathbf{k}'\sigma} \rangle. \quad (1.87)$$

As long as $V_{\mathbf{k}, \mathbf{k}'}$ can be regarded as a constant around the Fermi surface, this molecular field is simplified as

$$V \sum_{\mathbf{k}'} \langle n_{\mathbf{k}'\sigma} \rangle. \quad (1.88)$$

Since the integration range of \mathbf{k}' is far larger than the energy gap, $\sum_{\mathbf{k}'} \langle n_{\mathbf{k}'} \rangle$ can be regarded also as a constant, so that the effect of the Fock term is only to shift the chemical potential.

For an anisotropic case, this molecular field term depends on the angle, so that the effect of the Fock term cannot be absorbed into the chemical potential. However, the effect of the Fock term can be taken into account in a similar way as in Landau's Fermi liquid theory (see Sec. 2.2) as far as $V_{\mathbf{k}, \mathbf{k}'}$ is a constant with respect to $|\mathbf{k}|$.

1.3.6 Pair wave function

The most important quantity characterizing the superconducting phase is the “pair wave function” $F(\mathbf{r}) = \langle \psi_{\downarrow}(\mathbf{r}) \psi_{\uparrow}(0) \rangle$, or its spatial Fourier transform $F_{\mathbf{k}} = \int d\mathbf{r} F(\mathbf{r}) e^{-i\mathbf{k} \cdot \mathbf{r}} = a_{-\mathbf{k}, \downarrow} a_{\mathbf{k}, \uparrow}$. We already saw the physical significance of this quantity in evaluating the expectation value of the interaction term in Eq. (1.30): $F(\mathbf{r})$ behaves as the two-particle wave function. As we will see later, $F(\mathbf{r})$ still behaves as the pair wave function of the Cooper pairs even when we go beyond the BCS theory, and it is essential quantity in the superconducting phase.

At finite temperature, the expression of $F_{\mathbf{k}}$ is modified into

$$F_{\mathbf{k}} = u_{\mathbf{k}} v_{\mathbf{k}} \tanh \left(\frac{\beta E_{\mathbf{k}}}{2} \right) = \frac{\Delta_{\mathbf{k}}}{2E_{\mathbf{k}}} \tanh \left(\frac{\beta E_{\mathbf{k}}}{2} \right), \quad (1.89)$$

so that its spacial dependence is given as

$$F(\mathbf{r}) = \sum_{\mathbf{k}} \frac{\Delta_{\mathbf{k}}}{2E_{\mathbf{k}}} \tanh\left(\frac{\beta E_{\mathbf{k}}}{2}\right) \exp(i\mathbf{k} \cdot \mathbf{r}). \quad (1.90)$$

In the case of the s -wave pairing, $\Delta_{\mathbf{k}}$ and $E_{\mathbf{k}}$ are independent of the direction $\hat{\mathbf{k}}$. Therefore, we can perform the integration over the angle:

$$\sum_{\mathbf{k}} \exp(i\mathbf{k} \cdot \mathbf{r}) = N(0) \int d\varepsilon_k \int \frac{d\Omega_{\mathbf{k}}}{4\pi} \exp(i\mathbf{k} \cdot \mathbf{r}) = N(0) \int d\varepsilon_k \frac{\sin kr}{kr}. \quad (1.91)$$

Therefore, we find $F_{\mathbf{k}}$ for the s -wave pairing as

$$F(\mathbf{r}) = N(0) \int d\varepsilon_k \frac{\sin kr}{kr} \frac{\Delta_k}{2E_k} \tanh\left(\frac{\beta E_k}{2}\right). \quad (1.92)$$

To go further, therefore, let us assume as always the weak coupling limit. Then, we obtain $T_c \ll \varepsilon_F$ and we find $k_F \xi \gg 1$, where $\xi = \hbar v_F / \Delta(0)$ is the healing length. This healing length is of the order of the “pair radius” defined in Eq. (1.32).

One important remark on $F(\mathbf{r})$ is that it is not normalized to unity, but rather one can regard the integral of its squared as the number of Cooper pairs⁹:

$$N_{\text{Cooper}} \equiv \int d^3\mathbf{r} |F(\mathbf{r})|^2 = \sum_{\mathbf{k}} \frac{\Delta_{\mathbf{k}}^2}{4E_{\mathbf{k}}^2} \tanh^2\left(\frac{\beta E_{\mathbf{k}}}{2}\right). \quad (1.93)$$

It is clear that the main contribution to this integral comes from a small energy region $|\varepsilon| \sim \Delta(T) \sim k_B T$. In this region, we can approximate $\Delta_{\mathbf{k}}(T)$ by its value at the Fermi surface, simply denoted by $\Delta(T)$. In this approximation, the total number of Cooper pairs is given by

$$N_{\text{Cooper}} = |\Delta(T)|^2 N(0) \int \frac{d\varepsilon_k}{4E_k^2} \tanh^2\left(\frac{\beta E_k}{2}\right). \quad (1.94)$$

In the limit $T \rightarrow 0$, this must be on the order of $N\Delta(0)/\varepsilon_F$, where N is the total number of the fermions. One can obtain an important insight from this equation: for the old-fashioned BCS superconductors, the number of Cooper pairs is much less than that of the fermions. We can see this point easily by using $\Delta(0)/\varepsilon_F \sim 10^{-4}$. As the temperature is increased, the number of Cooper pairs decreases, and in the limit $T \rightarrow T_c$, we find $N|\Delta(T)|^2/T_c\varepsilon_F$.

Let us discuss general behaviors of the pair wave function $F(\mathbf{r})$. What we can expect is that

1. At short distance $r \ll k_F^{-1}$, some of the above approximations break down, and equations given above are not valid. Since the Coulomb repulsion between the two electrons becomes dominant when the two electrons come close, the pair wave function at short distance behaves as $F(\mathbf{r}) \propto \varphi(\mathbf{r})$, where $\varphi(\mathbf{r})$ is the relative wave function of the two colliding electrons in the free space¹⁰ with $E \sim \varepsilon_F$.

⁹Again, this physical meaning is a much more general property that goes beyond the BCS theory, although the above equation does no longer hold (we will come back this point later).

¹⁰The modification to the Coulomb interaction could be important in some applications.

2. In the intermediate region $k_F^{-1} \ll r \ll \hbar v_F / \Delta(0)$, we can find $F(\mathbf{r}) \propto \varphi_{\text{free}}(r)$, where $\varphi_{\text{free}}(\mathbf{r})$ is the wave function of two freely moving particles with zero center of mass momentum at the Fermi energy.
3. At large distance $r \gg \hbar v_F / \Delta(0)$, $F(\mathbf{r})$ falls off exponentially $F(r) \propto \exp(-r/\xi)$ with $\xi \sim \hbar v_F / \Delta(0)$. Here, the spatial extent of the pair wave function ξ can be shown to be only weakly T -dependent [2].

The bottom lines are that

1. The radius of the Cooper pairs is always of the order of $\hbar v_F / \Delta(0)$, and is very huge compared to the microscopic length scale. Even when we vary the temperature, the size of the pairs does not change significantly, and this point remains to be true.
2. Even at $T = 0$, the number of Cooper pairs N_{Cooper} is far smaller than that of the fermions N . As the temperature increase, N_{Cooper} decreases and finally it vanishes at $T = T_c$.

1.4 Generalization of the BCS theory

Here let us consider the generalization of the previous discussion.

1. From the beginning, we have assumed the Sommerfeld model; thus we have ignored the existence of the crystalline and the Coulomb interaction between the electrons. The periodic potential can be taken into account by replacing the free wave functions in the previous discussions with the Bloch waves

$$\psi_{\mathbf{k},n}(\mathbf{r}) = u_{\mathbf{k},n}(\mathbf{r})e^{i\mathbf{k}\mathbf{r}}. \quad (1.95)$$

2. Next, let us take the Coulomb interaction into consideration. Here, we apply Landau's Fermi liquid theory, and assume that the states of the interacting system can be labeled with those of the non-interacting system under the adiabatic switching of the interaction. Then, the net "polarization" of the states is given by

$$\sum_{|\mathbf{k}|} \langle n_{\mathbf{k},\sigma} \rangle. \quad (1.96)$$

As long as the net polarization remains unchanged across the normal-superfluid phase transition, the molecular field terms do not play any role. Therefore, the only effect of the interaction is to replace the bare mass with the effective mass $m \rightarrow m^*$, leaving the gap equation intact. They do affect, however, the responses to the external fields, just as in the normal state.

3. The Coulomb interaction

$$V_{\text{Coulomb}}(q) = \frac{e^2}{\varepsilon_o q^2} \quad (1.97)$$

is long ranged, so that it is difficult to treat it straightforwardly. However, if we take the screening effect into account, it becomes short ranged, and we can show that it does not have significant effect. In fact, if we use the random-phase approximation (RPA), the effective potential is modified due to the screening as

$$V_{\text{eff}}(q) = \frac{\kappa_o}{1 + q^2/q_{\text{TF}}^2}, \quad (1.98)$$

where κ_o is the static bulk modulus of the non-interacting Fermi gas and q_{TF} is the Thomas-Fermi wave number. Since this is valid only in the static limit, ω should be much smaller than $v_F q$, where v_F is the Fermi velocity. As long as we restrict ourselves to the classical superconductors, this condition is usually satisfied and the above expression can be used safely. If we assume that only the interaction for small q 's is important, the long-range part of the Coulomb interaction merely shifts the strength of the potential, and it has no effect on the gap equation. However, it does affect the responses and the value of T_c .

4. Finally, let us consider the strong coupling case. Generally speaking, this kind of interaction requires much more complicated treatments as Eliashberg has pointed out (see Sec. 4.1.1). However, it provides only fairly small corrections to the naive BCS theory. In fact, the ratio $\Delta(0)/k_B T_c$ can be 2.4 in Hg, and Pb at the largest, while it is about 1.76 in the BCS theory.

References

[1] A. J. Leggett, *Quantum Liquids* (Oxford University Press, New York, NY, USA, 2006).

[2] *Question from a student:* We have defined the pair radius by the effective radius of the pair wave function $F(\mathbf{r})$. Also we know that there is another length scale called the Ginzburg–Landau healing length, which diverges as $T \rightarrow T_c$. What is the difference between these two?

Answer: Thank you. A good question. What we talk about here is effectively the radius of the Cooper pair. So you may think it is the radius of the effective molecule of the Cooper pair, described in their relative coordinate. On the other hand, the Ginzburg–Landau healing length is, crudely speaking, the length which characterizes the behavior of the pair wave function in the bulk. If I consider the pair wave function around the bulk boundary, the pair wave function goes to zero at the wall. When we discuss the Ginzburg–Landau healing length, we are talking about the center of mass coordinate. Suppose that the pair wave functions go to zero at the wall, then it must have an exponential behavior. How long does it take to? The answer is the Ginzburg–Landau healing length.

Another possible interpretation of the Ginzburg–Landau healing length is that it is the length over which the order parameter has to distort such that the bending energy is equal to the bulk condensation energy. According to this criterion, it is not surprising, although not obvious, that the Ginzburg–Landau healing length tends to infinity in the limit $T \rightarrow T_c$.

Lec. 2 Superfluid ^3He : basic description

In this and next sections, we briefly review the ^3He system. First, we deal with a normal phase of ^3He by the famous Landau Fermi liquid theory. Next, we describe the theory of superfluid ^3He , where, unlike the simple BCS theory presented in the previous section, the anisotropy becomes important. Finally, the Ginzburg–Landau theory is formulated for both the singlet and triplet superfluids.

2.1 Introduction

The liquid ^3He has become available since the 1950s. Since it does not exist in nature, most of ^3He people actually use is produced from tritium through the reaction¹ ($^3\text{H} \rightarrow ^3\text{He} + e + \bar{\nu}$). ^3He is an inert atom having the stable electronic state $(1s)^2S_0$ with a huge excitation energy. Therefore, we can regard it as a point particle with a (nuclear) spin $1/2$, obeying the Fermi statistics just as an electron in metals.

The interaction potential between ^3He atoms is showed in Fig. 2.1. At short distance, it has a “hard-core” repulsive region, originating from the Pauli principle between the electrons. At large distance, on the other hand, the van der Waals interaction makes the potential attractive.

For $T \lesssim 100$ mK, the liquid ^3He behaves much like a textbook normal metal. For example, the specific heat C_V , Pauli spin susceptibility χ , viscosity η , spin diffusion constant D_S , and thermal conductivity κ behave as

$$C_V \propto T, \quad \chi = \text{const.}, \quad \eta, D_S \propto T^{-2}, \quad \kappa \propto T^{-1}. \quad (2.1)$$

It turns out, however, that the inter-atomic interaction is rather strong. For example, the spin susceptibility χ is 20 times larger than that for the ideal Fermi gas. How can we justify the above seemingly non-interacting behavior in the presence of such a strong interaction?

¹Recently, there is a shortage of ^3He in order to use it in neutron detectors, and its price is growing.

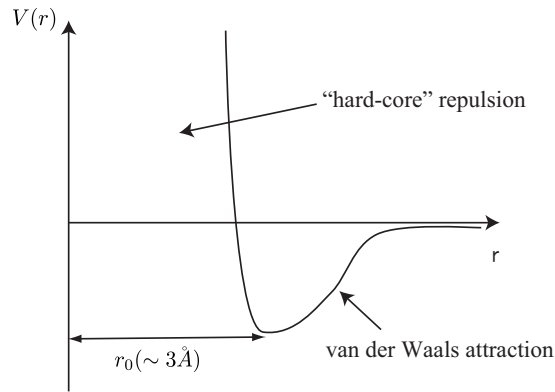


Fig. 2.1. The interaction potential between ${}^3\text{He}$ atoms.

2.2 Landau Fermi liquid theory

A very nice explanation of the normal liquid ${}^3\text{He}$ for $T \lesssim 100$ mK was given by the Landau Fermi Liquid theory. This theory is based on the following qualitative assumption about the behavior of the system: we turn on the interaction adiabatically to the free Fermi gas, and assume that the ground state and all low-energy excited states of the non-interacting system evolve continuously into those of the interacting system. Obviously, we exclude the possibility of any phase transitions in the above adiabatic process, such as the normal liquid-superconductivity phase transition, the disorder-ferromagnetic phase transition and the liquid-crystal phase transition.

The low-energy excited states are labeled by specifying the difference in the occupation number $\delta n(\mathbf{p}\sigma)$ of the state with the momentum \mathbf{p} and the spin σ measured from the ground state. As long as the above assumption holds, we are able to do this even if the interaction is pretty strong. The difference $\delta n(\mathbf{p}\sigma)$ can only take the following values (p_F : the Fermi momentum):

$$\begin{cases} \delta n(\mathbf{p}\sigma) = 0 \text{ or } -1 & (|\mathbf{p}| < p_F), \\ \delta n(\mathbf{p}\sigma) = 0 \text{ or } 1 & (|\mathbf{p}| > p_F). \end{cases} \quad (2.2)$$

The energy E of the whole system can be expanded as

$$E = E_0 + \sum_{\mathbf{p}\sigma} \varepsilon(\mathbf{p}\sigma) \delta n(\mathbf{p}\sigma) + \frac{1}{2} \sum_{\mathbf{p}\mathbf{p}'\sigma\sigma'} f(\mathbf{p}\mathbf{p}'\sigma\sigma') \delta n(\mathbf{p}\sigma) \delta n(\mathbf{p}'\sigma'), \quad (2.3)$$

where E_0 is the ground state energy of the interacting system. We defined $\varepsilon(\mathbf{p}\sigma)$ and $f(\mathbf{p}\mathbf{p}'\sigma\sigma')$ as the coefficients in this expansion, and f is called the Landau interaction function.

Now, we make use of the symmetry of the system to restrict the general form of the coefficients. First of all, $\varepsilon(\mathbf{p}\sigma)$ must be spin-independent and isotropic; i.e., $\varepsilon(\mathbf{p}\sigma) = \varepsilon(|\mathbf{p}|)$.

Since we are interested in the low-energy excitation, we expand it as

$$\varepsilon(\mathbf{p}\sigma) = \varepsilon(|\mathbf{p}|) \simeq \varepsilon(p_F) + v_F(|p| - p_F). \quad (2.4)$$

The effective mass m^* and the Fermi velocity v_F are defined as

$$m^* \equiv \frac{p_F}{v_F}, \quad v_F \equiv \left(\frac{d\varepsilon}{dp} \right)_{p=p_F}. \quad (2.5)$$

From the symmetry argument, we can also see that $f(\mathbf{p}\mathbf{p}'\sigma\sigma')$ is a function of $|\mathbf{p}|$, $|\mathbf{p}'|$, $\mathbf{p} \cdot \mathbf{p}'$ and $\sigma \cdot \sigma'$. Hence, it can be expanded in terms of the Legendre polynomials P_ℓ as

$$f(\mathbf{p}\mathbf{p}'\sigma\sigma') \simeq \sum_{\ell} (f_{\ell}^s + f_{\ell}^a \sigma \cdot \sigma') P_{\ell}(\hat{\mathbf{p}} \cdot \hat{\mathbf{p}}'). \quad (2.6)$$

Since the coefficients $f_{\ell}^{(s,a)}$ have the dimension of (energy) \times (volume) $^{-1}$, it is convenient to define dimensionless quantities

$$F_{\ell}^s \equiv \Omega \frac{dn}{d\varepsilon} f_{\ell}^s, \quad F_{\ell}^a \equiv \Omega \frac{dn}{d\varepsilon} f_{\ell}^a, \quad (2.7)$$

where Ω is the total volume of the system. For the liquid ^3He , the values of these parameters are

$$\begin{cases} m^*/m & \sim 3-6, \\ F_0^s & \sim 10-100, \\ F_{\ell}^s & \sim 1 \ (\ell \neq 0), \\ F_{\ell}^a & \sim 1. \end{cases} \quad (2.8)$$

The Landau Fermi liquid theory may be very informally summarized as follows:

- Instead of real particles with the bare mass m , we deal with “quasi-particles” with their **effective mass** m^* .
- The system is subject to the **molecular fields** which are proportional to F_{ℓ}^s and F_{ℓ}^a and generated by the **polarizations** of the system (see below).

Molecular fields

Now, we review the molecular field theory in order to examine the spin response. Using Eq. (2.7), we rewrite Eq. (2.6) as

$$f(\mathbf{p}\mathbf{p}'\sigma\sigma') = \left(\frac{dn}{d\varepsilon} \right)^{-1} \Omega^{-1} \sum_{\ell} (F_{\ell}^s + F_{\ell}^a \sigma \cdot \sigma') P_{\ell}(\hat{\mathbf{p}} \cdot \hat{\mathbf{p}}'). \quad (2.9)$$

If F_0^a is much larger than the other terms, we keep only this term in Eq. (2.3):

$$E = \frac{1}{2} \Omega^{-1} \left(\frac{dn}{d\varepsilon} \right)^{-1} F_0^a \sum_{\mathbf{p}\mathbf{p}'\sigma\sigma'} \sigma \cdot \sigma' \delta n(\mathbf{p}\sigma) \delta n(\mathbf{p}'\sigma'). \quad (2.10)$$

Since the total spin $\mathbf{S} = \sum_{p\sigma} \boldsymbol{\sigma} \delta n(p\sigma)$ is conserved, Eq. (2.10) is reduced to

$$E = \frac{1}{2} \Omega^{-1} \left(\frac{dn}{d\varepsilon} \right)^{-1} F_0^a \mathbf{S} \cdot \mathbf{S}. \quad (2.11)$$

This expression is the same as the energy of the free Fermi gas with total spin \mathbf{S} in the molecular field

$$\mathbf{H}_{\text{mol}} = - \left(\frac{dn}{d\varepsilon} \right)^{-1} F_0^a \mathbf{S}. \quad (2.12)$$

Since we know the spin response of the ideal Fermi gas to an external field $\mathbf{H}_{\text{ext}}(\mathbf{k}\omega)$, we obtain

$$\begin{cases} \mathbf{S}(\mathbf{k}\omega) &= \chi_0^{\text{sp}}(\mathbf{k}\omega) \mathbf{H}_{\text{tot}}(\mathbf{k}\omega), \\ \mathbf{H}_{\text{tot}}(\mathbf{k}\omega) &= \mathbf{H}_{\text{ext}}(\mathbf{k}\omega) + \mathbf{H}_{\text{mol}}(\mathbf{k}\omega), \\ \mathbf{H}_{\text{mol}}(\mathbf{k}\omega) &= - \left(\frac{dn}{d\varepsilon} \right)^{-1} F_0^a \mathbf{S}(\mathbf{k}\omega), \end{cases} \quad (2.13)$$

where $\chi_0^{\text{sp}}(\mathbf{k}\omega)$ is the spin response function of the noninteracting Fermi gas with the effective mass m^* . These relations are generalizations of the very familiar mean field theory of ferromagnetism.

We can easily derive the true spin response function

$$\chi_{\text{true}}(\mathbf{q}\omega) = \frac{\chi_0^{\text{sp}}(\mathbf{q}\omega)}{1 + (dn/d\varepsilon)^{-1} F_0^a \chi_0^{\text{sp}}(\mathbf{q}\omega)}. \quad (2.14)$$

By substituting $\chi_0^{\text{sp}} = \frac{dn}{d\varepsilon}$ into Eq. (2.14), we immediately obtain the static spin susceptibility

$$\chi = \frac{dn/d\varepsilon}{1 + F_0^a}. \quad (2.15)$$

This formula is exactly the same as the one in the Landau Fermi liquid theory. Here, we have derived it based on the molecular field theory and our knowledge on the ideal Fermi gas.

2.3 Effects of (spin) molecular field in ${}^3\text{He}$

2.3.1 Enhanced low-energy spin fluctuations

The left figure of Fig. 2.2 shows the frequency-dependence of the χ_0^{sp} of the free Fermi gas, while the right figure is $\chi_{\text{true}}^{\text{sp}}$ corresponding to the Fermi liquid. Their relation is described in Eq. (2.14) with dimensionless parameter $F_0^a \sim -0.7$. We notice that there is a peak for the Fermi liquid. Although this peak does not resemble the delta-function and thus does not represent a real propagating excitation, we can think of this peak as a sort of an elementary excitation, so-called “paramagnon”. The strong peak at low frequency suggests that the elementary excitation is long-lived. Thus, the excitation is also referred to as the “persistent spin fluctuation”.

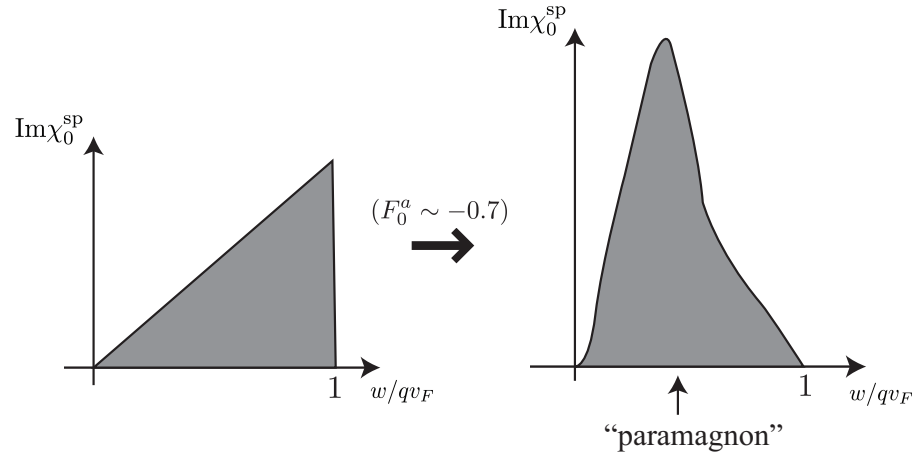


Fig. 2.2. The imaginary part of the spin susceptibility χ_0^{sp} .

2.3.2 Coupling of atomic spins through the exchange of virtual paramagnons

In metals, the effective electron-electron interaction arises from the exchange of virtual phonons. This is illustrated schematically in the left figure of Fig. 2.3. An electron attracts positive ions on the way and other electrons feel these positive charges. Hence, the effective electron-electron interaction is attractive.

The effective interaction between ^3He atoms due to spin fluctuations is illustrated schematically in the right figure of Fig. 2.3. In this case, virtual paramagnons mediate the attractive interaction between ^3He atoms, just as phonons do in metals. There are, however, several important differences between paramagnons and phonons. For example, the interaction due to the exchange of paramagnons is spin-dependent. In the limit $\mathbf{q}, \omega \rightarrow 0$, the interaction induced by the virtual paramagnon is always attractive in the spin-triplet state, while it is repulsive in the spin-singlet state.

2.3.3 Pairing interaction in liquid ^3He

Let us examine the possibility of forming Cooper pairs in the ^3He system. To this end, let us consider the interactions between ^3He atoms. The bare atom-atom potential shown in Fig. 2.1² has a strong hard core repulsion at short distance, much stronger

²The attractive part of the potential has the maximum around $r \sim r_0$, which we can assume to be of the order of the radius of the Cooper pairs. On the other hand, the Cooper pairs must be formed from states near the Fermi surface, $k \sim k_F$. Therefore, we infer the following relation

$$\ell \sim k_F r_0 \quad (\ell = 1, 2, \text{ or } 3), \quad (2.16)$$

where ℓ is the angular momentum.

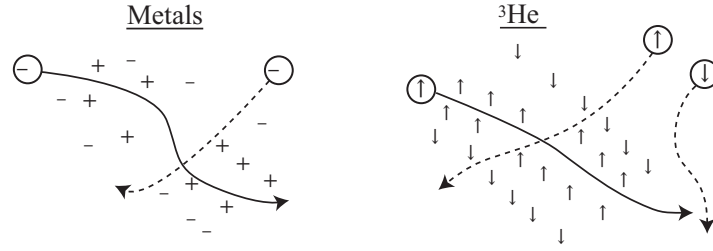


Fig. 2.3. The mechanism to induce the interaction in the liquid ${}^3\text{He}$ is analogous to that of metals.

than the Coulomb repulsion for electrons. Due to this strong repulsion, the Cooper pairs with zero angular momentum are disfavored in ${}^3\text{He}$. Furthermore, the effective interaction originated from the spin-fluctuation exchange, discussed above, is attractive for the spin-triplet case and repulsive for the spin-singlet case. Recalling that the Pauli principle constrains that states with even (odd) angular momentum ℓ must be in spin-singlet (triplet) state, we can expect, all in all, that the $\ell = 1$ or possibly $\ell = 3$ pairing with $S = 1$ may be favored³. Even before the experimental discovery of ${}^3\text{He}$, people discussed the possibility of $\ell = 1$: p -wave state. Now it is clear that we have to generalize the BCS theory to the $\ell \neq 0$ pairing.

2.4 Anisotropic spin-singlet pairing (for orientation only)

We begin with the easiest anisotropic pairing; that is, the $\ell = 2$ spin-singlet pairing. Our strategy here is basically using the usual BCS theory and making necessary modifications to describe the anisotropic pairing. Let us assume the BCS ansatz similar to Eq. (1.9),

$$\Psi_N = \left(\sum_{\mathbf{k}} c_{\mathbf{k}} \alpha_{\mathbf{k}\uparrow}^\dagger \alpha_{-\mathbf{k}\downarrow}^\dagger \right)^{N/2} |\text{vac}\rangle. \quad (2.17)$$

Note that $\alpha_{\mathbf{k}\sigma}^\dagger$ here creates *quasi-particles*, not bare particles, since there is a strong inter-atomic interaction. We have relations similar to Eqs. (1.57) and (1.69),

$$F_{\mathbf{k}} = \Delta_{\mathbf{k}}/2E_{\mathbf{k}}, \quad (2.18)$$

$$\Delta_{\mathbf{k}} = - \sum_{\mathbf{k}'} V_{\mathbf{k}\mathbf{k}'} \frac{\Delta_{\mathbf{k}'}}{2E_{\mathbf{k}'}} \tanh(E_{\mathbf{k}'}/2k_B T). \quad (2.19)$$

The pair wave function $F_{\mathbf{k}}$ and the gap function $\Delta_{\mathbf{k}}$ now depend on both the direction and the magnitude of the momentum \mathbf{k} . The interaction $V_{\mathbf{k}\mathbf{k}'}$ is a nontrivial function of

³The $\ell = 2$ pairing was considered in the original theory [1].

$\mathbf{k} - \mathbf{k}'$, and it can have a complicated form under the constraint that it must be invariant under the spatial rotation. Since we are only interested in behaviors of the system close to the Fermi surface and we can set $|\mathbf{k}|, |\mathbf{k}'| \sim k_F$, $V_{\mathbf{k}\mathbf{k}'}$ can always be expanded as

$$V_{\mathbf{k}\mathbf{k}'} = \sum_{\ell} V_{\ell} P_{\ell}(\hat{\mathbf{k}} \cdot \hat{\mathbf{k}'}), \quad (2.20)$$

where $P_{\ell}(\hat{\mathbf{k}} \cdot \hat{\mathbf{k}'})$ are the Legendre polynomials. If V_{ℓ} is negative for some ℓ_0 and if $|V_{\ell_0}|$ is appreciably larger than other V_{ℓ} 's, we keep only the ℓ_0 component, ignoring all other components. Now let us assume this is the case.

We can also decompose $\Delta_{\mathbf{k}}$ into spherical harmonics $Y_{\ell m}(\theta_{\mathbf{k}}, \phi_{\mathbf{k}})$ as

$$\Delta_{\mathbf{k}} = \sum_m \Delta_{\ell_0 m} Y_{\ell_0 m}(\theta_{\mathbf{k}}, \phi_{\mathbf{k}}). \quad (2.21)$$

To find coefficient $\Delta_{\ell_0 m}$, we consider the free energy and minimize it. Note that the optimal solution $\Delta_{\ell_0 m}$ can be a nontrivial *complex* number, which in turn means a non-zero angular momentum of the paired state. This is because, as we will see later, if the gap function $\Delta_{\mathbf{k}}$ is complex, the pair wave function $F_{\mathbf{k}}$ is also complex. More generally, $\Delta_{\ell_0 m} \neq 0$ for $\ell_0 \neq 0$ implies that some physical quantities, such as the density of states, would be anisotropic.

2.5 Digression: macroscopic angular momentum problem

In this section, let us consider one of the long-standing questions about the anisotropic pairing: can a superfluid state with an anisotropic coupling have a macroscopic angular momentum?

We take the BCS wave function Eq. (2.17) with the following coefficients:

$$c_{\mathbf{k}} = f(|\mathbf{k}|, \theta_{\mathbf{k}}) \exp(2i\phi_{\mathbf{k}}) \quad (d\text{-wave}). \quad (2.22)$$

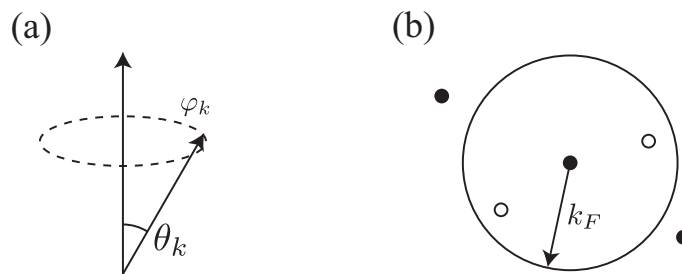


Fig. 2.4. (a) The definitions of $\theta_{\mathbf{k}}$ and $\phi_{\mathbf{k}}$. (b) The BCS ground state constructed from the Fermi sea, not from the Fock vacuum.

See Fig. 2.4 (a) for the definition of $\theta_{\mathbf{k}}$ and $\phi_{\mathbf{k}}$. With this wavefunction, we can calculate the commutator of the operator $\hat{\Omega}^\dagger$ defined in Eq. (1.8) and the generator of rotations around the ℓ -axis \hat{L}_z as

$$[\hat{L}_z, \hat{\Omega}^\dagger] = -i\hbar \frac{\partial c_{\mathbf{k}}}{\partial \phi_{\mathbf{k}}} \alpha_{\mathbf{k}\uparrow}^\dagger \cdot \alpha_{-\mathbf{k}\downarrow}^\dagger = 2\hbar \hat{\Omega}^\dagger. \quad (2.23)$$

Therefore, it turns out that

$$\hat{L}_z \Psi_N = N\hbar \Psi_N. \quad (2.24)$$

This result is somewhat counterintuitive because it implies that this d -wave superfluid state has a macroscopic angular momentum at any temperature below T_c ! Why did we get this seemingly unphysical result? Obviously, this is because we started from the Fock vacuum $|0\rangle$. All pairs of electrons below the Fermi sea gave finite contributions to the total angular momentum.

For comparison, let us change our starting point from the Fock vacuum $|0\rangle$ to the Fermi sea $|\text{FS}\rangle$, the ground state of the non-interacting system. The BCS ground state can be constructed by moving electron pairs from inside of the Fermi surface to outside of it, as shown in Fig. 2.4 (b). The corresponding formula would be

$$\Psi_N^{(m)} \equiv (\hat{\Omega}^+)^{N_+} (\hat{\Omega}^-)^{N_-} |\text{FS}\rangle \quad (N_+ - N_- = 2N_m), \quad (2.25)$$

where $\hat{\Omega}^\pm$ is defined as

$$\hat{\Omega}^+ = \sum_{k > k_F} c_{\mathbf{k}} \alpha_{\mathbf{k}}^\dagger \alpha_{-\mathbf{k}}^\dagger, \quad \hat{\Omega}^- = \sum_{k < k_F} c_{\mathbf{k}}^{-1} \alpha_{-\mathbf{k}} \alpha_{\mathbf{k}}. \quad (2.26)$$

We can easily convince ourselves that the state $\Psi_N^{(m)}$ is an eigenstate of \hat{L}_z with the eigenvalue $N_m \hbar$. If we use the result $N_m/N = \Delta/\varepsilon_F$ obtained in Lec. 1, we see that the eigenvalue is $L_z \sim N\hbar(\Delta/\varepsilon_F) \ll N\hbar$.

We therefore have these two different conclusions depending on the starting points. It turns out that these two ground states give the same prediction for almost all physical properties, except for the angular momentum as we have seen above. After all, which is the true value of the angular momentum of the superfluid ^3He under a specific geometry and a boundary condition? This problem is not fully resolved yet, and remains controversial even today.

2.6 Spin-triplet pairing

In this section, we will discuss the spin-triplet pairing in detail.

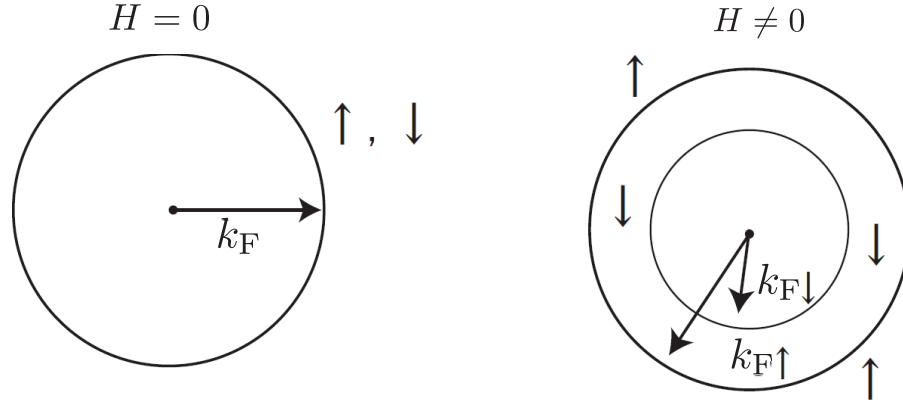


Fig. 2.5. The response to the external field.

2.6.1 Equal spin pairing (ESP) state

Let us start off with the simplest case, the equal spin pairing (ESP). With a suitable choice of the spin axes, the ESP state is characterized by the wavefunction

$$\Psi_N = \sum_{\mathbf{k}} \left(c_{\mathbf{k}\uparrow} \alpha_{\mathbf{k}\uparrow}^\dagger \alpha_{-\mathbf{k}\uparrow}^\dagger + c_{-\mathbf{k}\downarrow} \alpha_{\mathbf{k}\downarrow}^\dagger \alpha_{-\mathbf{k}\downarrow}^\dagger \right)^{N/2} |\text{vac}\rangle. \quad (2.27)$$

Although the Pauli principle implies $c_{\mathbf{k}\sigma} = -c_{-\mathbf{k}\sigma}$, there is no particular relation between $c_{\mathbf{k}\uparrow}$ and $c_{\mathbf{k}\downarrow}$ in general. Note that the above state is not equivalent to

$$\Psi_N^{(F)} = \left(\sum_{\mathbf{k}} c_{\mathbf{k}\uparrow} \alpha_{\mathbf{k}\uparrow}^\dagger \alpha_{-\mathbf{k}\uparrow}^\dagger \right)^{N/4} \left(\sum_{\mathbf{k}} c_{-\mathbf{k}\downarrow} \alpha_{\mathbf{k}\downarrow}^\dagger \alpha_{-\mathbf{k}\downarrow}^\dagger \right)^{N/4} |\text{vac}\rangle. \quad (2.28)$$

Equation (2.27) is a *coherent* superposition of $\uparrow\uparrow$ and $\downarrow\downarrow$ pairs, while Eq. (2.28) represents a Fock state. For a spin-conserving potential, the gap equation for $\sigma = \uparrow\uparrow, \downarrow\downarrow$ decouples:

$$\Delta_{\mathbf{k}\sigma} = - \sum_{\mathbf{k}'} V_{\mathbf{k}\mathbf{k}'} \frac{\Delta_{\mathbf{k}'\sigma}}{2E_{\mathbf{k}'\sigma}} \tanh \frac{1}{2} \beta \varepsilon_{\mathbf{k}'\sigma}. \quad (2.29)$$

One important remark for the ESP state is the spin susceptibility. Let us imagine that we prepare an ESP state with a certain pairing axis and apply a small magnetic field along the axis. The reactions of $\uparrow\uparrow$ pairs and $\downarrow\downarrow$ pairs to the magnetic field are completely independent, and thus the magnetic field does not affect the Cooper-pair formation. The spin susceptibility for the ESP state χ_{ESP} is therefore approximately equal to that of the normal state χ_n (Fig. 2.5).

2.6.2 General case

We consider the most general spin-triplet pairing state,

$$\Psi_N = \left(\sum_{\mathbf{k}\alpha\beta} c_{\mathbf{k}\alpha\beta} \alpha_{\mathbf{k}\alpha}^\dagger \alpha_{-\mathbf{k}\beta}^\dagger \right)^{N/2} |\text{vac}\rangle. \quad (2.30)$$

The coefficients $c_{\mathbf{k}\alpha\beta}$ must be an odd function of \mathbf{k} and symmetric with respect to α and β :

$$c_{\mathbf{k}\alpha\beta} = c_{\mathbf{k}\beta\alpha} = -c_{-\mathbf{k}\alpha\beta}. \quad (2.31)$$

For fixed \mathbf{k} , we can always choose the spin axis which makes $c_{\mathbf{k}\alpha\beta}$ diagonal; i.e., $c_{\mathbf{k}\uparrow\downarrow} = c_{\mathbf{k}\downarrow\uparrow} = 0$. This spin axis may not be unique, and also can depend on \mathbf{k} . What is worse, even if we use this axis, we cannot proceed much further. The gap equation and other formulas take too complicated forms in general.

These formulas are, however, enormously simplified if we restrict ourselves to the *unitary* case, where $|c_{\mathbf{k}\sigma}|^2$ is independent of σ . In this case, the pair wave function would be given by

$$F_{\mathbf{k},\alpha\beta} = \frac{\Delta_{\mathbf{k},\alpha\beta}}{2E_{\mathbf{k}}}, \quad (2.32)$$

where we have defined

$$E_{\mathbf{k}} \equiv (\varepsilon_{\mathbf{k}}^2 + |\Delta_{\mathbf{k}}|^2)^{1/2}, \quad |\Delta_{\mathbf{k}}|^2 \equiv \sum_{\beta} |\Delta_{\mathbf{k},\alpha\beta}|^2. \quad (2.33)$$

We can check that $|\Delta_{\mathbf{k}}|^2$ and hence $E_{\mathbf{k}}$ are independent of α .

If the potential is spin-independent, then the expectation value of the interactions term is reduced to

$$\langle \hat{V} \rangle = \sum_{\mathbf{k}\mathbf{k}'\alpha\beta} V_{\mathbf{k}\mathbf{k}'} F_{\mathbf{k}\alpha\beta} F_{\mathbf{k}'\beta\alpha}. \quad (2.34)$$

As a consequence, the gap equation is decoupled and does not mix the spins:

$$\Delta_{\mathbf{k}\alpha\beta} = - \sum_{\mathbf{k}'} V_{\mathbf{k}\mathbf{k}'} \frac{\Delta_{\mathbf{k}'\alpha\beta}}{2E_{\mathbf{k}'}}. \quad (2.35)$$

2.6.3 \mathbf{d} -vector (unitary states)

Let us introduce the \mathbf{d} -vector, which is very useful for describing the unitary state. In an arbitrary reference frame, the \mathbf{d} -vector is defined by

$$d_i(\mathbf{k}) \equiv -i \sum_{\alpha\beta} (\sigma_2 \sigma_i)_{\beta\alpha} F_{\alpha\beta}(\mathbf{k}), \quad (2.36)$$

where σ_i are Pauli matrices. For any given \mathbf{k} , we can choose the spin axis in such a way that $F_{\uparrow\downarrow}(\mathbf{k}) = F_{\downarrow\uparrow}(\mathbf{k}) = 0$. The definition of the unitary state further imposes the restriction,

$$|F_{\uparrow\uparrow}(\mathbf{k})| = |F_{\downarrow\downarrow}(\mathbf{k})| \equiv |F_{\mathbf{k}}|. \quad (2.37)$$

In this case, $F_{\mathbf{k}}$ can be written as

$$F_{\mathbf{k}} = (d_1(\mathbf{k}) + id_2(\mathbf{k}))/2, \quad d_3(\mathbf{k}) = 0. \quad (2.38)$$

Therefore, \mathbf{d} is a real vector up to an overall phase (i.e., $\mathbf{d} \times \mathbf{d}^* = 0$). In the xy -plane, the angle of the \mathbf{d} -vector with y -axis is $\frac{1}{2}\arg(F_{\uparrow\uparrow}/F_{\downarrow\downarrow})$, while the magnitude $|\mathbf{d}|$ is equal to $|F_{\mathbf{k}}|$.

In other words, the two-particle state of spin- $\frac{1}{2}$ particles of this form is given by

$$S = 1, \quad \mathbf{S} \cdot \mathbf{d} = 0. \quad (2.39)$$

Even in a more general reference frame, the unitary phase has $\mathbf{d}(\mathbf{k})$ such that $\mathbf{d}(\mathbf{k}) \times \mathbf{d}^*(\mathbf{k}) = 0$ for each \mathbf{k} . In the BCS case $\mathbf{d}(\mathbf{k})$ depends only on the direction $\hat{\mathbf{n}} = \mathbf{k}/|\mathbf{k}| \approx \mathbf{k}/k_F$, not on the magnitude $|\mathbf{k}|$. If the direction of $\mathbf{d}(\mathbf{k})$ is independent of \mathbf{k} , it represents the ESP state.

2.7 Ginzburg–Landau theory

2.7.1 Spin-singlet case

The Ginzburg–Landau theory was developed in the context of the old-fashioned superconductors. Actually, this theory was developed before the microscopic works of the BCS theory were done. We consider a general BCS state (not necessarily the ground state) in a uniform space. Let us define the order parameter of the system based on the pair wave function $F_{\mathbf{k}} \equiv \langle a_{\mathbf{k}\uparrow}^\dagger a_{-\mathbf{k}\downarrow}^\dagger \rangle = u_{\mathbf{k}} v_{\mathbf{k}}$:

$$\Psi(\hat{\mathbf{n}}) \equiv \sum_{|\mathbf{k}|} F_{\mathbf{k}}. \quad (2.40)$$

The pairing potential energy $\langle \hat{V} \rangle$ is given by

$$\langle \hat{V} \rangle = \sum_{\mathbf{k}\mathbf{k}'} V_{\mathbf{k}\mathbf{k}'} F_{\mathbf{k}} F_{\mathbf{k}'}^* = \int \frac{d\Omega}{4\pi} \int \frac{d\Omega'}{4\pi} V(\hat{\mathbf{n}}, \hat{\mathbf{n}}') \Psi(\hat{\mathbf{n}}) \Psi^*(\hat{\mathbf{n}}'). \quad (2.41)$$

We confine ourselves to the case where $\Psi(\hat{\mathbf{n}})$ contains only the $\ell = \ell_0$ component of the spherical harmonics $Y_{\ell m}(\hat{\mathbf{n}})$ which corresponds to the most negative component V_{ℓ_0} of $V(\hat{\mathbf{n}}, \hat{\mathbf{n}}')$ (see Eq. (2.20) and the discussion below). Then $\langle \hat{V} \rangle$ can be rewritten as

$$\langle \hat{V} \rangle = V_{\ell_0} \int \frac{d\Omega}{4\pi} |\Psi(\hat{\mathbf{n}})|^2. \quad (2.42)$$

Next we consider the kinetic energy $\langle \hat{K} - \mu \hat{N} \rangle = \sum_{\mathbf{k}\sigma} \varepsilon_{\mathbf{k}} \langle n_{\mathbf{k}\sigma} \rangle$, and the entropy $-TS$. It is clear that $\langle \hat{K} - \mu \hat{N} \rangle - TS$ is a sum of contributions $f\{\Psi(\hat{\mathbf{n}})\}$ from each point on the Fermi surface:

$$\langle \hat{K} - \mu \hat{N} \rangle - TS = \int \frac{d\Omega}{4\pi} f\{\Psi(\hat{\mathbf{n}})\}. \quad (2.43)$$

From symmetry considerations⁴, the function $f\{\Psi(\hat{\mathbf{n}})\}$ can be expanded as

$$f\{\Psi(\hat{\mathbf{n}})\} = f\{|\Psi(\hat{\mathbf{n}})|^2\} = \text{const.} + \alpha(T)|\Psi(\hat{\mathbf{n}})|^2 + \frac{1}{2}\beta(T)|\Psi(\hat{\mathbf{n}})|^4 + O(|\Psi(\hat{\mathbf{n}})|^6). \quad (2.44)$$

Hence the total free energy $F \equiv \langle \hat{K} - \mu\hat{N} + \hat{V} \rangle - TS$ is given by

$$F = \text{const.} + (V_\ell + \alpha(T)) \int \frac{d\Omega}{4\pi} |\Psi(\hat{\mathbf{n}})|^2 + \frac{1}{2}\beta(T) \int \frac{d\Omega}{4\pi} |\Psi(\hat{\mathbf{n}})|^4 + O(|\Psi(\hat{\mathbf{n}})|^6). \quad (2.45)$$

The explicit forms of $\alpha(T)$ and $\beta(T)$ are not necessary for our purpose. We will drop the constant term below.

If the coefficient $V_\ell + \alpha(T)$ is positive, the normal state $\Psi(\hat{\mathbf{n}}) = 0$ minimizes the free energy. In contrast, if the coefficient is negative, the order parameter $\Psi(\hat{\mathbf{n}})$ has a finite value. Therefore, the critical point T_c can be determined from the equation

$$V_\ell + \alpha(T) = 0. \quad (2.46)$$

By expanding $V_\ell + \alpha(T)$ around $T = T_c$ as $\alpha'(T_c)(T_c - T)$ ($\alpha'(T_c) < 0$) and $\beta(T)$ as $\beta \equiv \beta(T_c)$, we have

$$F = \alpha'(T_c)(T_c - T) \int \frac{d\Omega}{4\pi} |\Psi(\hat{\mathbf{n}})|^2 + \frac{1}{2}\beta \int \frac{d\Omega}{4\pi} |\Psi(\hat{\mathbf{n}})|^4 + O(|\Psi(\hat{\mathbf{n}})|^6). \quad (2.47)$$

Note that V_ℓ has been dropped out of the problem!

For the s -wave pairing, since $\Psi(\hat{\mathbf{n}})$ becomes a constant Ψ , we get the standard Ginzburg–Landau expression,

$$F = \alpha'(T_c)(T_c - T)|\Psi|^2 + \frac{1}{2}\beta|\Psi|^4 + O(|\Psi|^6). \quad (2.48)$$

Minimizing this with respect to Ψ gives $F = -(\alpha'(T_c)^2/2\beta)(T_c - T)^2$, which agrees with the BCS theory.

For the $\ell \neq 0$ pairing, the free energy F depends on the specific form of $\Psi(\hat{\mathbf{n}})$. By minimizing the free energy with respect to the overall magnitude of Ψ , we find

$$F = -(\alpha'^2/2\beta) \left(\overline{|\Psi|^2} \right)^2 / \overline{|\Psi|^4}, \quad (2.49)$$

where the average \overline{X} of a function $X(\hat{\mathbf{n}})$ is defined as $\overline{X} \equiv \int \frac{d\Omega}{4\pi} X(\hat{\mathbf{n}})$. Hence, the lowest free energy is achieved by minimizing the anisotropy of $|\Psi|^2$ over the Fermi surface.

2.7.2 Spin-triplet case

To examine the spin-triplet case, it is convenient to define

$$\mathbf{d}(\hat{\mathbf{n}}) \equiv \sum_{|\mathbf{k}|} \mathbf{d}_{\mathbf{k}}. \quad (2.50)$$

⁴The free energy should be invariant under the global gauge transformation $\Psi \rightarrow \exp(i\alpha)\Psi$, which is a natural consequence of the assumption that Ψ has the meaning of a Schrödinger-like wave function.

The potential energy and the kinetic energy become

$$\langle \hat{V} \rangle = \int \frac{d\Omega}{4\pi} \int \frac{d\Omega'}{4\pi} V(\hat{\mathbf{n}}, \hat{\mathbf{n}}') \mathbf{d}(\hat{\mathbf{n}}) \cdot \mathbf{d}^*(\hat{\mathbf{n}}') \rightarrow V_{\ell_0} \int \frac{d\Omega}{4\pi} |\mathbf{d}(\hat{\mathbf{n}})|^2, \quad (2.51)$$

$$\langle \hat{K} - \mu \hat{N} \rangle - TS = \int \frac{d\Omega}{4\pi} f\{|\mathbf{d}(\hat{\mathbf{n}})|^2\}. \quad (2.52)$$

Therefore the free energy F is

$$F = \alpha'(T_c)(T_c - T) \int \frac{d\Omega}{4\pi} |\mathbf{d}(\hat{\mathbf{n}})|^2 + \frac{1}{2}\beta \int \frac{d\Omega}{4\pi} |\mathbf{d}(\hat{\mathbf{n}})|^4 + O(|\mathbf{d}(\hat{\mathbf{n}})|^6). \quad (2.53)$$

As we can see, $|\mathbf{d}(\hat{\mathbf{n}})|^2$ in the spin-triplet case plays the role of $|\Psi(\hat{\mathbf{n}})|^2$ in the spin-singlet case. Hence, the lowest free energy is obtained by minimizing the anisotropy of $|\mathbf{d}(\hat{\mathbf{n}})|^2$ over the Fermi surface.

References

- [1] P. W. Anderson and P. Morel, Phys. Rev. **123**, 1911 (1961).

Lec. 3 Superfluid ^3He (continued)

In this section, we focus specifically on superfluid ^3He and some interesting topics.

3.1 Experimental phases of liquid ^3He

Figure 3.1 is the phase diagram of ^3He at the temperature below about 3 mK. Solid ^3He is also interesting, but in this lecture, we focus on the liquid phases of ^3He . As we saw in the previous section, at higher temperature (but below 100 mK), this liquid ^3He behaves very much like a pure textbook Landau Fermi liquid. The Landau Fermi liquid is basically very much like a free degenerated Fermi gas with two differences: (a) The real particle excitation in the free Fermi gas becomes the quasiparticle excitation in the Fermi liquid, and the effective mass m^* of the quasiparticle is different from an atomic mass m due to the inter-atomic interaction. (b) The system is subject to a set of molecular fields which generate various kinds of macroscopic polarizations.

So far, the liquid ^3He is known to have at least three new phases. Most of the phase diagram is occupied by the B phase, and the A phase exists between the B and the normal phases. The last one is the A1 phase, which only appears in a strong magnetic field. The phase transitions between the normal phase and the A phase, or the normal phase and the B phase are second-order phase transitions. On the other hand, the transition between

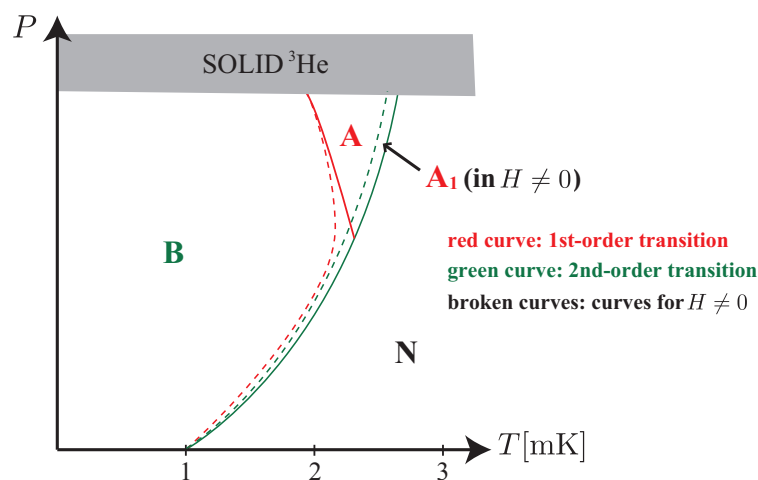


Fig. 3.1. Phase diagram of ^3He (See [1, 2]).

the A and B phases is a first-order phase transition, and this is typically accompanied by a certain amount of supercooling¹.

In the above paragraph, I avoid referring to the superfluid, because the concept of superfluid ${}^3\text{He}$ was originally based more on theoretical presumptions than on experimental phenomenologies. In fact, it is not easy to show that these phases are really superfluid in experiments², but here, we use a usual convention in referring to the phases of superfluid ${}^3\text{He}$.

3.2 Nature of the order parameter of different phases

It is believed that we are fairly confident in identifying the order parameters of pair wave functions of different phases of ${}^3\text{He}$. We can identify the order parameters by susceptibility, nuclear magnetic resonance (NMR) and also indirect arguments based on stability.

3.2.1 A phase

First of all, the A phase (spin-triplet) is believed to be characterized by the \mathbf{d} -vector. The \mathbf{d} -vector depends on the position on the Fermi surface, which we specify by $\hat{\mathbf{k}}$, and the \mathbf{d} -vector can be written down in the form

$$\mathbf{d}(\hat{\mathbf{k}}) = \hat{\mathbf{d}}f(\hat{\mathbf{k}}), \quad f(\hat{\mathbf{k}}) = \sin\theta_{\hat{\mathbf{k}}}e^{i\phi_{\hat{\mathbf{k}}}}, \quad (3.1)$$

where $\hat{\mathbf{d}}$ is a characteristic spin vector, which is independent of the position on the Fermi surface, $\hat{\boldsymbol{\ell}}$ is a characteristic vector describing the orbital space, and $\theta_{\hat{\mathbf{k}}}$ and $\phi_{\hat{\mathbf{k}}}$ are the polar angles of $\hat{\mathbf{k}}$ with respect to $\hat{\boldsymbol{\ell}}$ (see Fig. 3.2). This phase is usually known as the Anderson–Brinkman–Morel (ABM) state.

In the A phase, the pair wave function can be broken up into a spin wave function $\chi(\sigma)$ and a spatial wave function $F(\mathbf{r})$:

$$F(\mathbf{r}, \sigma) = F(\mathbf{r})\chi(\sigma). \quad (3.2)$$

Here, in the ABM state, $\chi(\sigma)$ is the state which satisfies $S = 1$ and $S_z = 0$ along $\hat{\mathbf{d}}$, and $F(\mathbf{r})$ is the state with the apparent angular momentum \hbar along $\hat{\boldsymbol{\ell}}$. The gap function in the ABM state is explicitly given by the formula here:

$$\Delta_{\hat{\mathbf{k}}} = \Delta_0 \sin\theta_{\hat{\mathbf{k}}} \exp(i\phi_{\hat{\mathbf{k}}}). \quad (3.3)$$

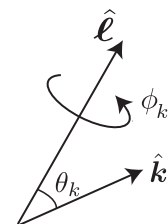


Fig. 3.2. Angles $\theta_{\hat{\mathbf{k}}}$ and $\phi_{\hat{\mathbf{k}}}$ are relative to $\hat{\boldsymbol{\ell}}$.

¹There are some very interesting problems associated with the supercooling, but we do not discuss in details here. See Ref. [2] for more details.

²The healing length of ${}^3\text{He}$ is at least of the order of a pair radius and much larger than that of ${}^4\text{He}$. Therefore, it is much easier to destroy the superfluidity in ${}^3\text{He}$ than in ${}^4\text{He}$. This is the main reason why ${}^3\text{He}$ experiments is difficult.

It is important that $\Delta_{\hat{\mathbf{k}}}$ is complex, and hence it has an angular momentum. Furthermore, the gap function has nodes at $\hat{\mathbf{k}} = \pm \hat{\boldsymbol{\ell}}$ (i.e., $\theta_k = 0, \pi$), which suggests the low-energy quasiparticles are more easily excited at low temperature compared with the fully gapped state.

The fact that the vector $\hat{\mathbf{d}}$ is independent of $\hat{\mathbf{k}}$ indicates the ABM state being the Equal-Spin-Pairing (ESP) state, which has a susceptibility equal to the normal state value. Thus, χ is not reduced so long as the magnetic field is applied perpendicular to $\hat{\mathbf{d}}$.

Alternative representation of the ABM state

We can use an alternative notation of the ABM state, in which the many-body wave function has the following form

$$\Psi_N = \text{const.} \left[\sum_{\mathbf{k}} c_{\mathbf{k}} \left(\alpha_{\mathbf{k}\uparrow}^\dagger \alpha_{-\mathbf{k}\uparrow}^\dagger + \exp(i\chi_d) \alpha_{\mathbf{k}\downarrow}^\dagger \alpha_{-\mathbf{k}\downarrow}^\dagger \right) \right]^{N/2} |\text{vac}\rangle, \quad (3.4)$$

where $\chi_d = -2\varphi_d$, and φ_d is the angle of \mathbf{d} in the xy -plane measured clockwise from the positive y -axis. This wave function brings out its ESP nature explicitly. There is a definite phase between the two up pairs and the two down pairs: the ESP state is a coherent superposition of them. Here, $c_{\mathbf{k}}$ is the orbital part of the wave function

$$c_{\mathbf{k}} = f(|\mathbf{k}|) \sin\theta_{\mathbf{k}} \exp(i\phi_{\mathbf{k}}). \quad (3.5)$$

3.2.2 A1 phase

Let us consider another phase, the A1 phase, which only appears under a strong magnetic field. If we take the coordinate axis such that the magnetic field is applied in the up (\uparrow) direction, the many-body wave function of the A1 phase is expressed as

$$\Psi_N = \text{const.} \left(\sum_{\mathbf{k}} c_{\mathbf{k}} \alpha_{\mathbf{k}\uparrow}^\dagger \alpha_{-\mathbf{k}\uparrow}^\dagger \right)^{N/4} \times (\downarrow \text{Fermi Sea}). \quad (3.6)$$

Crudely speaking, in the A1 phase, a pair of up spins form a Cooper pair, while down spins just behave like in the normal phase.

It is tempting to think that in the phase of this type, the spins are automatically polarized, but that is not true. Because this expression does not mean creating more particles in one spin direction \uparrow than the normal phase, they are just reorganized to make pairs in the real space. Therefore in this case, up spins have a gap on the Fermi surface which is the same as in the A phase, but down spins have no gap.

3.2.3 B phase: naive identification

The naive identification of the B phase is first proposed by R. Balian and N. R. Werthamer³ [4] in 1963, and this state is called the BW state. In the \mathbf{d} -vector notation, the state is described by $\hat{\mathbf{k}}$:

$$\mathbf{d}(\hat{\mathbf{k}}) \propto \hat{\mathbf{k}}. \quad (3.7)$$

In other words, the spin state is $S = 1, S_z = 0$ along $\hat{\mathbf{k}}$. It turns out that the orbital angular momentum satisfies $\hat{L}_z = 0$. Thus, in the BW state, we can show that the spin vector \mathbf{S} of the Cooper pairs is always directed oppositely to \mathbf{L} :

$$\mathbf{L} + \mathbf{S} \equiv \mathbf{J} = 0. \quad (3.8)$$

In the language of molecular physics, the BW state is 3P_0 state. In particular, by the Wigner–Eckart theorem, *any* anisotropy in physical properties must be determined by the value of \mathbf{J} . In this case $\mathbf{J} = 0$, which means all properties have to be isotropic, and the gap function Δ satisfies

$$|\Delta(\mathbf{n})| \propto |\mathbf{d}(\mathbf{n})| = \text{const}. \quad (3.9)$$

This means that Δ has no nodes (as it does not in the ABM state), and the number of quasiparticles is exponentially small ($\propto \exp(-\Delta/T)$) at low temperature. As to spin susceptibility χ , for any particular direction of the field, some pairs are formed in the $S_z = 0$ state and these pairs will not respond to the field. Therefore, χ is reduced from the normal-state value.

Combined with the result on the A phase, this has an important consequence that a magnetic field always advantages the A phase over the B phase.

3.3 Why A phase?

The very important question which arose soon after the phase diagram was discovered experimentally, is “Why should the A phase be there?”. To see this problem, remember the Ginzburg–Landau theory discussed in the previous section. For the pairing with given ℓ , it was shown that the free energy is minimized by the choice which minimizes the anisotropy of $|\mathbf{d}(\hat{\mathbf{n}})|^2$ over the Fermi surface. We can define this anisotropy by

$$K \equiv \frac{\overline{|\mathbf{d}|^4}}{\left(\overline{|\mathbf{d}|^2}\right)^2}, \quad (3.10)$$

and all we have to do is to *minimize* K .

Now we can estimate K by using the results of the gap function of each state, and see:

³Actually, there was an earlier discussion of this phase by Yu. Vdovin [3], but this work was not widely known outside the former Soviet Union.

For the ABM state, $|\mathbf{d}(\hat{\mathbf{n}})|^2 \propto \sin^2\theta \Rightarrow K_{\text{ABM}} = \frac{8/15}{(2/3)^2} = 6/5$.

For the BW state, $|\mathbf{d}(\hat{\mathbf{n}})|^2 = \text{const.} \Rightarrow K_{\text{BW}} = 1$.

Thus, in the generalized BCS theory, we *always* have $F_{\text{BW}} < F_{\text{ABM}}$!

This was the major problem when superfluid phases of ^3He were discovered experimentally, and some approaches were developed to examine this problem. The first approach is to generalize Ginzburg–Landau approach, and the second one is to consider spin fluctuation feedback. In the next two subsections, I will introduce these two approaches.

3.3.1 Generalized Ginzburg–Landau approach

In this approach, our discussion is only based on the symmetry of the states, and there is no particular assumption on energetics. Since $\mathbf{d}(\hat{\mathbf{n}})$ is a vector in spin space, and the orbital dependence is assumed to be p -wave, we can always write the quantities d_α as

$$d_\alpha(\hat{\mathbf{n}}) \equiv \sum_i d_{i\alpha} \hat{\mathbf{n}}_i, \quad (3.11)$$

where i is a spin subscript, and α is an orbital one. This means that all p -wave triplet states are completely parameterized by 9 complex quantities $d_{i\alpha}$, and the order parameter is defined in the 18-dimensional space.

Here, let us follow the original argument by Ginzburg and Landau, and assume the expansion:

$$F(T : \{d_{i\alpha}\}) = \alpha_0(T - T_c) \cdot O(|d|^2) + \beta(T) \cdot O(|d|^4) + \dots, \quad (3.12)$$

where $\alpha_0 > 0$ is a constant. Then, we consider some basic symmetries: invariance under global gauge transformations, and under rotations of the spin and orbital coordinate system separately. These symmetry conditions constrain the term of $O(|d|^2)$ to have the unique form

$$O(|d|^2) \propto \sum_{i\alpha} |d_{i\alpha}|^2, \quad (3.13)$$

which is $\int \frac{d\Omega}{4\pi} |\mathbf{d}(\hat{\mathbf{n}})|^2$, just as in the BCS theory.

For the $O(|d|^4)$ term, on the other hand, there are *five terms which are invariant* under the above symmetries. For example,

$$I_1 = \left| \sum_{i\alpha} d_{i\alpha}^2 \right|^2, \quad (3.14)$$

$$I_2 = \sum_{\alpha\beta ij} d_{\beta i}^* d_{\beta j}^* d_{\alpha i} d_{\alpha j}, \quad \text{etc.} \quad (3.15)$$

Here, note that I_1 is different from $I_4 \equiv (\sum_{i\alpha} |d_{i\alpha}|^2)^2 = 1$. We can write down any fourth-order invariants by the linear combinations of these five invariants⁴. Therefore in general,

⁴Readers interested in the other two invariants I_3 and I_5 may check them in Ref. [5].

setting some coefficients β_s , we obtain

$$O(|d|^4) = \sum_{s=1}^5 \beta_s I_s \equiv K_4. \quad (3.16)$$

I_s 's are fourth-order invariants characteristic of particular kinds of states (e.g., the ABM state, the BW state ...), but β_s 's are parameters which depend on energetic assumptions in general. Therefore we cannot determine β_s *a priori* unlike the simple BCS case.

Next, we should tackle the problem of finding $d_{i\alpha}$, which minimize the fourth-order free energy K_4 for given parameters β_s and normalization conditions:

$$\sum_{i\alpha} |d_{i\alpha}|^2 \equiv |\overline{d}|^2 = 1. \quad (3.17)$$

The problem is to find all possible states (all possible forms of $d_{i\alpha}$) which can be minima of free energy (i.e., minima of K_4) for some choice of the β_s under the above constraints. This problem is solvable in principle, but is quite messy and nearly unsolvable in reality without constraints. Therefore we restrict possible states to unitary states. Here, unitary states mean that for every $\hat{\mathbf{n}}$, $S_z = 0$ is satisfied in some set of spin axes.

If we assume this, the problem becomes simple, and it is found that only four states can be the extrema of free energy (for more details, see Ref. [5]):

1. The BW (“isotropic”) state: $d_{\alpha i} = \frac{1}{\sqrt{3}}\delta_{\alpha i}$
This state is already introduced. In the BW state, we have pairing in all possible directions.
2. The 2D (“planar”) state: $d_{\alpha i} = \frac{1}{\sqrt{2}}\delta_{\alpha i}(1 - \delta_{iz})$
This state is essentially very similar to the BW state because if the z -component is removed from the BW state, it becomes the planar state. This state is an ESP state, but is different from the ABM state.
3. The ABM (“axial”) state: $d_{yx} = -id_{zx} = \frac{1}{\sqrt{2}}$, all other $d_{\alpha i} = 0$
This state is already introduced.
4. The 1D (“polar”) state: $d_{zz} = 1$, all other $d_{\alpha i} = 0$
This state is also an ESP state.

Remarkable Theorem

For the BCS values of β 's, the BW state turns out to be most stable. If the non-BCS contributions to β are taken into account, however, other states may be more stable. In fact, the polar state can be more stable than the BW state only if the non-BCS contributions to β 's are comparable to BCS ones. For the ABM state, its energy become smaller

than that of the BW state for relatively small non-BCS contributions. Furthermore, we can show that the 2D (planar) state can *never* be the absolute minimum of free energy for any choice of β 's. Therefore, in general, *the BW or the ABM states are most likely to appear.*

It is important to note that in the above analysis, both orbital subscripts α 's and spin subscripts i 's always occur in pairs. Thus, I_s 's are invariant under spin and orbital rotation separately, and the BW state, the ABM state, etc. represent *classes* of states transforming into one another under these rotations.

3.3.2 Spin fluctuation feedback

In this subsection, we view the second approach which is much more based on physical mechanism. This approach is proposed by Anderson and Brinkman in 1973 [6].

The basic physical idea of Anderson–Brinkman theory is shown in Fig. 3.3. In a standard superconductor, which is described by the BCS theory, the mechanism of the formation of Cooper pairs is an exchange of virtual bosons, or phonons between the electrons. In the case of ^3He , quasiparticles also exchange bosonic degree of freedom called “spin fluctuation”, where additional quasiparticle and quasihole pairs are formed and the medium becomes virtually polarized by the strong inter-atomic interaction. Thus, the mechanism for the superfluidity sounds rather similar to the BCS one, but there is a critical difference. Unlike the superconductor, in the case of ^3He , the medium being polarized is precisely the medium in which Cooper pairs are formed, and the superfluid phase transition modifies the pairing interaction between quasiparticles. Therefore, the original force of the superfluidity, the spin fluctuation, is in turn modified in the presence of the superfluidity, and in general, we must include this “spin-fluctuation feedback”. The amount of this feedback effect depends on a particular kind of superfluid (the ABM state, the BW state, ...), and it is, in fact, significant in discussing the ABM and the BW states.

The spin-fluctuation-induced interaction (See Sec. 2.3) is given by

$$\hat{V}_{\text{eff}}(\mathbf{q}\omega) \approx -(F_0^a)^2 \chi_{\text{sp}}(\mathbf{q}\omega) \boldsymbol{\sigma}^{(1)} \cdot \boldsymbol{\sigma}^{(2)}, \quad (3.18)$$

where $\boldsymbol{\sigma}^{(1)}$ and $\boldsymbol{\sigma}^{(2)}$ are spin operators for each atom of the Cooper pairs. This interaction is attractive in the spin-triplet state, and repulsive in the singlet state. The point is that the spin susceptibility $\chi_{\text{sp}}(\mathbf{q}\omega)$ is *modified* by pairing. To obtain quantitative results, we need a microscopic complicated calculation [6], but we can easily obtain qualitative understanding by assuming

$$\delta\chi_{\text{sp}}(\mathbf{q}\omega) \propto \delta\chi, \quad (3.19)$$

where χ is a static spin susceptibility. Crudely speaking, we assume that the modification of the spin susceptibility is similar to the static part. With this assumption, we can immediately see that the BW state is disfavored. In fact, in the BW phase, the spin-fluctuation-induced attraction \hat{V}_{eff} gets smaller since the susceptibility is reduced $\chi < \chi_n$.

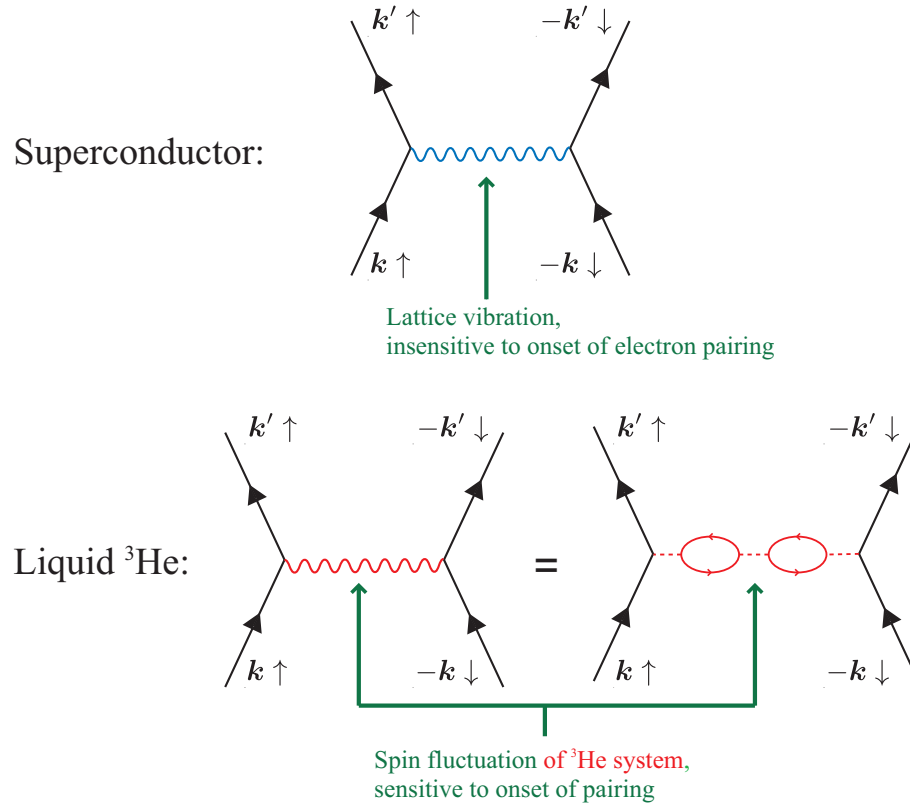


Fig. 3.3. Schematic illustration of the Anderson–Brinkman theory.

In the ABM phase, for fixed \mathbf{d} , $\delta\chi$ is actually *anisotropic*. In this case, we can write down the modification $\delta\chi$ and potential as

$$\delta\chi_{ij} \approx -f(T)d_id_j, \quad (3.20)$$

$$\Delta\langle\hat{V}_{\text{eff}}\rangle \approx -\delta\chi_{ij}\langle\sigma_i^{(1)}\sigma_j^{(2)}\rangle \approx +f(T)d_id_j\langle\sigma_i^{(1)}\sigma_j^{(2)}\rangle. \quad (3.21)$$

If we take the axis of \mathbf{d} in the z -direction, we find $\Delta\langle V_{\text{eff}}\rangle \propto d_z^2\langle\sigma_z^{(1)}\sigma_z^{(2)}\rangle$. In the ABM state, all Cooper pairs are in a state with $S = 1$, $S_z = 0$, so that the spins of the pairs in the z -direction are antiparallel and $\langle\sigma_z^{(1)}\sigma_z^{(2)}\rangle$ is strongly negative. Hence, in the ABM state, the spin-fluctuation attraction is increased in the ABM state over the normal-state value. If the spin-fluctuation feedback effect is strong enough, the ABM state may become even more stable than the BW state.

3.4 NMR in the new phase

The first experiment of the superfluid ${}^3\text{He}$ was the NMR experiments, which measure the susceptibility and the resonance frequency. First, we consider the susceptibility (Fig. 3.4.).

In the normal phase and the A phase, χ is constant (we actually know now by experimental results that there is a very small change for χ when we go into the A phase from

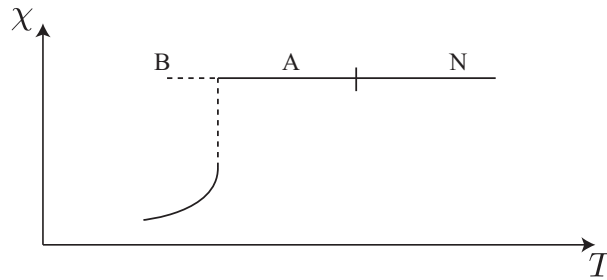


Fig. 3.4. The behavior of the susceptibility.

the normal phase), but in the B phase χ discontinuously drops. These phenomena are not particularly mysterious. The A phase could be an ESP state, which is composed of only $\uparrow\uparrow, \downarrow\downarrow$ pairs. Thus, there is no reduction in χ . The B phase could be the singlet or BW state, where $\uparrow\downarrow$ pairs are formed for both cases, and χ is expected to be reduced.

Next we consider the resonance frequency (Fig. 3.5 (a)), which is much more puzzling than the susceptibility. In the normal phase the resonance frequency ω_{res} is

$$\omega_{\text{res}} = \gamma H_{\text{ext}}, \quad (3.22)$$

where γ is μ_n/\hbar (μ_n : the nuclear moment) and H_{ext} is the external magnetic field. This is a standard Larmor frequency expression. When we go into the A phase, the early NMR experiments show that the resonance frequency shifts upward from the normal value

$$\omega_{\text{res}}^2 = \gamma^2 H_{\text{ext}}^2 + \omega_0^2, \quad (3.23)$$

which seems Pythagorean. This result is very well verified in other experiments. Through the phase transition from the A phase to the B phase, the resonance frequency appears to go back to the exactly same form as the normal state. By experiments

$$\omega_0^2(T) \approx A(1 - T/T_A), \quad \frac{A}{(2\pi)^2} \approx 5 \times 10^{10} \text{ Hz}^2. \quad (3.24)$$

Thus we need $H_0(\equiv \omega_0(T)/\gamma) \sim 30 \text{ G}$ (Fig. 3.5 (b)). However, the only spin-non-conserving force in problem is the nuclear dipole-dipole interaction, and the maximum associated field is less than 1 G even if the atoms approach very close! What develops the extra field H_0 which is perpendicular to the external field? Where does the effect come from? Is this the first indication of a radical breakdown of quantum mechanics?

3.5 What can be inferred from the sum rules?

From a simple sum-rule argument, if a single sharp resonance is observed (as in the experiments), then

$$\omega_{\text{res}}^2 = \gamma^2 H_{\text{ext}}^2 + \omega_0^2, \quad (3.25)$$

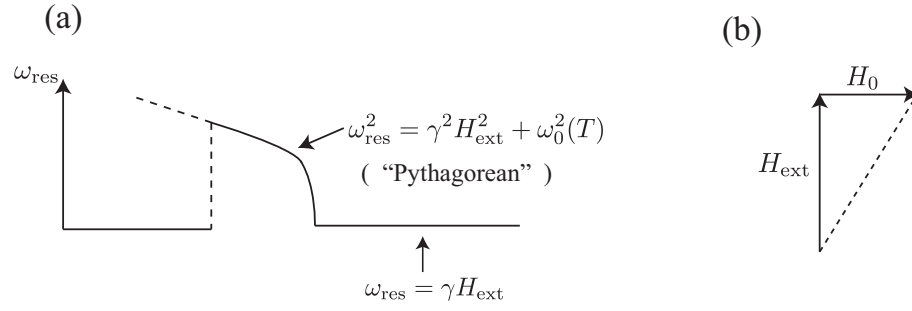


Fig. 3.5. (a) The behavior of the resonance frequency. (b) The extra field H_0 .

$$\omega_0^2 = \chi^{-1} \frac{\partial^2 \langle \hat{H}_D \rangle}{\partial \theta^2}, \quad (3.26)$$

where \hat{H}_D is the nuclear dipole energy and θ is the angle of simultaneous rotation of all spins (Fig. 3.6).

The second derivative of $\langle \hat{H}_D \rangle$ is expected to be

$$\frac{\partial^2 \langle \hat{H}_D \rangle}{\partial \theta^2} \sim \langle \hat{H}_D \rangle, \quad (3.27)$$

which is shown from the tensorial structure of \hat{H}_D that $\sum_{i=1}^3 \partial^2 \langle \hat{H}_D \rangle / \partial^2 \theta_i^2 = -\langle \hat{H}_D \rangle$ where θ_i is the i -th component of θ . This implies that the experimental value of $\omega_0^2(T)$ is

$$\langle \hat{H}_D \rangle(T) \sim K \left(1 - \frac{T}{T_A} \right), \quad K \sim 10^{-3} \text{ ergs/cm}^3. \quad (3.28)$$

This is a very large value. Since the end-to-end configuration is favored over the side-by-side one only by an energy

$$\Delta E \leq \frac{\mu_0 \mu_n^2}{r_0^3} \sim 10^{-7} \text{ K} \ll k_B T, \quad (3.29)$$

the “good” orientation is preferred to the “bad” one by (we consider $k_B T \sim 10^{-3} \text{ K}$)

$$\Delta E / k_B T \sim 10^{-4}. \quad (3.30)$$

The real situation is actually worse than this, since because of the Fermi degeneracy the thermal energy $k_B T$ should be replaced by $k_B T_F \sim 1 \text{ K}$, or $\Delta E / k_B T_F \sim 10^{-7}$. *Thus the vacuum expectation value of the dipole energy is much too small.*

3.6 Spontaneously broken spin-orbit symmetry

We consider here the spontaneously broken spin-orbit symmetry (SBSOS) in the liquid ^3He by an analogy with the behavior of ferromagnets (Fig. 3.7). For the ferromagnetic

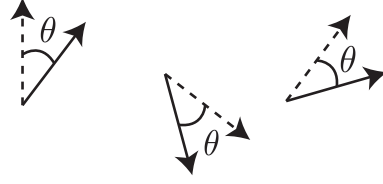


Fig. 3.6. θ is the angle of simultaneous rotation of all spins.

case, in the normal phase, the direction of spin vector is completely random. However, when we go into the ordered phase, all of the spin vectors become parallel,

$$\langle \mathbf{S} \rangle \neq 0. \quad (3.31)$$

This phase transition affects the response to an external field significantly. To see this, let us consider the Hamiltonian expressed with the two terms

$$\hat{H} = \hat{H}_0 + \hat{H}_z, \quad (3.32)$$

where \hat{H}_0 is the exchange interaction between spins, and \hat{H}_z is the Zeeman interaction term

$$\hat{H}_z = -\mu_B H_{\text{ext}} \sum_i S_{zi}. \quad (3.33)$$

While \hat{H}_0 is invariant under simultaneous rotation of all spins, the Zeeman term breaks the spin-rotation symmetry. In the paramagnetic phase ($T > T_c$), the spins behave independently. Thus the polarization value is approximately $\mu_B H_{\text{ext}}/k_B T \ll 1$, and the expectation value of the second term in Eq. (3.32) becomes

$$\langle \hat{H}_z \rangle \sim N (\mu_B H_{\text{ext}})^2 / k_B T, \quad (3.34)$$

which is usually a very small value. In contrast, in the ferromagnetic phase ($T < T_c$), \hat{H}_0 forces all spins to lie in parallel. Thus the polarization value is approximately 1, and the expectation value of the second term in Eq. (3.32) becomes

$$\langle \hat{H}_z \rangle \sim N \mu_B H_{\text{ext}}. \quad (3.35)$$

Next, we consider the liquid ^3He . The Hamiltonian can be expressed as

$$\hat{H} = \hat{H}_0 + \hat{H}_D, \quad (3.36)$$

where \hat{H}_0 is invariant under relative rotation of spin and orbital coordinate systems, and the dipolar-interaction \hat{H}_D is given by

$$\hat{H}_D = g_D \sum_{ij} \left(\frac{\sigma_i \cdot \sigma_j - 3\sigma_i \cdot \hat{\mathbf{r}}_{ij} \sigma_j \cdot \hat{\mathbf{r}}_{ij}}{(r_{ij}^3/r_0^3)} \right). \quad (3.37)$$

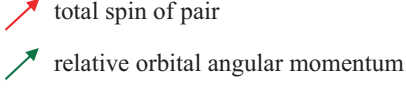
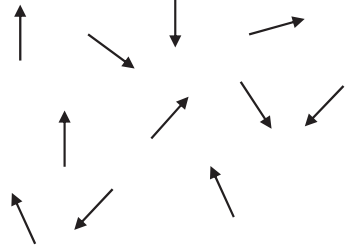
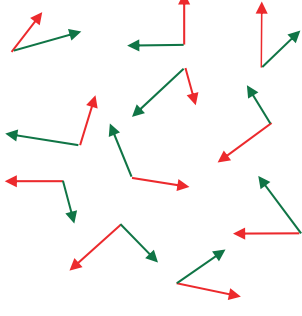
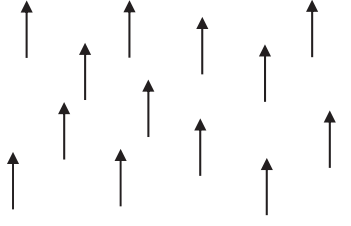
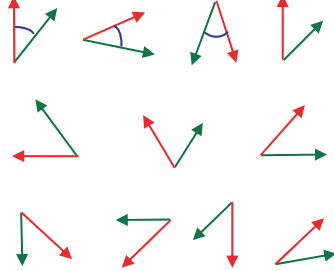
	<u>Ferromagnet</u>	<u>Liquid ^3He</u>
	 spin	 total spin of pair relative orbital angular momentum
Normal phase		
Ordered phase	 $\langle \mathbf{S} \rangle \neq 0$	 $\langle \mathbf{S} \rangle = 0, \langle \mathbf{L} \rangle = 0,$ but $\langle \mathbf{L} \times \mathbf{S} \rangle \neq 0$

Fig. 3.7. SBSOS with an analogy with ferromagnets.

This term *breaks* the relative spin-orbit rotation symmetry.

In the normal phase ($T > T_A$), the spins of the pairs behave independently. Therefore, the polarization value is approximately $g_D/k_B T \ll 1$, and

$$\langle \hat{H}_D \rangle \sim N g_D^2 / k_B T. \quad (3.38)$$

In the normal phase of the liquid ^3He , the direction of spin vector and the orbital angular momentum are completely random. There is no particular relationship between these vectors.

In the ordered phase ($T < T_A$), the directions of these vectors are still completely random, but all pairs have the same *relative* angles

$$\langle \mathbf{S} \rangle = 0, \quad \langle \mathbf{L} \rangle = 0, \quad (3.39)$$

$$\langle \mathbf{L} \times \mathbf{S} \rangle \neq 0. \quad (3.40)$$

Furthermore, all the Cooper pairs are in the same spin and orbital state. Therefore, \hat{H}_0 forces all pairs to behave similarly, and thus we find (as was found in Ref. [7])

$$\langle \hat{H}_D \rangle \sim Ng_D \sim 10^{-3} \text{ ergs/cm}^3. \quad (3.41)$$

3.7 Microscopic spin dynamics (schematic)

We consider the two important basic variables, the total spin \mathbf{S} and the orientation $\boldsymbol{\theta}$ of the spins of the Cooper pairs. By using *hydrodynamic (Born-Oppenheimer) approximation*, the Hamiltonian can be expressed as

$$\hat{H} = \hat{H}_0(\mathbf{S}) + \hat{H}_D(\boldsymbol{\theta}). \quad (3.42)$$

The set of semiclassical equations of motion can then be written as follows:

$$\frac{d\boldsymbol{\theta}}{dt} = \frac{\partial \langle \hat{H}_0 \rangle}{\partial \mathbf{S}} = H_{\text{ext}} - \chi^{-1} \mathbf{S}, \quad (3.43)$$

$$\frac{d\mathbf{S}}{dt} = \mathbf{S} \times H_{\text{ext}} - \frac{\partial \langle \hat{H}_D \rangle}{\partial \boldsymbol{\theta}}. \quad (3.44)$$

The last term of Eq. (3.44) expresses the dipole torque acting on the spin. From these equations, we can show that the linear NMR behavior is completely determined by eigenvalues of

$$\Omega_{ij}^2 \equiv \frac{\partial^2 \langle H_D \rangle}{\partial \theta_i \partial \theta_j}. \quad (3.45)$$

We can “fingerprint” A and B phases by NMR [2, 5]! In the ABM phase, we get a single resonance line. In the planer phase, alternatively, we get split resonances. Thus, these two phases can be easily resolved by the NMR experiments. The BW is much more interesting. The original BW state is $\mathbf{L} = -\mathbf{S}$, i.e., $\mathbf{J} = 0$. However, to minimize the dipole energy, the dipole torque rotates $\mathbf{d}(\hat{\mathbf{k}})$ by the angle of $\cos^{-1}(-1/4) = 104^\circ$ around the axis $\hat{\boldsymbol{\omega}}$. This means that the relative orientation of \mathbf{L} and \mathbf{S} is changed and \mathbf{J} no longer has a unique value. Under an external magnetic field, the “best” choice of this axis $\hat{\boldsymbol{\omega}}$ is parallel to H_{ext} . Thus, once θ is settled on its equilibrium value 104° , any further twisting perpendicular to $\hat{\boldsymbol{\omega}}$ is, to linear order, simply equivalent to a change in $\hat{\boldsymbol{\omega}}$ with θ fixed. Therefore, this twisting cannot give rise to a dipole torque, and there is *no* shift in transverse resonance. It only shifts the finite-frequency *longitudinal resonance*⁵.

⁵This shift in the longitudinal resonance also appears in the ABM phase.

3.8 Illustration of NMR behavior: A phase longitudinal resonance

Throughout the experiment, \mathbf{d} lies in the xy -plane (but may rotate), and we keep the orbital part of the pair wave function fixed. The spin part of the pair wave function is

$$\Psi_N(t) \approx (\exp(i\Delta\phi(t)/2) |\uparrow\uparrow\rangle + \exp(-i\Delta\phi(t)/2) |\downarrow\downarrow\rangle)^{N/2}, \quad (3.46)$$

where $\Delta\phi$ is the relative phase between $|\uparrow\uparrow\rangle$ and $|\downarrow\downarrow\rangle$. Note that this state is a coherent superposition of $|\uparrow\uparrow\rangle$ and $|\downarrow\downarrow\rangle$, not the mixed state. The variable canonically conjugate to $\Delta\hat{\phi}$ is the z -component of total (not Cooper-pair) spin \hat{S}_z , and the canonical commutation relation is defined as

$$[\hat{S}_z, \Delta\hat{\phi}] = 2i. \quad (3.47)$$

The dipole interaction does not conserve spin and scatters from $|\uparrow\uparrow\rangle$ to $|\downarrow\downarrow\rangle$ (and vice versa). Therefore, this interaction depends on the relative phase $\Delta\hat{\phi}$ as

$$\hat{H}_D = -\frac{g_D}{4} \cos\Delta\hat{\phi}. \quad (3.48)$$

In the adiabatic approximation, the polarization energy is

$$\hat{H}_0 = \hat{S}_z^2/2\chi - \hat{S}_z H_{\text{ext}}(t). \quad (3.49)$$

Equations (3.47)-(3.49) show the analogy with a simple quantum pendulum (Fig. 3.8), with the following correspondence:

$$\Delta\hat{\phi} \rightarrow \theta \text{ (the angle of pendulum with vertical),}$$

$$\hat{S}_z \rightarrow L \text{ (the angular momentum).}$$

Equations (3.47)-(3.49) define the problem of a (driven) simple quantum pendulum. Generally, in the real-life experiments and in the semiclassical limit, we can treat $S_z(t)$ and $\Delta\phi(t)$ as classical variables. The canonical equations for these classical variables can be written as

$$\frac{dS_z}{dt} = -\frac{\partial H}{\partial(\Delta\phi)} = -\frac{g_D}{2} \sin\Delta\phi, \quad (3.50)$$

$$\frac{d}{dt}(\Delta\phi) = \frac{\partial H}{\partial S_z} = 2 \left(\frac{S_z}{\chi} - H_{\text{ext}}(t) \right). \quad (3.51)$$

3.9 Digression: possibility of the “fragmented” state

The standard statement in a superconducting (superfluid) state is that the global $U(1)$ symmetry is spontaneously broken, which is experimentally untestable! What is really

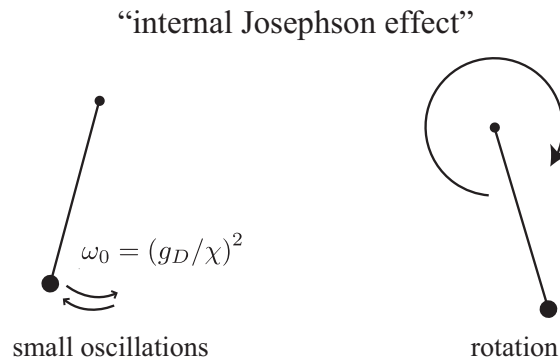


Fig. 3.8. The analogy with a simple quantum pendulum.

important is that the *relative* symmetry: relative phase of $|\uparrow\uparrow\rangle$ and $|\downarrow\downarrow\rangle$. We assume (cf. Eq. (3.46))

$$\Psi_N \sim (\exp(i\Delta\phi/2) |\uparrow\uparrow\rangle + \exp(-i\Delta\phi/2) |\downarrow\downarrow\rangle)^{N/2}, \quad (3.52)$$

where $\Delta\phi$ the definite relative phase, and essentially assume to be a classical value and we ignore its quantum fluctuations. Why can we neglect the fluctuation? We can ask the same question in a different manner. We can also think about the possibility for

$$\Psi_N \sim (|\uparrow\uparrow\rangle)^{N_\uparrow} (|\downarrow\downarrow\rangle)^{N_\downarrow}. \quad (3.53)$$

This state has no definite phase relation between $|\uparrow\uparrow\rangle$ and $|\downarrow\downarrow\rangle$, while it has a definite relative number

$$S_z = N_\uparrow - N_\downarrow. \quad (3.54)$$

Why we do not consider this possibility?

The answer is as follows. We consider the Hamiltonian

$$\hat{H} = \frac{\hat{S}_z^2}{2\chi} - \frac{g_D}{4} \cos\Delta\hat{\phi}, \quad (3.55)$$

in two cases: (a) $g_D \gg \chi^{-1}$, and (b) $g_D \ll \chi^{-1}$. In the case (a), the dominant term in Eq. (3.55) is the second term. Therefore $\Delta\phi$ is fixed, and S_z fluctuates. In contrast, in the case (b), the first term is dominant. Thus, S_z is fixed, and $\Delta\phi$ fluctuates. However in general $g_D \approx N$ and $\chi^{-1} \approx N^{-1}$. In the thermodynamic limit, the case (a) is always satisfied, and we need $N < 10^9$ to realize the latter⁶. While the case (a) corresponds to an ordinary BEC, the case (b) corresponds to the “fragmented” BEC, which we discuss in details in Sec. 4.2.

⁶In the ordinary bulk liquid, this condition is impossible. However, we can prepare a rather small system, e.g. in small inclusions of a liquid ^3He in a solid ^4He , so that the case (b) may be observed in such a case.

3.10 Superfluid ^3He : supercurrents, textures, and defects

It is important that the pair wave function is expressed by the spin orientation vector and orbital orientation vector. Before starting our discussions on the supercurrent, let us briefly summarize the behaviors of the spin and orbital orientation vectors in the uniform system. In the absence of any perturbation, the A phase is characterized by the spin orientation vector \mathbf{d} and orbital orientation vector $\boldsymbol{\ell}$, which in a uniform situation are in arbitrary directions. Similarly, the B phase is characterized by the rotation $\hat{\mathbf{R}}$ away from the $^3\text{P}_0$ state; $\hat{\mathbf{R}}$ again is arbitrary.

The dipole force (dominant perturbation in bulk) tends, in the A phase, to orient \mathbf{d} parallel (or anti-parallel) to $\boldsymbol{\ell}$ because the end-over-end configuration is formed by $\boldsymbol{\ell}$ lying perpendicular to the spins involved, which means $\boldsymbol{\ell}$ lies in parallel to \mathbf{d} , but the common orientation is still arbitrary. In the B phase, it fixes the angle of rotation \mathbf{R} to be $\cos^{-1}(-1/4) = 104^\circ$, but the rotation axis $\boldsymbol{\omega}$ itself is still arbitrary. The external magnetic field \mathbf{H}_{ext} tends to orient \mathbf{d} perpendicular to \mathbf{H}_{ext} in the A phase, while it tends to orient $\hat{\boldsymbol{\omega}}$ parallel to \mathbf{H}_{ext} in the B phase.

What happens if the orientation vectors vary in space? It turns out that superfluid currents appear. In this section, we briefly review the properties of the supercurrents in the superfluid ^3He and phenomena related to them.

3.10.1 Supercurrents

When the order parameter changes in space, there appears a current, in general. Since there are more than one degree of freedom in the triplet superfluid, there can be some non-trivial currents. We consider three situations where the order parameter varies in space. The simplest one is the situation where \mathbf{d} and $\boldsymbol{\ell}$ (or $\hat{\boldsymbol{\omega}}$) are fixed, and the only thing that can vary is the overall phase ϕ . In such a case, an ordinary superfluid mass flow similar to that in ^4He appears

$$\mathbf{v}_s(\mathbf{R}) = \frac{\hbar}{2m} \nabla \phi(\mathbf{R}), \quad (3.56)$$

where $2m$ comes from the formation of the Cooper pairs. The only special point is that in the A phase the superfluid density $\boldsymbol{\rho}_s$ is a tensor with its axis defined by $\boldsymbol{\ell}$ ($\rho_{s\perp} > \rho_{s\parallel}$, since more quasi-particles are excited parallel to $\boldsymbol{\ell}$ since there are nodes in the $\pm\boldsymbol{\ell}$ direction in the ABM state. See Sec. 3.2.1.). Just as in the superfluid ^4He , we can also expect vortices to appear.

The second case is where ϕ and $\boldsymbol{\ell}$ are fixed but \mathbf{d} is spatially varying (or ϕ fixed but $\hat{\boldsymbol{\omega}}$ varying). In this situation, the up-spin Cooper pairs are flowing in the different direction to the down-spin Cooper pairs. Therefore, there is no mass current, but there is a spin supercurrent.

The final case is where in the A phase \mathbf{d} is fixed but $\boldsymbol{\ell}$ (and ϕ) varies in space. This situation is more complicated than the others. Since $F(\mathbf{r}) \sim f(r)\sin\theta_k\exp(i\phi_k)$, the overall phase rotation is equivalent to the rotation around the $\boldsymbol{\ell}$ -axis. However, if $\boldsymbol{\ell}$ varies in space, such rotations are *not holonomic*, and $\nabla \times \mathbf{v}_s \neq 0$ in general [8].

3.10.2 Mermin–Ho vortex and topological singularities

If we continue to define \mathbf{v}_s in terms of infinitesimal rotations around $\boldsymbol{\ell}$, i.e., by

$$\mathbf{v}_s \equiv \frac{\hbar}{2m} \nabla \phi, \quad (3.57)$$

then we find

$$\nabla \times \mathbf{v}_s = \frac{\hbar}{4m} \sum_{ijk} \epsilon_{ijk} \ell_i \nabla \ell_j \times \nabla \ell_k. \quad (3.58)$$

This leads to the possibility of “coreless” vortices (Fig. 3.9.). If we start from a situation in which $\hat{\boldsymbol{\ell}}$ is constant (say parallel to $\hat{\mathbf{z}}$) in space and the condensate phase has a circulation of 4π around the annulus, then by rotating $\boldsymbol{\ell}$ locally around an axis in the xy -plane which is perpendicular to the radial vector at that point, we achieve a fixed state in which $\boldsymbol{\ell}$ is everywhere antiparallel to the z -axis and the phase is constant. Thus, we have achieved the phase which has no circulation around the contour in the middle.

A topological insulator in two dimensions is basically under the exactly same situation we get now. A very useful tool for analyzing the possible varieties of texture in $^3\text{He-A}$ and B is the branch of mathematics known as the homotopy theory.

Energetics will always pin $\boldsymbol{\ell}$ normal to the walls and experiments seem to be consistent with this hypothesis. For the A phase in a simply connected geometry, topological argument shows the ABM phase order parameter must have at least two topological singularities somewhere on the surface (most likely boojums, see Fig. 3.10.), and also, apart from these topological singularities, have all sorts of nonsingular textures (of $\mathbf{d}, \boldsymbol{\ell}, \boldsymbol{\omega}$).

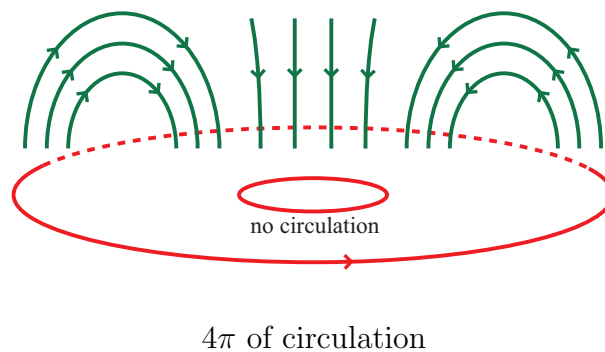


Fig. 3.9. Schematic illustration of the Mermin–Ho vortex.

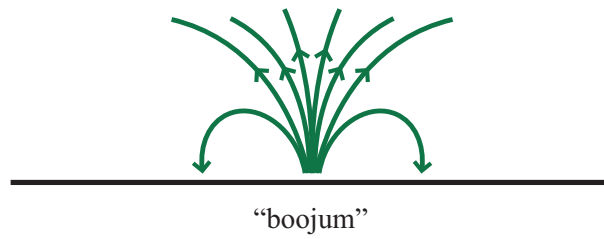


Fig. 3.10. Schematic illustration of the boojum texture.

References

- [1] D. Vollhardt and P. Wölfle, *The superfluid phases of helium 3* (CRC, 1990).
- [2] J. C. Wheatley, *Rev. Mod. Phys.* **47**, 415 (1975).
- [3] Y. A. Vdovin, *Application of Methods of Quantum Field Theory to Problems of Many Particles* (Gosatomizdat, Moscow, 1963).
- [4] R. Balian and N. R. Werthamer, *Phys. Rev.* **131**, 1553 (1963).
- [5] A. J. Leggett, *Rev. Mod. Phys.* **47**, 331 (1975).
- [6] P. W. Anderson and W. F. Brinkman, *Phys. Rev. Lett.* **30**, 1108 (1973).
- [7] *Question from a student:* Does this estimation depend on whether the anisotropic Fermi superfluid has the macroscopic angular momentum or not?
Answer: It is thought that all pairs away from the Fermi surface are independent as regards to their spins. Therefore, only the few close to the Fermi surface can affect this estimation. So the answer is “it is the same”.
- [8] *Question from a student:* What kind of current is it? It is neither superfluid mass current nor superfluid spin current.
Answer: No. It turns out that if ℓ is varying in space, in general there is a mass current, but the formula for it is more complicated.

Lec. 4 Definition and diagnostics of “exotic” superconductivity

What do we mean by “exotic” superconductors? To some extent, it is a matter of convention or a definition, but crudely speaking, one can isolate quite a large number of properties, which are common to the old-fashioned superconductors and not found in some of recent ones. The principal and common characteristics of the “classical”, or old-fashioned superconductors are

- (1) $T_c \leq 25$ K.
- (2) The normal state is well described by the Fermi-liquid theory.
- (3) The mechanism of Cooper-pair formation is the phonon-induced attraction.
- (4) The symmetry of the order parameter (the pair wave function) is the s -wave.

All of these properties are common to a wide class of materials, such as aluminum, lead, tin, etc. In fact, until 1986 one could say that all the superconductors have the transition temperature T_c less than 25 K, and they are all classical superconductors. Note that there are two exceptions to this “definition”: BKBO and MgB₂. BKBO and MgB₂ have transition temperatures $T_c \simeq 30$ K, and $T_c \simeq 40$ K, respectively, much higher T_c than that for the typical classical superconductors. Except for this extraordinarily high T_c , however, they seem to behave exactly like classical BCS superconductors, so we rather often classify them as classical superconductors.

In addition to the above four characteristics, there are three other properties which are usually but not always satisfied among many superconductors:

- (5) The crystal structure is essentially three-dimensional.
- (6) The superconducting state is not close to other broken symmetry phases (e.g., antiferromagnetic).
- (7) For alloys, the superconductivity is not particularly sensitive to stoichiometry.

“Exotic” superconductors, in contrast, fail to satisfy at least one of (1)-(7), as we can see from Table 4.1. The cuprates are the most non-BCS like of all the superconductors known today. That is why I will spend most of the time of the lectures to the cuprates.

Table 4.1. The list of the common or usual properties for the superconductors.

Property	Classical	Heavy-fermions	Organics	Ruthenates	Fullerenes	Ferropnictides	Cuprates
1. $T_c < 25$ K	(√)	√	√	√	×	×	×
2. Fermi liquid normal state	√	×	×	×	√	(√)	×
3. Phonon mechanism	√	×	?	?	√	×	×
4. Order parameter s -wave	√	?	?	×	√	(×)	×
5. Crystal structure 3D	√	√	×	×	×	×	×
6. No neighboring transition	√	×	√	√	√	×	×
7. Stoichiometry-insensitive	√	√	√	√	×	×	×
Maximum T_c [K]	40	2	15	2	40	56	150

How do we know whether the above properties are satisfied? The conditions for (1) the transition temperature, (5) crystal structure, (6) broken-unbroken symmetry phases, and (7) stoichiometry can be checked more or less by direct inspections. Whether (2) the normal state is well described by the Fermi liquid theory can be seen by Fermi liquid like signals: the specific heat is linear in temperature, the conductivity satisfies Bloch-Grüneisen formula, etc. Therefore, one can judge more or less from experiments and a little theory.

How about (3) and (4), the mechanism of the Cooper pair formation and the symmetry of the pair? I think the most obvious evidence for the phonon-induced attraction is the isotope effect, which can be seen from the quantitative agreement between the BCS theory and the experiment. A valid evidence for the symmetry of the pair to be s -wave can be obtained if many experimental quantities such as the specific heat fall off exponentially with temperature. This shows that the gap must have non-zero value everywhere on the Fermi surface. The certain and most obvious way that can happen is the pairs forming the isotropic state.

4.1 Diagnostics of the non-phonon mechanism

4.1.1 Absence of isotope effect

How do we find the mechanism to be phonon or non-phonon induced ones? The first consideration, as you might expect, has to do with the isotope effect. Let us have a brief review of the isotope effect in the BCS theory.

In the original BCS theory, the transition temperature is proportional to $M^{-1/2}$, where M is the isotope mass. This can be seen easily by assuming a constant interaction around the shell of the Fermi surface, recalling that the width of that shell is proportional to the Debye frequency, which is proportional to $M^{-1/2}$.

A theory of T_c for a realistic phonon-plus-Coulomb interaction is complicated and requires solutions of Eliashberg equations [1, 2]. McMillan [3] argued that a good analytic approximate solution of the Eliashberg equation is

$$T_c = \left(\frac{\Theta_D}{1.45} \right) \exp \left(- \left[\frac{1.04(1 + \lambda)}{\lambda - \mu^*(1 + 0.62\lambda)} \right] \right), \quad (4.1)$$

$$\lambda \equiv 2 \int_0^{\omega_D} \frac{\alpha^2(\omega)F(\omega)}{\omega} d\omega, \quad (4.2)$$

where $\alpha(\omega)$ is the phonon coupling function and $F(\omega)$ is the phonon density of state, and Θ_D is the Debye temperature. The quantity λ is proportional to the static local compressibility of the lattice, which is independent of the isotope mass M since it is irrelevant to the ionic motion. Then where, apart from the parameter Θ , does the isotope effect comes in? In this formula μ^* represents the Coulomb pseudopotential defined as

$$\mu^* \equiv \frac{N(0)\langle \hat{V}_c \rangle}{1 + N(0)\langle \hat{V}_c \rangle \ln(\varepsilon_F/\Theta_D)}, \quad (4.3)$$

where $\langle \hat{V}_c \rangle$ is the averaged Coulomb interaction. In an approximation of ignoring Θ_D -dependence of μ^* , T_c is simply proportional to Θ_D and then proportional to $M^{-1/2}$. Therefore, the “isotope exponent” $\alpha_I \equiv -\frac{\partial(\ln T_c)}{\partial(\ln M)}$ becomes

$$\alpha = \frac{1}{2}, \quad (4.4)$$

which is just the “textbook” BCS result.

If we take into account the dependence of μ^* on Θ_D with the formula (4.3), the isotope exponent becomes

$$\alpha_I = \frac{1}{2} \left[1 - \frac{1.04\mu^{*2}(1 + \lambda)(1 + 0.62\lambda)}{[\lambda - \mu^*(1 + 0.62\lambda)]^2} \right] < \frac{1}{2}. \quad (4.5)$$

Thus even if μ^* is small, α_I can deviate appreciably from 0.5 (and can even be negative!) in the BCS theory. Crudely and qualitatively speaking, therefore, we can reasonably say the following things:

- $\alpha_I \simeq 0.5 \Rightarrow$ probably phonon-mediated;
- $\alpha_I \ll 0.5 \Rightarrow$ probably but not certainly non-phonon-mediated;
- $\alpha_I > 0.5 \Rightarrow$ possibly phonon-mediated but the BCS theory certainly is inapplicable (no cases known so far).

This is a fairly a standard argument, which is usually given in literatures. However the above argument does not take into account other possible ways in which isotopic substitution could modify T_c , such as lattice distortion. For example, let us substitute the deuterium ^2D into the hydrogen ^1H in a superconductor. Since the deuterium has much a smaller zero-point energy than the hydrogen, it tends to modify the lattice structure. Therefore, even if we see the large isotope effect, we must not conclude the interaction must be phonon-mediated. It is possible that something more sophisticated occurs.

4.1.2 Absence of phonon structure in tunneling I-V characteristics

Recall that in the BCS theory the gap equation takes the form

$$\Delta_{\mathbf{k}} = - \sum_{\mathbf{k}'} V_{\mathbf{k}\mathbf{k}'} \frac{\Delta_{\mathbf{k}'}}{2E_{\mathbf{k}'}}. \quad (4.6)$$

However, in a realistic theory of a phonon-mediated interaction, the interaction potential $V_{\mathbf{k}\mathbf{k}'}$, even in a normal state, is energy dependent:

$$V_{\mathbf{k}\mathbf{k}'} = |g_{\mathbf{k}\mathbf{k}'}|^2 \frac{\varepsilon_{\mathbf{k}'} + \omega_{\text{ph}}(\mathbf{k} - \mathbf{k}')}{(\varepsilon_{\mathbf{k}'} + \omega_{\text{ph}}(\mathbf{k} - \mathbf{k}'))^2 - \varepsilon_{\mathbf{k}}^2}. \quad (4.7)$$

In this situation, it turns out that we have to modify the BCS calculation by a little bit and need the Eliashberg theory [1, 2]. I think the Eliashberg equation is for many people very non-intuitive, but most people believe that it describes the electron-phonon interactions well. If one solves the Eliashberg equation, the “gap” (off-diagonal field) becomes frequency-(energy-)dependent $\Delta \rightarrow \Delta(\omega)$ (but nearly independent of momentum). At $T = 0$, the gap equation becomes

$$\begin{aligned} \Delta(\omega) = & \frac{1}{Z(\omega)} \int_0^\infty d\omega' \text{Re} \left\{ \frac{\Delta(\omega')}{(\omega'^2 - \Delta^2(\omega'))^{1/2}} \right\} \\ & \times \left\{ \int_0^\infty d\Omega \alpha^2(\Omega) F(\Omega) \frac{2(\omega' + \Omega)}{(\omega' + \Omega)^2 - \omega^2} - \mu^* \right\}. \end{aligned} \quad (4.8)$$

Here $Z(\omega)$ is the renormalization function, given by the second Eliashberg equation.

McMillan and Rowell [4] pointed out that if we actually look at a tunnel junction between superconductors and normal metals the differential tunnel conductance measures $\Delta(\omega)$ by

$$\frac{(\partial I / \partial V)_S}{(\partial I / \partial V)_N} = \text{Re} \left\{ \frac{\omega}{(\omega^2 - \Delta^2(\omega))^{1/2}} \right\}, \quad \hbar\omega = eV. \quad (4.9)$$

Using this Eliashberg equation, we can reconstruct $\alpha^2(\Omega)F(\Omega)$ from $\Delta(\omega)$ obtained in this tunneling experiment. On the other hand, the phonon density of state $F(\Omega)$ can be directly measured by the neutron scattering, and $\alpha(\Omega)$ can be obtained by the fairly well calculations. Therefore, we can compare $\alpha^2(\Omega)F(\Omega)$ obtained by these two different methods, and see whether they give a consistent value. For the BCS superconductors, these two are known to agree very well.

In a qualitative point of view, if the origin of Cooper pairing is the phonon-mediated attraction, then peaks in neutron scattering spectrum (i.e., in $F(\Omega)$) must be reflected in the tunneling I-V characteristic. Conversely, absence of such a characteristic usually implies the non-phonon mechanism.

Of the existing groups of the “exotic” superconductors, the alkali fullerenes and possibly the organics are the only ones where the mechanism seems to be the phonon-mediated one. All the other groups in the Table 4.1 have the evidence for the non-phonon mechanism.

4.2 General properties of the order parameter

4.2.1 Definition of the order parameter

Since the many-body wave function is unlikely to be the simple BCS type, to discuss this subject we need a more general definition of the order parameter or the pair wave function [5]. The works of the superfluidity and superconductivity are started off from an early work by Penrose and Onsager [6] on the superfluid ^4He . Here, we parallel the discussion on the superfluid ^4He and on the superconductors to get a general way to describe the pairing in the superconductors.

Consider the two-particle reduced density matrix

$$\begin{aligned} \rho_2(\mathbf{r}_1\sigma_1, \mathbf{r}_2\sigma_2 : \mathbf{r}'_1\sigma'_1, \mathbf{r}'_2\sigma'_2 : t) &\equiv \langle \hat{\psi}_{\sigma_1}^\dagger(\mathbf{r}_1t) \hat{\psi}_{\sigma_2}^\dagger(\mathbf{r}_2t) \hat{\psi}_{\sigma'_2}(\mathbf{r}'_2t) \hat{\psi}_{\sigma'_1}(\mathbf{r}'_1t) \rangle \\ &= N(N-1)p_s \sum_{s, \sigma_3 \dots \sigma_N} \int d^3\mathbf{r}_3 \dots d^3\mathbf{r}_N \\ &\quad \Psi_S^*(\mathbf{r}_1\sigma_1, \mathbf{r}_2\sigma_2, \dots, \mathbf{r}_N\sigma_N : t) \Psi_S(\mathbf{r}'_1\sigma'_1, \mathbf{r}'_2\sigma'_2, \mathbf{r}_3\sigma_3 \dots, \mathbf{r}_N\sigma_N : t). \end{aligned} \quad (4.10)$$

Here p_s is the probability of the occupation of the many body state s . Crudely speaking, this is the best possible representation of “the effective behavior of two electrons averaged over behavior of remaining $N-2$ ”. Note all two-particle expectation values can be expressed in terms of ρ_2 . For example, if we consider the two-particle potential energy

$$\hat{V} \equiv \frac{1}{2} \sum_{ij} V(\hat{\mathbf{r}}_i - \hat{\mathbf{r}}_j), \quad (4.11)$$

its expectation value is given as

$$\langle \hat{V} \rangle(t) = \sum_{\sigma_1\sigma_2} \int \int d^3\mathbf{r}_1 d^3\mathbf{r}_2 V(\mathbf{r}_1 - \mathbf{r}_2) \rho_2(\mathbf{r}_1\sigma_1 \mathbf{r}_2\sigma_2 : \mathbf{r}_1\sigma_1 \mathbf{r}_2\sigma_2 : t). \quad (4.12)$$

Furthermore, the one-particle reduced density matrix can be given by

$$\rho_1(\mathbf{r}\sigma, \mathbf{r}'\sigma' : t) = \frac{1}{N} \sum_{\sigma_2} \int d^3\mathbf{r}_2 \rho_2(\mathbf{r}\sigma, \mathbf{r}_2\sigma_2 : \mathbf{r}'\sigma', \mathbf{r}_2\sigma_2 : t) + O(N^{-2}). \quad (4.13)$$

Thus, basically, if we know the two-particle reduced density matrix, we know all the physically meaningful quantities of the system. This, of course, does not mean we know all about the system. It is possible that the many-body wave functions are totally different but still give the same reduced density matrix¹, and for a certain physical quantity they give different values. However, for most practical purposes in the traditional condensed matter physics, the two-particle density matrix really gives all we need to know.

¹I know no particular case this occurs, but, for example, in the topological quantum computing that question can arise.

As a function of the variables $(\mathbf{r}_1\sigma_1, \mathbf{r}_2\sigma_2)$, the two-particle reduced density matrix ρ_2 is Hermitian by construction. Therefore, it can be diagonalized, i.e., always written in the form

$$\rho_2(\mathbf{r}_1\sigma_1, \mathbf{r}_2\sigma_2 : \mathbf{r}'_1\sigma'_1, \mathbf{r}'_2\sigma'_2 : t) = \sum_i n_i(t) \chi_i^*(\mathbf{r}_1\sigma_1, \mathbf{r}_2\sigma_2 : t) \chi_i(\mathbf{r}'_1\sigma'_1, \mathbf{r}'_2\sigma'_2 : t), \quad (4.14)$$

$$\sum_i n_i(t) = N(N-1), \quad (4.15)$$

where $\{\chi_i\}$ is an orthonormal set $(\chi_i, \chi_j) = \delta_{ij}$. Note that as Yang proved [5], the maximum value of any one n_i is $O(N)$, not $O(N^2)$. Another thing to notice is that ρ_2 must be antisymmetric under $(\mathbf{r}_1\sigma_1 \rightleftharpoons \mathbf{r}_2\sigma_2)$ etc. due to Fermi statistics, so must be eigenfunctions χ_i . The two-particle density matrix is a very intuitive way of looking at a behavior of the many-body system. If we just take two particles at random and look at the behavior averaged over all the other $N-2$ particles, then we have a certain probability proportional to $n_i(t)$ that we find the particular two-particle state of this form.

From now on we assume the states to be time-independent since we would like to consider the equilibrium state. In principle, there are three possibilities:

1. All eigenvalues $n_i \sim o(1)$ (normal state) (e.g., free Fermi gas).
2. Two or more eigenvalues are $O(N)$, and the rest eigenvalues are $o(1)$ (“fragmented” pseudo-BEC, usually disregarded²).
3. Only one eigenvalue is $O(N)$, and the rest eigenvalues are $o(1)$ (“simple” pseudo-BEC, i.e., Cooper pairing).

In the case 3, there is the “special” state which has the largest eigenvalue of ρ_2 . Let us denote the largest eigenvalue as $N_0 \sim O(N)$, and define

$$F(\mathbf{r}_1\sigma_1, \mathbf{r}_2\sigma_2) \equiv \sqrt{N_0} \chi_0(\mathbf{r}_1\sigma_1, \mathbf{r}_2\sigma_2), \quad (4.16)$$

which is the order parameter or the pair wave function. For the BCS case this definition reduces to the one given in Lec. 2. Note that from the orthonormality condition on the χ_i , we have

$$\sum_{\sigma_1\sigma_2} \int d^3\mathbf{r}_1 d^3\mathbf{r}_2 |F(\mathbf{r}_1\sigma_1, \mathbf{r}_2\sigma_2)|^2 = N_0. \quad (4.17)$$

Therefore, N_0 can be regarded as the “number of Cooper pairs” just as in the BCS case.

A possible alternative definition of F is

$$F(\mathbf{r}_1\sigma_1, \mathbf{r}_2\sigma_2) \equiv \langle N + 2 | \hat{\psi}_{\sigma_1}^\dagger(\mathbf{r}_1) \hat{\psi}_{\sigma_2}^\dagger(\mathbf{r}_2) | N \rangle, \quad (4.18)$$

²See discussion in Sec. 3.9 of spin triplet pairing in the limit $g_D \rightarrow 0$. For ${}^3\text{He}$, if the dipole energy and the number of the particles are small enough, the Cooper pairs are not the coherent superposition of $\uparrow\uparrow$ and $\downarrow\downarrow$ but half of them are $\uparrow\uparrow$ and the half are $\downarrow\downarrow$. Such state is a fragmented state. However, this is unusual because non-fragmented states almost always take over in the thermodynamic limit.

where $|N\rangle, |N+2\rangle$ are ground states (often “abbreviated” $\langle\hat{\psi}_{\sigma_1}^\dagger(\mathbf{r}_1)\hat{\psi}_{\sigma_2}^\dagger(\mathbf{r}_2)\rangle$ with implicit assumption of N -non-conservation).

If we define the center of mass coordinate and the relative coordinate by

$$\mathbf{R} = \frac{\mathbf{r}_1 + \mathbf{r}_2}{2}, \quad \mathbf{r} = \mathbf{r}_1 - \mathbf{r}_2, \quad (4.19)$$

then

$$F \equiv F(\mathbf{R}, \mathbf{r}, \sigma_1, \sigma_2). \quad (4.20)$$

For this lecture, we will usually be interested in the case in which F is independent of \mathbf{R} , i.e.,

$$F = F(\mathbf{r}, \sigma_1, \sigma_2). \quad (4.21)$$

This implies the translational invariance of the system. This is not quite accurate in a crystal, but crudely speaking, even for that case we will usually be more interested in the dependence on the relative coordinate than in dependence of the center of mass coordinate. Talking about the “symmetry of the order parameter”, we mean the dependence of F on $\mathbf{r}, \sigma_1, \sigma_2$.

4.2.2 Order parameter in a crystal³

For the moment, I am going to assume we can forget about spin-orbit coupling. I will come back to that at the end of this lecture. It turns out forgetting about the spin-orbit coupling does make the problem considerably simpler. In addition, we restrict ourselves for the moment to the case where only a single band⁴ intersects the Fermi surface⁵.

Let us take the Fourier transform of $F_{\alpha\beta}(\mathbf{r})$ in the Bloch basis, i.e.,

$$F_{\alpha\beta}(\mathbf{k}) \equiv \langle a_{\mathbf{k}\alpha}^\dagger a_{-\mathbf{k}\beta}^\dagger \rangle = -F_{\beta\alpha}(-\mathbf{k}), \quad (4.22)$$

where \mathbf{k} is the Bloch wave (not plane wave) and the last relation follows from the Fermi statistics. Because we neglect spin-orbit coupling, we can deal with the spin and the orbital wave function separately, i.e.,

$$F_{\alpha\beta}(\mathbf{k}) = s_{\alpha\beta} f(\mathbf{k}), \quad (4.23)$$

where $f(\mathbf{k})$ is the orbital wave function and $s_{\alpha\beta}$ is the spin wave function. As you know, we can adopt $s(\ell_s, m_s)_{\alpha\beta}$ ($\ell_s = 0$ or 1 , $m_s \leq \ell_s$) as a basis of the spin wave function,

³For exhaustive discussion, see Ref. [7].

⁴You might object here that I am talking implicitly in free electron language. This is indeed a very delicate point but I assume we can get away with this. The evidence is in certain exotic superconductors we can. Thus the idea of identifying different bands, even though it is, strictly speaking, a sort of non-electron kinds of scenario, still makes sense mostly.

⁵Not true for Sr_2RuO_4 , ferropnictides. etc.

where $s(\ell, m)_{\alpha\beta}$'s are defined as

$$\begin{cases} s(1, 1)_{\alpha\beta} &= \delta_{\alpha\uparrow}\delta_{\beta\uparrow}, \\ s(1, 0)_{\alpha\beta} &= \frac{1}{\sqrt{2}}(\delta_{\alpha\uparrow}\delta_{\beta\downarrow} + \delta_{\alpha\downarrow}\delta_{\beta\uparrow}), \\ s(1, -1)_{\alpha\beta} &= \delta_{\alpha\downarrow}\delta_{\beta\downarrow}, \\ s(0, 0)_{\alpha\beta} &= \frac{1}{\sqrt{2}}(\delta_{\alpha\uparrow}\delta_{\beta\downarrow} - \delta_{\alpha\downarrow}\delta_{\beta\uparrow}). \end{cases} \quad (4.24)$$

Note that $s(1, m_s)_{\alpha\beta}$ is symmetric, while $s(0, 0)_{\alpha\beta}$ is antisymmetric. By combining this fact with Eq. (4.22), we can conclude

$$\begin{aligned} s_{\alpha\beta}: \text{spin-singlet} &\Leftrightarrow f(\mathbf{k}): \text{even parity}, \\ s_{\alpha\beta}: \text{spin-triplet} &\Leftrightarrow f(\mathbf{k}): \text{odd parity}. \end{aligned}$$

Spin symmetry

In the spin-singlet case,

$$F_{\alpha\beta}(\mathbf{k}) = -(i\sigma_y)_{\alpha\beta}f(\mathbf{k}) = -\sqrt{2}s(0, 0)_{\alpha\beta}f(\mathbf{k}) \quad (4.25)$$

with $f(-\mathbf{k}) = f(\mathbf{k})$. In the spin-triplet case, we can define, just as for ${}^3\text{He}$,

$$\mathbf{d}(\mathbf{k}) \equiv -(i\sigma_y\boldsymbol{\sigma})_{\alpha\beta}F_{\beta\alpha}(\mathbf{k}) = -\text{tr}[(i\sigma_y\boldsymbol{\sigma})F(\mathbf{k})]. \quad (4.26)$$

In the last equation, we regard $F_{\alpha\beta}(\mathbf{k})$ as a two by two square matrix. Inversely, we can represent $F_{\alpha\beta}(\mathbf{k})$ in terms of $\mathbf{d}(\mathbf{k})$:

$$\begin{aligned} F_{\alpha\beta}(\mathbf{k}) &= i[\mathbf{d}(\mathbf{k}) \cdot \boldsymbol{\sigma}\sigma_y]_{\alpha\beta}/2 \\ &= \frac{1}{2}[(-d_1(\mathbf{k}) + id_2(\mathbf{k}))s(1, 1)_{\alpha\beta} + \sqrt{2}d_3(\mathbf{k})s(1, 0)_{\alpha\beta} + (d_1(\mathbf{k}) + id_2(\mathbf{k}))s(1, -1)_{\alpha\beta}], \end{aligned} \quad (4.27)$$

with $\mathbf{d}(-\mathbf{k}) = -\mathbf{d}(\mathbf{k})$. If $\mathbf{d}(\mathbf{k})$ is real, which is true for most of the cases we are interested in, $\mathbf{d}(\mathbf{k})$ represents the direction along which pair $(\mathbf{k}, -\mathbf{k})$ has $S_z = 0$. (i.e., $\mathbf{d} \cdot \mathbf{S}|F\rangle = 0$.)

In principle, we could take linear combinations of spin-singlet and triplet states. However, in the absence of spin-orbit coupling, we have to chose very pathological values of the parameters to realize such an ground state. Therefore, at least in the absence of spin-orbit coupling, the question of spin symmetry is very straightforward.

Orbital symmetry

What about the orbital symmetry? There is a rather delicate point here. Strictly speaking, once we get away from the simple BCS-like picture, we should not really assume the quantity $F_{\alpha\beta}(\mathbf{k})$, which is the order parameter or the effective wave function of pairs,

has much to do with the energy gap $\Delta_{\alpha\beta}(\mathbf{k})$. However, let us assume, at least as a minimal assumption, that the dependence of $F_{\mathbf{k}}$ on the magnitude of \mathbf{k} is not qualitatively different from the BCS form $\Delta_{\mathbf{k}}/2E_{\mathbf{k}}$, where $\Delta_{\mathbf{k}}$ is roughly independent of $|\mathbf{k}|$. If that is true, then the angular dependence of $F_{\alpha\beta}(\mathbf{k})$ on the Fermi surface is much the same as that of $\Delta_{\alpha\beta}(\mathbf{k})$.

The crucial point is that the possible forms of $F_{\mathbf{k}}$ are classified by transformation properties under the crystal symmetry operations, such as the reflection at $\mathbf{k} = 0$, rotation around a certain axis. If $F_{\mathbf{k}}$ transforms according to the identity representation, we call the superconductivity is “conventional”, or “s-wave” like (need not to be totally spherical since in a crystal we have only discrete rotational operation), otherwise “exotic”.

4.3 Diagnostics of the symmetry of the order parameter

Let me move on to the question: how one can diagnose the symmetry of the order parameter? It is difficult to obtain the whole form of the order parameter only by a single type of measurements. Each kind of experiments provides only partial information, such as its spin state, orbital state, node, etc. In this section, I introduce various methods to determine the symmetry of the order parameter.

4.3.1 Diagnostics of the spin state

The spin susceptibility (via the Knight shift)

The simplest way to observe the spin state of electrons in solid is to measure the Pauli susceptibility via the Knight shift. As shown in Fig. 4.1 (a), for the spin-singlet state, just like the BCS one, χ/χ_n falls to 0 as $T \rightarrow 0$ because the opposite spins are pairing up and it takes a finite pairing energy to break the pairs. We can apply the same argument to the ESP triplet states with $\mathbf{d}(\mathbf{n}) \parallel \mathbf{H}$. However, for the ESP triplet states with $\mathbf{d}(\mathbf{n}) \perp \mathbf{H}$, χ/χ_n remains approximately constant. To understand this behavior, let us take the ESP state with $\mathbf{d}(\mathbf{k}) = d(\mathbf{k})\hat{e}_z$ as an example. From Eq. (4.27), the pair wave function is given by

$$F_{\alpha\beta}(\mathbf{k}) = \frac{d(\mathbf{k})}{2}(\delta_{\alpha\uparrow z}\delta_{\beta\downarrow z} + \delta_{\alpha\downarrow z}\delta_{\beta\uparrow z}). \quad (4.28)$$

Therefore, if we apply a magnetic field in the z -direction ($\mathbf{d}(\mathbf{n}) \parallel \mathbf{H}$), we have to sacrifice the pairing energy to gain the Zeeman energy, from the reason I explained just above. However, if we change the spin axis from z to x , *the same state* can be re-expressed as

$$F'_{\alpha\beta}(\mathbf{k}) = \frac{d(\mathbf{k})}{2}(\delta_{\alpha\uparrow x}\delta_{\beta\uparrow x} - \delta_{\alpha\downarrow x}\delta_{\beta\downarrow x}). \quad (4.29)$$

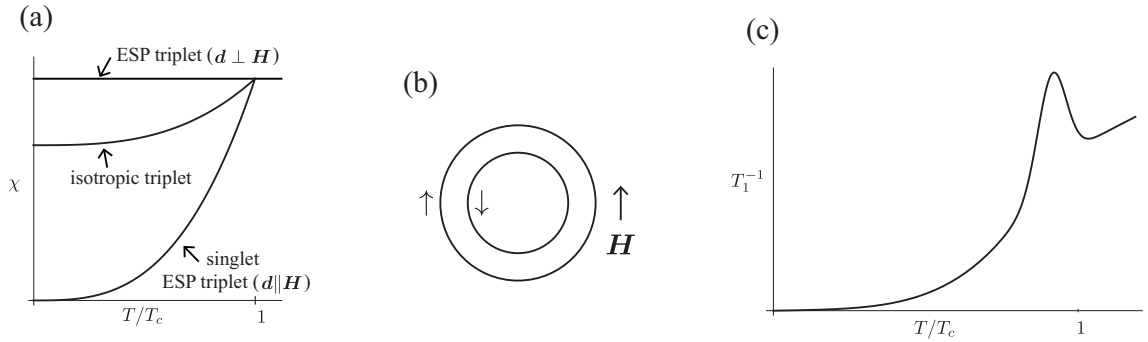


Fig. 4.1. (a) The Pauli spin susceptibility via the Knight shift. (b) A magnetic field generates a difference on the radius of the Fermi sphere between up and down spins. (c) The “Hebel–Slichter” coherence peak in the NMR.

Since the fermions with the same spin are pairing up or down in the x -direction, when we apply a magnetic field in the x -direction ($\mathbf{d}(\mathbf{n}) \perp \mathbf{H}$), the field does not interfere with the pair formation, and the susceptibility in this case is not be much different from that in the normal state. On the other hand, for a non-ESP triplet, (e.g., the BW-type state), some pairs are formed in a spin antiparallel configuration seen in the magnetic field axis, so that $0 < \chi/\chi_n < 1$. We can therefore conclude that

$$\begin{aligned} \chi(T=0) \neq 0 &\Rightarrow \text{Spin-triplet,} \\ \chi(T=0) = 0 &\Rightarrow \text{Either the spin-singlet, or the ESP triplet with } \mathbf{d} \parallel \mathbf{H}. \end{aligned}$$

The Chandrasekhar–Clogston (CC) limit on the upper critical field H_{c2} [8, 9]

Almost all exotic superconductors are extreme type-II. In an old-fashioned BCS-type superconductor, the upper critical field may be set by the Meissner effect. However, if the superconductor becomes very dirty, the upper critical field H_{c2} predicted from a naive “Meissner” effect becomes really enormous, on the order of 10^3 Tesla. Under those circumstances, the actual H_{c2} may be set by the second limiting effect. This effect is due to the fact that if we apply the large enough field, it is energetically advantageous to simply forget about the pairing and obtain the Zeeman energy, leaving the system in the normal state (Fig. 4.1 (b)). This may occur at the point when the field H becomes the order $\Delta(0)/\mu_B$. If the pairing is spin-singlet or the ESP state with $\mathbf{d} \parallel \mathbf{H}$, we expect this effect. Thus, we crudely conclude that

$$\begin{aligned} \text{Absence of the CC limit} &\Rightarrow \text{Spin-triplet.} \\ \text{Presence of the CC limit} &\Rightarrow \text{Spin-singlet or the ESP triplet with } \mathbf{d} \parallel \mathbf{H}. \end{aligned}$$

The “Hebel–Slichter” (HS) coherence peak in NMR

The prediction from the BCS theory is that if we measure the relaxation rate of nuclear spins of metal, in the normal phase, it is proportional to T . The spectacular prediction of the BCS theory, assuming a singlet pairing, is that if we go into the superconducting phase as we lower the temperature, it first rises due to the singularity ($\propto (E^2 - \Delta^2)^{-1/2}$) in the density of states at the edge of the gap, and then it drops (Fig. 4.1 (c)) [10]. The presence of this HS peak requires

- (a) Singularity in DOS at gap edge.
- (b) Absence of canceling factor ($\propto (E^2 - \Delta^2)$) in matrix element, due to coherence.

Unfortunately, (b) should still hold for the spin-triplet case, and thus the presence or absence of the HS peak does not give much information about the spin state. The peak is predicted to be half “canonical” size, but it is difficult to check this.

4.3.2 Diagnostics of the orbital state

Before I start off explaining the diagnostics of the orbital state, let me give two cautions:

- (1) Even if the order parameter transforms according to the identity representation of the crystal group, it may still have nodes. This is called “extended s-wave” (see Fig. 4.2 (a) as an example).
- (2) The order parameter $F_{\mathbf{k}}$ is a two-particle (“bosonic”) quantity, whereas the energy gap $\Delta_{\mathbf{k}}$ is single-particle (“fermionic”) quantity, since it is the actual gap in the single-particle spectrum. *Within the BCS theory*, the two are closely proportional as regards the angular dependence since

$$F_{\mathbf{k}} = \Delta_{\mathbf{k}}/2E_{\mathbf{k}}, \quad (4.30)$$

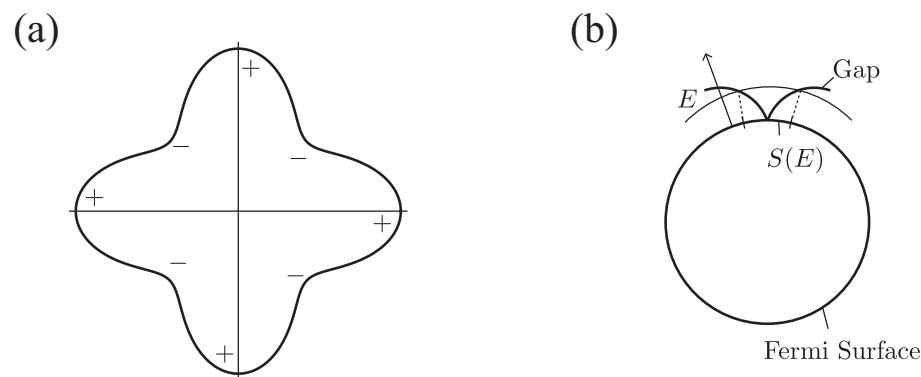


Fig. 4.2. (a) An example of the extended “s-wave” type gap. (b) An example of the 2D Fermi surface and the gap with the point node.

and in most of the range of \mathbf{k} , $E_{\mathbf{k}}$ does not have large dependence on the direction of \mathbf{k} . However, this need *not* necessarily be true in a more general theory. Thus, strictly speaking, one should try to distinguish carefully between those experiments which measure the energy gap $\Delta_{\mathbf{k}}$ and the order parameter $F_{\mathbf{k}}$.

Measurements of $|\Delta_{\mathbf{k}}|$

The most obvious thing we can measure is the actual magnitude of the gap $\Delta_{\mathbf{k}}$ ⁶, since there are several ways in doing this. As far as I know, there are only very indirect ways in measuring the actual complex quantity $\Delta_{\mathbf{k}}$ itself. On the other hand, there are some nice ways of measuring the complex quantity $F_{\mathbf{k}}$ ⁷. The main thing I am thinking in this context is so-called Josephson-type experiments. They have been very important in the analysis of the cuprates, and in somewhat (much less) important in the analysis of other exotic superconductors. I will discuss this in detail when I talk about the cuprates in Lec. 7.

Let us move on to the measurement of $|\Delta_{\mathbf{k}}|$.

- (a) The most direct measurements of $|\Delta_{\mathbf{k}}|$ are various kinds of spectroscopic measurements, such as ARPES and STM. In principle, this kind of experiments do directly measure $|\Delta_{\mathbf{k}}|$ as a function of \mathbf{k} and therefore as a function of position.
- (b) The more indirect thermodynamic measurement is via measurement of the density of states, $N_s(E)$. Since $N_s(E)$ is represented as

$$N_s(E) = \sum_{\mathbf{k}} \delta(E - E_{\mathbf{k}}) = N(0) \int_{|\Delta(\hat{\mathbf{n}})| \leq E} \frac{d\Omega}{4\pi} \frac{E}{\sqrt{E^2 - |\Delta(\hat{\mathbf{n}})|^2}}, \quad (4.31)$$

it is proportional to the area of the Fermi surface $S(E)$ where $|\Delta(\hat{\mathbf{n}})| \leq E$ is satisfied [11].

Figure 4.2 (b) illustrates an example of a 2D Fermi surface and a gap with the point node. We see that $S(E) \propto E$ if the gap function crosses its zero linearly at the node. This situation is generalized to

- 3D, point node: $N_s(E) \propto E^2$.
- 3D, line node: $N_s(E) \propto E$.
- 2D, point node: $N_s(E) \propto E$.

If $N_s(E) \propto E^n$, we know the low temperature behavior of physical quantities as follows (see chapter 7 of Ref. [12]):

Specific heat: $C_V \propto T^{n+1}$.

⁶In the triplet case, this is “total” gap and is proportional to $|\mathbf{d}(\mathbf{n})|$.

⁷This is something only realized comparatively recently.

Penetration depth: $\lambda(T) - \lambda(0) \propto T^n$.

Nuclear spin relaxation rate: $T_1^{-1} \propto T^{2n+1}$.

Knight shift: $K_s \propto T^n$ (for spin-singlet state).

Therefore, by measuring these quantity experimentally, we can determine the type of the node.

Note that in three dimensions, if the orbital angular momentum ℓ is larger than 1 (i.e., $\ell \geq 2$), the energy gap must *always* have nodes. For example, remember that when we talking about superfluid ^3He , I mentioned that in early days, people thought it is probably *d*-wave pairing. There is a general theorem which claims if it is *d*-wave, there must be at least two nodes on the Fermi surface. On the other hand, in two dimensions, it needs not have node for any ℓ , because we can have the order parameter $F_{\mathbf{k}} \sim \exp(i\ell\varphi)$ with angular momentum ℓ , but the magnitude of this is just a constant.

4.3.3 Effect of impurities

A digression: impurity scattering in the BCS (*s*-wave) superconductors

Let us consider the following Hamiltonian,

$$\hat{H} = \hat{H}_0 + \hat{V}, \quad \hat{H}_0 = \hat{K} + U(\mathbf{r}, \sigma), \quad (4.32)$$

where \hat{H}_0 (\hat{V}) is the single (two)-particle Hamiltonian, and \hat{K} is the kinetic term and $U(\mathbf{r}, \sigma)$ is an impurity potential. Let us forget about lattice potential for the moment. We denote eigenenergies and eigenfunctions and of \hat{H}_0 as ε_n and $\chi_{n\sigma}(\mathbf{r}, \sigma)$.

(A) Nonmagnetic impurities

If the impurity potential is independent of σ , i.e., $U(\mathbf{r}, \sigma) = U(\mathbf{r})$, then the system would be invariant under time-reversal. In that case, $\chi_n^*(\mathbf{r}, -\sigma)$ is also an eigenfunction, with same energy ε_n . We can therefore pair electrons in time-reversal states (Anderson's theorem). Pairing between the exact eigenstates ensures that the expenditure of \hat{H}_0 is minimal. In this case, the order parameter evaluated at the same point $F(\mathbf{r}, \mathbf{r}) \sim \sum_n |\chi_n(\mathbf{r})|^2$ is rather large because it is a sum of positive values, and hence we still get a large value for $-\langle \hat{V} \rangle$ even under the impurity. Thus, crudely speaking, the outcome of Anderson's theorem is that non-magnetic impurity do not do anything significant to *s*-wave superconductivity⁸.

(B) Magnetic impurities

If the impurity potential depends on σ (i.e., $U = U(\mathbf{r}, \sigma)$), time-reversal invariance is broken. Then we have two choices:

⁸In fact, if anything, it tends to raise T_c but I will not explain it further here.

(a) Pairing in the exact eigenstates ε_n of \hat{H}_0 .

Using the exact eigenstates still ensures the minimum expenditure of kinetic energy \hat{H}_0 . However, $F(\mathbf{r}, \mathbf{r})$ is much reduced, because the Cooper pairs are no longer formed in the time-reversal pairs. This is usually highly disadvantageous and thus this choice is hopeless.

(b) Pairing in the eigenstates of \hat{K} .

Firstly, we forget about the impurity and reconstitute the original “impurity-free” Fermi sea. This is advantageous since it gain the original BCS condensation energy E_c , originated from the large (not reduced) order parameter. However, it sacrifices the energy due to U of \hat{H}_0 :

$$\Delta E_U = +\frac{1}{2}N(0)\Gamma_U^2, \quad (4.33)$$

where Γ_U is, crudely speaking, the relaxation rate of the time-reversal operator. It becomes energetically disadvantageous when $\Delta E_U > E_c = \frac{1}{2}N(0)\Delta_0^2$, where Δ_0 is the gap for a pure system. Hence, we expect the superconductivity to disappear (at $T = 0$) at

$$\Gamma_U = \Delta_0. \quad (4.34)$$

Surprisingly, this very simple hand-waving argument is confirmed by the exact Abrikosov–Gor’kov theory [13].

Generalization to the exotic order parameter⁹

Let us generalize the above argument to the exotic order parameter. Even if impurities are *nonmagnetic*, exact eigenstates χ_n of \hat{H}_0 will now be complicated superposition of \mathbf{k} ’s from all over the Fermi surface. Thus, if we pair in χ_n ’s, $\langle \hat{V} \rangle$ will be very small, which is very disadvantageous. Therefore we must again “reconstitute” impurity-free eigenfunctions. It cost some energy due to the impurity, $\Delta E_U = \frac{1}{2}N(0)\Gamma_\ell^2$, (supposing there is a dominant ℓ in $V_{\mathbf{k}\mathbf{k}'}$; Γ_ℓ is the relaxation rate of ℓ -symmetry distortion). We compare the energy loss with the gain of the condensation energy. By analogy with the above argument, *superconductivity disappear when $\Gamma_\ell = \Delta_0$.*

4.4 Addendum: the effect of spin-orbit coupling

The discussion of the spin-triplet pairing in Lec. 2 and above implicitly assumes that the eigenstates of the single-particle Hamiltonian \hat{H}_0 are mostly¹⁰ invariant under the spin rotation and the orbital crystal group separately. Under these conditions, the pairing

⁹For more details cf. pp. 347-348 of Ref. [14].

¹⁰Except for dilute magnetic impurities, etc.

state can usually be classified into the spin-singlet and the triplet state, as discussed in Sec. 4.2.2. Mixing of these two possibilities requires rather pathological values of the parameters.

If \hat{H}_0 is *not* invariant under spin and orbital operations separately, on the other hand, there may be strong mixing of the spin and orbital degrees of freedom. The most obvious origin of this is *spin-orbit coupling*. Because it is scaled as Z^3 , it rapidly becomes important in heavy metals, e.g. U compounds. Under these conditions the only symmetries left are *parity* P and *time-reversal* T (both of which are preserved by spin-orbit coupling $\propto \boldsymbol{\ell} \cdot \boldsymbol{s}$), and we must use only these to classify the irreducible representations (see Ref. [7] for further details).

References

- [1] G. Eliashberg, *Sov. Phys. JETP* **11** (1960).
- [2] D. Scalapino, *In: Parks RD (eds) Superconductivity, vol 1* (Marcel Deklcer Inc, New York, 1969).
- [3] W. L. McMillan, *Phys. Rev.* **167**, 331 (1968).
- [4] W. McMillan and J. Rowell, *Phys. Rev. Lett.* **14**, 108 (1965).
- [5] C. Yang, *Rev. Mod. Phys.* **34** (1962).
- [6] O. Penrose and L. Onsager, *Phys. Rev.* **104**, 576 (1956).
- [7] G. E. Volovik and L. P. Gor'kov, *Sov. Phys. JETP* **61**, 843 (1985).
- [8] A. M. Clogston, *Appl. Phys. Lett.* **1**, 7 (1962).
- [9] A. M. Clogston, *Phys. Rev. Lett.* **9**, 266 (1962).
- [10] L. C. Hebel and C. P. Slichter, *Phys. Rev.* **113**, 1504 (1959).
- [11] P. W. Anderson and P. Morel, *Phys. Rev.* **123**, 1911 (1961).
- [12] J. F. Annett, N. Goldenfeld, and S. R. Renn, *Physical Properties of High Temperature Superconductors II* (World Scientific, New Jersey, NJ, USA, 1990).
- [13] A. A. Abrikosov and L. P. Gor'kov, *Sov. Phys. JETP* **12**, 1243 (1961).
- [14] A. J. Leggett, *Quantum Liquids* (Oxford University Press, New York, NY, USA, 2006).

Lec. 5 Non-cuprate exotic superconductivity

5.1 Alkali fullerides

5.1.1 Structure

Formula of this compound is A_3C_{60} , where A is some alkali element (Na, K, etc.) and C is a carbon. C_{60} molecule has a famous soccer-ball pattern, with 20 hexagons and 12 pentagons; its symmetry is icosahedron. While the carbon atom has a molecular orbital $1s^2 2s^2 2p^2$ in C_{60} molecule or solid, and $2s$ and $2p$ orbitals hybridize to form four sp^2 states. Of these, three are used up in the σ bonding (in-plane bonding), leaving one electron per carbon atom, i.e., 60 electrons per C_{60} molecule, in the p_z -like state. It is this last electron, which sticks out of the surface of the soccer ball, that controls the low-energy properties. Obviously the theory of the electronic states of the C_{60} molecule is quite complicated, so we will not go into its details and we only briefly summarize its important properties; C_{60} molecule has various molecular orbitals as usual. The highest occupied molecular orbital (HOMO) state is 5-fold orbitally degenerate, and the lowest unoccupied molecular orbital (LUMO) is 3-fold degenerate. In the single molecule, the HOMO-LUMO splitting is ~ 0.6 eV.

5.1.2 Fullerene crystals

When a large number of C_{60} molecules are put together, they form a so-called fullerene crystal. Its lattice has the face centered cubic structure; the cubic lattice parameter is

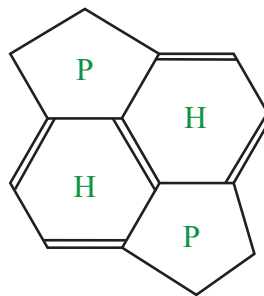


Fig. 5.1. Lattice structure of C_{60} .

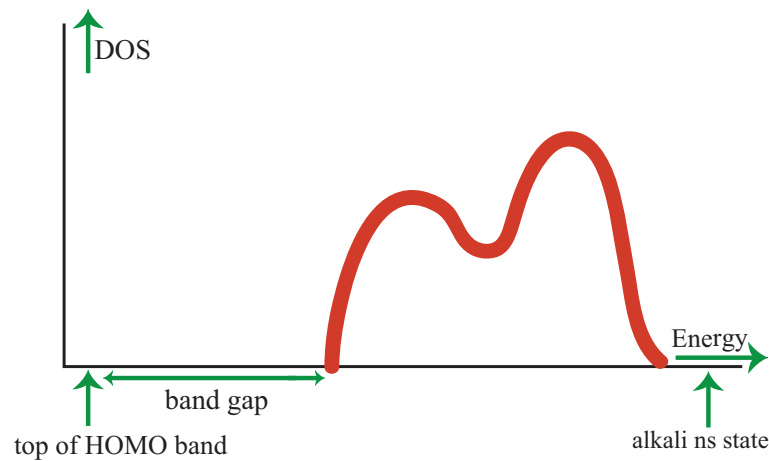


Fig. 5.2. Density of states of fullerene crystals.

$\sim 14.2 \text{ \AA}$, which roughly corresponds to the close-packing of C_{60} molecules. The complicated point which arises in connection with the crystals is that individual molecules can have two different orientations. Despite the fact that the molecules look pretty spherical, they are not exactly spherical, so there are two slightly different orientations for each molecule. Quite often, by just quenching the C_{60} into a solid state, one finds that the orientation of each molecule may be tuned to either of these two orientations. This phenomenon is called merohedral disorder, which is quite important for the detailed theory of transport, etc., but we do not go into its details here.

If C_{60} molecules are combined, they form a band structure. The density of states (DOS) of the band which evolves from the LUMO state is shown in Fig. 5.2. One finds a dip in the middle of the band, which is sensitive to the lattice parameter. This fact is important when one considers the origin of superconductivity.

5.1.3 Alkali fullerenes

A pure fullerene crystal, a simple collection of C_{60} molecules, is not superconducting but a fairly good band insulator with a band gap $\sim 1 \text{ eV}$. When alkali atoms are introduced to the crystal, there are certain positions in the crystal where alkali atoms are likely to locate. Since the energy levels of the intercalated alkali atoms are slightly above the LUMO band (Fig. 5.2), they will donate their s -electrons to the LUMO band. Thereafter, the ionized alkali atoms, the cores of the rare-earth metals, just serve as *spectators*, playing no important role in the behavior of the system (cf. *charge reservoir* atoms in cuprates).

The normal-state properties of fullerene crystal are roughly consistent with textbook picture of half-filled band: the specific heat $C_v \sim T$, the Pauli spin susceptibility $\chi \sim \text{const.}$, and the spin-lattice relaxation time $T_1 \sim T^{-1}$ etc. Note that experiments such as photoemission and plasmons confirm that the DOS at the Fermi energy $N(0) \equiv$

$\frac{1}{2} \left(\frac{dn}{d\varepsilon} \right) \Big|_{\varepsilon=\varepsilon_F}$, an important value for transport in normal and superconducting states, is strongly dependent on the lattice constant a .

5.1.4 Superconducting state

Superconductivity in A_xC_{60} occurs only when the filling of alkaline atoms x is almost equal to 3, but then has T_c up to ~ 40 K (Cs_3C_{60}). This high transition temperature is quite surprising because the intercalated graphite, for example KC_8 , has T_c lower than 1 K. T_c increases as the lattice spacing a is increased by the pressure or substitution; typically, the increase in T_c by the lattice spacing is given by

$$\frac{\partial T_c}{\partial a} \sim 33 \text{ K/\AA}. \quad (5.1)$$

This is consistent with the BCS result

$$T_c \sim \omega_D \exp(-1/N(0)V_0), \quad (5.2)$$

under the assumption that V_0 comes mainly from the intramolecular origin hence insensitive to a , and that the density of states $N(0)$ increases with a .

A_3C_{60} 's are strongly type-II. In fact, the pair radius is $\xi(0) \sim 26 \text{ \AA}$, which is less than twice the lattice spacings, and the London penetration depth is $\lambda(0) \sim 2400\text{-}4800 \text{ \AA}$. What are the characteristics of the pairing state? Behaviors of the spin-lattice relaxation time T_1 and the infrared reflectivity seem to suggest that the quasi-particle density of states is small when $|E| < \Delta \approx 1.76k_B T_c$, as it should be in the BCS theory. The Hebel-Slichter peak is seen in the muon spin resonance (μ SR) and ^{13}C NMR, which strongly indicate the pairing state has an s -state as in the BCS superconductors. So far, everything is consistent with the ordinary BCS superconductors except for one slight puzzling thing: the deviation of the London penetration depth from its zero temperature value does not follow an exponential law but some power law:

$$\Delta\lambda(T) \sim T^\alpha, \quad \alpha \sim 3. \quad (5.3)$$

What about the pairing mechanism? The isotope substitution ^{12}C by ^{13}C yields a large isotope exponent ≈ 0.4 ; remember that the isotope exponent value of the ideal BCS-type superconductor is exactly 0.5, and in real life there are various reasons for underestimating the value. This fact is therefore consistent with the phonon mechanism. However, one finds rather unusual situation in the ratio between the Debye frequency and the Fermi energy. Since carbon atoms are light and tightly bound in the solid, we have a large Debye frequency, and the Fermi energy is not that high. Then one obtains the ratio

$$\omega_D/\varepsilon_F \sim 0.3\text{-}0.6. \quad (5.4)$$

which is far larger than that of the BCS superconductors, typically $\omega_D/\varepsilon_F \sim 10^{-2}$. Therefore, even if the mechanism has phonon as its origin, details seem to be rather different from the BCS theory. The prevalent explanation is that alkali fullerides are pretty well described by the BCS theory, but that the strong molecular structure enables them to avoid the limit on T_c (cf. MgB_2).

5.2 Organics

There are various kinds of organic superconductors. Most of the extensively studied materials are quasi-2D crystals based on ET(BEDT-TTF) (bis(ethylene-dithio)-tetrathiafulvalene) (Fig. 5.3). Their structures have the form $(\text{ET})_2\text{X}$, where X is a monovalent anion (I_3^- , $\text{Cu}(\text{NCS})_2^-$...). The structure is slightly counterintuitive (Fig. 5.4 (a)): conducting layers consist of $(\text{ET})_2$, and the *blocking layers* consist of anions. Conventionally in the literatures, a -axis is taken parallel to the stacking direction of anion layers. These layers are pretty insulating, which makes difficult the electronic transportation along the a -axis. Pretty flat $(\text{ET})_2$ molecules line up along the b -axis, constructing metallic layers in the system. The distance between the insulating layers is quite large, $\sim 50 \text{ \AA}$.

5.2.1 Normal state

In the normal state, the conduction electron density is quite low ($\sim 10^{21} \text{ cm}^{-3}$). This feature is characteristic of quite a few classes of exotic superconductors including cuprates. They have a strong a -axis anisotropy¹: $\rho_a/\rho_{bc} \sim 10^2\text{-}10^3$, which is comparable to cuprates. Interestingly, clean samples made possible the de Haas-van Alphen (dHvA) type oscillation experiments. The dHvA-effects are electronic oscillatory effects under strong magnetic field. As a result of the fact that different orbits constitute the Fermi surface, various physical quantities such as susceptibility, resistivity etc. are periodic in the inverse of the magnetic field $1/B$. The dHvA experiment requires quite clean samples; crudely speaking, the period of cyclotron motion in the magnetic field must be smaller than the scattering time. This condition, although practically quite stringent, is satisfied in the organic superconductors. Figure 5.4 (b) shows a typical Fermi surface; everything is

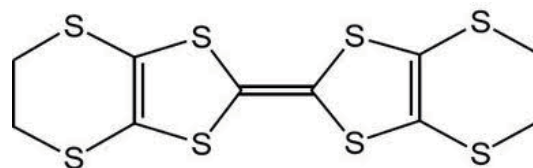


Fig. 5.3. Ethylene-dithio molecule.

¹Confusingly, the conventional notation calls the *hard* direction a , not c as in the cuprates.

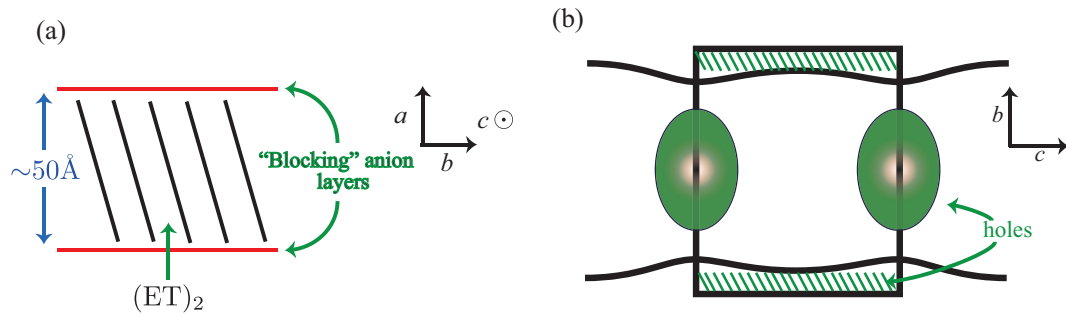


Fig. 5.4. (a) Crystal structure of organic superconductors. (b) Fermi surface of $(\text{K}(\text{ET})_2\text{Cu}(\text{NCS})_2)$.

strongly two-dimensional, i.e., cylindrical in three dimensions. This implies the conduction electrons cannot penetrate the *blocking* anion layers.

5.2.2 Superconducting state

The superconducting state typically has $T_c \sim 10\text{-}12$ K. Normally, superconductors with $T_c \sim 10$ K are not regarded as high- T_c . However, there is an argument as follows: the calculated in-plane hopping matrix element is small. This means that the bands which form in-plane are narrow and the Fermi energy is small. If one expresses T_c not in terms of Kelvin but rather as the fraction of Fermi energy/Fermi temperature, then the T_c value divided by T_F is comparable to that of cuprates. In this sense, the organic superconductors can be regarded as high-temperature superconductors.

The organic superconductors have the following physical properties:

- Extremely type-II ($H_{c1} \sim$ a few mT, $H_{c2} \sim 8\text{-}15$ T).
- Estimated pair radius $\xi_{\parallel} \sim 50$ Å in the *easy* plane, while $\xi_{\perp} \sim 5$ Å (\ll interlayer distance ~ 50 Å) along the *hard* axis.
- Symmetry: $C_V(T) \sim e^{-\Delta/T}$ for $T \rightarrow 0 \implies$ characteristic *s*-wave.
- Nuclear spin-lattice relaxation time: $T_1^{-1} \sim T^3 \implies$ *substantial low-energy DOS*. No Hebel–Slichter peak.
- Isotope effect: the substitution $^{12}\text{C} \rightarrow ^{13}\text{C}$ has $\alpha_I \sim 0.1$, but the substitution $^1\text{H} \rightarrow ^2\text{D}$ produces inverse isotope effect ($\alpha_I < 0$). This is consistent with the BCS theory, but the origin is more likely to be the effect of lattice deformation.

In my opinion, to be honest, no one is quite sure about the mechanism of high- T_c superconductivity in the organics. The simplest default option is that the organics are somewhat BCS-like, but electronic effects may be competitive.

5.3 Heavy fermions

Heavy fermions are actually the oldest class of exotic superconductors, discovered in 1979 [1]. Heavy fermion systems [2] are, in general, compounds which contain rare-earth elements (usually Ce) or actinide elements (usually U, and Pt). Heavy fermions have an extraordinary large specific heat even in the normal phase. In fact, the specific heat for the heavy fermion systems is 10 to 100 times larger than “textbook” values of ordinary metals: hence the name “heavy fermions”². All these materials are three-dimensional, and as far as I know, none of the heavy fermion material is strongly layered. This is actually somewhat remarkable because, as we will see, all the other classes of exotic superconductors really are strongly layered.

5.3.1 Normal-state behavior

For the normal-state behavior, there is a problem: at $T \sim 300$ K, the behavior of the heavy fermion systems, generally speaking, is quite different from that of textbook metals. It is not even universal in the class. For example, the resistivity $\rho(T)$ looks metallic for UPt₃ [3], while they behave as semiconducting for most others. However, the following property typically hold:

- $\chi \propto 1/T$
- $T_1^{-1} = \text{const.}$,
- $C_V = \text{const.}$,
- neutron scattering showing a simple Lorentzian peak centered at $T = 0$,

where χ is the magnetic susceptibility, and T_1^{-1} is the NMR relaxation time, and C_V is the specific heat. For typical rare-earth or actinide elements in heavy fermion systems, such as Ce³⁺ : $4f_1$, U⁴⁺ : $5f_2$, there are characteristic spare f -electrons. We would assume that these f -electrons are fairly tightly bound. Then, it is attractive to think, with the above properties in mind, a model with spare f -electrons of rare-earth or actinide elements, crudely speaking.

As T is lowered, on the other hand, it seems that in all cases, a crossover to a Fermi-liquid-like regime occurs³. In fact, at low temperature,

- $C_V = \gamma T$,
- $T_1^{-1} \propto T$,

²Note that this large effective mass is seen not only in the specific heat, but also in other quantities as well, in particular in the dHvA experiments.

³The temperature at which this crossover occurs depends on the system we are talking about. It can be as high as 100 K, or as low as 5 K.

- $\rho \propto A + BT^2$,

where ρ is the resistivity. Note that the constant term in the resistivity comes from an impurity scattering, while the T^2 term is what we get from electron-electron Umklapp scattering⁴. These behaviors look much like those of a Fermi liquid, but what is special to the heavy fermion system is that the coefficient γ in $C_V = \gamma T$ is enormous, up to ~ 1600 mJ/mole K² (CeCu₆ [4, 5]) (contrast “textbook” metal, $C_V \sim$ a few mJ/mole).

Hence the question for a normal state of the heavy fermion system arises: are we sure this specific heat is due to mobile electrons or not (since we can get this linear specific heat also from a localized electron)? I think that once the superconducting phase transition occurs, then it is rather clear that it has to be that of mobile electrons, since the jump in the specific heat at T_c is roughly the same as the BCS value. Thus, it is rather plausible that the electrons contributing to the large specific heat in the normal state and those forming the Cooper pairs in the superconducting phase are both mobile electrons, rather than localized ones.

Thus, the heavy fermion system at low temperature behaves as a standard Fermi liquid, but with the large effective mass. Note that this large effective mass is also confirmed by the measurement of the large Pauli susceptibility χ , typically 10 to 1000 times larger than that of textbook metals, and in the de Haas-van Alphen experiment.

We can imagine a naive model for the normal state as follows: suppose that f -electrons, fairly tightly bound, form very narrow band, with its width $\Delta \sim$ a few K. For $k_B T \gg \Delta$, all states in the band will be almost equally populated, which is equivalent to saying that electrons are localized on lattice sites independently. Then, it behaves as $\chi \propto 1/T$, $T_1^{-1} = \text{const}$, and small C_V . For $k_B T \lesssim \Delta$, we need a proper “band” picture with a large $m^* (\propto \Delta^{-1})$, which seems to account for the crossover to a Fermi-liquid behavior with a large effective mass.

At first sight, this argument sounds reasonable, and gives a good qualitative explanation for the normal-state behavior. However, unfortunately, there is a rather important point missing in it: it ignores the conduction (s or d) electrons. In fact, the conduction electrons interact with f -electrons and in general have complicated effects, in particular the Kondo effect [6, 7]. The Kondo effect occurs when we have conduction electrons moving in the presence of a localized single impurity with spin. The tendency for the conduction electrons and the impurity spin to form a singlet bound state gives rises to interesting phenomena which are studied in a vast amount of literature. In the heavy fermion system, the situation is much more complicated than this. The Kondo effect favors the singlet state between the conduction and the localized f -electrons. On the other hand, there is also the interaction between f -electrons mediated by a polarization of the conduction electrons (RKKY interaction [8, 9, 10]), which favors a magnetic ordering of f -electrons.

⁴Note that the electron-electron scattering in a free space does not give us a finite resistivity, since the momentum of colliding electrons, and thus the current must be conserved. In a crystal, however, the total momentum of the colliding electrons can change by modulus of the crystal lattice vector by the Umklapp process, so that it can have a resistivity of $\propto T^2$.

In fact, in many heavy fermion systems (even in some superconducting states), they show an antiferromagnetism at $T \lesssim 20$ K.

5.3.2 Superconducting phase

General remarks

We can classify heavy fermion systems into four classes as follows:

- 1) No phase transition occurs down to $T = 0$ (e.g., CeAl₃ [11]).
- 2) Show only a magnetic phase transition (e.g., CeCu₆ [4, 5]).
- 3) Show only a superconducting transition (e.g., UPt₃ [3], CeCu₂Si₂ [1], UBe₁₃ [12]...).
- 4) Both magnetic and superconducting transitions occur (e.g., UPdAl₃ [13], URu₂Si₂ [14], UGe₂ [15, 16] ...). In this class, magnetic order and superconductivity coexist (contrary to established “textbook” wisdom!).

The last class is, in some sense, the most interesting one. This is very surprising since up to the 1970s, it is strongly believed, as a kind of dogma, that a magnetic order and superconductivity cannot coexist. A qualitative reason for this, although it is a partial one, is that the magnetic ordering occurs for tightly bound electrons, such as f -electrons, whereas the superconductivity occurs for hybridized and delocalized conduction electrons.

In all cases known of the superconductivity in the heavy fermion system, the transition temperature can be never larger than of the order of a few Kelvin⁵: $T_c \lesssim 2$ K. This is actually quite remarkable because, as we have already seen and we will see further, there are other classes of exotic superconductors where T_c is much higher.

As to the mechanism, the most crucial observation is that, as far as we know, no heavy fermion superconductor shows any appreciable isotope effect. This strongly suggests, although it does not actually prove, that the mechanism for the superconductivity is not phononic but should be “all-electronic” one. I think that everyone would agree that, whatever may be the case for the other exotic superconductors, the mechanism is not phonon mechanism for heavy fermion superconductors.

Pairing states

The pairing states of the heavy fermion superconductors can be characterized by various methods, such as low temperature behavior of the specific heat C_V , nuclear relaxation

⁵In the class 4, $T_N \sim 10$ -50 K. We also note that there is some exceptions for this estimate of T_c . For example, PuCoGa₅, which is normally regarded as a heavy-fermion system, has a transition temperature $T_c = 18.5$ K.

Table 5.1. Properties of some heavy fermion superconductors, determined from experiments. AF stands for an antiferromagnetism, F for a ferromagnetism, and P for a paramagnetism. T_N is the Néel temperature.

System	Magnetism	T_c (K)	Parity	Gap nodes	Comments
UPt ₃ [3]	P	0.56	–	✓	
CeCu ₂ Si ₂ [1]	P	0.65	+ (?)	✓	
UBe ₁₃ [12]	P	0.9	– (?)	✓	
UPdAl ₃ [13]	AF	2.0	+	✓	$T_N = 14.5$ K
CeCoIn ₅ [17]	P	2.3	+	✓	probably $d_{x^2-y^2}$
UNiAl ₃ [18]	AF	1.0	–	?	$T_N = 4.6$ K
URu ₂ Si ₂ [14]	AF	0.8	–	?	$T_N = 17.5$ K
UGe ₂ [15, 16]	F	0.6	–	?	$T_{\text{Curie}} = 30$ K (at point of max T_c)

rate T_1^{-1} , electronic thermal conductivity κ_{el} , Knight shift, upper critical field H_{c2} , sensitivity of T_c to nonmagnetic scattering, or by an existence of multiple phases⁶. Some representative heavy fermions and their (suggested) symmetries are shown in Table 5.1.

Note that for the heavy fermion system, the spin-orbit coupling is not negligible and thus, we cannot separate the orbital and spin part as we did in BCS-like superconductors. In fact, for rare earth elements such as U or Ce, the spin-orbit coupling is, in fact, very large. In such a case, we have to classify them by the parity and time-reversal symmetry, as we discussed in Sec. 4.4. We also note that there is no evidence for the violation of the time-reversal symmetry in any heavy fermion, which is a rather interesting fact. Thus, the only important symmetry seems to be the parity, and it differs for different materials.

Most of the heavy fermion superconductors, as we can see, do appear to have a node in their gap, which can be seen, for example, by the power-law behavior of quantities such as C_V , or T_1^{-1} at low temperatures. Thus, the form of the gap is, at least, not simplest. It is conceivable that they are so-called extended s -wave superconductors, but it is generally thought that these are indeed exotic superconductors. Beyond that, it is really not that easy to say very much about the symmetries.

The thing I would like to comment on is that in Table 5.1 they do not appear to have a lot in common apart from the fact that they are not simple s -wave. That is rather surprising because, after all, they do have the normal state behavior in common, the low temperature Fermi-liquid-like phase. However, when they go into a superconducting phase, they seem to behave differently.

As for the magnetic properties, most of them are paramagnetic or antiferromagnetic. There is one case, recently discovered, which is ferromagnetic: UGe₂ [15, 16]. This is quite surprising because it has been used to be thought that a ferromagnetism is inconsistent

⁶For a simple s -wave picture, it is fairly difficult to account for multiple phases, so if there are multiple phases, it can be a strong evidence for the anisotropic pairing

with a superconductivity. It looks like the order parameter has an odd parity, which seems to be consistent with the ferromagnetism. An odd parity state suggests, crudely speaking, that the Cooper pairs are mostly triplet, so that a strong magnetic field does not suppress the spin-triplet pairing.

Note that not all of these have been entirely settled down. In fact, for example a superconductivity of UGe_2 is found around 2000 [15, 16], and there are a lot of work even recently.

5.4 Strontium ruthenate: Sr_2RuO_4

5.4.1 History

For the cuprates, the superconductivity starts to occur at the transition temperature up to $T_c \sim 150$ K [19, 20]. Typical crystal structure of the cuprates is illustrated in Figs. 5.5 (a) and (b). There are characteristic CuO_2 planes, and between them there are lanthanoides. The off-plane oxygens are different from the in-plane ones in that they are, in some sense, not directly connected to the superconductivity. It does seem rather clear that the CuO_2 planes are essential to the high- T_c superconductors. For all superconductors without CuO_2 planes, T_c is below 100 K. Therefore, at the moment when the cuprates were discovered, people started asking whether it is essential to have Cu, or we can replace it by other elements. An obvious replacement with Au, Ag did not work.

The crystal structure for Sr_2RuO_4 is shown in Figs. 5.6 (a) and (b). As we can see, it is extremely similar in its structure to the cuprates: the only differences are firstly that the Cu atom is replaced by Ru, and secondly the spacer is not Ba, but Sr.

It turns out, however, that the normal-state behaviors of Sr_2RuO_4 are quite dissimilar from those of cuprates. In addition, the transition temperature is quite different. For $\text{La}_{2-x}\text{Ba}_x\text{CuO}_4$ $T_c \sim 40$ K, while it turns out that $T_c \sim 1$ K for Sr_2RuO_4 regardless of

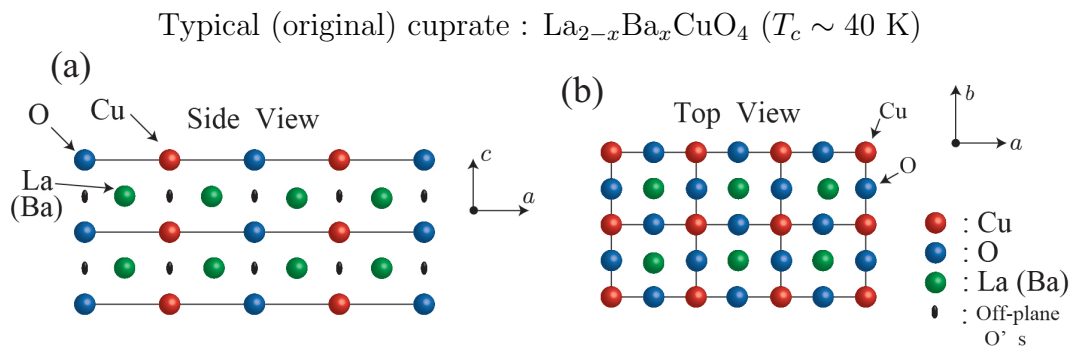


Fig. 5.5. (a) Crystal structure of cuprates for ac -plane (side view). (b) Crystal structure of cuprates for ab -plane (top view).

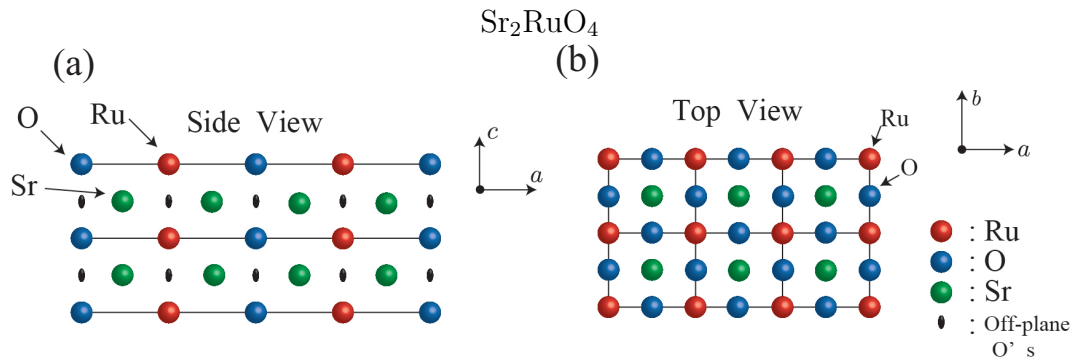


Fig. 5.6. (a) Crystal structure of Sr_2RuO_4 for ac -plane (side view). (b) Crystal structure of Sr_2RuO_4 for ab -plane (top view).

the optimistic hope that we would get a high- T_c superconductor from its similarity in the crystal structure.

5.4.2 Experimental properties of Sr_2RuO_4

We briefly review some important experimental properties of Sr_2RuO_4 . For more details, see Ref. [20].

Normal Phase

In the normal state for Sr_2RuO_4 , below $T \sim 25$ K, it appears to behave as a Fermi liquid in all three directions. Thus, the specific heat is a combination of the contributions from the electronic and phonon parts

$$C_V \sim \gamma T + \beta T^3. \quad (5.5)$$

For the susceptibility, we observe the Pauli susceptibility:

$$\chi \sim \text{const.} \quad (5.6)$$

For both the ab -plane and c -axis, the resistivity is

$$\rho \sim A + BT^2, \quad (5.7)$$

which is a characteristic form for a coherent Bloch wave transport limited by the impurity and electron-electron Umklapp scattering: the first term comes from the impurity scattering, while the second term from the Umklapp scattering. The value ρ_{ab} itself is considerably smaller compared with that of the cuprates, $\rho_{ab} \sim 1 \mu\Omega \text{ cm}$. This means that the samples are very pure systems, and indeed it turns out that one can make a very pure sample of Sr_2RuO_4 .

Table 5.2. Some of the Fermi liquid parameters for Sr_2RuO_4 . Note that the m_e is the bare electron mass, while m_{band} is the band mass.

	α -band	β -band	γ -band
k_F (\AA^{-1})	0.3	0.6	0.75
m^*/m_e	3.3	7.0	16.0
m^*/m_{band}	3.0	3.5	5.5

Another important feature of Sr_2RuO_4 is that it is a strongly anisotropic Fermi liquid. In fact, $\rho_c/\rho_{\text{ab}} \sim 10^3$, and this is comparable to those of typical cuprates. This strong anisotropy can be also seen in its band structure. We can reconstruct the Fermi surface from the de Haas-van Alphen kinds of experiments⁷, or we can calculate the band structure by the local density approximation (LDA). Both of them suggest that the Fermi surface consists of three strongly two-dimensional sheets: one hole-like sheet (called α -sheet), and two electron-like sheets (β - and γ -sheets). This is what we may expect from the strong anisotropy in the resistivity, which indicates that the hopping matrix element along the c -axis is far smaller than that for the inner-plane hopping. In fact, the deviation from the ideal two-dimensional Fermi surface is fairly small, of the order of $\sim 1\%$.

The behavior of electrons for each of the sheets is shown in Table 5.2. The Fermi momentum is of the order of a typical value, and it is not so much an exciting value. The effective mass is several times larger than the band mass, which is estimated by neglecting the electron-electron interaction and just solving an one electron problem. This indicates that electrons are strongly correlated, although it can be well described by the Fermi liquid.

Superconducting phase

People have expected that the transition temperature for Sr_2RuO_4 would be as high as those of the cuprates, but it turns out that T_c is not so high, although it does undergo a superconducting phase transition. The transition temperature for Sr_2RuO_4 is only about 1.5 K, and in that sense it was disappointing.

It turns out, however, that the susceptibility appears to be $\chi \sim \text{const.}$ in the superconducting state for all directions, which seems to indicate a triplet ESP state. I think this is fairly firm, and most people believe that the superconducting state of Sr_2RuO_4 is indeed a triplet ESP state.

⁷Although there are various ways to measure the band structure, if we are faced with some new materials and want to figure out what their band structures are, the most reliable way is the de Haas-van Alphen kinds of experiments, measuring a quantum oscillation with respect to the external magnetic field.

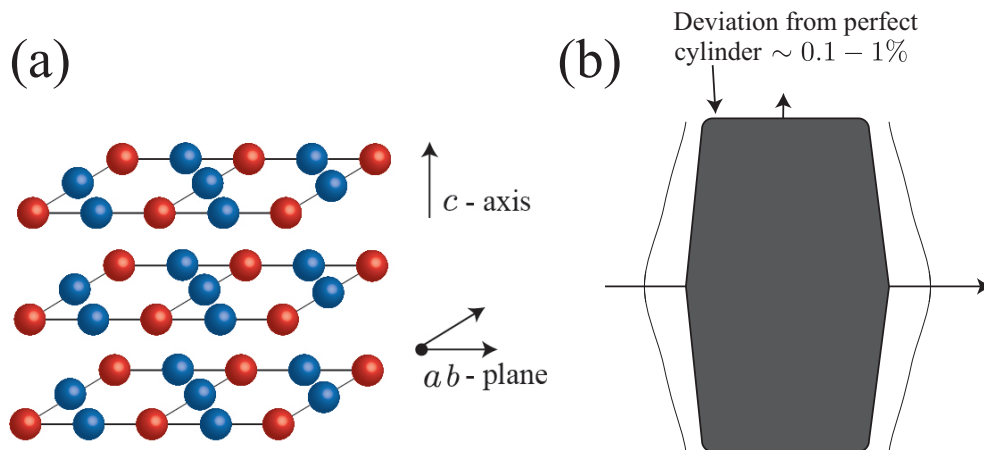


Fig. 5.7. (a) Crystal structure of Sr_2RuO_4 . (b) Schematic illustration of the Fermi surface of Sr_2RuO_4 .

With that in mind, let us suppose that the order parameter of Sr_2RuO_4 is indeed of the ESP form:

$$F(\mathbf{k}; \sigma_1, \sigma_2) = F(\mathbf{k}; \sigma_1, \sigma_2) = f(\mathbf{k})(|\uparrow\uparrow\rangle + |\downarrow\downarrow\rangle). \quad (5.8)$$

A crucial question arises: what is the orbital wave function of the pairs $f(\mathbf{k})$? Since it is a spin-triplet state, it has to be an odd parity state. This does appear to be consistent with some Josephson experiments, where it is shown that the order parameter seems to change its sign if we reflect it.

The most interesting question is whether the order parameter is real or complex. In the real case, such as $f(\mathbf{k}) \sim k_x$, the time-reversal symmetry is not broken. On the other hand, if it is complex, for example $f(\mathbf{k}) = k_x + ik_y$ ⁸, it can be broken. In the BCS theory, we know a priori, that the amplitude of order parameter $|\text{OP}|^2$ want to be as uniform as possible over the Fermi surface, although this is not always the case in a more general theory⁹.

It turns out that there are various experiments which are in favor of the time-reversal symmetry broken order parameter. Some of the experiments are as follows:

- **Muon spin rotation**

In the muon spin rotation experiment, we essentially measure an effective magnetic field where the muon is sitting after it is trapped to somewhere. Generally speaking, in the normal state under a zero external magnetic field, the muon sees indeed no local magnetic field. If, on the other hand, we have a system where the time-reversal symmetry is spontaneously broken, then you would expect to see that the muon spin rotates, and indeed we will see it. What is peculiar for Sr_2RuO_4 is that the signal of

⁸This state has an angular momentum along z -axis, and you can easily see that the time-reversal symmetry is broken.

⁹³He is one counterexample for this, where we could not exclude the possibility for the polar phase, which does not breaks the time-reversal symmetry.

the time-reversal symmetry breaking starts to appear at the superconducting phase transition [21]. This experimental fact suggests that the time-reversal symmetry is spontaneously broken in the superconducting state.

There is one worrying factor there: the direction of the local magnetic field. An obvious option for this is in the direction along the symmetry axis, that is along the c -axis. However, this is not the case, and in fact we have a finite component in the ab -plane. This is what remains to be understood.

- **Magnetic field dependence and telegraph noise in I_c of Josephson junctions interpreted in terms of switching of domains.**

If the time-reversal symmetry is broken as $k_x + ik_y$, there is also an equal possibility for having $k_x - ik_y$ state. There is an argument based on a macroscopic electromagnetic effect that it is likely to have various domains of them. Experimentalists interpreted the telegraph noise in I_c of Josephson junctions as the switching between these two states [22].

- **Kerr effect in zero magnetic field.**

Kerr effect is a measurement of the rotation of the polarization of the light when it passes through the material. If this rotation occurs, that is again a direct evidence of the time-reversal symmetry breaking. An experiment has observed the rotation and has confirmed this time-reversal symmetry breaking [23].

So far, so good. For an “ideal” $k_x + ik_y$ state, the energy gap has no node $|\Delta| \sim |F| \sim \text{const.}$, so that the number of quasi-particles for $T \ll T_c$ should be exponentially small. This should be seen in the measurement of the specific heat, thermal conductivity and so on. However, unfortunately what we find is a power-law behavior for most of these quantities. Whether this power-law is due to the existence of nodes in the gap is somewhat controversial. In principle, there is a critical test for this: Josephson junction test (see Fig. 5.8), which I shall talk in more detail in Sec. 7.4.

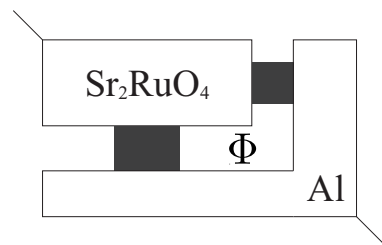


Fig. 5.8. Schematic illustration of the Josephson experiment.

5.5 Ferropnictides

Ferropnictides are discovered in January 2008 [24]; please note that much experimental data may not be definitive¹⁰.

5.5.1 Composition

There are two major elements, each containing a transition metal (usually Fe) and a pnictide, element in nitrogen column of periodic table (usually As). We have two main classes of parent compounds:

1111: (RE)(TM)(PN)O (example: LaFeAsO)

122: (AE)(TM)₂(PN)₂ (example: BaFe₂As₂)

where RE=rare earth, TM=transition metal, PN=pnictide and AE=alkaline earth. To realize superconductivity at high temperature, one has to dope carriers into the system; for example, LaFeAsO_{1-x}F_x for 1111, and Ba_{1-x}K_xFe₂As₂ for 122. The third class is LiFeAs, FeSe (11 system), etc. Most works on (1111) in this section refer to LaFeAsO_{1-x}F_x.

5.5.2 Structure (1111 compounds)

The left figure in Fig. 5.9 shows the lattice structure of LaFeAsO. This material is composed of LaO layers and FeAs layers. Crudely speaking, the valence state in the parent compound is probably (La³⁺O²⁻)⁺(Fe²⁺As³⁻)⁻; La³⁺ and O²⁻ have doubly closed shell, Fe²⁺ has 3d⁶, and As³⁻ has closed shell. In some sense, it looks like the iron is oxidized, while Fe 3d and As 4p orbitals hybridize. If we substitute fluorine for oxygen, the embedded extra electron moves to the FeAs layer; if one substitutes by 10 percent (LaFeAsO_{0.9}F_{0.1}), the carrier density is $\sim 10^{21}$ cm⁻³, which again is comparable to that of cuprates.

One interesting thing about the iron-arsenide compounds is that they obviously have various things in common with the cuprates. The most important point is the strong two-dimensionality of the system. Another thing they have in common is the *charge reservoir*, the atoms which originally supply an extra charge. In LaFeAsOF, for example, the fluorines are substituted with the oxygens in the LaO planes, and they supply the extra charge. On the other hand, superconductivity itself almost certainly occurs in metallic FeAs layers. The charge reservoir is separated from the layers where superconductivity occurs. That again we see is characteristic of the cuprates. 1111s are electron-doped, which means the compound has surplus electrons, while 122s are hole-doped; this fact is interesting in comparison with the cuprates.

¹⁰For a review of high-temperature superconductivity in ferropnictides, see Ref. [25].

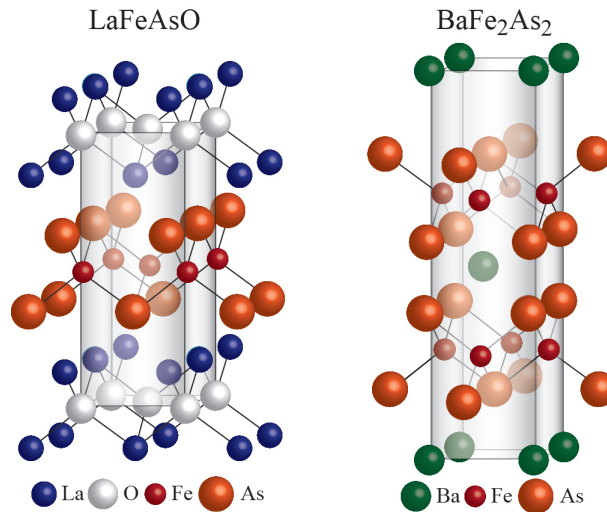


Fig. 5.9. Lattice structures of ferropnictides.

5.5.3 Phase diagram

Figure 5.10 (a) shows the phase diagrams of ferropnictides. The parent compounds are antiferromagnetic metal. In case (a), the crystallographic phase transition appears slightly over the antiferromagnetic phase transition. In case (b), the 1st order phase transition exists at the doping level $p = 0.05$, where the doping per unit formula p is equal to the stoichiometry x in this case (see Sec. 6.2 for more details). The carrier doping suppresses the antiferromagnetic order, and superconductivity appears at the doping level $x \simeq 0.05$. In case (a), near $x \simeq 0.05$, the superconductivity and antiferromagnetism coexist at low temperature, while in case (b) there is no coexistence. The dependence of T_c on doping is weak; maximum in $T_c(x)$ at $x \sim 0.12-0.15$ is *shallow*.

The phase diagrams of ferropnictides look quite similar to that of the cuprates (Fig. 5.10 (b)). One also has a superconducting dome and an antiferromagnetic phase where the carrier density is low. However, there are clear differences. In the cuprates, as we shall see later, the antiferromagnetic phase is not a metal but rather a Mott insulator. Furthermore, in the underdoped region, an anomalous *pseudogap phase* exists.

5.5.4 Experimental properties (normal state)

- $C_V \sim \alpha T + \beta T^3$,
- $\chi \sim A + BT$,
- ρ (DC conductivity) $\sim A + BT^2$,
- Hall coefficient $\sim A + BT$.

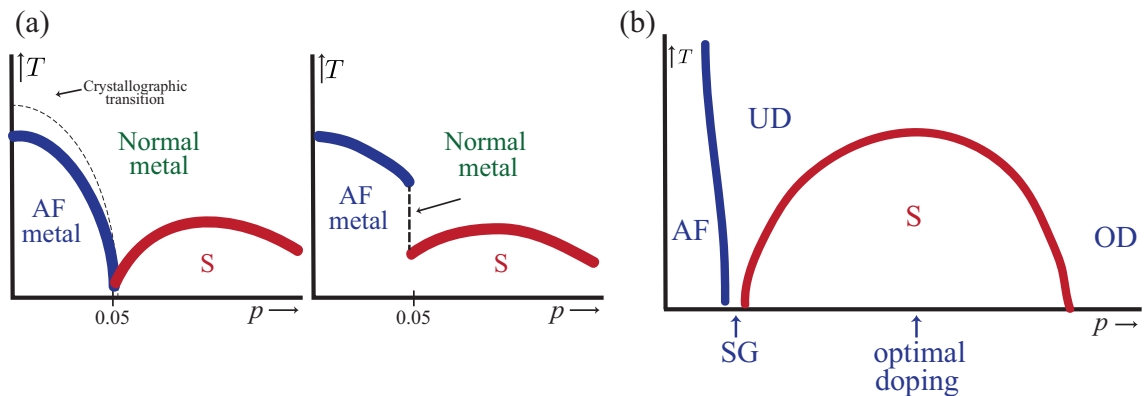


Fig. 5.10. (a) Phase diagrams of ferropnictides. (b) Phase diagram of the cuprates.

What are the properties of the normal phase? Crudely speaking, the specific heat C_V has the electron contribution αT and the phonon contribution βT^3 . The susceptibility χ has a constant A plus BT . For the DC conductivity, so far, the anisotropy of resistivity has not been measured carefully. People have measured a parent anisotropy rate, but it is indirect and not totally reliable. Since this is a quite delicate point, it is advisable to check up the up-to-date literature. For some reasons it seems difficult, at least to date, to prepare these metals in a large single crystal form, and there has not been any anisotropy measured. However, overall, the DC conductivity in the ab -plane is given by $A + BT^2$, where A is typical of impurities and B of the electron-electron Umklapp process. Furthermore, at room temperature, the DC resistivity is $\sim 3 \text{ m}\Omega$, which is comparable to that of cuprates. The Hall coefficient goes like $A + BT$, and its value is not dramatically different from textbook values.

5.5.5 Band structure

What about the band structure? If one performs angle-resolved photoemission spectroscopy (ARPES), quantum oscillation experiments, and the local density approximation (LDA) calculation, one finds the Fermi surface shown in Fig. 5.11 (a). Two holelike Fermi surfaces, which are not qualitatively different, are around the Γ point (0,0); two electronlike Fermi surfaces are around the M point (π, π) ¹¹ (be careful about notation!). There is also one fairly 3D band around Γ point.

There is one important point here. In 1111 systems, the Fermi surface is quite two-dimensional (*barrel-like*), while in 122 systems, it is much more three-dimensional. This suggests that the Fermi surface changes its shape along the z -direction (Fig. 5.11 (b)). Additionally, magnetism is much stronger in 122.

¹¹The number of Fermi surfaces varies depending on compounds, carrier concentrations, etc.

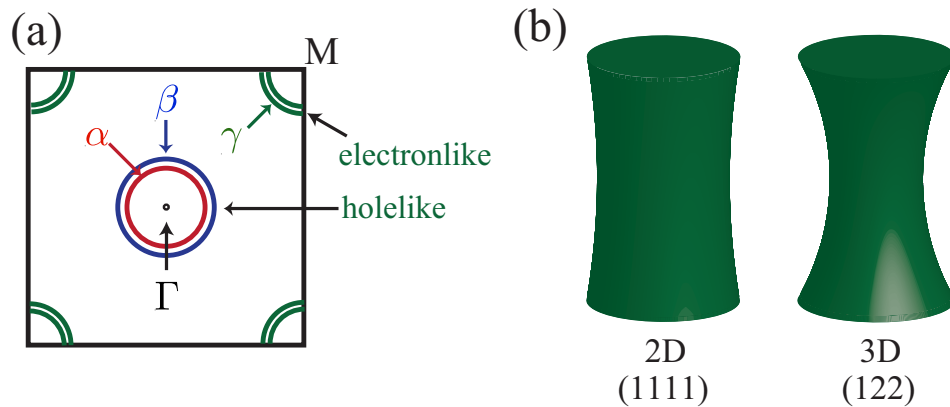


Fig. 5.11. (a) Fermi surface of ferropnictides. (b) Fermi surfaces in three dimensions.

5.5.6 Superconductivity

When I asked if a metal containing iron could be a good high-temperature superconductor, in the past most people answered in the negative. In fact, iron does have magnetic moment $\sim \mu_B$ as is measured by neutron scattering, and this magnetic moment would be destructive to superconductivity. However, the ferropnictides show superconductivity; T_c rises up to ~ 56 K in (doped) 1111, 38 K in 122, 20 K in 11. We also note that T_c is only weakly dependent on the carrier concentration x (e.g., $\text{LaFeAsO}_{1-x}\text{F}_x$).

5.5.7 Experimental properties (superconducting state)

All ferropnictides are strongly type-II, with extrapolated $H_{c2}(0) \sim 55\text{T}$. This value exceeds the Chandrasekhar–Clogston limit. The anisotropy is relatively small (~ 2 – 3). The zero-temperature penetration depth and the zero-temperature pair radius are $\lambda_{ab}(0) \sim 1600$ – 2400 Å, and $\xi_{ab}(0) \sim 20$ Å, respectively. ARPES shows that, on all sheets, the superconducting gap is only weakly \mathbf{k} -dependent.

What about the low-temperature behaviors of NMR and the penetration depth? Unfortunately, again experimental data in the literature are mutually inconsistent, but favor power law. Importantly, the Knight shift goes to zero as $T \rightarrow 0$ for *all* directions of magnetic field; this fact strongly indicates spin-singlet pairing. Isotope-effect experiments are mutually inconsistent, but most recent ones give a small value of α_1 ; this suggests that the mechanism is probably non-phonon.

Another reason why people tend to believe rather strongly it is not a phonon mechanism is that by now the actual theoretical techniques for calculating electron-phonon superconductivity are pretty well evolved. Most experts in this area are fairly confident that phonon mechanism by no means gives the critical temperature 55 K.

5.5.8 Pairing state

The Knight shift fairly strongly suggests the singlet spin state. Since the crystal has a tetragonal symmetry, main candidates are nodeless s -state and $d_{x^2-y^2}$ -state with nodes along the diagonal directions. We will come back to this point much more in detail in the context of cuprates. ARPES data suggests nodeless state, i.e., s -wave state. At low or zero temperature, however, various quantities such as T_1 and λ favor nodes.

Again, the extra complication is that in this case there are several bands, which causes the second Fermi surface. There is no particular reason why the gap must have the same sign on all sheets of the Fermi surface. Theory based on spin-fluctuation mechanism (most obvious non-phononic mechanism) predicts that the gap changes sign between the electronlike and holelike sheets (s^\pm -wave). Experimental evidence claimed in favor of this assignment: Josephson-like experiment on polycrystalline sample shows half flux quanta [26], which is characteristic to s^\pm state. STM again showed indirectly that s^\pm -state is favored [27]. Unfortunately, there has been no true Josephson experiment yet; one needs more carefully prepared single crystals. We may have them in the future.

Since ferropnictide superconductors have only 3-years history right now¹², one needs more time to settle the mechanism of the pairing state. One thing I could say pretty sure is that it is spin-singlet. Beyond that, we have yet to answer.

¹²This lecture was done at The University of Tokyo in 2011.

References

- [1] F. Steglich, J. Aarts, C. D. Bredl, W. Lieke, D. Meschede, W. Franz, and H. Schäfer, *Phys. Rev. Lett.* **43**, 1892 (1979).
- [2] G. R. Stewart, *Rev. Mod. Phys.* **56**, 755 (1984).
- [3] G. R. Stewart, Z. Fisk, J. O. Willis, and J. L. Smith, *Phys. Rev. Lett.* **52**, 679 (1984).
- [4] Y. Ōnuki, Y. Shimizu, and T. Komatsubara, *J. Phys. Soc. Jpn.* **53**, 1210 (1984).
- [5] G. R. Stewart, Z. Fisk, and M. S. Wire, *Phys. Rev. B* **30**, 482 (1984).
- [6] J. Kondo, *Prog. Theo. Phys.* **32**, 37 (1964).
- [7] A. Hewson, *The Kondo problem to heavy fermions Vol. 2* (Cambridge Univ Pr, 1997).
- [8] M. A. Ruderman and C. Kittel, *Phys. Rev.* **96**, 99 (1954).
- [9] T. Kasuya, *Prog. Theo. Phys.* **16** (1956).
- [10] K. Yosida, *Phys. Rev.* **106**, 893 (1957).
- [11] H. Ott, O. Marti, and F. Hulliger, *Solid State Comm.* **49**, 1129 (1984).
- [12] H. R. Ott, H. Rudigier, Z. Fisk, and J. L. Smith, *Phys. Rev. Lett.* **50**, 1595 (1983).
- [13] C. Geibel *et al.*, *Z. Phys. B* **84**, 1 (1991).
- [14] T. Palstra, A. Menovsky, J. Berg, A. Dirkmaat, P. Kes, G. Nieuwenhuys, and J. Mydosh, *Phys. Rev. Lett.* **55**, 2727 (1985).
- [15] S. Saxena *et al.*, *Nature* **406**, 587 (2000).
- [16] A. Huxley, I. Sheikin, E. Ressouche, N. Kernavanois, D. Braithwaite, R. Calemczuk, and J. Flouquet, *Phys. Rev. B* **63**, 144519 (2001).
- [17] C. Petrovic, P. Pagliuso, M. Hundley, R. Movshovich, J. Sarrao, J. Thompson, Z. Fisk, and P. Monthoux, *J. Phys.: Cond. Matt.* **13**, L337 (2001).
- [18] C. Geibel *et al.*, *Z. Phys. B* **83**, 305 (1991).

- [19] Y. Maeno, H. Hashimoto, K. Yoshida, S. Nishizaki, T. Fujita, J. Bednorz, and F. Lichtenberg, *Nature* **372**, 532 (1994).
- [20] A. P. Mackenzie and Y. Maeno, *Rev. Mod. Phys.* **75**, 657 (2003).
- [21] G. Luke *et al.*, *Nature* **394**, 558 (1998).
- [22] F. Kidwingira, J. Strand, D. Van Harlingen, and Y. Maeno, *Science* **314**, 1267 (2006).
- [23] J. Xia, Y. Maeno, P. T. Beyersdorf, M. M. Fejer, and A. Kapitulnik, *Phys. Rev. Lett.* **97**, 167002 (2006).
- [24] Y. Kamihara, T. Watanabe, M. Hirano, and H. Hosono, *J. Am. Chem. Soc.* **130**, 3296 (2008).
- [25] J. Paglione and R. L. Greene, *Nature Physics* **6**, 645 (2010).
- [26] C. Chen, C. Tsuei, M. Ketchen, Z. Ren, and Z. Zhao, *Nature Physics* **6**, 260 (2010).
- [27] T. Hanaguri, S. Niitaka, K. Kuroki, and H. Takagi, *Science* **328**, 474 (2010).

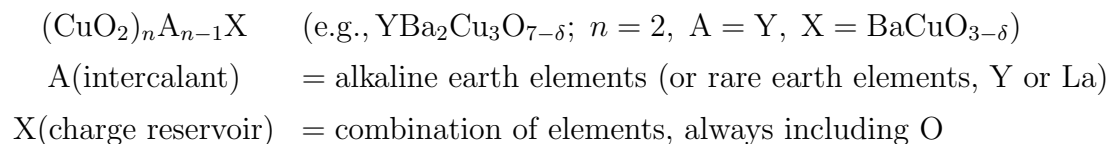
Lec. 6 Cuprates: generalities, and normal state properties

When the cuprate superconductors were originally discovered in 1986, it was a great surprise; they were the first materials to show reproducible superconductivity above 100 K. We know that at least 300 cuprates are superconductors and many of them, several dozens, actually have transition temperatures $T_c \sim 110\text{-}120$ K. One important point is that, though most cuprate materials are superconductors often with very high transition temperatures, there is a small class of cuprates which does not show superconductivity under any condition.

6.1 Basic chemical properties

6.1.1 Composition

The chemical composition of the cuprates is very characteristic and typical. We here introduce a very natural (but unconventional) notation:



This notation reflects a characteristic structure of the cuprates.

6.1.2 Structure

Figure 6.1 (a) shows the side view of the cuprates with $n = 2$, in which we can see that there are two copper oxide planes. Between them there are various materials X, which always contain oxygens, and these oxygens are frequently called apical oxygens. The reason for this nomenclature is that if we consider the positions of the apical oxygens in the three-dimensional picture they sit in the apices of the octahedron with the oxygens included in the CuO_2 plane. The intercalants A sit between the planes in the case of more than one copper oxide planes per unit cell.

A rather important characteristic of the cuprate superconductors is that we very often find homologous series. The homologous series is a sequence of materials with the same

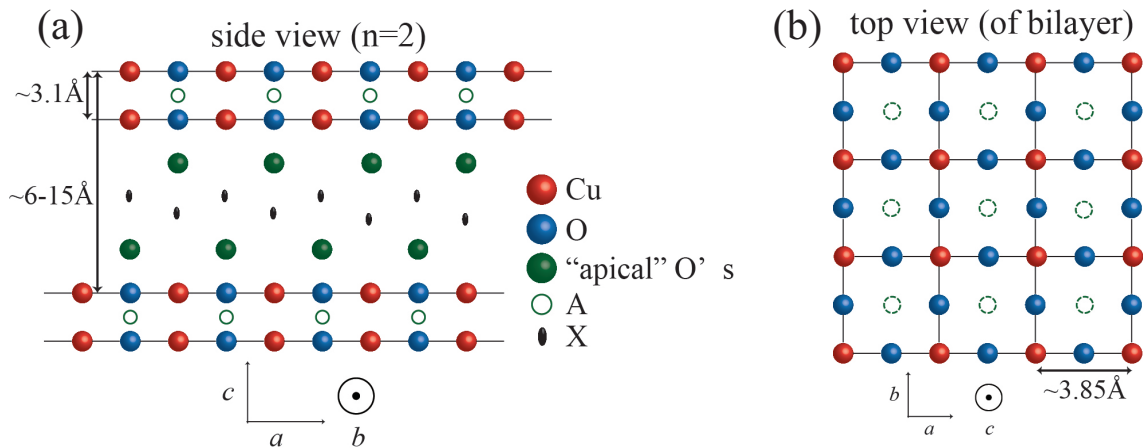
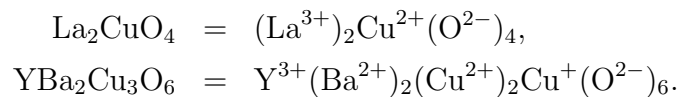


Fig. 6.1. (a) Side view of cuprates with $n = 2$. (b) Top view of cuprates with $n = 2$.

intercalant A and the same charge reservoir X but with a different number of layers (e.g., $\text{Tl}_2\text{Sr}_2\text{CuO}_6$, $\text{Tl}_2\text{Sr}_2\text{CaCu}_2\text{O}_8$, $\text{Tl}_2\text{Sr}_2\text{Ca}_2\text{Cu}_3\text{O}_{10}$, \dots), which is schematically shown in the Fig. 6.2 (a).

The superconductivity in the cuprates occurs in the neighborhood of what is called parent compounds. We can often start (for a given X) with a stoichiometric compound (“parent” compound) when valences balance, i.e., the total charge becomes neutral;



The state of the copper in the plane is Cu^{2+} : the copper starts with a $(3d^{10})(4s)^1$ electron state and loses two electrons and then becomes a $3d^9$, so that there is one hole in the d -shell per formula unit. This is typical for all the parent compounds of the cuprates. If we have a structure of this type, then we have an odd number of electrons per unit cell. Naively thinking, the system ought to be a metal. However, the system becomes an antiferromagnetic Mott insulator (Fig. 6.2 (b)): the electrons are localized at the copper atoms and order antiferromagnetically.

6.2 Doping

Suppose one starts with a “parent” compound, say La_2CuO_4 , and replaces a fraction x of La with Sr per unit cell, i.e.,



Since La has valence 3+ and Sr has 2+, the effect of this replacement is to add $-x$ electrons, i.e., x holes, per formula unit. In this case, the holes have nowhere to go but to the CuO_2 plane, and hence we are fairly confident that p , the doping per CuO_2 unit, is equal to the chemical stoichiometry x .

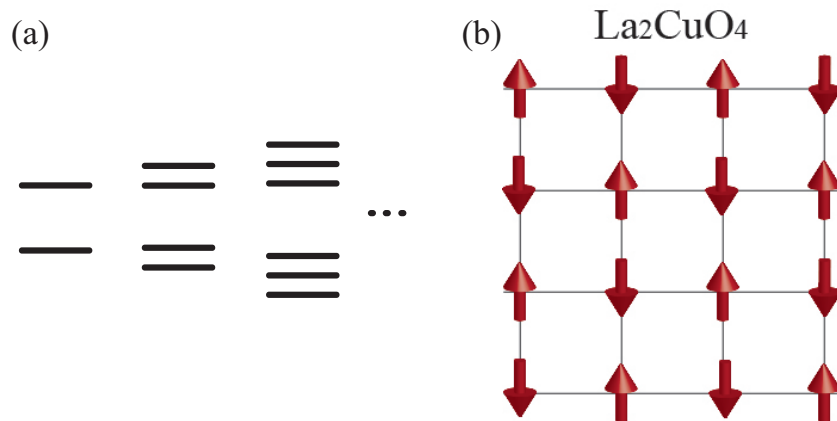
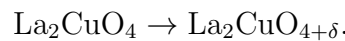


Fig. 6.2. (a) Homologous series. (b) Antiferromagnetic Mott insulator.

Alternatively, let us consider adding δ oxygen atoms per formula unit,



In this case, since the valence of O is 2−, the effect is to add 2δ holes per CuO_2 unit, i.e., $p = 2\delta$. In multiplane materials ($n > 1$), one must remember that any added holes have to be shared between the n planes per unit cell. Hence, naively, for example $\text{YBa}_2\text{Cu}_2\text{O}_{6+\delta}$, we expect $p = \frac{1}{2}(2\delta) = \delta$. However, in this case there are other complications because the added holes can go elsewhere than to the CuO_2 planes (e.g., in the “chains”). The chains are very specific for this compound, and then this is a complication special to this material.

What can we guess about the orbit(s) occupied by the holes in the CuO_2 plane? There is a general belief based on the quite reliable band structure obtained from atomic physics calculations; both the original one hole per CuO_2 unit in the parent state and any added holes by the doping occupy mainly the $3d_{x^2-y^2}$ orbital. However, this orbital may be somewhat hybridized with the p_x or p_y states on the neighboring oxygens (Fig. 6.3).

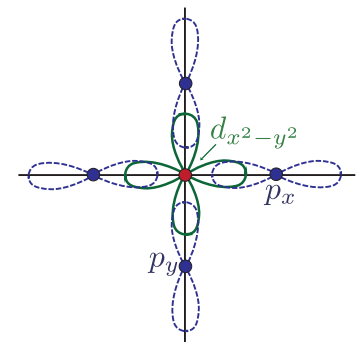


Fig. 6.3. Hybridization of the orbitals.

A vast majority of the cuprate superconductors are hole-doped; if we start from the parent compound we add not extra electrons but extra holes. However, there are also a few electron-doped cuprates. The best known electron-doped cuprates is NCCO ($\text{Nd}_{1-x}\text{Ce}_x\text{CuO}_4$). Properties of the electron-doped materials are qualitatively very similar to the hole-doped ones [1, 2].

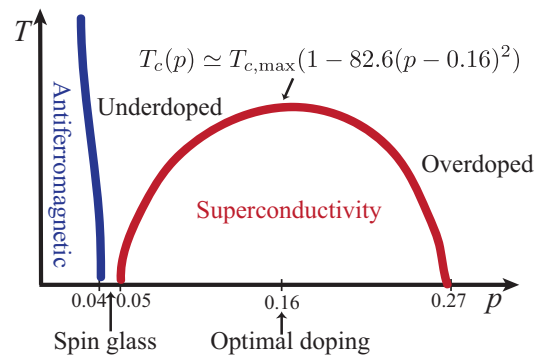


Fig. 6.4. Phase diagram of cuprates. The doping dependence is universal, and the temperature dependence (i.e., $T_{c,\max}$) is strongly material-dependent.

6.3 Construction of phase diagram

There are various factors controlling the interesting behavior of the cuprates, but the two most important ones are temperature T and the number of holes p per CuO_2 unit in the plane. How do we fix p ? There are two possibilities:

- (a) All added holes are known to go to CuO_2 planes (e.g., $\text{La}_{2-x}\text{Sr}_x\text{CuO}_4$).
- (b) The destination of the added holes are ambiguous (e.g., YBCO).

In the former case, we can simply fix p from x (or δ). However, in the latter case, we should fix p pragmatically. In most cases, what one usually does in practice is, if there exists another cuprate corresponding to the case (a) and an accessible region in the phase diagram has some overlap with it, we fix p so that we get the same p -dependence. This is important because there is no cuprate which can be explored in the whole range of p that is interesting to us. Therefore, we have to overlay different materials in the phase diagram. This might seem to be a little bit skew, but so far this is consistent with experiments.

Phase diagram of the cuprates

The phase diagram of the cuprates is shown in Fig. 6.4. As one goes from a Mott insulating parent compound to small values of the doping p , it remains antiferromagnetic. However, at the doping $p \simeq 0.04$, the system comes into a mysterious phase, usually thought of a spin glass phase. Then the superconducting phase appears roughly between $0.05 < p < 0.27$. To some extent, this universality of the p -dependence is a matter of construction because we simply decided to measure p so that the p -dependence is consistent. At least everything goes well and is consistent in this way; the p -dependence is universal and always the superconducting dome starts at $p = 0.05$ and terminates at $p = 0.27$. On the other hand, the dependence on the T -axis is rather non-universal; for Bi-2201 $T_{c,\max} \sim 10$ K, while for Hg-2223, one with the highest T_c , the transition

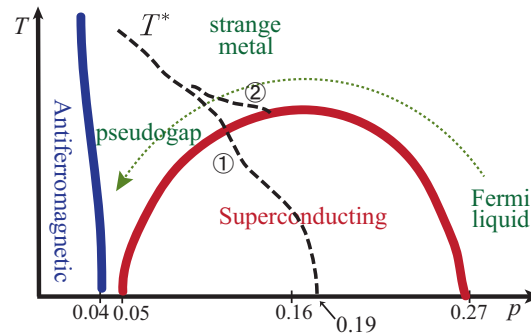


Fig. 6.5. T^* -line: locus of “crossover” behavior in various experimental quantities (C_V , χ , ρ_c, \dots).

temperature can be as large as $T_{c,\max} \sim 160$ K under 20 GPa. This problem is a huge mystery.

In the region $p > 0.27$, superconductivity does not appear and the system is well described by the genuine Fermi-liquid theory. On the other hand, in the region $0.04 < p < 0.05$, it is far from the Fermi-liquid state.

Here is an interesting question: let us consider a virtual path in the phase diagram which goes above the superconducting dome and connects these two regions (the dotted arrow in Fig. 6.5). Is there any point of a phase transition or any steep crossover? Apparently, there is no actual phase transition, but there is a so-called T^* -line. This roughly corresponds to a relatively sharp crossover line.

Although there is much controversy, most people claim that the Fermi-liquid region first changes to the strange metal region, and the pseudogap regime appears between the antiferromagnetic phase and the superconducting dome. Roughly speaking, there is a sharp crossover in various physical quantities between the strange metal regime and the pseudogap regime.

There are some interesting and controversial questions related to this T^* -line. The first one is about the property of the T^* -line;

1. Does it really correspond to a hidden phase transition not seen apparently or just a crossover?

Another one is about the low- T behavior;

2. Does the T^* -line (i) intersect the superconducting dome, or (ii) join smoothly onto the $T_c(p)$ line?

This question has arisen because it was very difficult to change p until quite recently. Now there is an argument which strongly favors the option (i) [3].

Table 6.1. Transition temperatures of various homologous series.

Common name	X group	n=1	2	3	4	5
Hg-12, $n-1, n$	HgBa ₂ O _{3+δ}	98	126	135	125	110
Tl-22, $n-1, n$	Tl ₂ Ba ₂ O ₄	95	118	125	112	105
Tl-12, $n-1, n$	TlBa ₂ O _{3-δ}	70(?)	103	123	112	107
Pb-22, $n-1, n$	PbSr ₂ O _{3+δ}	~40	97(?)	122	107	
Bi-22, $n-1, n$	Bi ₂ Sr ₂ O ₄	10-20	89	107		

6.4 Determinants of T_c

As noted, $T_{c,\max}$ varies enormously between different cuprates. What else determines T_c other than the doping p ? Correlations with

- the degree of the orthorhombic anisotropy,
- the degree of buckle of the planes,
- the distance to apical the oxygens,
- the chemical environment of the planes,

have been suggested, but none of them is “overwhelming”. On the other hand, in the homologous series, we can see a universal dependence of the maximum transition temperature $T_{c,\max}$ on the number of CuO₂ planes n , as shown in Table 6.1. As n goes to two from one and to three from two, $T_{c,\max}$ also goes up. Beyond $n = 3$, $T_{c,\max}$ decreases as n increases. Note that there is often a relation $\Delta T_{c(2-3)} \simeq \frac{1}{3} \Delta T_{c(1-2)}$.

I think probably it is not significant that T_c falls beyond $n = 3$. For all different members in the homologous series, we need to dope all of the planes, and if we get too many planes then they are just run out of the doping. Therefore, I suspect that the feature of the drop in T_c beyond $n = 3$ may be rather trivial.

There is one digression I just want to make about “the dogs which did not bark in the night-time”. This refers to the class of the cuprates which never become superconducting. There is a little-noticed fact that I think very interesting; without exception, all of these non-superconducting cuprates are either bi/tri-layer with alkaline-earth spacers (Sr, Ba) which are heavier than Ca. I think this is not due to the basic effect of the replacement

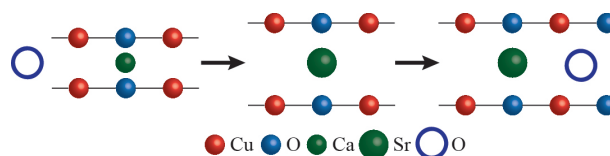


Fig. 6.6. Schematic illustration of the intruder O atoms.

Table 6.2. Notable features of various cuprates.

Compound	Common name	Notable features
$\text{La}_{2-x}\text{Sr}_x\text{CuO}_4$	LSCO	(almost) earliest HTS, large crystals
$\text{YBa}_2\text{Cu}_3\text{O}_{6+\delta}$	YBCO	first liquid-nitrogen temperature superconductors whose $T_c \sim 90$ K, “E. coli” of cuprates
$\text{Bi}_2\text{Sr}_2\text{Ca}_{n-1}\text{Cu}_n\text{O}_{(n+2+\delta)}$	BSCCO	“baklava”, good for ARPES, EELS, etc. most anisotropic high- T_c superconductor known.
$\text{HgBa}_2\text{Cu}_n\text{Ca}_{n-1}\text{O}_{2(n+1)}$	HgBCO	record holder for T_c (~ 160 K at 20 GPa).
$\text{Nd}_{1-x}\text{Ce}_x\text{CuO}_4$	NCCO	electron-doped
$\text{Ca}_{1-x}\text{Sr}_x\text{CuO}_2$	∞ -layer	no reservoir group X, infinite set of CuO_2 planes separated by alkaline earth ions Ca/Sr.

of Ca with Sr or Ba, but rather due to the effect of what I call the “intruder” oxygens. This is shown schematically in Fig. 6.6.

Let us start from the bilayer La compound where the intercalant is Ca. This is a superconductor with $T_c \sim 55$ -60 K. Then, we replace Ca by Sr, which is slightly bigger than Ca. The larger Sr intercalant atoms widen the distance between the CuO planes, and the oxygens are more likely to enter the aperture between the copper oxide planes, which depresses the transition temperature T_c . However, no one knows the reason why the intruder oxygens are so destructive to superconductivity.

6.5 Other remarks: carrier density and list of cuprate superconductors

At the “optimal” doping ($p \simeq 0.16$), the density of the (extra) holes in the plane is about $1.5 \times 10^{14} \text{ cm}^{-2}$. Hence the three-dimensional density is around $1\text{-}2 \times 10^{21} \text{ cm}^{-3}$ and interestingly that is quite comparable to strontium-ruthenates, ferroplnictides, This is rather interesting, since the high-temperature superconductivity does seem to require a rather low electron density.

Before we go into experimental techniques for the cuprates, here we list some interesting cuprates in the Table 6.2.

6.6 Experimental properties of the normal state: general discussion

First of all, unlike most of the other superconductors we are familiar with, the properties of the cuprates do seem to be very strongly dependent, not just on the doping, but on the impurities. For example, if we deliberately put Zn into a place of some of the copper in the CuO planes, this in fact has an enormous effect on the superconductivity. In the early days, arguments about some of the early experiments were completely spoiled by the impurity effect. We have to always bear in mind that, in particular with new experimental techniques, the experimental facts presented here are subject to revision.

Secondly, it is easy to vary temperature T at a fixed doping p , but it is much more difficult to vary p at a fixed T . Quite recently, people have started taking up a new kind of techniques; they prepare thin films of the cuprates, and then try to dope them electrically. However, one has to be cautious because the doping in this case only extends to the first few layers, and we may be probing the surface property rather than the bulk property.

Thirdly, many types of experiments can only be done on particular cuprates. For example, the ARPES is typically done on BSSCO and YBCO, and the neutron scattering on LSCO and YBCO. We always have to bear in mind that even if we have measured some spectacular properties on one cuprate, we are not sure whether they apply to all. Generally speaking, people tend to assume it does, but there is no warranty and sometimes naive application is quite dangerous.

It turns out that some regions of the phase diagram are relatively conventional. First, the least controversial phase is the Mott antiferromagnetic insulator phase in the low-doping region. Our knowledge suggests that this is just a standard antiferromagnetic insulator described by the nearest-neighbor Heisenberg Hamiltonian

$$\hat{H} = J \sum_{\langle ij \rangle} \hat{\mathbf{S}}_i \cdot \hat{\mathbf{S}}_j, \quad (6.1)$$

with $J_{\text{in-plane}} \sim 1000$ K and $J_{\text{bilayer}} \sim 200$ K. This is consistent with experimentally observed $T_N \sim 300$ K at $p=0$ for LSCO, 500 K for YBCO. YBCO has a higher Néel temperature than LSCO, probably because YBCO has two CuO layers, while LSCO has only one.

Second, in the overdoped regime again, most people agree that the system is approximately a standard Fermi liquid; the system becomes more conventional as one dopes more in the overdoped regime. Finally, in the narrow spin-glass region of the doping $0.04 < p < 0.05$, a few experiments suggest the resistivity $\rho(T)$ increases without limit as one decreases the temperature; if one could reach $T = 0$, which is impossible in real life, the system would be a perfect insulator. This behavior is rather similar to what we find in disordered granular films.

6.7 Experimental properties at the optimal doping

6.7.1 Electronic specific heat

Let us move on to the controversial regimes. First of all, let us consider the optimal doping $p \sim 0.16$, where T_c takes its maximum value. What about the thermodynamic properties? It is known that the electronic part of the specific heat behaves as $C_V^{\text{el}} = \gamma T$ at least up to the room temperature [4]. The coefficient γ per CuO_2 unit is about $\gamma \simeq 6.5 \text{ mJ/mol}(\text{CuO}_2)\text{K}^2$, which is almost the same for LSCO, YBCO, and Tl-2201. If one interprets the value with the Fermi liquid theory, the density of states is given by

$$N(0) \simeq 1.4 \text{ eV}^{-1}\text{spin}^{-1}(\text{CuO}_2 \text{ unit})^{-1}. \quad (6.2)$$

This value is about four times the two-dimensional free electron value $ma^2/2\pi\hbar^2$. The specific heat above T_c does appear to be consistent with the Fermi liquid model with the mass enhancement $m^*/m \sim 4$. Given the tight-binding structure of the cuprates, this mass enhancement seems quite reasonable.

6.7.2 Magnetic properties

The Pauli spin susceptibility χ , determined mostly from the Knight shift on YBCO, is approximately independent of T [5]. There is one interesting point here; the in-plane Knight shift for Cu is much larger than that for Y or O. This is significant for people who believe in the spin fluctuation theory. The nuclear spin relaxation rate T_1 is inversely proportional to the temperature, i.e., $T_1^{-1} \propto T$, which is known as the Korringa relation. So far, all the properties of the normal phase at the optimal doping appear to be pretty much Fermi-liquid like.

6.7.3 Transport

Cuprates are very strongly layered materials. Almost all the transport properties are strongly anisotropic. Quoted results below are values in the ab -plane unless otherwise stated [5, 6].

If one measures the DC resistivity of the cuprates at the optimal doping, *all* the cuprates have $\rho \propto T$ from $T \sim 800 \text{ K}$ all the way down to T_c (down to $T \sim 10 \text{ K}$ for Bi-2201). Above 800 K the situation becomes more complicated because the oxygens get disturbed, and thus one usually does not think about that regime. Except for this high-temperature regime, the resistivity appears to be exactly linear to the temperature, which is quite a remarkable fact.

What happens if one goes away from the optimal doping? It turns out that the resistivity generally behaves as $\rho \propto T^\alpha$, where α varies continuously. In the overdoped limit,

$\alpha = 2$, which is consistent with the Fermi-liquid theory if the electron-electron Umklapp scattering is taken into account. If one moves from the overdoped regime to the optimal doping regime, α changes from 2 to 1. If one moves further into the underdoping regime, α becomes smaller than 1 and finally less than 0.

If one thinks about the conductivity rather than the resistivity, since the conductivity is simply a sum of contributions from different planes, one can define the conductivity per CuO plane. One obvious question is whether this value is universal for all cuprates. The answer is generally no. However, for higher- T_c materials, the resistivity per plane, i.e., the inverse of the conductivity per plane, seems to be approximately universal

$$R_{R.T.} \sim 3 \text{ k}\Omega \sim 0.12R_Q, \quad (6.3)$$

where $R_{R.T.}$ and R_Q are the resistivity at the room temperature and the quantum universal resistance, respectively¹. In the lower- T_c materials, on the other hand, the conductivity, in general, is much smaller. This may be rather trivially understood from the following argument: almost universally² in all lower-temperature cuprates, the dopants sit close to CuO_2 planes. Therefore, they provide extra scattering mechanisms.

Can the $\rho \propto T$ law at the optimal doping be explained by the phonons? It is well known that at least at high temperatures, ordinary metals are described by the Fermi-liquid theory and show a linear- T dependence for $T \gtrsim \Theta_D$. This resistivity is caused by the scattering of electrons by phonons. Is this what is going on at the optimal doping? Almost certainly not. First of all, the Debye temperature of most cuprates is typically about the room temperature, but the linear behavior is still exactly linear down to far lower temperatures than the Debye temperature³. Furthermore, in a naive calculation based on what we know about the phonon spectrum and the electron-phonon coupling in the cuprates, it looks as if the phonon contribution should give us a resistivity larger than this. Thus, the phonon mechanism seems to be unable to explain the linear law, and something more subtle is going on here.

As for the AC conductivity $\sigma(\omega)$, on the other hand, the following Drude form is well known for ordinary metals

$$\sigma(\omega) \sim \frac{ne^2\tau/m}{1 + i\omega\tau}. \quad (6.4)$$

We can therefore ask whether the resistivity of cuprates fits well with this formula. The answer is yes, only if the relaxation time τ is allowed to be a function only of ω , with the behavior

$$\tau(\omega) \sim \max(\omega, k_B T / \hbar). \quad (6.5)$$

¹In in two dimensions, the resistivity has the same dimension as the resistance.

²Bi-2201 seems to be a special exception.

³One should be cautious here; it is known that in some textbook metals like Re, the linear law of resistivity persists well below Θ_D . Re has the Debye temperature 300 K and the linear behavior persists down to 75 K. Thus even if the linear behavior is observed down to a far lower temperature than the Debye temperature, it is not a sufficiently convincing argument against phonons.

The early model of the normal state of cuprates, the so-called marginal Fermi liquid theory, is essentially based on the same assumption.

For the Hall angles for pure samples in the high-field ~ 8 T, one normally finds

$$\cot \Theta_H \propto T^2. \quad (6.6)$$

A rather odd thing to be remarked; if one plots the thermoelectric power at low temperatures, it does not look so spectacular. If one plots it as a function of the doping, however, the room temperature value, as a function of the doping, crosses zero almost exactly at the optimal doping for all the known cuprates [7]. In fact, if one wants to know whether a certain material at the room temperature becomes a superconductor, the thermoelectric power at the room temperature can thus be a good criterion.

So far, we have talked about the ab -plane transports. What about the c -axis? The c -axis resistivity at the optimal doping is rather interesting. It always appears to vary as

$$\rho(T) \propto T^\alpha. \quad (6.7)$$

However, the power α can range from -1 to $+1$ for different cuprates, which is quite puzzling. There have been a large number of papers trying to explain this fact.

6.7.4 Spectroscopic probes: Fermi surface

If one is dealing with some materials, the obvious question is whether they have any Fermi surface and, if they have, what the Fermi surface looks like. Two most useful probes of the Fermi surface in a metal are angularly resolved photoemission spectroscopy (ARPES) and quantum-oscillation phenomena.

In the late 1980s, it was recognized that ARPES should be a particularly nice way for examining cuprates⁴. In ARPES, one shines light with a given frequency, and measures the momentum and energy of the electrons kicked out. If one deals with a three-dimensional metal, there would be a slight problem there; although the momentum is conserved in the transverse direction, the component normal to the surface is likely to change when the electron emerges from the metal. In the cuprates, very luckily, one can essentially treat it as a two-dimensional problem, and the above problem does not appear. ARPES essentially measures the spectral function $A(\mathbf{k}, \varepsilon)$, the probability of finding an electron with its momentum \mathbf{k} and energy ε in the thermal equilibrium state. For non-interacting electrons, it would be proportional to $\delta(\varepsilon - \varepsilon_{\mathbf{k}})$, because if one electron has a Bloch wave \mathbf{k} it has the definite energy corresponding to the wave vector. One expects that the coefficient of the delta function is essentially 1 when \mathbf{k} is inside the Fermi surface, and 0 for the other. However, this is not the case, in general, for interacting cases including the cuprates.

⁴For a review of ARPES studies on cuprate superconductors, see Ref. [8].

The quantum-oscillation phenomena occur in thin materials under a high magnetic field, in which various quantities such as the magnetization and the resistivity oscillate as a function of the magnetic field. The oscillation is not periodic in the field itself but rather in the inverse of the field. Let us refer to the class of these effects as de Haas-van Alphen (dHvA) effects. The quantum oscillations were, for a long time, thought to be almost impossible in the cuprates. However, in the last three years or so, researchers have succeeded in doing dHvA experiments. The dHvA-type experiments measure the area(s) of those parts of the Fermi surface corresponding to the closed orbits, the classical motion in the magnetic field. One cannot say anything about their shape or position through dHvA experiments. Because of the strongly two-dimensional (layered) nature of the cuprates, the magnetic field is always applied along the c -axis, and it simply measures the areas of the two-dimensional Fermi surface(s), which is a much simpler situation than in three-dimensional metals.

6.7.5 Results of ARPES experiments at the optimal doping

First of all, $A(\mathbf{k}, \varepsilon)$ does not look like $\delta(\varepsilon - \varepsilon_{\mathbf{k}})$ at all; an incoherent background seems to be $\sim 90\%$ of the total weight. We do get the peak but it is just 10% of the total weight. Crudely speaking, this result suggests that if indeed the cuprates at the optimal doping are well described by the Fermi liquid theory, they are very *bad* ones. However, the energy-integrated function, which indicates whether the state \mathbf{k} is occupied, does show a jump ($\sim 10\%$) as a function of $|\mathbf{k}|$ for a given direction $\hat{\mathbf{n}}$. Since the Fermi surface is defined as the locus of the points where the discontinuity occurs, this fact gives us a well-defined Fermi surface. This function for cuprates at the optimal doping is shown in Fig. 6.7. Filled states are located at the center of the first Brillouin zone, and the hole-like Fermi surface is located at the zone corner (π, π) . Luttinger's theorem states that the volume enclosed by the Fermi surface is directly proportional to the particle density, and it allows us to calculate the hole density: $n_h \sim 1.19$ ($\sim 1 + p$, as naively expected). This is

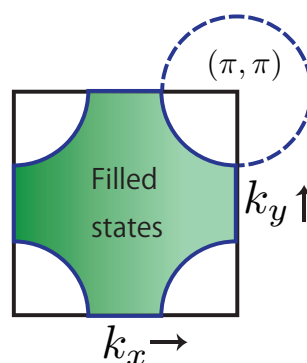


Fig. 6.7. Energy-integrated function of the cuprates.

a rather important result; at least, at the optimal doping, it is consistent with the Fermi liquid picture. Moreover, the number of electrons occupying the Fermi sea is exactly 1 plus p , where the former contribution (1) is originally there in the parent compound, while the latter one (p) is added by the doping. It turns out that dHvA experiments on a somewhat overdoped side are consistent with this result.

6.7.6 Neutron scattering

Neutrons couple mainly to electron spins, and the cross-section $\sigma(\mathbf{q}, \omega)$ measures the spin-fluctuations. For fixed \mathbf{q} , the cross-section as a function of ω in the normal state has no marked structure. However, for fixed ω , the cross-section as a function of \mathbf{q} has a marked peak at $\mathbf{q} = (0.5\pi/a, 0.5\pi/a)$ [9]. Importantly, the \mathbf{q} value is precisely equal to the Bragg vector of the magnetic superlattice in the antiferromagnetic phase, which of course is measured independently. This suggests that the strong antiferromagnetic spin fluctuations, which are there in the original pure antiferromagnetic phase, do seem to persist quite strongly into the non-magnetic phase.

6.7.7 Optics (ab -plane)

Most of the direct experiments measure the optical reflectivity $R(\omega)$ [9]. Unfortunately, the optical reflectivity measures a raw and nasty combination of the real and imaginary parts of the dielectric function:

$$R(\omega) = \frac{(1 - \text{Re } \varepsilon(\omega))^2 + (\text{Im } \varepsilon(\omega))^2}{(1 + \text{Re } \varepsilon(\omega))^2 + (\text{Im } \varepsilon(\omega))^2}. \quad (6.8)$$

To obtain anything about the individual part, one can exploit the fact that the real and imaginary parts are related by the Kramers–Kronig relations:

$$\text{Re } \varepsilon(\omega) - 1 = \text{P} \int_{-\infty}^{\infty} \frac{d\omega'}{\pi} \frac{\text{Im } \varepsilon(\omega')}{\omega' - \omega}, \quad (6.9)$$

$$\text{Im } \varepsilon(\omega) = -\text{P} \int_{-\infty}^{\infty} \frac{d\omega'}{\pi} \frac{\text{Re } \varepsilon(\omega') - 1}{\omega' - \omega}. \quad (6.10)$$

Using either of these equations, and with a knowledge of $R(\omega)$ in all frequencies, one can, in principle, obtain $\text{Re } \varepsilon$ and $\text{Im } \varepsilon$.

There is, however, a more direct way to measure these optical quantities. In the last few years, two or three groups have done ellipsometric measurements. In this method, we can directly measure the complex dielectric constant $\varepsilon(\omega)$ individually without using the Kramers-Kronig relation.

The most important quantity in the optical data is the loss function,

$$L(\omega) = -\text{Im} \frac{1}{\varepsilon(\omega)}. \quad (6.11)$$

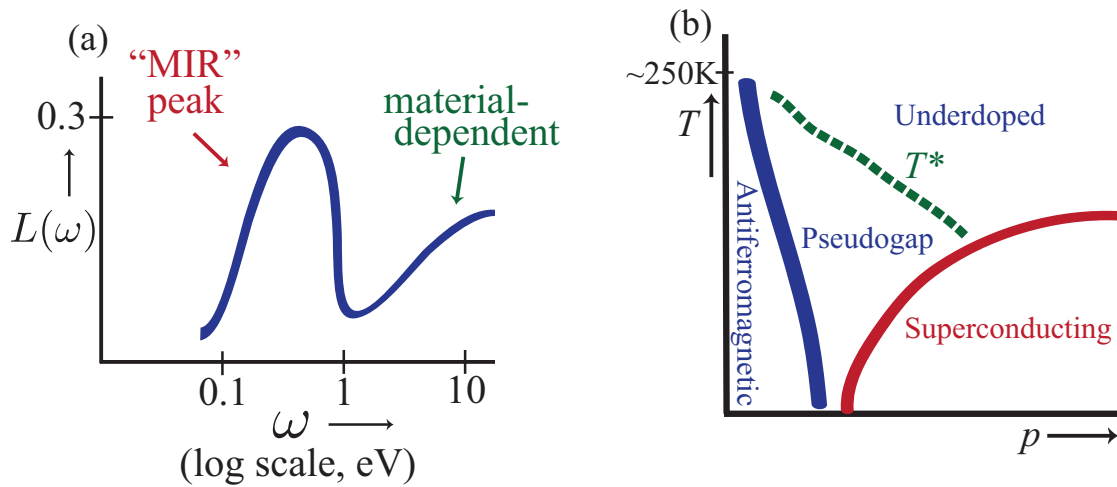


Fig. 6.8. (a) Loss function $L(\omega)$. (b) Phase diagram in the underdoped regime.

Can we expect this quantity to be universal between cuprates? First of all, note that $\epsilon(\omega)$ is a three-dimensional quantity, and therefore, it is sensitive both to the CuO_2 plane density and the charge reservoir contribution to $\text{Re}\epsilon$. The charge reservoir is, generally speaking, pretty insulating. It is not likely to make much contribution to the measured properties. The shape of the loss function in logarithmic scale is given in Fig. 6.8 (a). Surprisingly, it looks as if the mid-infrared (MIR) peak, which is always seen in optics in the cuprates, is only weakly material-dependent.

The behavior is not much interesting below 0.1 eV. Between 0.1-1 eV, one always obtains a strong and broad MIR peak; this peak is very characteristic of all cuprates, including non-superconducting ones. Then $L(\omega)$ drops drastically. The energy value at which $L(\omega)$ takes the minimum value, typically 1-2 eV for the cuprates, roughly corresponds to the plasma frequency. After that, $L(\omega)$ again rises; this behavior is material-dependent.

Not just optics show this behavior. Incidentally, this behavior is consistent with the electron energy-loss spectroscopy (EELS) experiments [10], which directly measure the loss function $L(\mathbf{q}, \omega)$ of impinged electrons through the interaction with a solid. In the normal phase, one sees the MIR peak up to $\mathbf{q} \sim 0.1 \text{ \AA}^{-1}$, beyond which it looks somewhat attenuated.

6.8 Experimental properties at the underdoped regime

6.8.1 Pseudogap

Let us move on to the underdoped regime [11]. The pseudogap region as shown in Fig. 6.8 (b) is, from an experimental point of view, not superconducting. Presumably, the

system does not have any long-range order⁵. However, there are considerable evidences that below the T^* -line the fermionic excitation spectrum has an *energy gap* similar to that of the superconducting phase. Some of the evidences are listed below:

- (a) Specific heat: $C_V \sim \gamma T$ for $T \gg T^*$, but for $T \leq T^*$ it drops well below the T -linear behavior [12].
- (b) Static spin susceptibility from the Knight shift: $\chi \sim \text{const.}$ for $T \gg T^*$, and it drops below that value for $T \leq T^*$. Interestingly, if we define the so-called Wilson ratio $S/\chi T$ (rather than C_V/χ), it is almost independent of T for *all* T .
- (c) Nuclear spin relaxation rate: $T_1^{-1} \propto T$ (Korringa law) for $T \gg T^*$, and it falls below the T -linear behavior for $T \leq T^*$.
- (d) Transport: both the in-plane resistivity $\rho_{ab}(T)$ and the c -axis resistivity $\rho_c(T)$ drop for $T \leq T^*$ at frequency $\omega \leq 500 \text{ cm}^{-1}$ (corresponds to $\sim 750 \text{ K}$).

What do all of these suggest? Remember that the resistivity is certainly always limited by the electron-electron scattering. If the resistivity drops, this means less scattering, or less carriers, which then suggests a reduced DOS below $E \sim$ a few 100 K. However, this does not directly suggest an actual energy gap. The direct observation of the finite energy gap requires different kinds of experiments. If we perform experiments at the optimal doping, we find nothing spectacular, but experiments at the underdoped regime give us something unconventional:

- (e) Tunneling: a gap-like feature is seen in tunneling characteristics, above T_c and up to the room temperature. The tunneling characteristic of metals between normal metals like Cu and cuprates in the underdoped regime looks somewhat similar to

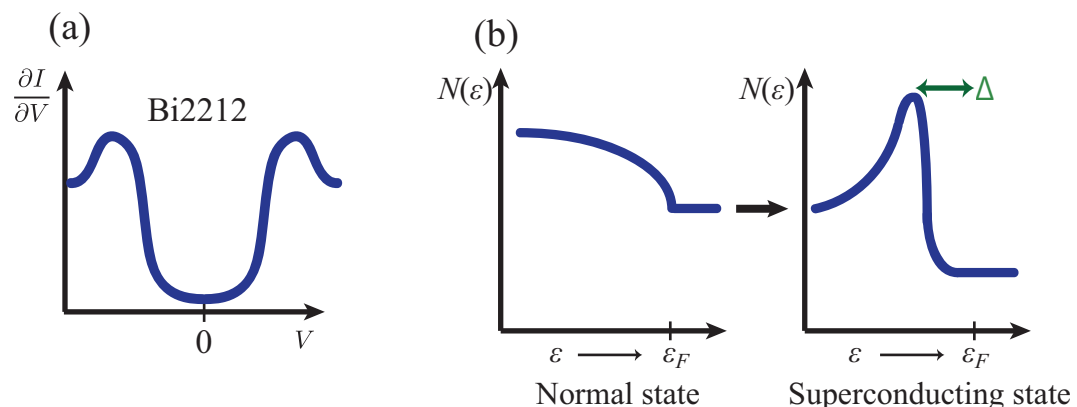


Fig. 6.9. (a) Tunneling result for the underdoped cuprates. (b) Gap opening in the density of states at ε_F .

⁵I will come back to the topic about the precise relationship between the superconductivity and the long-range order in Sec. 8.2.

the standard tunneling result of normal-metal superconducting materials (Fig. 6.9 (a)).

(f) ARPES (see below): can detect the feature more directly.

There are some recent and somewhat controversial evidences for the spontaneous breaking of the rotational $\frac{\pi}{2}$ invariance in the pseudogap regime. We may get a stripe-like structure then [13]. Also, controversially, some researchers claim the spontaneous violation of time-reversal symmetry.

6.8.2 ARPES in the pseudogap regime: the puzzle of the Fermi surface

Let us discuss ARPES in the pseudogap regime. How the Fermi surface behaves in the pseudogap regime? In the superconducting state at the optimal doping, the diffuse normal-state ARPES spectrum develops into a sharp peak which is pulled well back from the Fermi energy (Fig. 6.9 (b)). The \hat{n} -dependent difference is usually taken as a measure of the gap; it is of $d_{x^2-y^2}$ form, i.e., 0 at (π, π) and largest along the crystal axes. We will come back to this point in the next lecture. At the optimal doping and on the overdoped side, the $\Delta(\hat{n}, T)$ so defined appears to vanish for $T > T_c$. However, in the underdoped regime, a gap of similar $d_{x^2-y^2}$ form is seen in the superconducting state and *persists* above T_c [14, 15]; $\Delta(\hat{n}, T)$ appears to be more or less T -independent, but the amplitude of the peak decreases, and it disappears around the room temperature.

There is a puzzle here; ARPES data appear to show (modulo the gap) that even in the pseudogap regime the Fermi surface is well-defined and is quite similar to that seen at the optimal and overdoped values of p , i.e., the large ($\sim 1 + p$) Fermi surface (Fig. 6.7). Unfortunately, the dHvA oscillations seem to indicate equally definitively that the Fermi surface(s) is very small. Supposing 4-fold rotational symmetry, because dHvA experiments do not provide information about the exact locus of the Fermi surface in the momentum space, one possible case is that the small pocket-like Fermi surfaces appear around $(\pm\frac{\pi}{2}, \pm\frac{\pi}{2})$ (Fig. 6.10). Even under this assumption the total hole concentration in the Fermi sea would be only $\sim p$, not $1 + p$.

One possible resolution is that, because dHvA has to be conducted at high magnetic field (~ 20 T), it might qualitatively change the nature of the ground state. Remember that in the overdoped regime, dHvA and ARPES show a large Fermi surface. This fact seems to imply that there is a qualitative change in the Fermi surface when one sweeps across the phase diagram from the overdoped regime to the underdoped regime. At least under large fields, there must be a discontinuity or a crossover in the qualitative nature of the ground state as a function of the doping.

Here are obvious questions; where exactly does the change occur? What kind of change is this, a general phase transition or a crossover? It is difficult to avoid the following

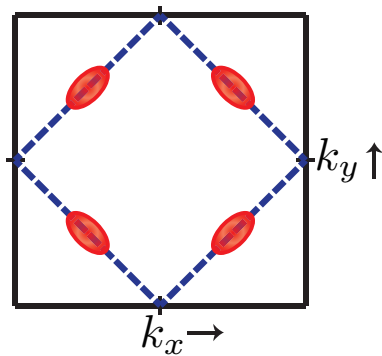


Fig. 6.10. A possible Fermi surface in the underdoped regime according to dHvA experiment.

conclusion: unfortunately, to the best of our knowledge, the existing dHvA experiments cannot answer them. This is certainly something which researchers must be working on in the next few years.

References

- [1] *Question from a student:* You said that there is a sequence with different n and then the conducting layers will be accumulated and get more three dimensionality. Then, how would T_c change? Does the more three dimensionality indicates higher T_c ?
Answer: Yes, indeed. You are absolutely right. I will come back to this later in more detail, but, generally speaking, almost always if I add more layers it does increase T_c up to $n = 3$ and after it goes down.
- [2] *Question from a student:* So far, in the high- T_c superconductors such as the cuprates and the ironpnictides, there are two layers, the superconducting layer and the insulating layer. Is that a requirement for the high- T_c ?
Answer: A nice question. I would say that we know not only the cuprates and the ferropnictides but also the organics, which are high-temperature superconductors in some sense. It may be important that the metallic planes are separated by the insulating layers, but I think in some sense more important point is that the places which supply the doping are separated from the CuO_2 planes or the equivalent ones for the other compounds. For example let us go back to LSCO, which is not a very good high-temperature superconductor: it has the transition temperature only about 40K. I think the reason is, at least for the large part, that the doped Sr sits actually right above the CuO_2 planes. Therefore, it acts as the impurities which scatter the electrons. In most of the rather high-temperature material, such as bismuth, thallium, mercury compounds, the doping sits away from the copper oxide planes. I suspect this is a rather trivially important point for the high- T_c .
- [3] *Question from a student:* Do you mean that there are two phases in the superconducting dome because of T^* -line intersecting the superconducting phase?
Answer: No. As far as we know at least, the T^* -line corresponds to the relatively sharp quantitative crossover but not the phase transition. Unfortunately, many of the properties which undergo discontinuities here tend to vanish in the superconducting phase. So it is not easy to follow this transition. What one can do is to apply the strong magnetic field⁶ in order to suppress superconductivity, and for the low T_c compounds that is possible. Then, you will rather see a crossover as a function of the doping.

⁶One can also track the T^* -line in the superconducting dome by adding zinc instead of applying the magnetic field to suppress the superconductivity [16].

- [4] J. Tallon, T. Benseman, G. Williams, and J. Loram, *Physica C* **415**, 9 (2004).
- [5] M. A. Kastner, R. J. Birgeneau, G. Shirane, and Y. Endoh, *Rev. Mod. Phys.* **70**, 897 (1998).
- [6] S. Ono, Y. Ando, T. Murayama, F. F. Balakirev, J. B. Betts, and G. S. Boebinger, *Phys. Rev. Lett.* **85**, 638 (2000).
- [7] S. D. Obertelli, J. R. Cooper, and J. L. Tallon, *Phys. Rev. B* **46**, 14928 (1992).
- [8] A. Damascelli, Z. Hussain, and Z.-X. Shen, *Rev. Mod. Phys.* **75**, 473 (2003).
- [9] M. R. Norman and C. Pépin, *Rep. Prog. Phys.* **66**, 1547 (2003).
- [10] N. Nücker, H. Romberg, S. Nakai, B. Scheerer, J. Fink, Y. F. Yan, and Z. X. Zhao, *Phys. Rev. B* **39**, 12379 (1989).
- [11] J. L. Tallon and J. W. Loram, *Physica C* **349**, 53 (2001).
- [12] J. W. Loram, K. A. Mirza, J. M. Wade, J. R. Cooper, and W. Y. Liang, *Physica C* **235-240**, 134 (1994).
- [13] C. V. Parker, P. Aynajian, E. H. da Silva Neto, A. Pushp, S. Ono, J. Wen, Z. Xu, G. Gu, and A. Yazdani, *Nature* **468**, 677 (2010).
- [14] C. Renner, B. Revaz, J.-Y. Genoud, K. Kadowaki, and O. Fischer, *Phys. Rev. Lett.* **80**, 149 (1998).
- [15] A. Matsuda, S. Sugita, and T. Watanabe, *Phys. Rev. B* **60**, 1377 (1999).
- [16] S. H. Naqib, J. R. Cooper, J. L. Tallon, R. S. Islam, and R. A. Chakalov, *Phys. Rev. B* **71**, 054502 (2005).

Lec. 7 Cuprates: superconducting state properties

I want to spend most of this lecture on the properties of cuprates in the superconducting phase. This has been the major topic of research over the last 25 years. One should bear in mind that like the normal state properties, the properties in the superconducting states do tend to be somewhat doping-dependent. They are actually less doping-dependent than the normal state properties. I will quote results at the optimal doping unless otherwise stated. To give you an orientation, I will compare them with the BCS predictions wherever possible.

7.1 Experimental properties

7.1.1 Structural and elastic properties and electron density distribution

These quantities are measured, for example, by the X-ray scattering. As far as we know, they do not change substantially at T_c or below, as in the BCS prediction.

7.1.2 Macroscopic electromagnetic properties

- i) Strongly type-II.
- ii) Strongly anisotropic.

The penetration depth along the c -axis¹ is much greater than that in the ab -plane, $\lambda_c \gg \lambda_{ab}$. This means that the pair radius, or the coherence length, is far less in the c -axis direction $\xi_c \ll \xi_{ab}$.

We can actually measure the upper critical field fairly close to T_c [1]. If we extrapolate² it to $T = 0$, their values are $H_{c2}(0) \sim 50$ T for $\mathbf{H} \parallel \mathbf{c}$, and ~ 400 T for $\mathbf{H} \perp \mathbf{c}$. If we interpret these results by the BCS theory, the corresponding coherence lengths are $\xi_{ab}(0) \sim 15\text{-}30$ Å, and $\xi_c(0) \sim 2\text{-}3$ Å. Note that $\xi_c(0) \sim 2\text{-}3$ Å is smaller than the

¹The penetration depth in the c -axis corresponds to the current flowing along the c -axis. That does not mean the penetration of the magnetic field in the c -axis direction.

²This is much greater than the field we can obtain with the existing magnets, so these are just extrapolations.

actual spacing of the unit cell dimension in the c -axis. Notice, incidentally, that there is another way within the BCS theory of getting the coherence length from the transition temperature: $\xi_{ab}(0) = 0.18\hbar v_F/k_B T_c$. The estimate done by this formula agrees well with the one obtained from the upper critical field (if we use $m^*/m = 4$).

7.1.3 Specific heat and condensation energy

There is a jump in the specific heat at T_c , as expected by the BCS theory. The amount of the jump is $\frac{C_s - C_n}{C_n}(T_c) \cong 1.6-2$ [2], which is somewhat larger than the BCS value 1.4. At the optimal doping, the shape of the peak is relatively sharp, while in the underdoped and overdoped regimes, the peak is considerably more rounded. That is to be expected on the underdoped side, but it is puzzling on the overdoped side.

For $T < T_c$, the specific heat falls off sharply, as in the BCS theory. In contrast, for $T \rightarrow 0$ it goes as a power law, probably T^n . It is probably consistent with $n = 1$ (but I think it is dubious. I will come back this point later).

The condensation energy is rather striking. The condensation energy as a function of the doping has a sharp peak at $p \approx 0.19$. Remember that this doping value is not the “optimal” value $p \approx 0.16$ corresponding to the maximum T_c , but it is rather the point, at least approximately, where the T^* -line intersects the axis if we extrapolate it. This may be significant, since the T^* -line is often interpreted as an indication of the quantum phase transition at $T = 0$, and if that idea is right, the point $p \approx 0.19$ is exactly where the quantum phase transition occurs. Note, however, that at finite temperature, the T^* -line itself represents a crossover rather than a phase transition.

It is interesting to work out the condensation energy in terms of the CuO_2 unit. It turns out that the maximum condensation energy is ~ 33 J/mol at $p \approx 0.19$, corresponding to $\Delta U_{ns}(0) \cong 2$ K/ CuO_2 unit. This value does seem to be relatively independent of the compounds.

7.1.4 NMR

The relaxation time T_1^{-1} drops precipitately below T_c , and appears to behave as $T_1^{-1} \propto T^3$ as $T \rightarrow 0$, which is consistent with the point node [3]. χ behaves rather like that of the BCS theory in $T \gtrsim 0.5T_c$. Below that temperature, the value is larger than the BCS value, again probably consistent with the power law.

7.1.5 Penetration depth

The penetration depth is one of the most frequently measured quantities. There are several different methods for measuring the penetration depth:

(a) Magnetization-related

There is a method related to the magnetization. Unfortunately, because of the anisotropy, the theory is not in a simple form, and thus it is not so reliable.

(b) Fraunhofer diffraction in Josephson junction

This method has been used for some classical superconductors, but it is not widely used in the cuprates so far.

(c) μ SR (muon spin rotation)

It is generally believed that this method is reliable.

(d) Microwave surface impedance

I think this is the most reliable method to measure the penetration depth. In particular, the group of Bonn and Hardy at the university of British Columbia has specialized in this measurement, and it does appear to agree, at least approximately, with the muon spin resonance result. Therefore, I have a certain amount of confidence in this method.

Let us discuss the superconducting fraction ρ_s/ρ , which is proportional to λ^{-2} , rather than discussing the penetration depth directly. In the ab -plane, near T_c , it is probably $\rho_s/\rho \propto (T_c - T)^{2/3}$. This is interesting: this behavior is exactly what we obtain in the $3D$ XY -model, a complex scalar field theory. In ^4He , this power-law dependence, with its power not exactly $2/3$, but nearly $2/3$, has been extremely well verified. Therefore, it seems that the superconductivity in the cuprates has the same universality class with ^4He .

For $T \rightarrow 0$, things become slightly complicated. In pure samples, the correction appears to behave linearly $\rho_s/\rho = 1 - \alpha T$, while in dirty samples, the correction is quadratic $\rho_s/\rho = 1 - \alpha' T^2$. These facts are consistent with a gap with a point node. The value of the penetration depth at $T = 0$ is $\lambda(0) \sim 1000 \text{ \AA}$ for YBCO at the optimal doping in the b -axis direction, while it can be as large as $\lambda(0) \sim 4000 \text{ \AA}$ for LSCO.

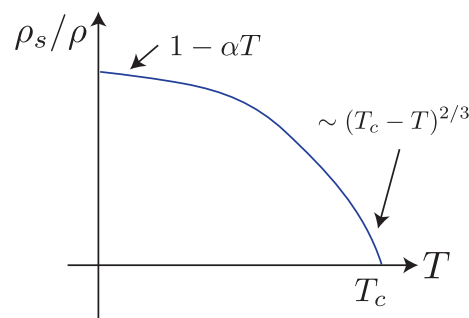


Fig. 7.1. Temperature dependence of the superfluid density.

It is interesting to ask how well do the data on the ab -plane penetration depth $\lambda_{ab}(0)$ agree with the “naive” (quasi-London) prediction

$$\lambda^{-2}(0) = n_{3D}e^2\mu_0/m^*. \quad (7.1)$$

We can fit with the data $m^* = 4m$, which is consistent with the effective mass in the normal state value of the specific heat, and with $n_{3D} = 10^{22} \text{ cm}^{-3} \times p_{\text{eff}}$, where p_{eff} is the effective number of carriers per CuO_2 unit. We must take here *not* $p_{\text{eff}} = p$, *but rather*

$$p_{\text{eff}} = 1 + p. \quad (7.2)$$

In other words, we must count not only the excess ones over the parent compound, but rather all the holes in the Cu $3d^9$ band. This is a rather important conclusion. Therefore, in terms of the superconductivity, it is not just the added electrons, but rather all the electrons in the d -band are playing the role.

There is one puzzling thing: in YBCO, $\lambda_a(0) \cong 1600 \text{ \AA}$, while $\lambda_b(0) \cong 1000 \text{ \AA}$. If we square them up to get the superfluid density, the value in the b -axis is 2.5 times larger than that in the a -axis. At first sight, that appears to say that the chains, which are pointing along the b -axis, are carrying 3/2 as much contribution as both planes! That is really quite surprising, and as far as I know, there has been no solution to this puzzle.

The c -axis penetration depth is far larger than that in the ab -plane: from $\lambda_c(0) \sim 11,000 \text{ \AA}$ for YBCO, to $\sim 100 \mu\text{m}$ ($=0.1 \text{ mm}$!) for Bi-2212. These values are much larger than what we find in the typical BCS superconductors. When we underdope them, these values increase very rapidly. This is not surprising: particularly, in the case of YBCO, as one underdopes, one certainly depletes the chains, which are forming the bridges between the planes. Thus, we decrease the contact along the c -axis.

The temperature dependence of the c -axis penetration depth at low temperature is much weaker than in the ab -plane, and it may be fit by $\rho_s/\rho \sim 1 - \alpha T^5$.

An interesting question we may ask is as follows: what will happen if we model the interlayer contact as a Josephson junction and apply the standard Ambegaokar–Baratoff formula $I_c(0)R_n = \pi\Delta(0)/2e$, which relate the critical current I_c of the Josephson junction and the energy gap. With a little bit of algebra, we find

$$\lambda_c^{-2}(0)\rho_c d_{\text{int}}/\Delta(0) = \text{const.}, \quad (7.3)$$

where d_{int} is the mean spacing between the multilayers. This agrees reasonably well with experiments, which suggests that the idea of modeling the inter-plane contact as a set of Josephson junction works.

7.1.6 AC conductivity

Both in the BCS superconductors and in the cuprates, the behaviors of the AC conductivity are really quite complicated, but there are two qualitative differences:

i) In the cuprates, $\sigma(\omega)$ is appreciable for $\omega < 2\Delta(0)$, while for the BCS superconductors $\sigma(\omega) = 0$ since there is no single electron state there.

ii) For finite ω , $\sigma(\omega)$ rises immediately below T_c , and thereafter drops, which suggests that $\sigma(\omega)$ is limited by the electron-electron scattering, and the number of electrons taking part in the scattering will later drop below T_c . That is self-consistent with the behavior of the thermal conductivity, as we shall see next.

7.1.7 Thermal conductivity

We can use the kinetic-theory formula

$$\kappa = \frac{1}{3} C_V \bar{v} \ell \quad (7.4)$$

for both the phonon and electron contributions to the thermal conductivity. From this formula, we obtain

$$\kappa_{\text{ph}}/\kappa_{\text{el}} \sim (T/\Theta_D)^2 (\ell_{\text{ph}}/\ell_{\text{el}}) \quad (7.5)$$

for $p \sim 1$, where Θ_D is the Debye temperature, ℓ_{ph} and ℓ_{el} are the mean free paths of electrons and phonons. We have used $c_s/v_F \sim \omega_D/\varepsilon_F$ here.

For the BCS superconductors, $\kappa_{\text{ph}}/\kappa_{\text{el}} \ll 1$ at T_c , so that $\kappa \sim \kappa_{\text{el}}$. Therefore, the thermal conductivity is proportional to the number of normal electrons, which falls off rapidly below T_c .

For the cuprates, since the transition temperature is high and the electron mean free path is short, it turns out that $\kappa_{\text{ph}}/\kappa_{\text{el}} \gtrsim 1$. In other words, the phonon contribution is quite important near T_c . As an experimental fact, we know that κ rises below T_c and thereafter drops. We can argue, probably, that the phonons are dominant, which is limited by the scattering with electrons. This effect of scattering then drops below T_c , since the number of normal electrons decreases. However, it is also possible that even though the electrons are dominant, we still get this scattering. Therefore, it is not entirely clear how much is due to electrons and phonons.

7.1.8 Tunneling

We can see a very characteristic difference in tunneling experiments [4, 5, 6]. In the BCS model, the differential conductance measured in the tunneling experiment $G \equiv \partial I/\partial V$ is flat in the normal state, while in the superconducting state,

$$G_s(E)/G_n = \frac{\varepsilon}{\sqrt{\varepsilon^2 - \Delta^2}} \theta(\varepsilon - \Delta), \quad (7.6)$$

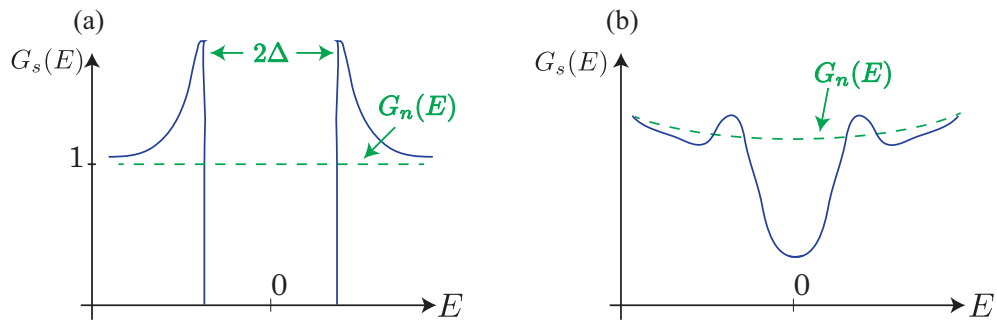


Fig. 7.2. (a) Tunneling density of states for a BCS superconductor. (b) Tunneling density of states for a typical cuprate (ab -plane).

which is illustrated in Fig. 7.2 (a). It is zero for the energy smaller than the gap, while for the energy larger than the gap, there is a characteristic peak from the increase in the number of states. In the cuprates, first of all there is some energy dependence as $G_n(E) \sim a + b(E)$, while in the superconducting state it has an interesting feature as illustrated in Fig. 7.2 (b). As you can see, there is (i) a “dip” beyond the peak which is not present in the BCS superconductor. Secondly, (ii) $G_s(E = 0) \neq 0$, which would rather strongly indicate that there is a non-zero density of electronic state at the zero energy. Finally, (iii) the peak-to-peak distance, which is “ 2Δ ” in the BCS theory, is typically $\sim 7-8k_B T_c$ for the ab -plane tunneling, whereas in the BCS theory it is only $3.5k_B T_c$. It turns out, however, that it is closer to the BCS theory for the c -axis tunneling, and also for the overdoping. The fact that the overdoping region is close to the BCS theory is consistent with a rather general observation that perhaps all the cuprates become more BCS-like toward the overdoping (the normal state becomes more normal Fermi liquid-like, and it becomes BCS-like in the superconducting state).

7.1.9 ARPES

A typical behavior of the ARPES spectra [7, 8, 9] is illustrated in Fig. 7.3 (a). First of all, we do have both in the normal and superconducting states a very apparent discontinuity, or something looking like more or less a discontinuity, at what we identify as the Fermi energy. However, the discontinuity is rather small both in the normal and superconducting states, and it is only something like 10% of the whole value; it appears that the background is not zero. Another interesting feature is that there is a dip beyond the peak just as in the tunneling spectrum. Furthermore, as we go into the superconducting state, there appears a “pullback” $\Delta\varepsilon$ of the spectrum from the normal state Fermi energy, typically $\Delta\varepsilon(\pi, 0) \sim 4-5k_B T_c$. The most interesting feature of this pullback is the dependence of $\Delta\varepsilon(\mathbf{n})$ or the peak height on the angle on the Fermi surface. Both the pullback and the peak height take their maxima in $(\pi, 0)$ and $(0, \pi)$ directions in the Brillouin zone, while they take minima, in fact they go to zero, in (π, π) direction. This would then indicate

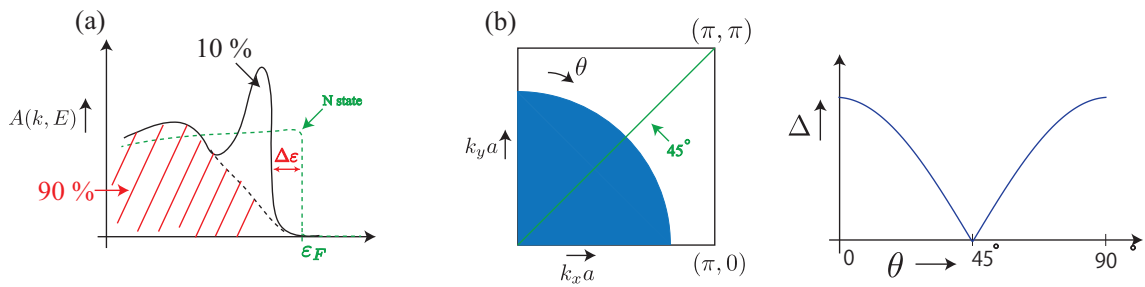


Fig. 7.3. (a) ARPES spectrum of a typical cuprate in the anti-nodal direction. (b) First Brillouin zone of the cuprates, and the orientation dependence of the energy gap ($d_{x^2-y^2}$ symmetry).

that, at least as seen in the ARPES data, the “gap” has a node in (π, π) direction. People have tried to fit the gap numerically to simple formulae, but I do not think that is the crucial point. One sometime worries if it does not fit some simple formulae, but I think there is no reason to expect that.

7.1.10 Neutron scattering (YBCO, LSCO, and Bi-2212)

Remember that in the normal state, the neutron scattering cross section $\sigma(\mathbf{q}, \omega)$ is fairly strongly peaked as a function of \mathbf{q} at $\mathbf{q} = (0.5\pi/a, 0.5\pi/a)$ (magnetic superlattice values), but featureless as a function of frequency. In the superconducting state in YBCO [9, 10, 11] and Bi-2212 [12], nothing changes in the “even” channel (both planes in the c -axis contribute in phase). On the other hand, in the “odd” channel (both planes in the c -axis contribute out of phase, i.e., $q_z = \pi/d$, where d is the interlayer spacing), there is a striking peak seen around $\mathbf{q} = (0.5\pi/a, 0.5\pi/a)$ with $\omega \sim 41$ meV. It is only seen in the odd channel, not seen in LSCO [9], which only has a single plane and there is no odd channel for it. Thus, we can ask a very obvious question: is this peak is peculiar to *bilayer* cuprates? I have been trying hard to find any recent data on that (the above is quite early observation, first done in the late 1990s), and I am rather sure that people have been trying to do experiments on a single layered material. However, I have not been able to find any published result for this experiment. Thus, we do not know whether it is peculiar to bilayer cuprates. My guess would be that it strongly is, considering the fact that it appears only in the odd channel. In any case, no one is quite sure what is significant for this strong peak, although it is a very striking feature.

7.1.11 Optics

In the BCS theory, the superconductivity affects only those single electron states with their energy of the order of $\Delta \sim k_B T_c$, so that the optical behavior at frequency $\omega \gg \Delta$ is not so affected by the superconductivity. In fact, with a calculation based on the BCS

theory, we can indeed show that the effect is of the order of $(k_B T_c / \hbar \omega)^2$. If we put the values for the cuprates and $\hbar \omega \sim 1$ eV, the result is $\sim 10^{-4}$, which is probably too small to be seen. In reality, the changes of the spectra in superconducting state are $\sim 2\text{-}5\%$ [13, 14, 15]. Even at 5 eV, we still see appreciable changes in the optical spectrum at T_c and below T_c .

More precisely, the original measurements are done for the reflectivity $R(\omega)$, which is the easiest kinds of measurements we can do about the optics. If we define a quantity $\eta(\omega)$ as

$$\eta(\omega) \equiv \frac{R_s(\omega)}{R_n(\omega)} - 1, \quad (7.7)$$

we obtain a curve drawn in Fig. 7.4. What is striking is that the zero crossing of $\eta(\omega)$ occurs almost exactly where the normal state reflectivity $R_n(\omega)$ has the minimum. That then might suggest

$$\eta(\omega) = -\delta(\partial R_n / \partial \omega) \quad (7.8)$$

where δ is the average downward shift of the “initial” state (no change in the final state). Unfortunately, the relation does not work for the following reasons:

(a) It requires $\delta \sim \Delta$, which in turn implies, apparently, that the initial states are strongly concentrated over the energy range $\sim \Delta$ near ε_F . It does appear that there is no obvious reason for this to happen.

(b) While the above assumption does seem qualitatively to fit the data on the reflectivity, recent ellipsometric experiments [14, 15] have shown that it does *not* seem to fit $\varepsilon_1(\omega)$ and $\varepsilon_2(\omega)$.

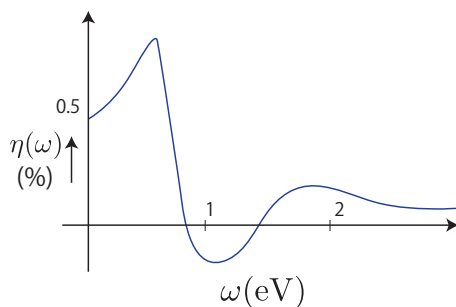


Fig. 7.4. Behavior of $\eta(\omega)$ as defined in Eq. (7.7).

7.1.12 Electron energy loss spectroscopy (EELS)

Unfortunately, for reasons I do not understand, only a few EELS experiments were done in the early days of the cuprates, in the late 1980s and early 1990s [15, 16]. We actually have a lot of data in the normal state and the mid-infrared peak can be seen. For the superconducting states, on the other hand, the published data can be found only at low energy $\omega \lesssim 100$ meV. This is probably because they expected to see the energy gap, which I think is, a priori, a bad idea. In fact, we may not see the gap with the EELS. Crudely speaking, the low energy EELS data is strongly overscreened and it is possible that we do not see anything interesting there. Unfortunately they did not go into the mid infrared regime ($\omega \sim 0.5$ -1 eV), although I wish they had. Now my colleagues are going to do that.

7.2 What do we know for sure about superconductivity in the cuprates?

In the last twenty five years, there have been hundreds of microscopic theories on what is going on in the cuprates. No one can agree which of these theories are correct. Thus, let us discuss here what we can say for sure about the superconductivity in the cuprates, without adopting any particular microscopic theory, but rather just by looking at experimental properties of the cuprates with some very basic theoretical considerations.

1. “Cooper pairs” are formed in the cuprate superconductors.

For the BCS superconductors, it is an almost universal belief that the onset of superconductivity coincides with the onset of the off-diagonal long range order (ODLRO). In other words, *superconductivity is due to the formation of Cooper pairs*. More technically, the basic “topology” of many-body wave function is

$$\Psi_N \sim \mathcal{A}[\phi(\mathbf{r}_1\sigma_1; \mathbf{r}_2\sigma_2)\phi(\mathbf{r}_3\sigma_3; \mathbf{r}_4\sigma_4) \cdots \phi(\mathbf{r}_{N-1}\sigma_{N-1}; \mathbf{r}_N\sigma_N)], \quad (7.9)$$

where ϕ is the *same* “molecular” wave function for all pairs (quasi-BEC of Cooper pairs). For most purposes, it is more convenient to work in terms of closely related (but different) quantity

$$F(\mathbf{r}_1, \mathbf{r}_2, \sigma_1, \sigma_2) = \langle \psi_{\sigma_1}^\dagger(\mathbf{r}_1)\psi_{\sigma_2}^\dagger(\mathbf{r}_2) \rangle. \quad (\text{“pair wave function”}) \quad (7.10)$$

“Macroscopic wave function” of Ginzburg and Landau, $\Psi(\mathbf{R})$, is just $F(\mathbf{r}_1, \mathbf{r}_2, \sigma_1, \sigma_2)$ for $\sigma_1 = -\sigma_2 = +1$, and $\mathbf{r}_1 = \mathbf{r}_2 = \mathbf{R}$, i.e., the wave function of the center of mass of Cooper pairs.

Why do we assume these forms “pairing hypothesis” for old-fashion superconductors? One good reason is that one spectacular prediction of this hypothesis is that

flux is quantized in $hc/2e$. With the flux quantization and Josephson experiments (see Sec. 7.4 for more details.), it is shown that this pairing hypothesis to be exactly satisfied for old-fashion superconductors. Those experiments are also done for the cuprates, and sure enough we obtain the same quantization, and the pairing hypothesis is also exactly satisfied.

2. “Universality” of high- T_c cuprate superconductors with very different chemical compositions, etc.

Almost all agree that *the main actors in the superconductivity are electrons in CuO_2 planes*. It is not necessarily true that CuO_2 planes are the main actor just because all the cuprates have them in common³. However, it is widely believed that CuO_2 planes are the main actors.

We know that charge reservoirs are very important but not all the cuprates have charge reservoirs (the “infinite layer” cuprates do not have charge reservoirs but they are still very good high- T_c superconductors).

3. Spin state of the Cooper pairs is singlet.

For simplicity, we assume that we can neglect the spin-orbit interaction, because oxygen and copper are light (atomic masses: 16 and 29) and thus the spin-orbit interaction is small at least within CuO_2 planes. Then, we can do the simple analysis in terms of the spin wave function and the orbital wave function.

What do we know, first of all, about the spin wave function? We discussed before that at least in the BCS theory, the Pauli spin susceptibility drops rapidly for spin-singlet and remain constant for spin-triplet, as shown in Fig. 7.5. Experimental results in the NMR (χ_s, T_1, \dots) imply the latter. Therefore it is fair conclusion that the spin state of the cuprates is *singlet* (not triplet), i.e.,

$$F(\mathbf{r}_1, \mathbf{r}_2, \sigma_1, \sigma_2) = \frac{1}{\sqrt{2}}(\uparrow\downarrow - \downarrow\uparrow)F(\mathbf{r}_1, \mathbf{r}_2). \quad (7.11)$$

4. Copper pairs are formed out of electrons in the same band.

Some years ago, J. Tahir-Kheli made an interesting proposal [17]. He said why do we always assume that Cooper pairs are formed from time-reversal states that are from the same band. There may be another possibility that they are formed by taking one electron from one band and second electron from another. He claims that the theory may explain some of the experimental properties. In particular, it might give a natural explanation on why superconductivity is so strongly peaked as a function of doping. However, according to his theory, we always expect a substantial

³As an example, one of my colleagues pointed out that whole class of airplane have wheels in common but they are not the main part of flight.

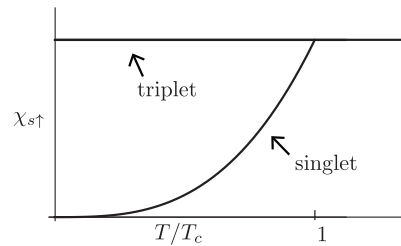


Fig. 7.5. Spin susceptibility as a function of temperature.

FIR absorption just above the gap edge, which is certainly not seen experimentally. Thus, I do not believe the theory is totally correct, and we can conclude with a good confidence that the Copper pairs are formed from the states with the opposite spins and opposite momenta (i.e., the time-reversed states) in the same band.

5. Small Cooper pair size, and large effect of fluctuations.

As we discussed in Sec. 7.1.2, the order-of-magnitude estimates from T_c and H_c shows that the in-plane “radius” of Cooper pairs ξ_0 is typically 15-30 Å, and it is the order of a few lattice spacings a : $\xi_0/a \sim 3-10$. Compared with value for the BCS superconductors, $\xi_0/a \sim 10^4$ for Al for example, it is far smaller. This implies that the fluctuations ought to be much more important in the cuprates than in the BCS superconductors. This is certainly true. For example, while the resistivity is smooth in the normal phase and drops vertically⁴ when it enters the superconducting phase for Al, the transition is slightly rounded for BSCCO. When we apply a stronger magnetic field (~ 10 T), it becomes so rounded that it is very difficult to say where exactly the T_c is.

6. Irrelevance of the inter-layer tunneling.

In the normal state, the c -axis resistivity is very high. One can interpret the resistivity in terms of electrons’ hopping from one plane to the next, being somehow disturbed by fluctuations and decay. The average time taken for electrons to hop between planes is much greater than $\hbar/k_B T$. This has a significant implication: crudely speaking, $\hbar/k_B T$ is of the order of the characteristic time associated with superconducting state. Thus, the large hopping time strongly suggests that the pairs in different multilayers can be regarded effectively as *independent*. In other words, in order to analyze the superconducting behaviors of the cuprates, it is sufficient, at least in the first approximation, to focus on a single plane. This has not always been the universal view; in the first ten to fifteen years of the subject, Anderson’s interlayer tunneling theory, which rejected this point of view and claimed that the hopping in the c -axis is crucial, was rather appreciated. However, one

⁴Basically, it is very difficult to measure the width of superconducting transition in Al because it is too small.

critical experiment in 2000 or so has led most of us, including Anderson himself, to disbelieve his theory. Therefore, the c -axis hopping is negligible.

7. Absence of substantial isotope effect and “folk-theorems” on T_c .

At least in higher- T_c cuprates, no substantial isotope effect has been seen. In lower- T_c cuprates, and even in higher- T_c ones in strongly overdoped or underdoped regimes, we do have the isotope effect. This tends to suggest that phonons are playing very minor roles. The isotope effect appears only when electronic effects are strongly suppressed.

A “folk-theorem” on T_c is another evidence for the non-phonon mechanisms. Band theorists, using such methods as the local density approximation (LDA), claim to be very good at predicting T_c with the BCS scheme: i.e., with the hypothesis of the electron-phonon coupling. They say that we will never get higher T_c than 40 K in the phonon mechanism. Thus, basically⁵ the phonon alone is not enough to explain the higher T_c .

7.3 Symmetry of the order parameter (gap)

In the BCS theory, the fermionic gap $\Delta(\mathbf{n})$ has almost the same \mathbf{n} -dependence as the order parameter $\Psi(\mathbf{n})$. In a more general theory, however, this is *not* guaranteed, but it seems very unlikely that the symmetries of these two quantities are totally different.

As we have seen, NMR experiments indicate that the order parameter is spin-singlet, i.e.,

$$F(\mathbf{r}_1, \mathbf{r}_2, \sigma_1, \sigma_2) = \frac{1}{\sqrt{2}}(\uparrow_1\downarrow_2 - \downarrow_2\uparrow_1)F(\mathbf{r}_1, \mathbf{r}_2), \quad (7.12)$$

where $F(\mathbf{r}_1, \mathbf{r}_2)$ and $F_{\mathbf{k}}$ are even-parity. We assume relevant symmetry is that of CuO₂ plains, i.e., (approximately) tetragonal. Then symmetry group is C_{4v} (symmetry group of square) with the fundamental operations below:

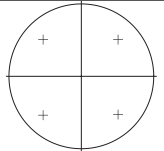
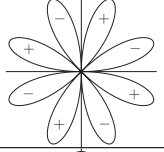
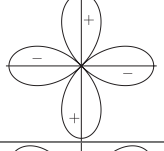
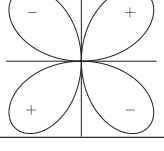
- (a) Rotation through $\pi/2$ around z -axis ($\hat{R}_{\pi/2}$).
- (b) Reflection in crystal axis, e.g. (100) (\hat{I}_{axis}).
- (c) Reflection in a 45° axis, e.g. (110) ($\hat{I}_{\pi/4}$).

Note that the operations (a)-(c) are not independent:

$$\hat{I}_{\text{axis}}\hat{I}_{\pi/4}\hat{R}_{\pi/2} \equiv 1. \quad (7.13)$$

⁵There is one or two exceptions against this folk-theorem. Tsuei *et al.* suggested we could somehow get a phonon mechanism without the isotope effect, but there is no positive evidence of this mechanism [18].

Table 7.1. Four allowed symmetries of the order parameter in the cuprates.

	Informal name	Group theoretic notation	$\hat{R}_{\pi/2}$	\hat{I}_{axis}	Representative state
	s^+	A_{1g}	+1	+1	1
	s^- ('g')	A_{2g}	+1	-1	$xy(x^2 - y^2)$
	$d_{x^2-y^2}$	B_{1g}	-1	+1	$x^2 - y^2$
	d_{xy}	B_{2g}	-1	-1	xy

It is rather trivial to see $\hat{I}_{\text{axis}}^2 \equiv \hat{I}_{\pi/4}^2 \equiv 1$. Moreover, since we restrict ourselves to the case where $F_{\mathbf{k}}$ is even parity, $\hat{R}_{\pi/2}^2 F_{\mathbf{k}} = F_{-\mathbf{k}} = F_{\mathbf{k}}$ for any $F_{\mathbf{k}}$ under consideration, which means⁶ $\hat{R}_{\pi/2}^2 = 1$.

As a result, all of these operators can only have eigenvalues ± 1 , which determines *only four possible irreducible representations* (all one-dimensional). Table 7.1 gives the overview of these possible cases. You should not take the figures so seriously; for example, it is still possible that the s -wave gap has nodes in the directions of 30° and 60° . When we talk about the symmetry of the gap, we should be thinking of only how the order parameter behaves under symmetry operations.

Here is an interesting question: are we actually sure that the order parameter belongs to a single irreducible representation? Could it not belong to more than one representations? In general, yes it could. However, with the following argument, we exclude this possibility. If i labels the different irreducible representations, the free energy can be expanded as

$$F(T) = \sum_{ij} \alpha_{ij}(T) \psi_i^* \psi_j + \frac{1}{2} \sum_{ijkl} \beta_{ijkl}(T) \psi_i^* \psi_j^* \psi_k \psi_l, \quad (7.14)$$

with a help of the global U(1) symmetry. Quite generally, invariance of the free energy under the above lattice symmetry operations implies $\alpha_{ij} = \alpha_j \delta_{ij}$. Thus, the first terms should be $\alpha_i |\psi_i|^2$. For the second term, the order parameters of the different representa-

⁶In two dimensions, π rotation around z -axis is identical with the parity operation.

tions can couple, so that it can make a complicated behavior in general.

If we assume more than one $\psi_i \neq 0$ contribute to the free energy, we automatically have two phase transitions. Crudely speaking, the order parameter with a stronger attraction starts to take non-zero values in the first phase transition, and the other one with a weaker attraction becomes non-zero in the second phase transition. This is certainly not seen experimentally. (For these two phase transitions to be coincide, we need very pathological fine-tuning of parameter.) Thus we can conclude that

the order parameter belongs to a single irreducible representation.

According to the above argument, the order parameter must be just one of the four forms, s , $d_{x^2-y^2}$, d_{xy} and s^- . However, people usually concentrate on the first two, because s -wave is favored by some types of theory (e.g., phonon) and $d_{x^2-y^2}$ is favored by the spin-fluctuation theory.

How to tell?

- (a) $d_{x^2-y^2}$, d_{xy} , s^- must have (at least) four nodes on Fermi surface. s need not. Thus, exponential decrease of quasiparticle-associated quantities (χ , T_1^{-1} , $\Delta\lambda(T)$...) certainly implies s -wave. Experimentally, all these quantities have power-law dependences consistent with two-dimensional point node. Does this inevitably exclude s -wave? Unfortunately not, because even the s -wave state may have nodes allowed by symmetry, i.e, the “extended s -wave” (see Fig. 7.6).
- (b) More specifically, $d_{x^2-y^2}$ (and s^-) must have nodes at (π, π) , whereas s (and d_{xy}) would have nodes at (π, π) only by pathology. Thus, the observation of nodes suggests $d_{x^2-y^2}$. The ARPES data indeed indicates such nodes. However,
 - i) The “gap” seen in ARPES may not simply be the superconducting gap (cf. pseudogap regime).
 - ii) The “extended s -wave” state of the form $F(\theta) = A + B \cos 4\theta$ ($0 < B - A \ll A$) may be difficult in practice to distinguish from $d_{x^2-y^2}$ (Fig. 7.6).

Therefore, we need experiments which are directly sensitive to the *sign* (or more generally *phase*) of order parameter, such as the Josephson (“phase-sensitive”) experiments.

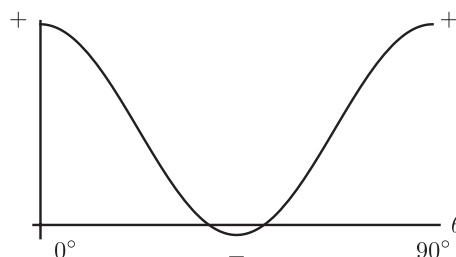


Fig. 7.6. Extended s -wave state, described as $F(\theta) = A + B \cos 4\theta$ ($0 < B - A \ll A$).

7.4 Josephson experiment in cuprate (and other exotic) superconductors

The Josephson experiment as a tool to determine the phase of the order parameter was first suggested in the context of the p -wave superconductivity [19]. The first experiment done in this direction was in 1993 with my colleagues [20].

The Josephson effect occurs for any geometry, including a superconductor-normal-superconductor junction (Fig. 7.7), and a SQUID geometry (Fig. 7.7 (b)). For the former case, to the lowest order in Ψ , the Josephson energy or the simple s -wave case is given by

$$E_J \propto -\text{const.}(\Psi_1^*\Psi_2 + \Psi_2^*\Psi_1) \sim -\text{const.} \cos \Delta\varphi. \quad (7.15)$$

where $\Delta\phi$ is the phase difference between the two superconductors. In the SQUID geometry, the critical current shows an interesting behavior: the critical current is maximum at $\Phi = n\Phi_0$, and minimum at $\Phi = (n + 1/2)\Phi_0$. This can be understood easily by using

$$\sum_i \Delta\varphi_i = 2\pi\Phi/\Phi_0 \quad (7.16)$$

where $\Delta\varphi_i$ is the change of phase across the junction, and Φ is the flux through trapped in the circuit⁷. For $\Phi = n\Phi_0$, we can consider the simplest case $\Phi = 0$. In this case, the phase drops in the two paths are the same. On the other hand, for $\Phi = (n + 1/2)\Phi_0$, there is π -phase difference, so that the Josephson current interferes destructively and takes its minimum.

Let us start to see how these goes for the Josephson experiment in the cuprates. Basically, the Josephson experiment are based on the following two principles:

- (a) If two bulk superconductors separated by the Josephson junction, and they are described by Hamiltonian \hat{H} , which is invariant under symmetry group G , then the Josephson coupling energy must be similarly invariant under G .

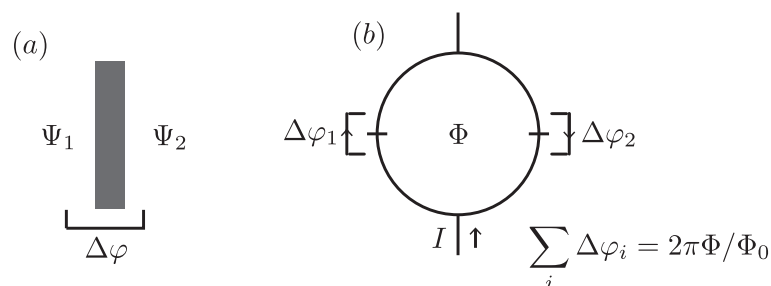


Fig. 7.7. Various geometry of the Josephson experiments.

⁷ Ψ and $\Delta\varphi_i$ are defined consistently here.

(b) For a circuit, as shown in Fig. 7.8 (b), we again find the fundamental equation Eq. (7.16).

We always assume the lowest-order Josephson energy (which is testable via Fraunhofer diffraction pattern etc.) is given by Eq. (7.15).

Application (a) alone Let us consider $\pi/2$ rotation around z -axis on the system shown in Fig. 7.8 (a). The Pb order parameter Ψ_{Pb} is invariant, i.e., $\Psi_{\text{Pb}} \rightarrow +\Psi_{\text{Pb}}$. If YBCO is s -wave (s or s^-), $\Psi_{\text{YBCO}} \rightarrow +\Psi_{\text{YBCO}}$, then the lowest-order Josephson effect allowed. On the other hand, if YBCO is d -wave ($d_{x^2-y^2}$ or d_{xy}), $\Psi_{\text{YBCO}} \rightarrow -\Psi_{\text{YBCO}}$, the lowest-order Josephson effect *forbidden* (otherwise, the free energy cannot be invariant under the $\pi/2$ rotation around the z -axis). Thus, this difference can be a crucial test for the symmetry of the order parameter of exotic superconductors.

Application (b) alone Since the order parameter in Pb Ψ_{Pb} is invariant under $\pi/2$ rotation, Ψ_{Pb} takes the same value at junctions 1 and 2. If YBCO is s -wave, the situation is the same as in conventional DC SQUID, so that $I_c(\Psi)$ is maximum at $\Psi = n\Psi_0$, and minimum at $\Psi = (n + 1/2)\Psi_0$. On the other hand, if YBCO is d -wave, the sign of Ψ changes between junction 1 and 2 in YBCO. This means that we effectively add π to the right hand side of Eq. (7.16), which then implies that the critical current I_c is maximum at $\Psi = (n + 1/2)\Psi_0$, and minimum at $\Psi = n\Psi_0$. The latter is what precisely D. Wollman *et. al.* have found in the experiment [20]; there have been about twenty phase-sensitive experiments by different groups as well. The conclusion from all these experiments is that:

the order parameter of the cuprates is $d_{x^2-y^2}$.

Some experiments prepared beautiful “tricrystal ring”, and exploit in some sense both principles (a) and (b) (see pp. 345-346 of Ref. [21] for more detail), and got the same conclusion.

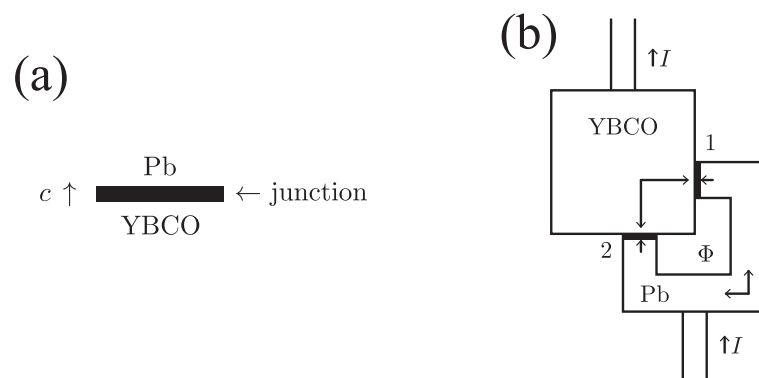


Fig. 7.8. (a) Pb and YBCO are separated by Josephson junction which is invariant under $\pi/2$ rotation around z -axis. (b) The setup for π -junction experiment [20].

7.5 What is a “satisfactory” theory of the high- T_c superconductivity in the cuprates?

It is interesting to ask a rather sociological question: how will we know when we have a “satisfactory” theory of the high- T_c superconductivity in the cuprates? Right now, if I go to my dozens of colleagues and ask, “do we understand high- T_c superconductivity”, every one of them says “Yes!”. If we then ask “OK, then what is the correct theory?”, we get totally different theories. That is not satisfactory at all.

How should we get out of this? By definition, we have a satisfactory theory if 90% or 95% of people agree. Apart from that, do we have a more objective criterion? I think we should, at least, be able to:

- (A) give a blueprint for building a robust room-temperature superconductor,
- OR (B) assert with confidence that we will never be able to build a (cuprate-related) room temperature superconductor,
- OR (C) say exactly why we cannot do either (A) or (B).

The above two (A) and (B) may sound demanding because strictly speaking, we cannot do them even for the BCS theory. However, in the BCS theory, we can do (A) and (B), given a particular material with its certain information, such as the phonon spectrum, phonon matrix element, band structures etc. Right now, to best of my knowledge, there is no theory which satisfies any of these three conditions.

Let us ask a few more specific questions:

- (1) Are the cuprates unique in showing high- T_c superconductivity⁸?
- (2) If so, what is special about them?
(e.g., band structure, two-dimensionality, antiferromagnetism, etc.)
- (3) Should we think of high- T_c superconductivity as a consequence of the anomalous normal-state properties, or vice versa?
- (4) Is there a second phase transition associated with the T^* -line? If so, what is the nature of the low temperature (“pseudogap”) phase⁹?
- (5) If yes to (4), is the phase transition relevant to high- T_c superconductors or a completely unconnected phenomenon?
- (6) Why does T_c depend systematically on n in homologous series?

⁸This depends on what we call the high- T_c superconductors, but nowadays people would say no since the recent discovery of the ferropnictides, at least, is a counterexample.

⁹Right now, there is no positive evidence for the phase transition. Everything looks, at least, consistent with the idea of a smooth crossover. However, some people believe that it corresponds to a sort of hidden phase transitions, and suggest that the pseudogap phase breaks the time-reversal symmetry, rotational symmetry, or some other kinds of symmetries.

References

- [1] D. N. Basov and T. Timusk, *Rev. Mod. Phys.* **77**, 721 (2005).
- [2] J. Tallon and J. Loram, *Physica C* **349**, 53 (2001).
- [3] J. Tallon, G. Williams, and J. Loram, *J. Phys. Chem. Solids* **59**, 2145 (1998).
- [4] C. Renner, B. Revaz, J.-Y. Genoud, K. Kadowaki, and O. Fischer, *Phys. Rev. Lett.* **80**, 149 (1998).
- [5] A. Matsuda, S. Sugita, and T. Watanabe, *Phys. Rev. B* **60**, 1377 (1999).
- [6] N. Hussey, *Adv. Phys.* **51**, 1685 (2002).
- [7] M. R. J. C. Campuzano, M. R. Norman, arXiv:cond-mat/0209476v1 (2002).
- [8] A. Damascelli, Z. Hussain, and Z.-X. Shen, *Rev. Mod. Phys.* **75**, 473 (2003).
- [9] M. Norman and C. Pepin, *Rep. Prog. Phys.* **66**, 1547 (2003).
- [10] H. Mook, D. Pengcheng, S. Hayden, G. Aeppli, T. Perring, and F. Dogan, *Nature* **395**, 580 (1998).
- [11] P. Dai, H. Mook, S. Hayden, G. Aeppli, T. Perring, R. Hunt, and F. Doğan, *Science* **284**, 1344 (1999).
- [12] H. Fong, P. Bourges, Y. Sidis, L. Regnault, A. Ivanov, G. Gu, N. Koshizuka, and B. Keimer, *Nature* **398**, 588 (1999).
- [13] M. J. Holcomb, C. L. Perry, J. P. Collman, and W. A. Little, *Phys. Rev. B* **53**, 6734 (1996).
- [14] H. Molegraaf, C. Presura, D. Van Der Marel, P. Kes, and M. Li, *Science* **295**, 2239 (2002).
- [15] M. Rübhausen, A. Gozar, M. V. Klein, P. Guptasarma, and D. G. Hinks, *Phys. Rev. B* **63**, 224514 (2001).
- [16] R. B. Phelps, P. Akavoor, L. L. Kesmodel, A. L. Barr, J. T. Markert, J. Ma, R. J. Kelley, and M. Onellion, *Phys. Rev. B* **50**, 6526 (1994).

- [17] J. Tahir-Kheli, Phys. Rev. B **58**, 12307 (1998).
- [18] C. C. Tsuei, D. M. Newns, C. C. Chi, and P. C. Pattnaik, Phys. Rev. Lett. **65**, 2724 (1990).
- [19] V. B. Geshkenbein, A. I. Larkin, and A. Barone, Phys. Rev. B **36**, 235 (1987).
- [20] D. A. Wollman, D. J. Van Harlingen, W. C. Lee, D. M. Ginsberg, and A. J. Leggett, Phys. Rev. Lett. **71**, 2134 (1993).
- [21] A. J. Leggett, *Quantum Liquids* (Oxford University Press, New York, NY, USA, 2006).

Lec. 8 Exotic superconductivity: discussion

In this last lecture, I certainly do not want to try to review the whole field of exotic superconductivity that would be quite impossible. I would like to do mainly three things:

- (1) Discuss what properties are shared by all the exotic superconductors.
- (2) Give a brief review of existing theoretical approaches.
- (3) General considerations on energy saving in all “electronic” (non-phonon) superconductors.

In this last part of the lecture, I will be talking largely about some ideas I have been playing with over last more than ten years. Some of those are published and some are not. This idea is, though not fully recognized in the community, quite interesting since it is a rather different approach from many of conventional approaches in the literatures.

8.1 Common properties of all exotic superconductors

Trivially, the most obvious common property is the superconductivity itself. What does the “superconductivity” exactly mean, and what does it imply? In the original experiment by H. K. Onnes, he applied constant current through, aluminum and measured voltage drop across it (Fig. 8.1 (a)). He found that the resistivity drops sharply to zero at T_c .

This original experiment is rather simple from an experimental point of view, but this is not the simplest experiment, theoretically speaking. There are two kind of much simpler

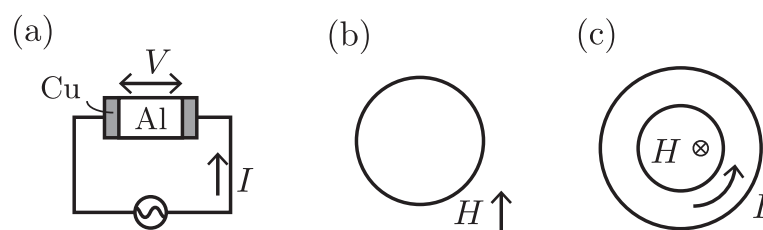


Fig. 8.1. (a) Cu is in the normal state, while Al is in the superconducting state. We apply constant current through them and measure the voltage drops across Al. (b) Experimental setup for the Meissner effect (c) Experimental setup for the persistent current.

ones. The first one is the Meissner effect. In this experiment, one takes a simply connected superconducting sample and hangs it up in zero magnetic field initially (Fig. 8.1 (b)). If one applies a magnetic field in the normal state (above T_c), the magnetic line just goes straight through it. When one cools down the sample below T_c , then the magnetic field lines suddenly appear to be totally expelled from the metal. In other words, superconductors show perfect diamagnetism.

It is important to realize that the Meissner effect is a true *thermal-equilibrium* effect. We have not changed anything other than temperature. Thus, the Meissner effect cannot simply be the consequence of zero-resistivity and it goes beyond that. The zero-resistivity would tell us that the system may not come into equilibrium with the boundary conditions, but here what is happening is coming out of equilibrium.

The second well-known phenomenon on the superconductivity is the persistent current. One first takes a system with ring geometry and applies a magnetic field through it (Fig. 8.1 (c)). Then, makes the sample into superconducting state and sets up some kinetic current by turning the magnetic flux down from finite value to zero. What one finds is that the current circulate for an astronomically long time. It is, however, rather easy to demonstrate that this *cannot* be an equilibrium effect and this is in fact an astronomically long-lived *metastable* effect.

There is no a priori guarantee that these two phenomena always go together, but it seems to come together, in all superconductors known to date.

8.2 Phenomenology of superconductivity

The following phenomenology are established mainly by London, Landau and Ginzburg during 1938-50. The theory postulates that the superconducting state is characterized by Schrödinger-like “macroscopic wave function” $\Psi(\mathbf{r})$, which can be analyzed into the magnitude and the phase:

$$\Psi(\mathbf{r}) = |\Psi(\mathbf{r})| \exp(i\phi(\mathbf{r})). \quad (8.1)$$

The crucial point is that the phase must be single valued modular 2π like the Schrödinger wave function.

It further postulates that the current is given in a similar form to what we obtain in the single particle quantum mechanics:

$$\mathbf{J}(\mathbf{r}) \propto |\Psi(\mathbf{r})|^2 (\nabla\phi(\mathbf{r}) - e^* \mathbf{A}(\mathbf{r})) \quad (8.2)$$

where e^* is an effective charge ($e^* = 2e$ in the BCS theory) and \mathbf{A} is a gauge potential.

Under these two simple assumptions, let us see how far we can explain the two major phenomena of superconductivity.

8.2.1 Meissner effect

The Meissner effect turns out to be the exact analog of atomic diamagnetism (for example, xenon gas). We apply the magnetic vector potential to a simply connected system and see what happens. It basically induces a diamagnetic current, which is opposite inside to the vector potential.

First of all, because we are thinking of a bulk superconductivity in a simply connected geometry, $\int \nabla\phi(\mathbf{r}) \cdot d\mathbf{l} = 0$. Thus, it is allowed to assume $\nabla\phi(\mathbf{r})$ itself remains 0 even when we apply magnetic field. Then, we obtain $\mathbf{J} = -\frac{ne^2}{m}\mathbf{A}$, which directly leads

$$\nabla^2\mathbf{B} = \lambda_L^{-2}\mathbf{B} \Leftrightarrow \mathbf{B} = \mathbf{B}_0 \exp(-z/\lambda_L), \quad (8.3)$$

where $\lambda_L = \sqrt{m/\mu_0 ne^2}$ is the London penetration length and z is the distance from the surface. Thus if we apply the magnetic field to the surface, it falls exponentially.

This argument can be applied to both a single atom and superconductors. However, there is a big difference between them. If we put the typical values and evaluate λ_L , it is almost the same for both the single atom and superconductors (perhaps the order of $\sim 1000 \text{ \AA}$). On the other hand, the size of the atom is much less than that of superconductors. Thus, in the case of atom, it shields only a small fraction of the applied field, while superconductors show almost complete diamagnetism.

8.2.2 Persistent current

We can define a winding number $n \equiv (2\pi)^{-1} \int \nabla\phi(\mathbf{r}) \cdot d\mathbf{l}$. n is conserved *unless* $|\Psi(\mathbf{r})| = 0$ across some cross section, which is highly unfavorable energetically. As a direct consequence, $J \sim n$ is conserved for an astronomically long time.

8.2.3 Summary

What was essential in the above argument? For these two phenomena to occur, there must exist a *complex* order parameter $\Psi(\mathbf{r})$ such that

- (a) Nonzero values of $|\Psi(\mathbf{r})|^2$ are (locally) stable.
- (b) Spatial gradients of the phase of $\Psi(\mathbf{r})$ correspond to charge currents.

An overwhelmingly natural guess at the nature of such an order parameter is as follows: $\Psi(\mathbf{r})$ represents *macroscopically occupied eigenfunction of n -particle density matrix*, i.e., the system possesses off-diagonal long range order (ODLRO). More rigorous arguments (Yang [1], Kohn and Sherrington [2]) claim to show rigorously that

ODLRO is a necessary and sufficient condition for superconductivity.

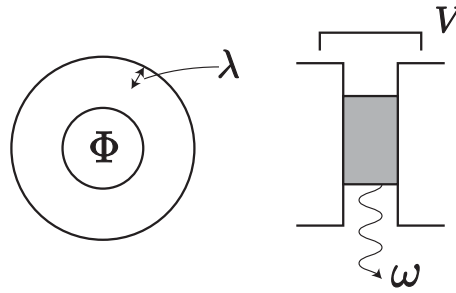


Fig. 8.2. Experimental setups for flux quantization (left) and AC Josephson junction (right).

In strict two dimensions, we know from other exact theories that we cannot get the ODLRO but the system can go through a Kosterlitz–Thouless (KT) phase transition and essentially behave like a superconductor. Thus this is not a totally reliable theorem but I do not know any counterexample in three dimensions. Historically, in the 1980s, “anyon superconductivity” was claimed to be a superconductivity without the ODLRO. However, it turned out that anyon superconductors are just a kind of the standard BCS superconductors and thus not an counterexample.

Even if this “theorem” is true, it says nothing about the value of n . Since electrons are fermions, n must be even. Yet, in principle, n could be 4, 6, ... Then why can we assume $n = 2$? Two kinds of experiments are particularly persuasive (Fig. 8.2):

- (a) In a (thick) ring geometry, total trapped flux Φ through the hole is quantized in units of h/ne .
- (b) In the AC Josephson effect, the principal frequency of current, when we apply voltage V between Josephson junctions, should be $\omega = neV/\hbar$.

Both of these experiments have been done not only on old-fashioned superconductors but also on exotic superconductors, and all results seem to be entirely consistent with $n = 2$. There is no evidence for any value of n other than 2 in any superconductor. Thus, we can reasonably conclude that

superconductivity is due to the formation of Cooper pairs.

That is the one thing all superconductors most surely have in common.

8.3 What else do exotic superconductors have in common?

Apparently, exotic superconductors do not have much in common, apart from superconductivity itself. Even if we exclude alkali fullerenes¹,

- (a) Not all are non-phonon mechanism (still controversial: some evidences suggest that the mechanism of organics is phonon, and others show against that).
- (b) Not all are quasi-two-dimensional (most heavy Fermions are three-dimensional).
- (c) Not all are close to an antiferromagnetic phase (some heavy Fermions, Sr_2RuO_4 do not have the phase).

However, if we restrict ourselves to “high-temperature” superconductors (the cuprates, ferropnictides, organics), then we get the following common features:

- (a) All are strongly two-dimensional.
- (b) All have an antiferromagnetic phase close to the superconducting phase.
- (c) All have charge reservoirs well separated from superconducting layers.

8.4 Theoretical approaches (mostly for the cuprates)

1. Generic “BCS-like” approach.

Crudely speaking, what BCS did was to try to isolate a particular physical effect which they believe, in some sense, is the key to the superconductivity in metals of aluminium and lead. This fundamental physical effect was the effective attraction between the electrons supplied by the exchange of virtual phonons. Next, they wrote down the effective low energy Hamiltonian, which they believed encapsulated and expressed this fundamental physical feature. This is, of course, the famous BCS Hamiltonian, which was spectacularly successful.

Recently, there have been lots of attempts to do something very similar on exotic superconductors. Typically one, tries to isolate what he/she thinks might be important effects (for example, the exchange of some kinds of excitons, and the formation of d -density wave, bipolarons, and whatever). One then, arbitrarily writes down some kinds of postulated low energy effective Hamiltonian, which involves these particular physical effects, and then move on to calculations. There are thousands

¹Remember that when we discussed alkali fullerenes in Lec. 5, we concluded that all the evidences of alkali fullerenes indicate they are probably just standard BCS superconductors due to the phonon mechanism, and the only difference is the strong molecular structure that may explain the high- T_c in this case. Thus, they are not genuine exotic superconductors.

of papers in the literature which carry out this kinds of properties. Of course, they usually claim that they can explain at least some certain experimental data.

I think there are a number of problems in this kind of approaches. Obviously, we have no particular reason to believe any one of these effective Hamiltonians is going to be the right description. For the BCS theory, we were very lucky; before BCS did it, there was no particular reason to believe that this approach worked for electron-phonon interaction, but it did. Furthermore, none of these (to the best of my knowledge, except spin-fluctuation theory which is a bit different and I will treat it somewhat differently) has ever made any prediction ahead of experiments.

2. Approaches based on the Hubbard model (which involves less guess than the first class).

There are a large number of theoretical approaches in the literature based on some forms of the Hubbard model. The simplest form of the Hubbard model is

$$\hat{H}_{\text{eff}} = -t \sum_{\sigma, (i,j) \in \text{n.n.}} a_{i\sigma}^\dagger a_{j\sigma} + U \sum_i n_{i\uparrow} n_{i\downarrow}, \quad (8.4)$$

where n.n. in the summation stands for the nearest neighbors. As long as we focus on one relevant electronic orbital per site, then we do not have to worry about parallel spin interaction because of the Pauli principle. This is very simple looking Hamiltonian. However, as far as we know, it is not analytically soluble even in two dimensions. Therefore, we have to resort to some possible strategies:

- (a) Digital numerical simulations: even for most powerful computers available, we can solve the problem typically up to only $\sim 10 \times 10$ sites, and it is not obvious this is enough to give us a reasonable thermodynamic result.
- (b) Analog simulation: last ten years lots of amazing things have happened in the experiments on ultracold atoms in optical lattices. It turned out that atoms in optical lattices under appropriate conditions are marvelous simulations of the Hubbard model (much better than electrons in real solids). People have just about started right now using this technique.
- (c) “Guesses” at analytic solution: one kind of rather plausible results is that we start from the BCS type wave function, and then project off all terms having doubly occupied sites by the Gutzwiller projection operator, $\Psi_N = \hat{\mathcal{P}}_G \Psi_{\text{BCS}}$, reflecting the strong repulsion between two electrons on the same site. Some people claim qualitatively good explanation on experiments taking this approach.

One problem of the Hubbard model in general is that the model may omit important physical effects (e.g., long-range part of Coulomb interaction).

3. Antiferromagnetic (AF) spin fluctuation exchange

In all high- T_c superconductors, the superconducting phase occurs close to the AF phase (Fig. 8.3). Moreover, both the NMR and the neutron scattering data in the cuprates suggest that the in-plane spin susceptibility $\chi(\mathbf{q}, \omega)$ in normal phase is featureless as a function of ω , while they are strongly peaked as a function of \mathbf{q} at $\mathbf{q} = \mathbf{Q} \equiv (\pm\pi/a, \pm\pi/a)$, the superlattice Bragg vector in the AF phase, as shown in Fig. 8.4.

This is often expressed as a possible ansatz for $\chi(\mathbf{q}, \omega)$ ($\equiv \chi_{\text{NAFL}}(\mathbf{q}, \omega)$)² [3]. Pines *et. al.* [3] postulated a crude phenomenological ansatz that, far from pseudo-Bragg vectors \mathbf{Q} , $\chi_{\text{NAFL}}(\mathbf{q}, \omega)$ has Fermi liquid-like form:

$$\chi_{\text{NAFL}}(\mathbf{q}, \omega) \cong \frac{\chi_{\mathbf{q}}}{1 - i\omega/\Gamma_{\mathbf{q}}} \cong \frac{\chi_0}{1 - i\omega/\Gamma_0}. \quad (8.5)$$

This is not particular interesting. However, when we are very close to a pseudo-Bragg vector,

$$\chi_{\text{NAFL}}(\mathbf{q}, \omega) \cong \frac{\chi_{\mathbf{Q}_i} (\gg \chi_{\mathbf{q}})}{1 + (\mathbf{Q}_i - \mathbf{q})^2 \xi^2(T) - i\omega/\omega_{\text{SF}}} \quad (8.6)$$

where $\omega_{\text{SF}} (\ll \Gamma_0)$ is the AF fluctuation frequency, and $\xi(T)$ is the AF correlation length. What this approach emphasizes is that the particular nearly antiferromagnetic spin fluctuations are playing an important role.

Ansatz³ : single electrons couple strongly to AF spin fluctuations, whose exchange then generates an effective electron-electron attraction. This is similar to what is going on in ³He, except that in ³He, what they are trying to exchange is paramagnon, related to the close ferromagnetic phase.

Unfortunately, the question of what is correct coupling constant is rather controversial. People usually put the value of the constant by hand or try to do some approximate calculations to evaluate it. However, there has been an argument in the literature which states

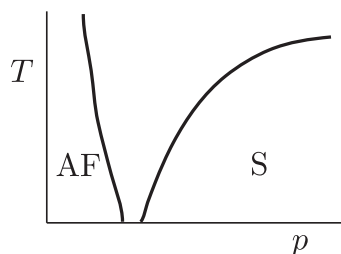


Fig. 8.3. The well-known phase diagram for the cuprates. S is the superconducting phase and AF is the antiferromagnetic phase. p represents the density of holes.

²NAFL stands for Nearly antiferromagnetic Fermi liquid.

³Not directly testable in experiment.

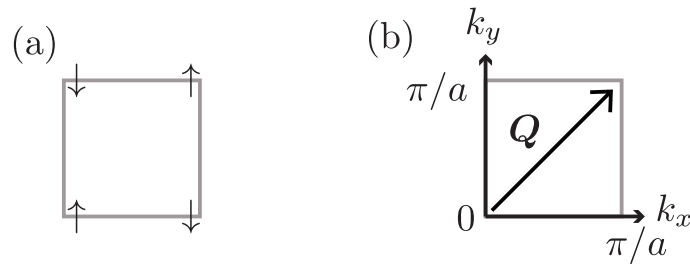


Fig. 8.4. (a) The AF spin order in real space. (b) The superlattice Bragg vector \mathbf{Q} in \mathbf{k} -space.

that the coupling constant is actually zero. There are certain amount of controversies about that, but let us here suppose that the coupling constant is not zero and see the striking prediction of the spin-fluctuation theories (rather generic):

- (a) The points on the Fermi surface most strongly connected by \mathbf{Q}_i are roughly at $(\pi/a, 0)$, $(0, \pi/a)$ etc. (Fig. 8.4). Then, we can expect the gap becomes maximum there. Thus we expect the gap is singlet, as indicated by ARPES.
- (b) The sign of the pair wave function $F_{\mathbf{k}}$: scattering processes should as far as possible leave $F_{\mathbf{k}}$ invariant. However, the emission of the virtual spin fluctuations flips the spin, changes momentum by \mathbf{Q} . If a state is singlet, spin-flip is equivalent with multiplying (-1) . Hence to preserve $F_{\mathbf{k}}$, momentum change by \mathbf{Q} ($A \rightarrow B$ in Fig. 8.4) must also multiply (-1) .

Hence, from (a) $F_{\mathbf{k}}$ must be large at $(\pi/a, 0)$ (b) $F_{\mathbf{k}}$ must change sign under $\hat{R}_{\pi/2}$. Of the four even-parity irreducible representations of C_{4v} (s , s^- , $d_{x^2-y^2}$ and d_{xy}), only $d_{x^2-y^2}$ works⁴. Thus,

spin-fluctuation theories unambiguously predict $d_{x^2-y^2}$ symmetry.

As I said, that is the only prediction I know, in the whole history of the high temperature superconductivity, where theorists made a non-trivial prediction which was later confirmed by experiments. This is an appreciable credit of the spin-fluctuation theories. The main criticism directed to the spin-fluctuation theories is that we just have too many fitted parameters.

8.5 Which energy is saved in the superconducting phase transition?

Let us start on the last part. I believe that the arguments in this section are at a more general level than much of the theories I have talked about so far. Let me give a review of

⁴See Lec. 7.

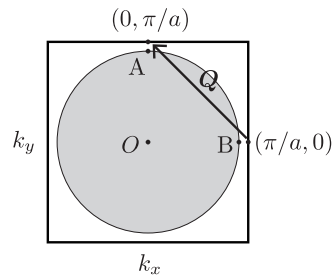


Fig. 8.5. Antiferromagnetic spin fluctuations connect the point on the Fermi surface close to $(\pi/a, 0)$, $(0, \pi/a)$.

this interesting theory, where some of these are published [4] and some not published yet. We start with a very general question: do we know anything about the energy which is saved or not in the superconducting phase transition? Actually, it turns out that this is just the case for different questions, and it can be applied to any other phase transition.

8.5.1 Virial theorem

We start with a really basic level, non-relativistic limit of the famous Dirac Hamiltonian:

$$\hat{H} = \hat{K} + \hat{V}, \quad (8.7)$$

$$\hat{K} = \sum_i \frac{\hat{p}_i^2}{2m} + \sum_\alpha \frac{\hat{P}_\alpha^2}{2M}, \quad (8.8)$$

$$\hat{V} = \frac{1}{8\pi\epsilon_0} \left\{ \sum_{i,j} \frac{e^2}{|\mathbf{r}_i - \mathbf{r}_j|} + \sum_{\alpha,\beta} \frac{(Ze)^2}{|\mathbf{R}_\alpha - \mathbf{R}_\beta|} - 2 \sum_{i,\alpha} \frac{Ze^2}{|\mathbf{r}_i - \mathbf{R}_\alpha|} \right\}. \quad (8.9)$$

Let us imagine the following thought experiment⁵: let us imagine we cool the system down to zero temperature, but forbid it to form Cooper pairs. Then, basically speaking, we have got the “best” normal ground state of fermions. Let us relax that constraint and allow them to form Cooper pairs. We know that this is what we see in experiments. Why is it? It is because, trivially, it saves the energy by forming the Cooper pairs. In other words, trivially, the energy of the best superconducting ground state must be below that of the best normal state.

There is a very simple argument done by Chester [5] in the context of the old-fashioned superconductivity, and he simply uses the sum rules. At zero pressure, we obtain

$$\langle \hat{H} \rangle = \langle \hat{K} \rangle + \langle \hat{V} \rangle, \quad (8.10)$$

$$\langle \hat{K} \rangle = -\frac{1}{2} \langle \hat{V} \rangle \quad (8.11)$$

⁵This argument works not only for the superconductivity.

from the virial theorem. Remember that the virial theorem works because we have a simple form of the interaction. Thus, the expectation value for the total Hamiltonian is

$$\langle \hat{H} \rangle = \frac{1}{2} \langle \hat{V} \rangle. \quad (8.12)$$

Therefore, since $E_{\text{cond}} \equiv \langle \hat{H} \rangle_{\text{N}} - \langle \hat{H} \rangle_{\text{S}} > 0$, the total Coulomb energy (electron-electron, electron-nuclei, and nuclei-nuclei) must be smaller in the superconducting phase:

$$\langle \hat{V} \rangle_{\text{S}} < \langle \hat{V} \rangle_{\text{N}}. \quad (8.13)$$

This is a very general statement. Conversely, according to this relation, the total kinetic energy (the kinetic energy of electrons plus the kinetic energy of nuclei) must be increased in the the superconducting phase transition. That is a theorem, and we cannot get out of that. This is a rather strong constraint to certain kinds of theories, in which they claim that the kinetic energy is actually saved in the the superconducting phase transition. Such theories can never be true unless we redefine the kinetic energy in some ways: otherwise, this theorem kills them.

Let us now go on further from the Dirac Hamiltonian, and go on to an intermediate-level description. Let us do the partition of electrons into “core” electrons and “conduction” electrons. Since there are experiments showing that the phonons do not play a major role in the cuprates, let us ignore the phonons. Then, we have an effective Hamiltonian for the conduction electrons as follows:

$$\hat{H} = \hat{K}_{\text{eff}} + \hat{V}_{\text{eff}} \quad (8.14)$$

$$\hat{K}_{\text{eff}} = \sum_i \frac{\hat{p}_i^2}{2m} + \hat{U}(\mathbf{r}_i) \quad (8.15)$$

$$\hat{V}_{\text{eff}} = \frac{1}{8\pi\epsilon_0} \sum_{i,j} \frac{e^2}{\epsilon |\mathbf{r}_i - \mathbf{r}_j|}, \quad (8.16)$$

where \hat{U} is the potential of the static lattice, and ϵ is a high-frequency dielectric constant (contribution to the dielectric constant from the core ions). We ignore the c -axis now. I will later argue that almost certainly the only part of the kinetic energy we have to worry about is in the ab -plane: basically forget about the c -axis, since that contribution turns out to be very small. It is important to be aware, though it is not often remarked in the literatures, that the interaction term is not the bare Coulomb interaction. Why not? It is because it is going to be screened by atomic cores, and we know from experiments, that this effect is not small. In fact, typically, the high-frequency dielectric constant of the cuprates is somewhat 4 to 5. Therefore, it is a big effect.

Let us assume that $U(\mathbf{r}_i)$ is independent of ϵ . This is not obvious, and it could be relaxed, but for the moment, let us just play with it. Then, the only point where ϵ comes in is the interaction part. If this is right, we can compare two systems which have the same

form of $U(\mathbf{r})$ and carrier density, *but different* ε . Let us imagine that we can somehow do that comparison. What do we then expect? Is it better for the high-temperature superconductivity to have a large value of ε , that is a weak Coulomb interaction, or the opposite, small ε , and therefore a strong Coulomb interaction? Naively speaking, one would say “look, the repulsion is not good for the superconductivity, and it is better to set the repulsion down. In that way, we might be able to get an effective attraction.” This is, in fact, not true. What we will get is the opposite. We can just apply the Hellman-Feynman theorem, and obtain

$$\frac{\partial \langle \hat{H} \rangle}{\partial \varepsilon} = \left\langle \frac{\partial \hat{V}}{\partial \varepsilon} \right\rangle = - \left\langle \frac{\hat{V}}{\varepsilon} \right\rangle. \quad (8.17)$$

Therefore, provided $\langle \hat{V} \rangle$ decreases in the normal to superconducting phase transition, then $\frac{\partial E_{\text{cond}}}{\partial \varepsilon} < 0$. In other words, “other things” ($U(\mathbf{r}), n$) being equal, it is advantageous to have as strong a Coulomb repulsion as possible. At first sight, it is counterintuitive. I think it is somewhat plausible to look in the following way: forget everything you have ever known about the BCS theory, effective attraction. What is happening is that there is an enormous amount of the repulsion in the normal phase, but by forming Cooper pairs, this repulsion somehow manages to decrease. The more repulsive energy we have in the normal phase, the more chances of it to be released. Intuitively speaking, that is how it works. This is a rather remarkable conclusion, and other things being equal, we want to have a stronger Coulomb repulsion as possible for the high-temperature superconductivity.

Here is an example, which I think a possible manifestation of this. Let us consider a single plane Hg-1201, and compare that with a central plane of Hg-1223. What do we know about these two materials? Of course, there are other effects which distinguish these two, but let us focus here on the screening of the Coulomb repulsion. Since both have the same CuO_2 plane, the screening by Cu and O is essentially the same. For the inter-layer materials, there is a difference. For Hg-1201, there is BaO_2 sitting between the planes, which has a large polarizability, contributing to a large dielectric constant. Thus, for Hg-1201 the Coulomb repulsion is well screened. On the other hand, for Hg-1223, there is Ca^{++} between the layers, which has a little polarizability since it forms a closed shell structure. Thus, the Coulomb interaction in the central plane is not screened. Thus, the conclusion from the above argument is that the transition temperature for Hg-1223

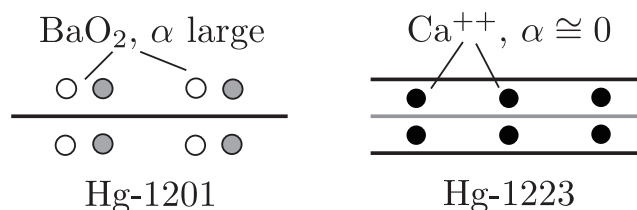


Fig. 8.6. Schematic illustration of the crystal lattice for Hg-1201 and Hg-1223.

is higher than that of Hg-1201: this is true indeed. I do not claim that this is the only reason for the difference in the value of T_c , but at least it is going in the right direction⁶.

8.5.2 Energy consideration in “all-electronic” superconductors

Let us now turn to the general question: what do we know the way in which the energy is saved or not saved in “all-electronic” superconductors? Again, I will start from the intermediate level description (neglect phonons, inter-cell tunneling):

$$\hat{H} = \hat{T}_{(\parallel)} + \hat{U} + \hat{V}_c, \quad (8.18)$$

where $\hat{T}_{(\parallel)}$ is the in-plane electron kinetic energy, \hat{U} is the potential energy of conduction electrons under the static field of the lattice, and \hat{V}_c is the inter-conduction electron Coulomb energy (intra-plane and inter plane). That is all we assume: we *do not* add spin fluctuations, excitons, anyons... If they are there, they should come out from the above Hamiltonian automatically. We know, from the previous section, that at least one of $\langle \hat{T} \rangle$, $\langle \hat{U} \rangle$, $\langle \hat{V}_c \rangle$ must be decreased by the formation of Cooper pairs. The default option for this is $\langle \hat{V}_c \rangle$: this is not necessarily true, but just to have a starting point, let us assume so.

An important observation, although it is not noted in much of literatures, is that there is a rigorous relation (sum rule):

$$\langle \hat{V}_c \rangle \sim - \int d^d \mathbf{q} \int d\omega \operatorname{Im} \left\{ \frac{1}{1 + V_{\mathbf{q}} \chi_0(\mathbf{q}, \omega)} \right\}, \quad (8.19)$$

where $V_{\mathbf{q}}$ is a Coulomb interaction (repulsive), and $\chi_0(\mathbf{q}, \omega)$ is a bare density response function. For the three-dimensional case, this is

$$\langle \hat{V}_c \rangle_{3D} \sim \int d^3 \mathbf{q} \int d\omega (-\operatorname{Im} \varepsilon(\mathbf{q}, \omega)^{-1}), \quad (8.20)$$

where $\operatorname{Im} \varepsilon(\mathbf{q}, \omega)^{-1}$ is called the loss function. Thus, this sum rule is a relation between the interaction energy and the loss function.

Let us raise a question: *where in the space of (\mathbf{q}, ω) is the Coulomb energy saved (or not)?* An interesting point is that quite independent from any microscopic theory, in principle, this can be answered by experiments. It can be answered to an extent by an optics, or X-rays, but the best answer will be obtained from the electron energy-loss spectroscopy (EELS) (I will come back to this point in Sec. 8.5.6).

Let us discuss the property of Eq. (8.19), especially in the case $V_{\mathbf{q}} \chi_0(\mathbf{q}, \omega) \ll 1$ and $V_{\mathbf{q}} \chi_0(\mathbf{q}, \omega) \gg 1$.

A. $V_{\mathbf{q}} \chi_0(\mathbf{q}, \omega) \ll 1$

Suppose that $V_{\mathbf{q}} \chi_0(\mathbf{q}, \omega) \ll 1$. This typically means $q \gg q_{\text{TF}}^{(\text{eff})} \sim \min(k_{\text{F}}, k_{\text{TF}}) \sim 1 \text{ \AA}^{-1}$.

⁶This argument may be too naive because for Hg-1223 it neglects the polarizability of the other CuO_2 planes.

By expanding the denominator, and we find

$$\langle \hat{V}_c \rangle_{\mathbf{q}} \cong +V_{\mathbf{q}} \int d\omega \operatorname{Im} \chi_0(\mathbf{q}, \omega) = V_{\mathbf{q}} \langle \rho_{\mathbf{q}} \rho_{-\mathbf{q}} \rangle_0. \quad (8.21)$$

This means that in order to decrease $\langle \hat{V}_c \rangle_{\mathbf{q}}$, $\langle \rho_{\mathbf{q}} \rho_{-\mathbf{q}} \rangle_0$ must *decrease*. However, if we have anything like the BCS theory, the change in the density correlation function in the superconducting phase transition $\delta \langle \rho_{\mathbf{q}} \rho_{-\mathbf{q}} \rangle_{\text{pairing}}$ can be written as

$$\delta \langle \rho_{\mathbf{q}} \rho_{-\mathbf{q}} \rangle_{\text{pairing}} \sim \sum_{\mathbf{p}} \Delta_{\mathbf{p}+\mathbf{q}/2} \Delta_{\mathbf{p}-\mathbf{q}/2}^*. \quad (8.22)$$

Now we arrive at an interesting point: if $\Delta_{\mathbf{p}}$ has the same sign over the Fermi surface, this term should be positive. That means that the formation of the Cooper pairs increases the Coulomb energy, which is exactly what we do not like. That gives us a strong argument that the gap should change its sign over the Fermi surface. From this point of view, it becomes not a big surprise that so many of the exotic superconductors appear to have also exotic pair wave functions, i.e., gap symmetries.

B. $V_{\mathbf{q}} \chi_0(\mathbf{q}, \omega) \gg 1$

Let us consider the opposite case $V_{\mathbf{q}} \chi_0(\mathbf{q}, \omega) \gg 1$. This typically means $q \ll q_{\text{TF}}^{(\text{eff})}$. Then, we find

$$\langle \hat{V}_c \rangle_{\mathbf{q}} \cong \frac{1}{V_{\mathbf{q}}} (-\operatorname{Im} \chi_0(\mathbf{q}, \omega)^{-1}). \quad (8.23)$$

This tells us that in order to decrease $\langle \hat{V}_c \rangle_{\mathbf{q}}$ (i.e., decrease T_c), we should *increase* $\operatorname{Im} \chi_0(\mathbf{q}, \omega)$, which is consistent with an increase in $\langle \rho_{\mathbf{q}} \rho_{-\mathbf{q}} \rangle_0$. In other words, *an increased correlation leads to an increased screening, which in turn means a decrease of the Coulomb energy.*

8.5.3 Eliashberg vs. Overscreening

In the standard Eliashberg approach, crudely speaking, we generate an effective attraction between pairs of electrons, as in Fig. 8.7 (a), the electron with \mathbf{k} and $-\mathbf{k}$ will form a pair with that attraction. The attraction may be an exchange of some kinds of bosons, such as phonons, spin fluctuations, or excitons, but it must be attractive.

In the overscreened picture, as illustrated in Fig. 8.7 (b), the main effect of pairing is not coming from the electrons interacting in the opposite momentum, but from all momenta $\mathbf{k}_1, \mathbf{k}_2$. The contribution comes from the modification of the interaction energy between those electrons. The great advantage of this picture is that it does not require an attractive interaction in the normal phase. Thus it is a different picture from the Eliashberg types of theories.

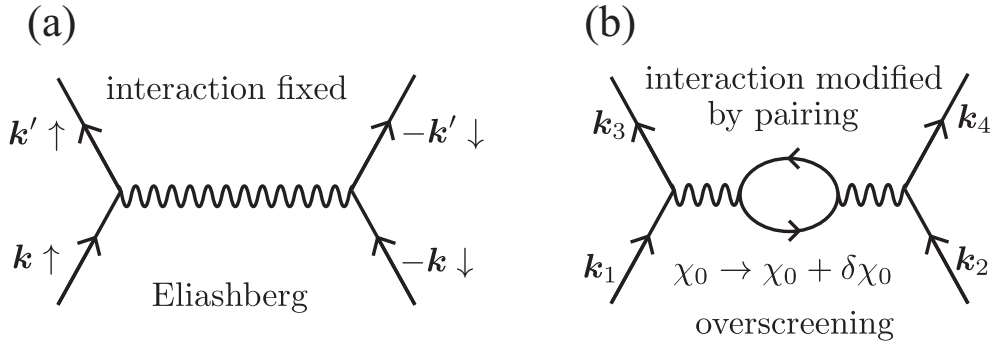


Fig. 8.7. (a) Feynman diagram for the Eliashberg type of interaction between electrons. (b) Feynman diagram for the overscreened interaction between electrons.

8.5.4 Role of two-dimensionality

Let us turn to a generic question: can we get any insight into why so many, or all, of the high-temperature superconductors are strongly two-dimensional? To consider this, use the sum rule again:

$$\begin{aligned} \langle \hat{V} \rangle &= -\frac{1}{2} \sum_q \int \frac{d\omega}{2\pi} \text{Im} \left\{ \frac{1}{1 + V_q \chi_0(q, \omega)} \right\} \\ &= -\frac{1}{2} \frac{1}{(2\pi)^{d+1}} \int_0^\infty d^d q \text{Im} \left\{ \frac{1}{1 + V_q \chi_0(q, \omega)} \right\}. \end{aligned} \quad (8.24)$$

Here, note that V_q depends on the dimension. In three dimensions, $V_q \sim q^{-2}$, and from the definition, $1 + V_q \chi_0(q, \omega) \equiv \varepsilon_{\parallel}(q, \omega)$, we find

$$\langle \hat{V} \rangle \sim \int q^2 dq \int d\omega \left\{ -\text{Im} \frac{1}{\varepsilon_{\parallel}(q, \omega)} \right\}. \quad (8.25)$$

Note that we have the loss function in the right-hand side. Therefore, the “small” q region is strongly suppressed in the integral⁷.

In two dimensions, on the other hand, $V_q \sim q^{-1}$, so that

$$V_q \chi_0(q, \omega) \sim q \frac{d}{2} (\varepsilon(q, \omega) - 1), \quad (8.26)$$

where d is an inter-plane spacing. Then, we obtain⁸,

$$\begin{aligned} \langle \hat{V} \rangle &\sim \int q dq \left\{ -\text{Im} \frac{1}{1 + q \frac{d}{2} (\varepsilon_{3D}(q, \omega) - 1)} \right\} \\ &\sim \frac{1}{d} \int dq \left\{ -\text{Im} \frac{1}{\varepsilon_{3D}(q, \omega)} \right\}. \end{aligned} \quad (8.27)$$

⁷The similar argument is used in the original paper of Hubbard [6] to justify that the small q region is not essentially important, so that we can neglect the long-range part of the interaction.

⁸Note that the high-frequency dielectric constant for the cuprates is rather large, so that the term $q \frac{d}{2} (\varepsilon_{3D}(q, \omega) - 1)$ can be dominant even for a low momentum.

Thus, the linear q factor in the integration is canceled by the linear q dependence on the right-hand side of Eq. (8.26), and the small q contribution may be as important as large q part. That raises an important question: in 2D-like high-temperature superconductors (cuprates, ferropnictides, organics...), *is the saving of the Coulomb energy, mainly at small q ?*

8.5.5 Constraints on the Coulomb saved at small q

What do we know about constraints on the saving of the Coulomb energy at small q [4]? To answer this question, let us recall

$$\langle \hat{V} \rangle = V_q \langle \rho_q \rho_{-q} \rangle = \frac{V_q}{2\pi} \int_0^\infty \text{Im} \chi(q, \omega) d\omega. \quad (8.28)$$

Here and from now on, we are using the “full” density response $\chi(q, \omega)$, not the “bare density response”. Note that the dimension can be arbitrary in the following discussion. From the sum rule for the full density response function, we obtain

$$J_{-1} \equiv \frac{2}{\pi} \int_0^\infty \frac{d\omega}{\omega} \text{Im} \chi(q, \omega) = \chi(q, 0) \quad \text{Kramers–Kronig relation}, \quad (8.29)$$

$$J_1 \equiv \frac{2}{\pi} \int_0^\infty \omega d\omega \text{Im} \chi(q, \omega) = \frac{nq^2}{m} \quad \text{f-sum rule}, \quad (8.30)$$

$$J_3 \equiv \frac{2}{\pi} \int_0^\infty \omega^3 d\omega \text{Im} \chi(q, \omega) = \frac{q^2}{m^2} \langle A \rangle + q^4 \frac{n^2}{m^2} V_q + o(q^4). \quad (8.31)$$

The third equation is a generalized Mihara–Puff relation [7], and

$$\langle A \rangle \equiv -\frac{1}{\pi} \sum_k (\mathbf{k} \cdot \hat{\mathbf{q}})^2 U_{-k} \rho_k. \quad (8.32)$$

There is, in fact, a strong argument that $\langle A \rangle$ should be positive here. Note that in two dimensions, the term in $\langle A \rangle$ is dominant at small q compared with the V_q term. From the general Cauchy–Schwartz inequalities (for arbitrary dimension), we obtain

$$\frac{1}{2} \sqrt{V_q^2 J_{-1} J_1} \geq \langle \hat{V} \rangle_q \geq \frac{1}{2} \sqrt{V_q^2 J_1^3 / J_3}, \quad (8.33)$$

or equivalently,

$$\frac{\hbar\omega_p}{2} + o(q^2) \geq \langle \hat{V} \rangle_q \geq \frac{\hbar\omega_p}{2} \frac{1}{\sqrt{1 + \frac{\langle A \rangle}{nm\omega_p^2}}} + o(q^2). \quad (8.34)$$

It is interesting to see from this inequality that for $\langle A \rangle = 0$ (for example, the “jellium” model⁹), *there is no saving of the Coulomb energy for $q \rightarrow 0$ up to $o(q^2)$.* In other

⁹The jellium model is a model where we assume a uniform background of positive charge, rather than a periodic potential produced by the ion.

words, if indeed a lot of the Coulomb energy is saved in the low-energy part for the high-temperature superconductors, it is crucial to have the lattice!

Here, let me show a further argument on why the small q region may be important. Let us get back to the question which, in principle, can be answered by experiment:

Where in the space of q and ω is the Coulomb energy saved (or not)?

Let us, at this point, go over to a question at first totally different:

Why does T_c depend on n , the number of layers?

As we have discussed for Ca-spaced homologous series, T_c rises with n at least up to $n = 3$ (this point is noncontroversial). This rise *may* be fitted by the formula (for “not too large” n)

$$T_c^{(n)} - T_c^{(1)} \sim \text{const} \left(1 - \frac{1}{n}\right). \quad (8.35)$$

Note that this formula *is* controversial. A possible explanation is as follows:

A . Boring explanation

The superconductivity is a single-plane phenomenon, but multi-layering affects properties of individual planes, such as doping, band structure, screening by off-plane ions...

B . “Interesting” explanation: inter-plane effects

Inter-plane effects play an important roles. Some of the examples are listed below:

1. Anderson inter-layer tunneling model¹⁰.
2. Kosterlitz–Thouless theory.
3. Inter-plane Coulomb interactions (we know that they are present!).

Primarily, what about the third possibility? For sure, we know that they are there. The point is whether they are important or not. We have to have the electron-electron interaction between neighboring planes if they are not negligible. If we take the effect of the Coulomb interaction from electrons in the nearest plane, and perform the Fourier transform, we obtain

$$V_{\text{int}}(q) \sim q^{-1} \exp(-qd), \quad (8.36)$$

where q is the in-plane wave vector, and d is the intra-multilayer spacing, which is typically $d \sim 3.5 \text{ \AA}$.

If the option 3 is right, then even in the single-plane materials, a dominant region of q is $q < d^{-1}$!

¹⁰Although this idea is abandoned, but it is still interesting.

8.5.6 Mid-infrared optical and EELS spectra of the cuprates

Then, where in ω is energy saved? Here I use the WILLIE SUTTON principle¹¹: we can only save the energy for making the superconducting phase transition in regions of \mathbf{q} and ω where there is a lot of energy stored up in the normal phase. Thus, to achieve a high-temperature superconductor, we have to specify where the energy is saved in the normal phase. This can be investigated in experiments.

Optics

Optics show that there is a lot of energy saved in the long-wavelength, mid-infrared regime, as we can see from the measurement of the loss function $L(\omega) \equiv -\text{Im}\varepsilon^{-1}(\omega)$ shown in Fig. 8.8.

EELS

EELS measures $q \rightarrow 0$ shape of the loss function, and verifies that (roughly) the same shape persists for finite q . (at least up to $\sim 0.3 \text{ \AA}$).

Thus, it looks like that that's where the money is! That's where the energy is saved in the normal phase!

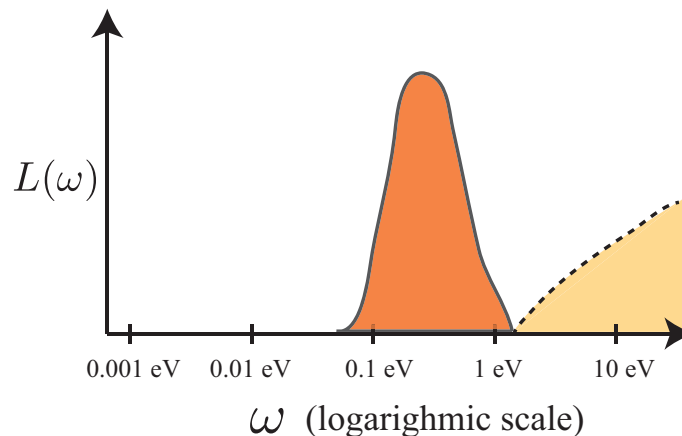


Fig. 8.8. Schematic illustration of the loss function $L(\omega)$ measured by an optical measurement. The large peak corresponds to the mid-infrared peak, while the contribution in the higher-energy part is a rather material-dependent part, coming from each atoms.

¹¹WILLIE SUTTON is a famous bank robber in the US in the 1930s. One of the reason he is notorious is when journalists interview him, “why do you rob banks?”. Then he replies, “Because that’s where the money is!”.

Then, that is the obvious guiding principle we can use for the realization of high-temperature superconductors.

If the saving of the Coulomb energy is mainly in the low- q , mid-infrared regime, then we can expect that a certain change in the shape of spectrum should appear in the normal-to-superconducting phase transition: this should be able to be observed in the EELS spectrum. In fact, from the sum rule, we expect that $\text{Im}\varepsilon^{-1}$ must *decrease* in the phase transition in the mid-infrared regime. This means that $\text{Im}\left(\frac{\delta\varepsilon}{\varepsilon_n^2}\right) > 0$, where $\delta\varepsilon$ is the change of the dielectric constant through the phase transition. To estimate this quantity from experiments, we should know both the real part and imaginary part of the dielectric constant. Unfortunately, in most experiments, they only show such quantities as the reflectivity, effective plasma frequency, and so on, and there are few papers which show both the real and imaginary part explicitly. There is one paper which does show both¹², and there is a very interesting piece of data in it [8]: both in the real part and the imaginary part, they have a strong frequency dependence. However, for any frequency, they are exactly the opposite to each other. That is, the real part of ε is exactly minus of the imaginary part:

$$\varepsilon_n(\omega) \cong \frac{\omega_p^2}{\omega^2}(-1 + i), \quad (8.37)$$

where ω_p is the plasma frequency. This equation means

$$\varepsilon_n^{-2} \sim \frac{\omega^4}{2\omega_p^4}i. \quad (8.38)$$

If this is right, we can conclude that a condition $\text{Re}\delta\varepsilon < 0$ is required in the mid-infrared regime. We now apply the Kramers–Kronig transform to see what it implies for the imaginary part, and we obtain

$$\int_0^\infty \omega'^4 \left\{ \frac{1}{2} \log \left| \frac{\omega_e + \omega'}{\omega_e - \omega'} \right| - \frac{\omega_e}{\omega'} \right\} \text{Im}\delta\chi(q, \omega') d\omega' < 0 \quad (\omega_e \sim \omega_p). \quad (8.39)$$

It is important to note that the bracket part in this equation is positive for $\omega' > \bar{\omega}_e$, where $\bar{\omega}_e$ is some characteristic frequency of the order of the plasma frequency $\bar{\omega}_e \sim \omega_e \sim \omega_p$. On the contrary, it is negative for $\omega' < \bar{\omega}_e$. If indeed a lot of energy is saved in the low-momentum, mid-infrared regime, what we would expect from this is that the spectral weight transfers from $\omega > \omega_p$ to $\omega < \omega_p$: a transfer into the mid-infrared regime. The experimental data and the presentation in the literatures are complicated, but I believe that this in fact is entirely consistent with what they actually see in the experiment.

Even if it works, however, I do not want you to care too much. The reason we should not worry is that the optics measure $q \ll \xi^{-1}$, whereas the saving of the Coulomb energy should be mainly from $\xi^{-1} < q \lesssim q_{\text{TF}}$. *Therefore, what we really need is the EELS experiment!* Although there have been EELS experiments in the normal phase in the

¹²Admittedly, they measured the reflectivity, and then used the Kramers–Kronig relation to obtain the dielectric constant, but it seems that they are right.

mid-infrared regime, and there have been also done in the superconducting regime, there has been no experiment which has shown the changes in going from the normal to superconducting phase in the mid-infrared regime. I have been leaning on various experimental groups for 15 years to do these experiments, and at last my colleagues P. Abbamonte, and J. Zuo at UIUC are going to do this experiment. Hopefully, in a year or two, we will know the result of the experiment. That will be a really crucial test for this argument.

8.6 How can we realize room temperature superconductors?

Let us just assume that the above idea is checked in the EELS experiment, and ask what are good ingredients for enhancing T_c . The possible ways are as follows:

1. Two-dimensionality (a weak tunneling contact between layers, but a strong Coulomb contact).
2. Strongest possible Coulomb interaction (intra-plane and inter-plane).
3. Strong Umklapp scattering may give rise to a wide and strong mid-infrared peak.

What we have actually shown is that in the absence of the lattice potential, we will not get the saving of the energy. Thus, the lattice is crucial. One of the effect of the lattice is to give rise to the Umklapp scattering, although there are of course many other effects. If there is a strong Umklapp scattering, it gives rise to a wide and strong mid-infrared peak. Since the wide and strong mid-infrared peak is a very characteristic thing in the cuprates, it seems that this argument works. However, note that although we know for sure that there is such a peak, we are not sure about its origin, and the Umklapp process is only one possibility. For example, a strong antiferromagnetic fluctuation may be the origin for the mid-infrared peak.

Anyway, the EELS experiment will show whether the above argument works or not, and these guidelines are correct or not.

Finally, I will make my bet on robust room-temperature superconductors. I do not think we will get it in my lifetime unless I am very lucky ($\sim 10\%$). But, I suspect in your lifetime, we will probably get a robust room temperature superconductor ($> 50\%$). Hopefully, this kind of argument may be somewhat helpful in finding new materials and so forth.

Thank you

References

- [1] C. N. Yang, *Rev. Mod. Phys.* **34**, 694 (1962).
- [2] W. Kohn and D. Sherrington, *Rev. Mod. Phys.* **42**, 1 (1970).
- [3] P. Monthoux and D. Pines, *Phys. Rev. B* **50**, 16015 (1994).
- [4] M. Turlakov and A. J. Leggett, *Phys. Rev. B* **67**, 094517 (2003).
- [5] G. V. Chester, *Phys. Rev.* **103**, 1693 (1956).
- [6] J. Hubbard, *Proc. R. Soc. A* **276**, 238 (1963).
- [7] N. Mihara and R. D. Puff, *Phys. Rev.* **174**, 221 (1968).
- [8] A. El Azrak, R. Nahoum, N. Bontemps, M. Guilloux-Viry, C. Thivet, A. Perrin, S. Labdi, Z. Z. Li, and H. Raffy, *Phys. Rev. B* **49**, 9846 (1994).

Index

- ^3He
- A phase of —, 42, 43
 - A1 phase of —, 42, 44
 - B phase of —, 42, 45
 - Cooper pair in —, 32
 - Normal liquid —, 29, 42
 - superfluid —, 43
- ABM state, 43, 46, 47, 55
- Abrikosov–Gor’kov theory, 74
- Alkali fullerenes, 78
- Ambegaokar–Baratoff formula, 120
- Anderson pseudospin representation, 16
- Anderson’s interlayer tunneling theory, 127, 151
- Anderson’s theorem, 73
- Anderson–Brinkman theory, 48
- Anyon superconductivity, 139
- ARPES, 108
- in the cuprates, 109, 122
 - in the pseudogap regime, 113
- BCS wave function, 11, 12
- BKBO, 61
- Bloch state, 25, 67
- Bloch–Grüneisen formula, 62
- Boojum texture, 58
- Broken pair (BP) states, 18
- BW state, 45–47
- Chandrasekhar–Clogston limit, 70
- Charge reservoir, 78, 98
- Classical superconductor, 61
- Coherence length, 118
- Condensation energy, 74
- in the cuprates, 118
- Conductivity
- in the cuprates, 120
- Critical field
- Upper — in the cuprates, 117
- Cuprates
- AC conductivity in —, 120
 - ARPES in —, 109, 113, 122
 - Condensation energy in —, 118
 - Crystal structure of —, 86, 99
 - dHvA experiment in —, 113
 - Doping in —, 99
 - EELS in —, 125
 - Ellipsometric measurements in —, 110, 124
 - Hall angle in —, 108
 - Isotope effect in —, 128
 - Knight shift in —, 106, 112, 118
 - List of —, 104
 - Loss function in —, 110
 - Luttinger’s theorem in —, 109
 - Microwave surface impedance in —, 119
 - Muon spin rotation in —, 119
 - Neutron scattering in —, 110, 123
 - Nuclear spin relaxation rate in —, 106, 112, 118
 - Optical reflectivity in —, 110, 124
 - Pair radius in —, 117, 127
 - Penetration depth in —, 117, 118, 120
 - Phase diagram of —, 93, 101
 - Resistivity in —, 106, 112
 - Specific heat in —, 112, 118
 - Superconducting fraction in —, 119
 - Thermal conductivity in —, 121

- Thermoelectric power in —, 108
 Tunnel conductance in —, 112, 121
 Upper critical field in —, 117
- d*-vector**, 37
- de Haas-van Alphen (dHvA) effect, 80,
 88, 109
 — in the cuprates, 113
- Debye frequency (temperature), 21, 63
- Density matrix
 Reduced density matrix, 65
- Dipole-dipole interaction
 — in ^3He , 50–52
- Electron energy-loss spectroscopy (EELS),
 111, 152
 — in the cuprates, 125
- Eliashberg equation, 26, 63, 64
- Ellipsometric measurements
 — in the cuprates, 110, 124
- Equal spin pairing (ESP) state, 36, 69, 88
- Excited pair (EP) state, 18
- Exotic superconductor, 61
 Common properties of —, 136
- Extended *s*-wave state, 71, 130
- Fermi liquid theory, 25, 29, 62
- Ferropnictides, 62, 91
- Far infra-red (FIR) absorption, 126
- Flux quantization, 125, 139
- Fock term, 13, 23
- Fragmented BEC, 56, 66
- Fullerene crystal, 77
- Gap equation, 20
 — at zero temperature, 17
 — at finite temperature, 20
 — for ESP state, 36
 — for general triplet states, 37
- Ginzburg–Landau theory, 38
 Generalized —, 46, 129
- Groud pair (GP) state, 18
- Gutzwiller projection, 141
- Hall angle
 — in the cuprates, 108
- Hartree term, 13
- Healing length, 24
 Ginzburg–Landau —, 27
- Heavy fermion, 82
 — superconductor, 62
 Normal state of —, 82
- Hebel–Slichter coherence peak, 71
- Hellman-Feynman theorem, 146
- Homologous series, 98, 103, 133, 151
- Hubbard model, 141
- Intercalant, 98
- Isotope effect, 21, 62
 — in the cuprates, 128
- Isotope exponent, 63
- Josephson experiment, 72, 89, 125
 AC Josephson effect, 139
 Principles of —, 131
- Kerr effect, 90
- Knight shift, 69, 73
 — in the cuprates, 106, 112, 118
- Kondo effect, 83
- Korringa relation, 106
- Kosterlitz–Thouless (KT) phase, 139, 151
- Kramers–Kronig relation, 110, 150
- London penetration length, 138
- Loss function
 — in the cuprates, 110
- Luttinger’s theorem, 109
- Macroscopic angular momentum, 34
- Meissner effect, 137, 138
- Mermin–Ho vortex, 58
- MgB_2 , 61, 80
- Microwave surface impedance
 — in the cuprates, 119

- Mid-infrared (MIR) peak, 111, 152
- Mihara–Puff relation, 150
- Muon spin rotation, 89
— in the cuprates, 119
- Neutron scattering
— in the cuprates, 110, 123
- NMR
Hebel–Slichter peak in —, 71
— in ^3He , 49, 55
- Nuclear spin relaxation rate, 73
— in the cuprates, 106, 112, 118
- Off-diagonal long range order (ODLRO),
125, 138
- Old-fashioned superconductor, 61
- Optical lattice
— in ultracold atoms, 141
- Optical reflectivity
— in the cuprates, 110, 124
- Organic superconductor, 62, 80
- Pair radius, 14, 24, 25
— in the cuprates, 117, 127
- Pair wave function, 23, 66
— at zero temperature, 13, 18
— at finite temperature, 20
- Paramagnon, 31
- Parent compound, 99
- Penetration depth, 73, 118
London —, 138
— in the cuprates, 117, 118, 120
- Persistent current, 137, 138
- Planar (2D) state, 47
- Polar (1D) state, 47
- Pseudogap regime, 102, 111
- Quasi-particle, 19, 33
- Random-phase approximation (RPA), 26
- Reduced density matrix, 65
- Resistivity
— in the cuprates, 106, 112
- RKKY interaction, 83
- Screening, 26, 146, 148, 151
Overscreening, 148
- Sommerfeld model, 10, 25
- Specific heat, 62, 72
— in the cuprates, 112, 118
- Spectators, 78
- Spin fluctuation
Persistent — in ^3He , 31
— feedback, 48
— theory in the cuprates, 142
- Spin-orbit coupling
Effect of —, 74
— in heavy fermions, 85
- Spontaneously broken spin-orbit symmetry (SBSOS), 51
- Strontium Ruthenate, 62, 86
- Sum rule, 147
f-sum rule, 150
— in ^3He , 50
- Superconducting fraction
— in the cuprates, 119
- Supercurrent, 57
Mass —, 57
Spin —, 57
- T^* -line, 102, 133
- Thermal conductivity
— in the cuprates, 121
- Thermoelectric power
— in the cuprates, 108
- Tunnel conductance
— in the classical superconductors,
64
— in the cuprates, 112, 121
- Umklapp scattering, 83, 87, 93, 107, 154
- Virial theorem, 145
- WILLIE SUTTON principle, 152